TO DESIGN A FRAMEWORK FOR REDUCTION OF SPECKLE NOISE IN SYNTHETIC APERTURE RADAR IMAGES

Thesis

SUBMITTED TO

BABASAHEB BHIMRAO AMBEDKAR UNIVERSITY

(A Central University)

Lucknow

BABASAHEB BHIMRAO AMBEDKAR UNIVERSITY
LUCKNOW
प्रज्ञा शील करुणा
ESTABLISHED 1996

FOR THE DEGREE OF

Doctor of Philosophy

In

INFORMATION TECHNOLOGY

By

Prabhishek Singh
(Enrolment No. 1292/15)

Under the Supervision of

Dr. Raj Shree

Department of Information Technology

BABASAHEB BHIMRAO AMBEDKAR UNIVERSITY

(A CENTRAL UNIVERSITY)

LUCKNOW-226025, INDIA

2018

Dedicated to

my

Mother & Father

DECLARATION

I, Prabhishek Singh, solemnly declare that this thesis of research on **"TO DESIGN A FRAMEWORK FOR REDUCTION OF SPECKLE NOISE IN SYNTHETIC APERTURE RADAR IMAGES"** is my original work. The study has been conducted under the guidance of Dr. Raj Shree, at Department of Information Technology, Babasaheb Bhimrao Ambedkar University (A Central University), Lucknow (U.P.), India-226025. It is further declared that to the best of my knowledge and belief it has not been submitted earlier for the award of any degree. The thesis is essentially free from all kinds of plagiarism.

Dated: 24/04/18

Prabhishek Singh

(Prabhishek Singh)

Research Scholar
Department of Information Technology
Babasaheb Bhimrao Ambedkar University
(A Central University)
Lucknow, (U.P.), India-226025

CERTIFICATE

This is to certify that the thesis titled **"TO DESIGN A FRAMEWORK FOR REDUCTION OF SPECKLE NOISE IN SYNTHETIC APERTURE RADAR IMAGES"** submitted by **Mr. Prabhishek Singh** is an original research work and has not been previously submitted in part or full for the award of any other degree or diploma to this or any other University.

The thesis submitted to Babasaheb Bhimrao Ambedkar University, Lucknow satisfies all the requirements as stipulated in the *Doctor of Philosophy (Ph.D.) regulations-1999 as amended in 2008/2010/2013* and it is fit for submission and evaluation for the award of the degree of Doctor of Philosophy of the University.

Date: 24/04/18

24/04/18

Supervisor

24/04/18.

Head of the Department

ACKNOWLEDGEMENT

I thank God the almighty for his shower of blessings without which nothing would have been possible.

It is with a profound sense of gratitude; I would like to express my heartfelt thanks to each one who has been involved with my thesis, over the last few years, all who had made this great endeavour possible.

First and foremost, I am deeply indebted to Assistant Professor and my supervisor **Dr. RAJ SHREE**, Department of Information Technology, Babasaheb Bhimrao Ambedkar University (A Central University), Vidya Vihar, Raebareli Road, Lucknow, for her constant source of inspiration and guidance in the pursuit of my doctorate study and in preparing this thesis. I am extremely grateful to her for her constant assistance and inestimable help right from the planning till the execution of this entire Ph. D. thesis work. Her extreme energy, creativity and excellent technical and management skills have always been a constant source of motivation for me. The perfection that she brings to each and every piece of work that she does always inspired me to do things right at first time. She is a great person and one of the best mentors, I always be thankful to her. I will always be obliged to her for her wholehearted support and kindness extended to me during my entire course.

I would like to extend my sincere gratitude to **Prof. (Dr.) R. A. Khan**, Professor and Head, Department of Information Technology, Babasaheb Bhimrao Ambedkar University (A Central University), Vidya Vihar, Raebareli Road, Lucknow, for his invaluable support. I will remain indebted to him for his valuable suggestions during the entire thesis work and providing thoughtful feedback to improve its content. I will always be gratified to him for his unconditional support and kind-heartedness extended to me during my entire course.

I would like to thank to all the **experts** from India and abroad for their valuable observation during review process. I would also like to thank to all the **faculty members** and **office staff** of the Department for their cooperation and continuous support extended during the thesis work.

I would like to thank and acknowledge **Dr. RS Kamlavanshi**, retired Associate Professor, Department of Plant Pathology, CS Azad University of Agriculture and

Technology, Kanpur and **Dr. Satya Kumar**, Professor, Department of Plant Pathology, College of Agriculture, GB Pant University of Agriculture and Technology, Pantnagar, Uttrakhand. I would also like to thank and acknowledge **Dr. Shankar Lal**, former ADG (Crop Science), ICAR, Delhi & Former Director, Indian Institute of Pulses Research, Kanpur, for their constant motivation, encouragement and help in writing and organising this thesis.

I also sincerely thank my friend **Dr. Manoj Diwakar**, Assistant Professor and Head, Department of Computer Science and Information Technology, Uttaranchal University, Arcadia Grant, Chandanwari, Premnagar, Dehradun, Uttarakhand, for his encouragement and technical support extended to me during the period of my course. I will always remain indebted to him for his support not only in my thesis work but also during the entire course of my doctrate degree. I also sincerely thank my friend and senior, **Ganesh Chandra**, research scholar, Department of Computer Science, Babasaheb Bhimrao Ambedkar University (A Central University), Vidya Vihar, Raebareli Road, Lucknow for his encouragement and expertise extended in the statistical analysis.

On a personal note, I feel that I can by no means repay the endless efforts of all members of my family to keep me motivated even from the first day of my primary school education until the last minutes of this work. I especially want to thank my mother **Mrs. Sarla** for her willingness to keep me awake by sacrificing her sleep, to my father **Mr. Sunder Lal** for his continuous support that puts me back to work when I felt tired, my sister-in-law **Dr. Poonam Majumder Singh** for her continuous support and motivation that puts me active again whenever I felt low and to my elder brother **Dr. Abhishek Singh** who always being my ideal. This work could not be completed without them. This journey would not have been possible without the unparalleled support of my family.

I wish to dedicate this work to my parents, my brother and my sister-in-law and my teachers for their extreme support in my entire endeavour till date. I thank you all from the core of my heart.

PRABHISHEK SINGH

ABSTRACT

Image Restoration is one of the most investigated field of image processing. It is the process of taking a noisy or degraded image as input image and estimating the noise-free image that is approximately equivalent to the reference image using some image restoration technique. The reason behind this degradation may be motion blur, noise, camera mis-focus etc. Image restoration is implemented by reversing the procedure that distorts the image. This is executed by imaging a point source and use the point source image, which is called the Point Spread Function (PSF) to restore the image details lost to the distorting process.

In this research work, image restoration is done on Synthetic Aperture Radar (SAR) images that are already influenced by the speckle noise. SAR is one form of radar that is fixed on the satellites and aircrafts that captures the high-resolution images of large area of the earth surface from different view angles. SAR images are formed by the consistent interaction of the emitted microwave radiation with target areas. This consistent interaction originates arbitrary constructive and destructive noisiness that results into granular pattern on captured SAR image. This granular pattern of noise is known as speckle noise. This noise is multiplicative in nature. A granular pattern of speckle noise in the SAR image corresponds to the "salt-and-pepper" kind of noisy effect. The granular pattern of speckle noise is the interference or fading pattern. Speckle is the scattering phenomenon but not the noise. The consistent interaction of high-frequency radar waves with a complex set of scatterers are possibly the restrictive aspect of SAR processing system design and application. Speckle noise creates a negative impact on the SAR image. It has adverse effect on the SAR image. Eliminating speckle noise from the SAR image is one the challenging task as SAR images are already influenced by the speckle noise. The process of eliminating or reducing speckle noise from the SAR image is called as the SAR image despeckling.

The main objective of image despeckling is to eliminate the speckle noise, preserve the important details of SAR images such as texture, edges, structures, corners, maintaining the smoothness in the homogeneous region of the image and preserving the fine details in the heterogeneous region. Usually SAR images are high dimensional images and preserving the edge and corner components is one major issue. Anisotropic diffusion also called Perona-Malik diffusion is used to reduce noise without disturbing the significant parts of the image. A homomorphic despeckling method is proposed using anisotropic diffusion in db2 based type wavelet transform. The linear and non-linear filters are applied on the approximate part of the

image to remove blurring. Method noise thresholding is used to restore the unfiltered part of the despeckled image. The proposed method is applied and tested on correlated speckle noise as well as uncorrelated speckle noise on the real dataset of SAR images. The performance of the proposed method is evaluated by its visual quality and by using other metrics such as Peak Signal-to-Noise Ratio (PSNR), Structural similarity index metric (SSIM), Universal Image Quality Index (UIQI) and Root Mean Square Error (RMSE). The performance and computational time are calculated and compared with standard filters and methods. The critical analysis of the result shows that proposed method gives the brilliant outcome in terms of structure and edge preservation and noise suppression.

This proposed method is the hybrid combination of the Bayesian method in transform domain (homomorphic filtering in wavelet domain) and non-Bayesian method (anisotropic diffusion). This unique hybrid combination presents image quality with good visual appearance. The computational cost of this method is highly efficient. The concept of method noise is implemented as the post-processing step. It enhances the quantitative results as well as visual quality of the image. If this hybrid combination and easy use of method noise can give such good results, then a way better and intelligent use of method noise can give much better results. The results of this method motivate to go for designing a new method with more intelligent use of method noise.

Theoretically, multiplicative noise is considered as the ratio of the standard deviation to the signal value. The new despeckling method works on db2 based 2D-Discrete Wavelet Transform (DWT) using wavelet thresholding, Directional Smoothing Filter (DSF) and intelligent use of method noise thresholding. The method is designed to despeckle the simulated as well as real speckled SAR images. It uses a hybrid combination of DSF, wavelet thresholding using enhanced Bayesian shrinkage rule and method noise thresholding for despeckling purpose. After DWT decomposition, the approximate component is directed to DSF followed by method noise thresholding and detailed components are directed to wavelet thresholding followed by method noise thresholding. This method validates the efficient use of method noise and explains how its intelligent use can enhance the result of the algorithm over other efficient methods. The quality assessment of the proposed method is done by visual appearance and measures such as PSNR, SSIM, UIQI, Equivalent Numbers of Looks (ENL), Noise Variance (NV), Coefficient of Variation (CV), Mean Squared Error (MSE), Correlation Coefficient (CC) and preservation of mean values before and after despeckling. The

effectiveness of the proposed method is demonstrated by matching it to well-known speckle noise removal methods on SAR images.

The post-processing operation of method noise in the first despeckling method presents decent result. This concludes with the new idea of using the concept of method noise in more intelligent way for better results. The second despeckling method is completely based on the use of method noise. The method noise is used for fine detail preservation. The other filter used in this technique is DSF that is specifically used for edge preservation. This method is an edge preserving despeckling technique. This method offers a new intelligent use of method noise in two different ways. The concept of method noise is used three times in this method. Firstly on the low frequency components, secondly on the high frequency components and lastly as a post-processing operation. This new way of implementing the method noise enhances the result. The proposed method 1 and 2 works on global filtering. According to literature available, the despeckling results using local filtering shows better result than the global filtering. In both method, the decomposition level is manually set by experimenting the method from level 1-7 and the optimal results are obtained at 3 level. The cost of second method is computationally low. The local filtering and automatic selection of decomposition level leads to design a new despeckling method.

A new despeckling technique for speckled SAR images is designed using a local correlation based fusion of high-frequency coefficients in DWT with method noise thresholding. The decomposition level is decided by analyzing the texture of the input image at each decomposition level by calculating entropy. The core idea of this proposed technique lies in the selection of decomposition level in 2D-DWT based on entropy parameter and on the fusion of high-frequency coefficients. On decomposition, the low-frequency coefficients remain untouched and the high-frequency coefficients are thresholded using two different shrinkage rules in parallel. Therefore the Bayesian and Bivariate shrinkage methods are applied to the high-frequency coefficients in parallel. After performing two different thresholding methods, the improved high-frequency coefficients are fused using local correlation based strategy. The threshold value is calculated using correlation coefficient (CC) of two improved high-frequency coefficients. Later again the CC is evaluated between the two improved high-frequency coefficients using small size mask for the fusion strategy. The CC is now compared with the threshold value for the fusion purpose. On the basis of defined fusion strategy, the average and maximum operation are applied to perform the fusion of high-frequency coefficients. The despeckling method is followed by method noise

thresholding in order to preserve the fine details of the image. The performance of the proposed method is assessed using metrics such as Signal-to-Noise Ratio (SNR), PSNR, SSIM and visual appearance of the despeckled image. The experimental results demonstrate the effectiveness of proposed work over prior works on SAR image despeckling.

List of Tables

List of Figures

TABLE OF CONTENTS

1. INTRODUCTION

1.1 Background

All the information that is gathered for detecting and tracking ships, ocean wave forecasting, agricultural monitoring, military system, assessment of damages after flood and earthquake is acquired through SAR images. If the quality of the SAR image is good, then enough useful information can be obtained but if the quality of the SAR image is bad, then there is problem in obtaining useful information. This chapter briefly explains the radar, its types, working and applications. The process of SAR image creation is discussed. The reason of roughness and brightness found in the SAR image is discussed with the relevant facts. The different type of

problems related to SAR image is shown in the tabular form; out of them the problem of speckle noise is targeted and explained in detail. In the last four sections, motivation, problem statement, and objectives, contribution to the work and thesis organization is discussed in the detail.

1.2 Radar

Radar (**RA**dio **D**etection **A**nd **R**anging [1], [2] or **RA**dio **D**irection **A**nd **R**anging [3], [4]) is a system that uses radio waves to detect and determine the velocity, angle or range of objects. It is used to detect aircraft, ships, guided missiles and weather formations. A radar system consists of a transmitter that emits high-frequency electromagnetic waves. The transmitting and receiving antenna are used for transmitting the radar waves and receiving the backscattered information. The receiving antenna and processor determines the characteristics of the objects.

Radar is categorized into two types:

- Active radar and
- Passive radar.

In active radar, an antenna emits high-frequency radio waves on the objects of the earth surface and echoes back the backscattered information of the object. This type of radar is called as mono-static. In Figure 1.1, the variable T denotes the time delay that is equal to the total time taken by the signal to be transmitted to the object and reflected back i.e. $t_{transmitted}$ + t_{echo}. Here the location of the transmitter and receptor is same.

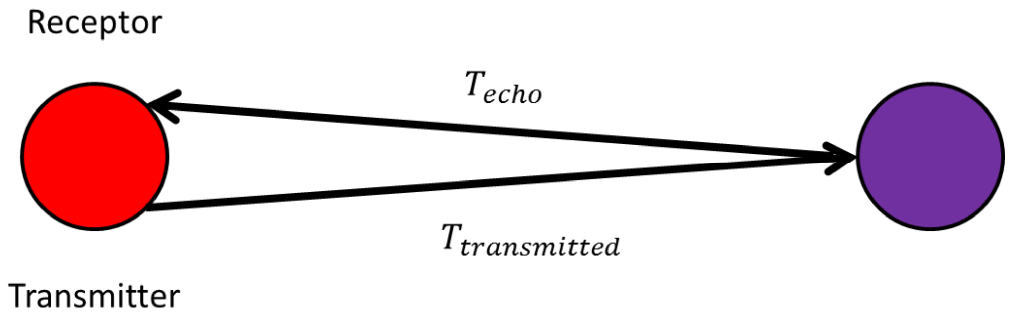

Figure 1.1 Basic mechanism of an active radar system

In a passive radar system, the location of the transmitter and receptor is different. A passive radar system depends on the signal spread from a dissimilar location. This type of radar

system is called bi-static. In the Figure 1.2, t1+t2 = t3+t4. This condition is true for every object that is positioned on the ellipse of Figure 1.2. For both of the objects in Figure 1.2, from the receptor point of view, the time delay between the original signal and the reflected signal is exactly the same. The performance of the passive radar system is highly dependent on the number of transmitters and receptors and their geometry.

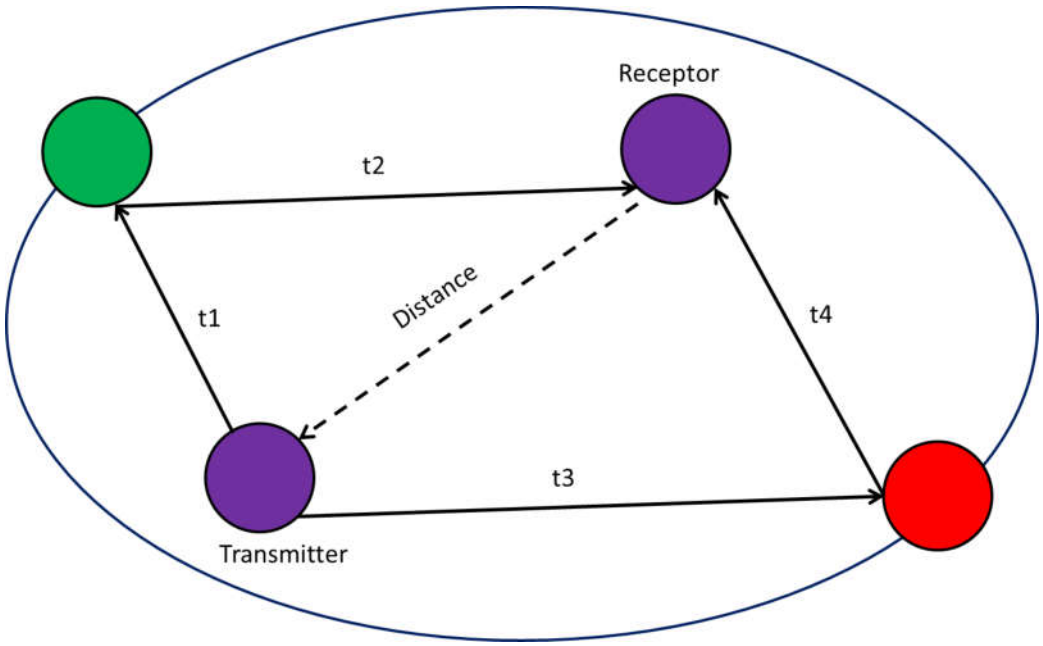

Figure 1.2 Basic mechanism of a passive radar system

Radar is categorized into two main groups on the basis of antenna size:

- Real Aperture Radar (RAR)
- Synthetic Aperture Radar (SAR)

1.2.1 RAR (Real Aperture Radar)

RAR are the non-coherent radars that are controlled by the physical length of the antenna. It is active radar that transmits high-frequency radar waves from the antenna to the particular piece of terrain that one wants to obtain the image. This transmitted radar waves is of the narrow-angle beam in the range direction at right angles to the flight direction called as the azimuth direction and receives the backscattering from the targets which will be transformed to a radar image from the received signals, as shown in Figure 1.3. The image resolution is defined by the length of the antenna. It is impractical to design a large antenna in order to get a high-resolution image because in that case, an antenna has to be at least many times of the length of wavelength in order to minimize the bandwidth of transmitted signal [5]. If in case,

such antenna is made then it is very problematic to mount such antenna, which requires 1 km diameter length of the antenna to get 25 meters resolution with L band (=25 cm) and 100 km distance from a target, a RAR hence has a practical constraint for refining the azimuth resolution.

1.2.2 SAR (Synthetic Aperture Radar)

In SAR imaging, an antenna transmits the microwave pulses towards the earth surface. This high-frequency microwave energy scattered back to the spacecraft is measured as shown in Figure 1.3 [160]. The SAR makes use of the radar principle to form an image by utilizing the time delay of the backscattered signals. SAR is the coherent radar that is attached to the satellites and aircrafts that captures the high-resolution images of the wide surface area of the earth. SAR overshadows photographic and other optical imaging abilities as it has the advanced capability of taking images in varying weather conditions, day and night due to a different wavelength of camera sensors. SAR works over the sensors of the wavelength of 1 cm to 1 m, whereas optical sensors use wavelengths near that of visible light or 1 micron. Due to this difference, SAR has the capability to see through clouds and storms, whereas optical sensors are unable to do so. On comparing with RAR, SAR increases the size of the antenna or aperture synthetically to raise the azimuth resolution. In SAR, the data processing of received signals and phases from moving targets with a small antenna is a complicated process.

When radar waves hit the earth surface, the proportion of energy scattered back to the sensor as shown in Figure 1.3 depends on many factors [6], [160]:

- Physical factors such as the dielectric constant of the surface materials which also depends strongly on the moisture content.
- Geometric factors such as surface roughness, slopes, orientation of the objects relative to the radar beam direction.
- The types of land cover (soil, vegetation or man-made objects).
- Microwave frequency, polarisation and incident angle.

Due to the cloud-penetrating property of microwave, SAR is able to acquire “cloud-free” images in all-weather [6]. This is especially useful in the tropical regions which are frequently under cloud covers throughout the year. Being an active remote sensing device, it is also capable of night-time operation [7], [160].

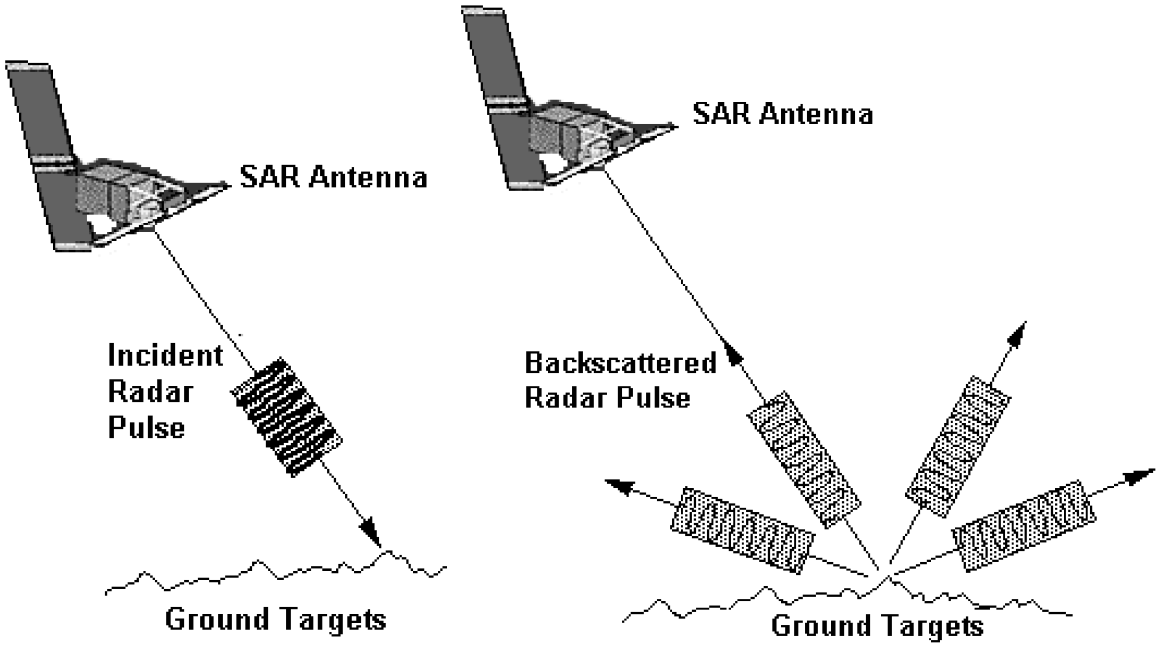

(a) **(b)**

Figure 1.3 (a) A radar pulse is transmitted from the antenna to the ground (b) The radar pulse is scattered by the ground targets back to the antenna [160]

1.3 Different Types of SAR

SAR imaging is divided into following types on the basis of the nature of application:

1.3.1 Strip mapping Mode SAR

The traditional SAR image processing is based on the strip mapping mode [12], [13] as shown in Figure 1.4(a). This mode is used when the large terrain is to be captured. Here the terrain data is acquired without staring at any particular location. Heavy computation is required. In this SAR mode, a large unit of backscattered energy is bounced back and received by the antenna, which takes more computation time for handling this much data.

1.3.2 Spotlight Mode SAR

The flying SAR system stares at an exact a scene typically on the ground [12], [13] as shown in Figure 1.4(b). It captures small terrain area than strip mapping mode hence requires less computation cost. It captures multiple SAR images of same spot of the terrain to get the more accurate data. Here multiple SAR images are captured within a time interval of seconds.

Since the area of the captured region is not large, so the amount of reflected energy received by the antenna is not much. Due to this, the computational time is less.

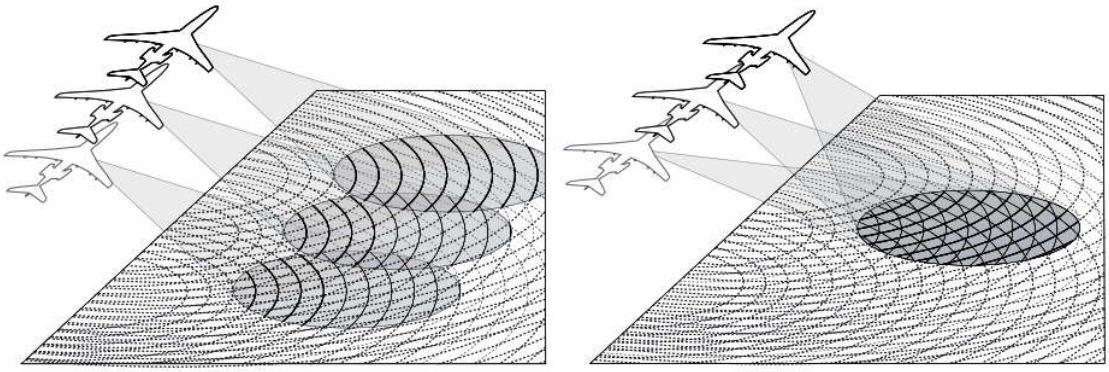

(a) **(b)**

Figure 1.4 Types of SAR (a) Stripmap SAR [12] (b) Spotlight SAR [12]

Spotlight mode is used in the applications where lower mapping, low processing time and low cost is the need. This mapping is heavily used by fighter aircraft to keep inform the navigation system by tracing the recognized landmarks [13].

1.3.3 Inverse SAR (ISAR)

Inverse synthetic aperture radar (ISAR) is a radar technique that uses the radar imaging concept to create a 2D-high resolution image of a target. It is analogous to traditional SAR, except that ISAR technology uses the movement of the target rather than the emitter to create the synthetic aperture. ISAR is mainly used for capturing or mapping the moving or rotating targets. The ISAR is critically used in the war application like the movement of aircrafts and ships [13].

1.4 Applications for SAR

SAR has now become one of the valued remote sensing tools for both soldierly and noncombatant users. Various soldierly SAR applications are intelligence gathering, battlefield survey, and weapons supervision. The noncombatant applications include topographic planning, geology and mining, oil spill observation, sea ice observation, oceanography, agricultural and land use monitoring and planetary or celestial examinations [8]. The observation and interpretation of the earth using SAR have following wide practical applications as discussed below.

1.4.1 On the ocean

- Man-made illegal or accidental spills are visible in SAR images.
- Ships can be detected and tracked.
- Natural leakage from oil deposits can also be observed, providing hints for the oil industries.
- Scientists are studying the radar backscatter from the ocean surface which is related to wind and current fronts, eddies, and internal waves.
- In shallow waters SAR imagery allows one to infer the bottom topography.
- The topography of the ocean floor can be mapped using the very precise ERS Altimeter because the sea bottom relief is reflected on the surface by small variations of the sea surface height.
- Ocean wave forecasting and marine climatology.
- Regional ice monitoring. This is essential for navigation in ice-infested waters.

1.4.2 On the land

- Monitoring lands of forestry and agriculture.
- Some geological or geomorphological features are enhanced in radar images thanks to the oblique viewing of the sensor and to its ability to penetrate (to a certain extent) the vegetation cover [8].
- SAR data can be used to georeference other satellite imagery to high precision, and to update thematic maps more frequently and cost-effectively, due to its availability regardless of weather conditions.
- In the aftermath of a flood, the ability of SAR to penetrate clouds is extremely useful. Here SAR data can help to optimize response initiatives and to assess damages.
- Detection of small surface movements caused by earthquakes, landslides or glacier advancement [8].

1.5 SAR Image Creation

SAR is also like a camera that captures images. Both SAR and optical camera have the different penetrating capability. This penetrating capability depends upon the capturing phenomenon. In order to create an image, the optical camera depends on the light while SAR relies on radar signals which it transmits. This significant difference of SAR allows capturing

the images in pure darkness and also permits to see through clouds, rain, fog, and snow. Creating a SAR image requires a heap of data and terrific calculating power [9].

In general, the basic working principle of radar i.e. RAR is to calculate the time taken by the radio wave to travel from an antenna to object and back to the antenna. Radar computes this traveling distance from an antenna to object and back to the antenna using time interval but this kind of radar can only trace an object and measure its speed. To create an image, a significantly greater heap of data and terrific calculating power is needed. It needs an exceptionally elongated antenna. But in SAR, it uses a smart way of synthetically creating a long antenna by moving a small antenna to cover a long distance. After receiving all data, it saves it and starts processing it [9].

As the airplane flies and moves forward, the SAR antenna transmits the high-frequency radio waves also called radar waves in the direction of the ground. In the middle of the pulses, the antenna collects backscattered high-frequency radio waves that have bounced off objects on the ground. These backscatter pulses contain information that includes the total distance traveled by the pulses to make the round trip to and from the plane. It also contains the information about the movement of the SAR whether it is moving in the direction of or against from the object on the ground. The backscattered pulses are recorded and if the pulses are recorded to be very close to each other, then the plane with the SAR antenna is moving towards the ground and if the pulses are recorded to be far from each other the plane is moving away from the ground [9].

From the huge amount of backscattered pulse data collected, there are certain pulses that show a specific pattern, this specific pattern denotes that those pulses are bounced off from the same location. During this process the information related to distance is known from the exact location where the plane was when it sent and received the pulses that fit the pattern, it's a simple matter to plot the point of the object on the image it's creating [9]. The point on the image is plotted, but the brightness of the point is still not known. SAR determines the brightness by the intensity of the signal it receives. An object such as a tree absorbs some of the radar energy and so it appears gray. A metal object-oriented toward the SAR antenna reflects a lot of the energy back, so it appears bright [9].

In SAR image processing, there are a thousand calculations needs to be performed for each and every pixel and such image is shown below of Washington, D.C., which is made up of several million pixels in Figure 1.5.

Figure 1.5 SAR image of Washington, D.C. took on a snowy night in 1994. [11]

1.6 Roughness and Brightness of SAR Image

The brightness and darkness in the SAR images are due to the structure surface of the target object on the ground. The roughness of the surface decides the brightness of the SAR images. When the antenna transmits the high-frequency radar waves and they hit the ground, only a portion of the signals reflects backs to the antenna. The antenna has the capability of both transmitting and receiving the radar signals.

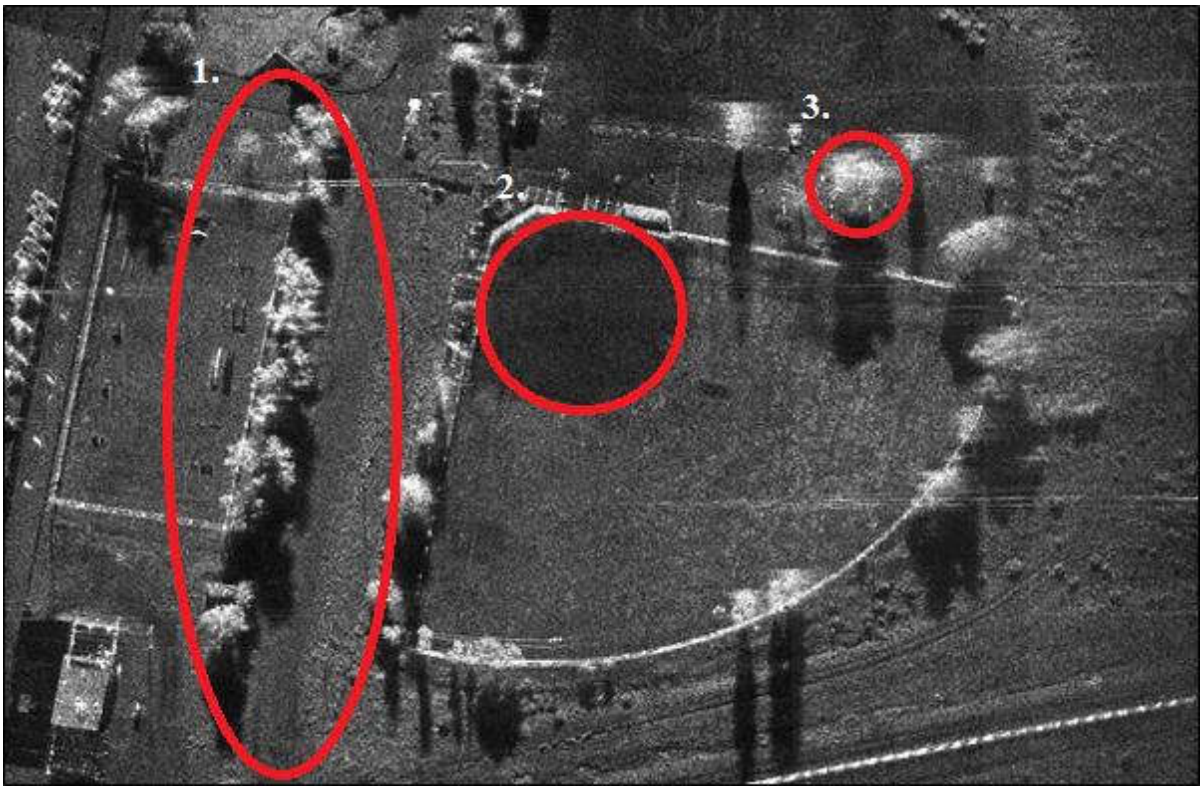

Figure 1.6 Dark and Bright areas of the SAR images

When the adequate portion of the radar signals reflects back to the antenna then those parts are shown bright in the SAR image. When a very small portion of the radar signals is reflected back to the antenna then those areas are projected dark in the SAR images. There are certain factors over which the returning radar signals depends upon like electrical properties, roughness, the geometrical positioning of the surface and the polarization direction of the returning radar wave. Figure 1.6 shows the bright and dark areas in the SAR image.

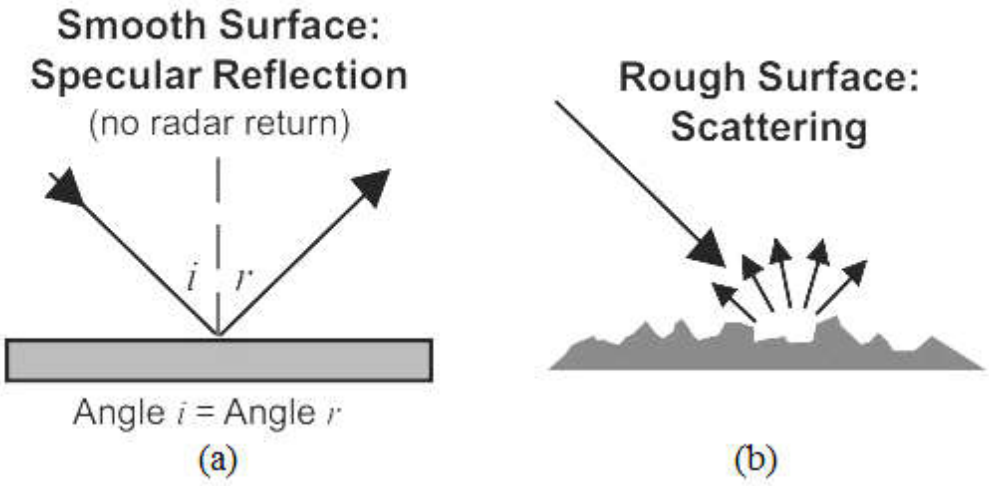

Figure 1.7 Surface orientation (a) Smooth surface (b) Rough surface

Figure 1.7 shows the surface orientation of the target ground over which the radar signals hit. The smooth and rough surfaces are shown in the above figure. When radar signal hits the smooth surface of the terrain as shown in Figure 1.7(a) the angle of incidence of the radar signal is almost equal to the angle of reflection of the reflected radar signal. This means that there is either no radar return or a very little energy returns back to the radar antenna. In this case, the projection is shown dark in the SAR image. This type of case is mainly seen in the calm water body like a river which has a specular reflection [15].

When radar signal hits the rougher surface which has a random and irregular surface orientation, then the radar energy is reflected back in many directions as shown in Figure 1.7(b). In this case, a small portion of the radar energy is reflected back and received by the SAR antenna which produces a bright signature in the SAR image. This type of case is mainly seen in SAR images of rocky mountains and trees.

The orientation of the local surface of the target region relative to radar wave travel path is responsible for the variation of brightness in the SAR images. Other various surface orientations responsible for variation in brightness are shown in Figure 1.8. When radar

signal hit the surfaces that are perpendicular to the travel path of the signal then this scenario generates the strongest return as they are directly facing the sensor shown in Figure 1.8(a).
The slopes that face away from the SAR sensor produce the weak returns of the target information. Similarly, the slopes of the hills are steeper than the depression angle then they are not illuminated by the radar signals and are completely shadowed and in this case, least or no information of the returned back to the antenna which also appears darker in the SAR image. As the depression angle becomes smaller causing more gentle back slopes to become shadowed.

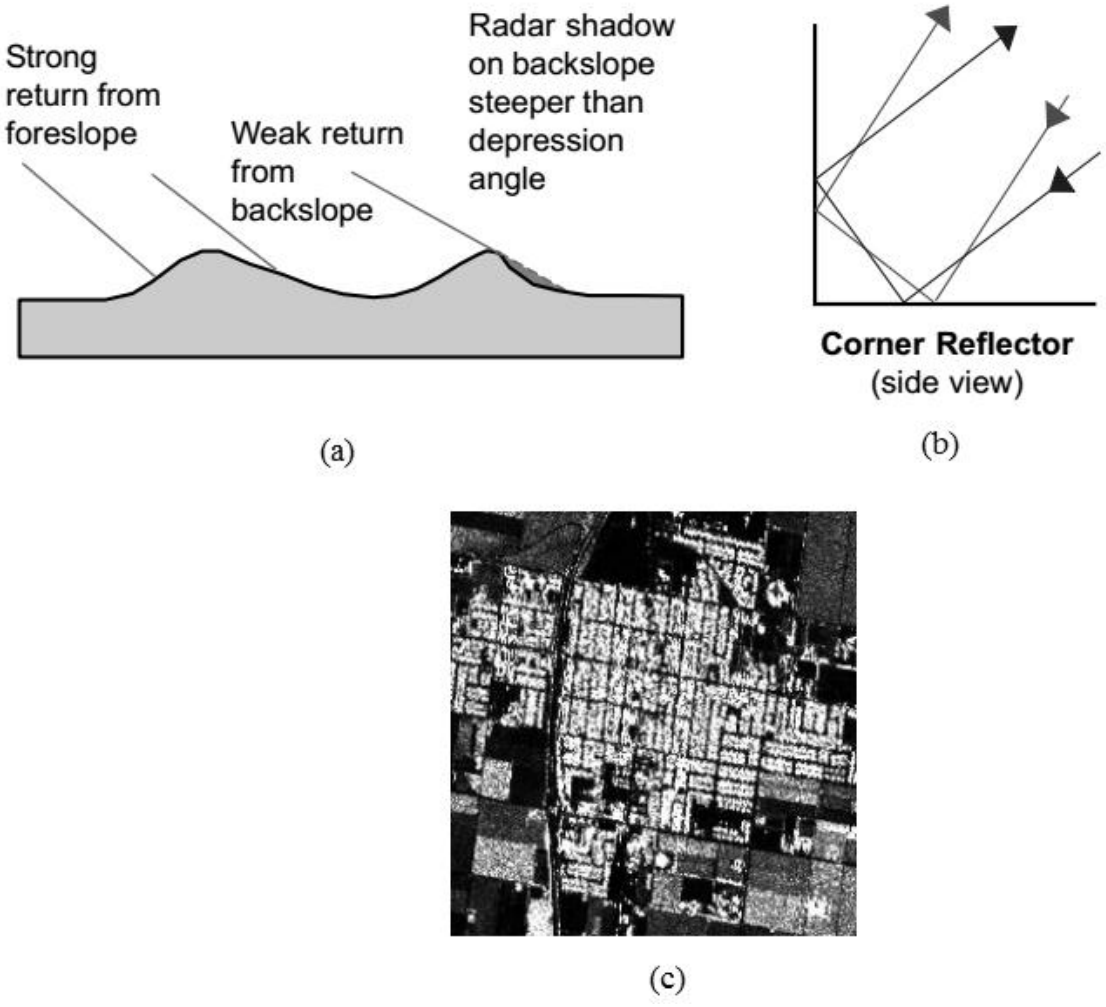

Figure 1.8 Surface orientation affecting the brightness of the SAR images

The visual appearance of the buildings in the populated area is bright and clear in the SAR image because of the corner reflector shape as shown in Figure 1.8(b) and (c). In Figure 1.8(b), corner reflector is shown that produces the strongest return of the radar signals. It can be noticed that the radar signals when hit the surface it completely reflects back to the SAR sensor regardless of the depression angle. The objects with metal surfaces like bridges and

towers of power line appear brighter in the SAR images because the value of the dielectric constant is high [14]. The dry natural materials like rammed earth and earth sheltering have low dielectric constants, but the occurrence of humidity in the soil, snow, or vegetation raises this value and their radar reflectivity too. SAR image processing assesses humidity content of surface materials.

1.7 Problem in SAR Image

There are a number of reasons of disturbance in the performance of the SAR system and degradation in the quality of SAR image. Some of the reasons are nonlinearities of the SAR subsystem that damage the ability of the system resolution. Noise is one frequently seen problem in SAR images whose major source is image acquisition [10]. Other sources of noise introduction are the position of sensor and velocity errors that result in geometric distortion in the SAR image. Major occurring problems in the SAR image are discussed in Table 1.1.

Table 1.1 Real problems in SAR images [13]-[16]

Real effects on SAR images	Major sources
Geometric distortion	• Change in position: movement variation and changes in platform attitude (high and low frequencies) cause distortion due to the platform of spaceborne or airborne. • Rotation of earth, topographic effect and curvature cause distortion due to earth. • Deviation in sensor mechanism and viewing geometry: panoramic effect causes distortion due to the sensor. • Refraction and turbulence cause distortion due to the atmosphere. • Time-variations or drift and clock synchronicity cause distortion due to measuring instruments.
System nonlinear effects	• Amplitude error and phase error degrades the system impulse response function (IRF). • Thermal noise damages the dynamic range of the system. • Quantisation error, bit error noise and system nonlinearities damage the azimuth resolution and dynamic range of IRF.

Range migration	• Linear drift because of elliptical orbit and earth rotation. • The appearance of hyperbola shaped reflection as target move towards the synthetic aperture. • Curvature depends on range compressed response due to which SAR handles the two-dimensional space-variant problem. • High velocities of airplanes and satellite-borne SAR system.
Speckle Noise effects	• SAR images are shaped by the constant interaction of the transmitted high-frequency radar waves with target areas. This constant interaction causes random constructive and destructive nosiness that result in salt and pepper noise all over the image. This noise scatters all around the image and suffers from the speckle noise effects and degrades the quality of the SAR image. It is a granular pattern noise that inherently exists in the SAR image. • The existence of numerous elemental scatterers with an arbitrary distribution within a resolution cell.

1.8 Noise in SAR Image

The granular pattern that usually found in the SAR image either during image acquisition or due to arbitrary constructive or destructive interference is called as speckle noise. It appears like 'salt and pepper' noise due to its granular pattern. The consistent interaction of high-frequency radar waves with a complex set of scatterers is possibly the least implicit and restrictive aspect of SAR processing system design and application.

Non-consistent sensors usually employ diffraction limited physical apertures for the focusing of incident electromagnetic radiation, followed by detectors which are sensitive to the total intensity of the radiation incident upon them.

In contrast, a SAR transmits a very precise signal towards its target and, when the reflected radiation returns, a SAR records not only the amplitude of that signal but its phase as well. It is the phase information which allows for the post-facto coherent summation of the many thousands of recorded signals in the correlator during the aperture synthesis operation. Coherent signals have properties that are considerably different from their noncoherent counterparts. The coherent interference between targets contained within a resolution cell is the basis for much of the scintillation of coherent radar imagery, an effect often referred to as

speckle. Thus, there is a wide variation in the SAR image, even when a uniform input is given. This variation can be considered as a form of noise. In the classical sense, the speckle is not really noise and there is information to be obtained from it because speckle is the radar signature of the target under a particular set of circumstances [20].

The traditional speckle pattern is shown in Figure 1.9. Basically, speckle is not a noise but a scattering phenomenon [18]. However, in the SAR image processing, speckle is modeled as multiplicative noise as shown in Eq. (1.1) [17].

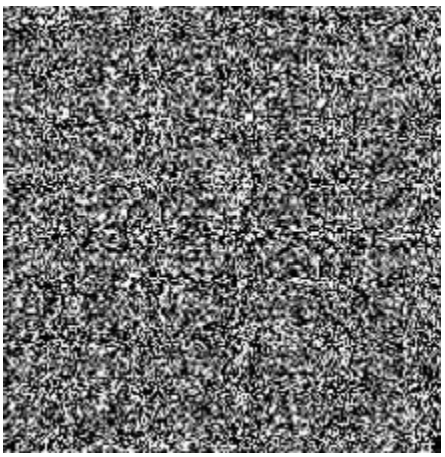

Figure 1.9 Classical speckle pattern [20]

Speckle noise is modeled as multiplicative noise. Therefore the resultant signal is the product of speckle signal and original noise [46]. Let I (i, j) is the degraded pixel of an observed image and S (i, j) be the noise-free image pixel which is to be recovered. With the multiplicative noise model,

$$I(i,j) = S(i,j) * N(i,j) \quad \text{.....(1.1)}$$

In which N (i, j) depicts the multiplicative noise with unit mean and standard deviation [19]. An inherent characteristic of SAR images is the presence of speckle noise. Speckle noise is random and deterministic in an image [30]. Speckle has a negative impact on SAR images. Radical reduction in contrast resolution may be the main reason for the poor effective resolution.

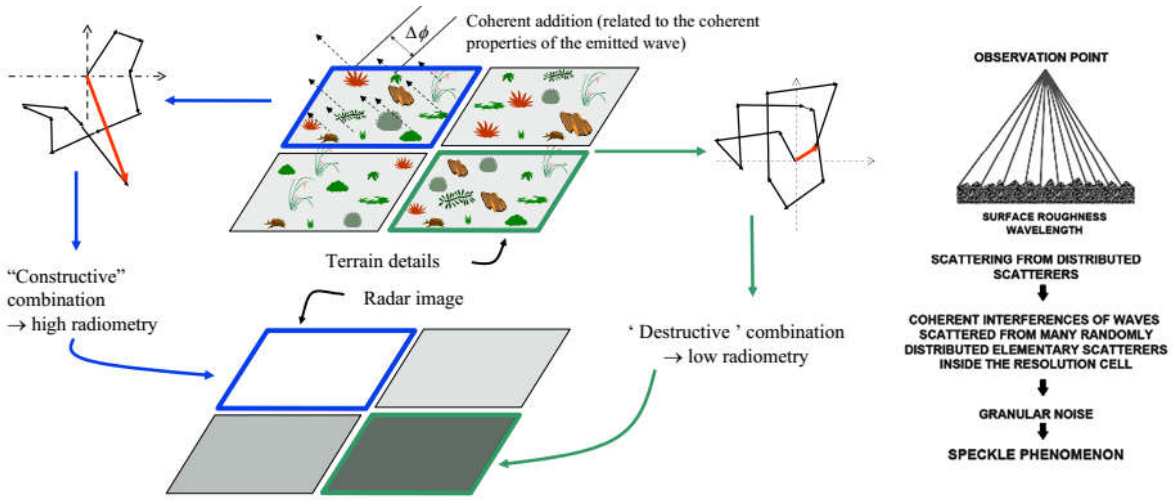

(a) **(b)**

Figure 1.10 Speckle phenomenon (origin) [18], [20]

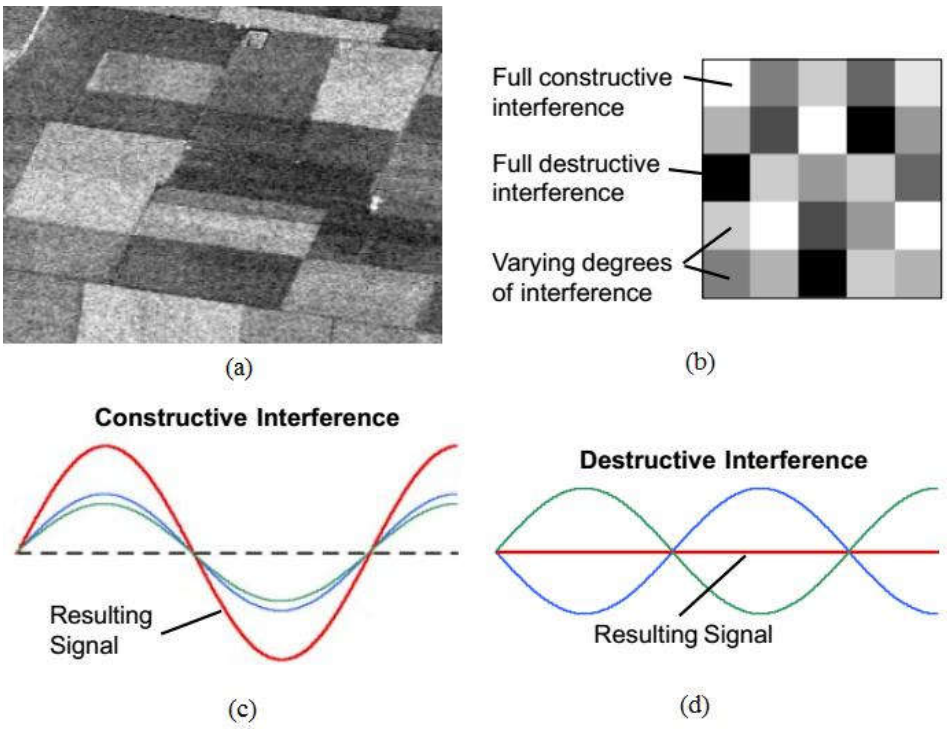

Figure 1.11 Plotting bright and dark point of the speckled image

Speckle is the interference or fading pattern. In a fully developed speckled image, the bright points show where the interference is constructive and the dark points show where the interference is destructive as shown in Figure 1.10(a) and (b). The constructive and destructive interferences are shown and plotted in Figure 1.11(a)-(d).

1.9 SAR Image Dataset

The proposed methods discussed in the thesis are experimented on several real SAR images. The experimental result of the proposed methods on real SAR dataset is shown in the Figure 1.12. The real SAR data is taken from the open public database. The SAR image is shown in Figure 1.12(a) is Ka-band image of a variety of military vehicles in the desert near Albuquerque, NM, taken from the Sandia National Laboratories, Airborne ISR, available at http://www.sandia.gov/RADAR/imagery/ [11]. The SAR image is shown in Figure 1.12(b) is Space Radar Image of Kilauea, Hawaii - Interferometry 1, taken from the database of Jet propulsion laboratory, California Institute of Technology, available at https://photojournal.jpl.nasa.gov/catalog/PIA01763. The SAR image is shown in Figure 1.12(c) is the aerial photography of the cemetery of Cologne, Germany which is available at open public access database [70], [71]. The SAR images are shown in Figure 1.12 (d) and (e) are taken from the open public database available at http://eo.belspo.be/.

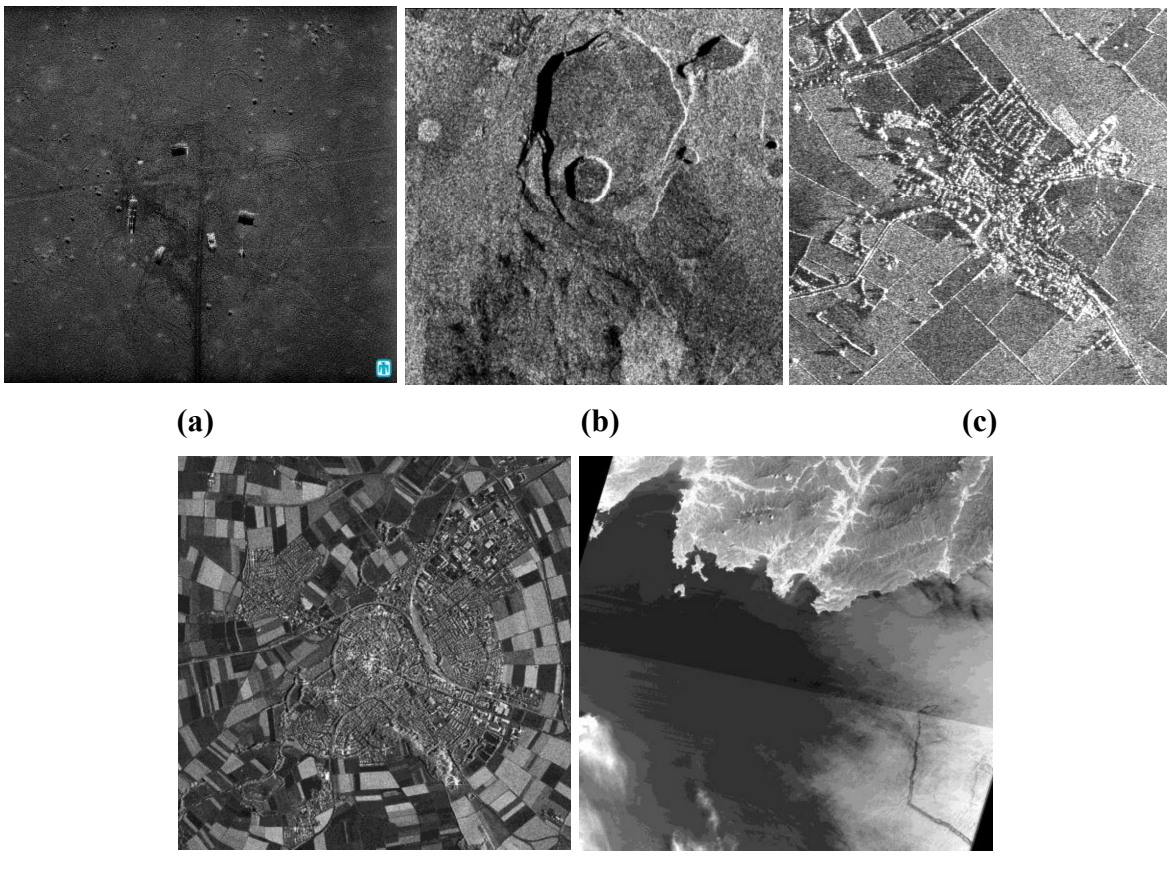

(a) **(b)** **(c)**

(d) **(e)**

Figure 1.12 SAR image dataset

1.10 Motivation

The SAR image despeckling is a rapidly advancing field. In the past decade, there are numerous research articles on SAR image despeckling. There are standard filters and various methodologies available for the despeckling of SAR image. These despeckling methodologies depend upon the nature of the speckled SAR image. The despeckling is performed on simulated as well as on the real speckled SAR image. The speckle distribution in simulated and real speckled SAR image is different. In simulated speckled SAR images, the speckle distribution is uniform. In the real speckled SAR images, the speckle scattering phenomenon is unknown. Therefore an effective and robust despeckling technique is required that can process both types of speckled images. Apart from despeckling, SAR image quality assessment is another issue, as the performance metrics of both categories of speckled SAR images are different. The quality of despeckled SAR image is assessed by various quantitative metrics and visual appearance of the despeckled SAR image.

The despeckling process is a bit difficult than normal denoising of digital images, as, in SAR image, the type of noise found is speckle noise that is multiplicative in nature. Before applying any despeckling process on the speckled SAR image, it is required to handle the multiplicative nature of speckle noise. Therefore homomorphic filtering is applied on speckled SAR images that implement log and exponential transform for transforming the multiplicative nature of speckle noise into additive nature. The log and exponential function are the overhead operations that increase the time complexity of the method and also degrade the image up to a certain level. Therefore it is required to preserve the fine details of the image. The major challenge during the despeckling process is the preservation of the fine details like edges and corners in the image, smoothness in the homogeneous areas and preservation of texture in the heterogeneous areas in the SAR image. Since the SAR images are low contrast images, so information preservation is a bit difficult than in normal optical images. The following specified issues are main priorities in the despeckling process:

- No artifacts generation during the despeckling process.
- The edges and image boundaries should be well preserved. Special care is needed to avoid over smoothing and over sharpening.
- Visibility of low contrast objects should be maintained.
- Texture preservation.
- Smoothness in the homogeneous regions of the SAR image.

- Preservation of non-homogeneous regions of the SAR image.

1.11 Problem Statement and Objectives

The major goal behind the thesis is to estimate and obtain a despeckled SAR image from the distorted or speckled SAR image while preserving the significant details of image such as texture, edges, structures, and corners. The developed despeckling method is experimented on simulated and real speckled SAR images. Since there are many despeckling methods developed in the past years but still there is a lot of scope for progressive enhancement. The research work is performed using Bayesian and Non-Bayesian methods in the transform domain. The research is grounded on wavelet transform.

The first objective of research work is to develop a new homomorphic and method noise thresholding based despeckling of SAR image using anisotropic diffusion. The preservation of edges is a critical task. Anisotropic diffusion is implemented to handle this issue. A homomorphic despeckling method is proposed using anisotropic diffusion in db2 based 2D-Discrete Wavelet Transform (DWT). The approximate part of the image is handled by the linear and non-linear filters in order to eliminate blurring. The method noise thresholding is applied to restore the unfiltered components of the despeckled SAR image. The proposed method is applied and tested on correlated speckle noise as well as uncorrelated speckle noise on the real dataset of SAR images.

The second objective of the work is to develop an improved despeckling method for simulated and real speckled SAR images using the hybrid combination of directional smoothing filter (DSF) and method noise thresholding. The preservation of fine details during the despeckling is the major task. The DSF is an edge-preserving filter. The approximate component is directed to DSF followed by method noise thresholding and detailed components are directed to wavelet thresholding followed by method noise thresholding. The research justifies the efficient use of method noise and explains how its intelligent use can enhance the despeckling result of the method. The proposed algorithm works on db2 based 2D-DWT using wavelet thresholding. The method is designed to despeckle the simulated and real speckled SAR images.

The third objective is to develop a SAR image despeckling technique using a local correlation based fusion of high-frequency coefficients in DWT using method noise thresholding. The

decomposition level is set by analyzing the texture feature of the input image at each level by entropy metric. This method of selecting the decomposition level preserves the maximum information possible. The main idea behind the proposed work lies in the selection of decomposition level in 2D-DWT based on entropy parameter for maximum information retrieval and fusion strategy for enhanced wavelet coefficients. On decomposition, the low-frequency coefficient is not processed and the high-frequency coefficients are thresholded by two distinct shrinkage rules in parallel. Bayesian and Bivariate shrinkage methods are used to threshold the high-frequency coefficients. After performing two different thresholding methods in parallel on detailed component, the enhanced high-frequency coefficients of these two thresholding methods are fused using local correlation based strategy. The threshold value is calculated using correlation strategy, and then the correlation coefficients are compared with the threshold value for the fusion purpose. Based on the strategy defined the average and maximum operation are performed for the fusion of high-frequency coefficients.

The despeckling results are analysed by evaluating the performance of the proposed method by metrics like Signal to Noise Ratio (SNR), Peak Signal to Noise Ratio (PSNR), Structural Similarity Index Measure (SSIM), Universal Image Quality Index (UIQI), Equivalent Numbers of Looks (ENL), Noise Variance (NV), Coefficient of Variation (CV) and Mean-squared Error (MSE). It also statistically analyses the effects of speckle noise on SAR images.

1.12 Contribution to Work

The research work is entirely based on despeckling the SAR images using method noise thresholding and image fusion in wavelet transform. The concept of RADAR and its types i.e. RAR and SAR with its merits and demerits are discussed. Various applications of SAR are discussed. The entire process of SAR image creation is discussed with the clear reason for the presence of bright and dark points in the SAR images. All the problems related to SAR images are discussed in detail and explaining their effect on the SAR images with their major sources. A specific noise problem in the SAR image i.e. speckle noise is targeted and all the perspectives related to the speckle noise in the SAR images is explained. The pioneer research work i.e. traditional and non-traditional methods of despeckling are discussed in the chapter 2 right from beginning to the current period. The strength and limitation of each work are discussed in brief.

The preliminaries of the research work including the theories related to the proposed methodology are discussed. It analyses the effect of speckle noise over SAR images at different noise variance level. Further, homomorphic filtering needed for nature transformation of speckle noise from multiplicative to additive is discussed. It discusses the general model of wavelet-based SAR image despeckling. The DWT and CWT are discussed in detail with their merits and demerits in respect of SAR image despeckling. The concept of method noise is applied and experimented on the various standard SAR image despeckling techniques. The advantage of using method noise in despeckling is discussed. The dual nature of MSE metric used for performance evaluation is verified in with and without reference indexes. Various quantitative metrics used for performance evaluation are discussed in two cases i.e. with and without-reference indexes.

The new speckle reduction methods for both simulated and real speckled SAR images are proposed. The proposed methods are based on various Bayesian and non-Bayesian method in transform domain using method noise thresholding and fusion concept in wavelet transform. The first proposed method i.e. HMN-AD is homomorphic and method noise thresholding based despeckling of SAR image using anisotropic diffusion and is successfully experimented on simulated and real speckled SAR images. It efficiently preserves the fine details and smoothness in the image and removes the blurriness. The second proposed despeckling algorithm i.e. HMN-DSF is based on the hybrid combination of directed smoothing filter and method noise thresholding using wavelet transform. It is also successfully experimented on simulated and real speckled SAR images. It is an edge-preserving technique. The third proposed despeckling method i.e. HMN-CF is a SAR image despeckling technique using a local correlation based fusion of high-frequency coefficients using DWT. It displays the best despeckling results in terms of visual appearance and quantitative measure.

The application of method noise in SAR image despeckling is new and has vast scope in this area. The concept of fusion in SAR image despeckling is also new and enhances the performance than normal despeckling method but is comparatively costly. The despeckling results of all proposed methods are shown in visual, graphical and tabular form. The HMN-CF has the highest execution time than the other two but its despeckling results are better than them. The proposed methods are validated by hypothesis testing using paired T-test by analyzing the quantitative values before and after despeckling of SAR images.

1.13 Thesis Organization

The thesis is comprised of six chapters including an introduction, literature survey, preliminaries, proposed methodology, experimental results with discussion and conclusion.

Chapter 1 discussed the background of the RADAR including its types i.e. RAR and SAR, types of SAR, its applications, SAR image creation, the presence of dark and bright points in the SAR image, problems in the SAR, speckle noise. It also discusses the motivation, problem statement, objectives and significance of the work.

Chapter 2 discusses the major literature work related to SAR image despeckling. It reviews all the standard "state of art" filters and pioneer conventional and non-conventional works in SAR image despeckling. The merits and demerits are discussed with the brief description.

Chapter 3 discusses the various wavelet transform used in SAR image despeckling like DWT with their merits and demerits. It discusses the few linear and non-linear filters used in the proposed methodology. The importance of homomorphic filtering over non-homomorphic filtering is also discussed. It briefly discusses various performance measures used in the SAR image despeckling in two different cases: with and without reference indexes. The concept of method noise is discussed. The effect of speckle noise over SAR image at various noise variance levels is also discussed. The dual and diverse nature of MSE metric is further discussed in the chapter.

Chapter 4 discusses the proposed methodology. It explains the proposed method of SAR image despeckling using framework and step-by-step procedure.

Chapter 5 shows the results of the proposed method. The despeckling result of various traditional and non-traditional methods is compared with the proposed method. The performance of the proposed method is analyzed using various performance metrics like PSNR, MSE, CV, ENL etc. It also analyses the data before and after the despeckling process and then validates the proposed methods 1, 2 and 3 by hypothesis testing using paired T-test.

Chapter 6 concludes the work with a major contribution. It also proposes the future scope of the work.

1.14 Conclusion

The chapter briefly introduces the basic theory of Radar and its types. It also introduces the SAR and its main types. Various applications related to SAR imaging are discussed. The major problem found in the SAR image is targeted in this chapter i.e. speckle noise. Speckle noise is multiplicative in nature. Its effects on the SAR image are more adverse than additive noises. This is one of the most challenging tasks in satellite imagery. Reducing speckle noise from SAR images is the main problem statement of this thesis while preserving the fine details of the SAR image i.e. edges, lines, texture and maintaining the smoothness in the homogeneous areas. All the contributions of this thesis are also discussed.

2. LITERATURE SURVEY

2.1 Background

A mass of despeckling filters, methods, and techniques can be acquired by linking the dissimilar domains of estimation (spatial, homomorphic, wavelet, and homomorphic-wavelet), A non-comprehensive evaluation and classification of approaches are presented in this chapter. The major literature related to Bayesian and non-Bayesian methods are discussed in this section in the chronological order of the year. Most of the traditional and non-traditional works are discussed in this section. The merits and demerits of the work are also mentioned in their discussion.

2.2 Categorization of SAR Image Despeckling Methods

A lot of despeckling techniques can be derived by merging the different domains like spatial and transform domain in Bayesian approach and non-Bayesian approach. This section classifies the speckle reduction methods in SAR images in various domains as shown in Figure 2.1. The despeckling methods are divided into two categories: Bayesian and non-Bayesian methods. The Bayesian method is further researched in spatial and transform domain. The initial research on SAR image despeckling is performed in the spatial domain and the results were acquired by assuming on the statistical properties of reflectivity and speckle. The output results in this domain are satisfactory.

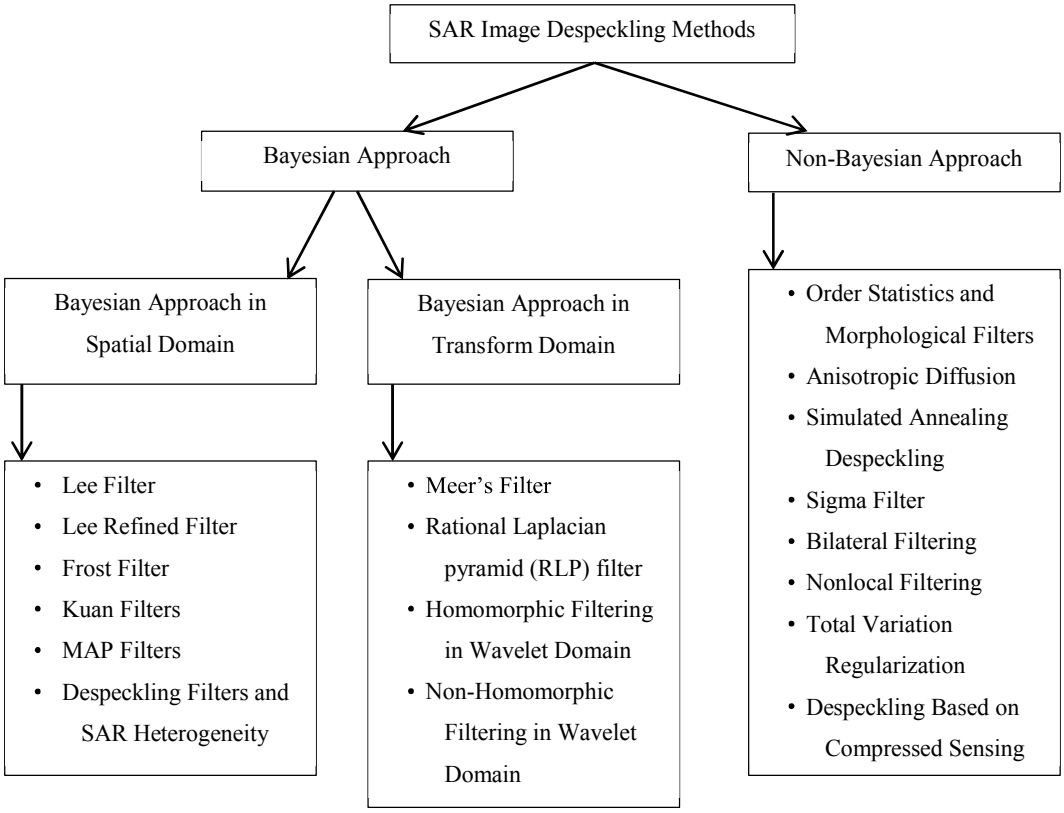

Figure 2.1 Classification of SAR image despeckling methods

2.3 Major Related Work

Lee JS [21] in 1980 used the neighborhood intensity values in the kernel. All the pixels are processed separately. During the movement of kernel, the local statistics of the pixels within the kernel are taken into consideration. Minimum Mean Square Error estimator (MMSE) calculates the weight function. This filter efficiently eliminates the speckle noise but the fine details are distorted in the image. This originally first paper [21] contains the solution for both additive noise and multiplicative speckle noise. [21] is reportedly the first ever model-based despeckling filtering method. Later the solution was systematically established in [22] and revised in [23] incorporated with the sigma filter. The Lee filter has a drawback of losing edge details as they left noisy after despeckling.

The Lee refined filter [24] in 1981 was intended to remove the demerit of remaining noisy edge boundaries left by Lee filter. In order to improve this filtering methodology, as 7×7 sliding window is moved over a SAR image and edge is detected, then the system practices the local gradient to evaluate its orientation. At maximum 8 edge-directed non-square masks

are allowed. The local mean and local variance is evaluated and implemented within the local 7 × 7 mask that better fits the edge orientation. If no edge is detected, the estimates are computed on the whole 7 × 7 window. The major demerit of this filter is it only works using the fixed mask size 7 × 7.

The Frost filter [25] in 1982 is an exponentially weighted averaging filter and is adaptive in nature. An optimal MMSE filter is used for smoothing images. The speckle noise is reduced by this filter and fine details are preserved in the image. Its major demerit is blurriness in the output despeckled images. An ideal framework for the SAR imaging process is derived in [25] and smoothening is shown. The SAR imaging framework demonstrates that the SAR image is degraded by multiplicative speckle noise. The framework leads to the smoothing radar images using optimum (minimum MSE) filter. The local block processing is applied here inside the homogeneous areas of the SAR image which preserves the edge and texture information and provides the minimum MSE value inside this region. This filter shows better computationally complexity and performance of this adaptive filter is qualitatively and quantitatively compared with several traditional filters using real and speckle added SAR images. With the advancement of time, there is no much advancement or development in the Frost filter either by researchers or others, except only some heterogeneity adjustment were made to all spatial Bayesian filters [26] by Kuan in 1985.

Kuan [26] in 1985 proposed a method based on the advancement to Lee's algorithm. It is an adaptive noise smoothing filter. It is adapted to local changes in image statistics based on a non-stationary mean, non-stationary variance image model. This filter can deal with various noises which depend on signal characteristics. This filter is capable of smoothing the speckled SAR image whose speckle distribution and image statistics is unknown. Film-grain and Poisson signal-dependent restoration problems are also considered as examples. Also, prior knowledge about the original image is also not required. The demerit of Kuan filter is over smoothing of edges and textures and the computational complexity of the algorithm is also very high.

A. Lopes [33] in 1990 analyzed the best-renowned filters. It is done by analyzing the experiments related to the local coefficient of variation of the despeckled SAR image, which defines the heterogeneous region properties of the observed SAR image. Some applied benchmarks are then bringing together to it to adapt the filters in order to make them more well-organized and proficient. Later the filters are verified on a speckle added original SAR

image and real speckled SAR image. As it is believed, the new fresh innovative filters perform superior, i.e., it average and smooth the uniform regions better and maintains texture and edges information, linear features, and point target responses efficiently at the same time.

P. Perona and J. Malik [45] in 1990 introduced a concept of anisotropic diffusion and proposed a new description of scale-space, and a category of procedures used to understand a diffusion method is familiarized. This technique is widespread in image processing. The main motive of this technique was to reduce the image noise and preserving of the fine details of the image especially edges, lines and other details which are necessary for the understanding of the image. Y. Yu and S. T. Acton [60] in 2002 smartly fitted the concept of anisotropic diffusion [45] in the reducing the speckle noise and applied it on the coherent images. This research shows better performance in terms of mean preservation, speckle reduction, and edge localization. The performance is better than traditional methods and conventional anisotropic diffusion method. Y. Yu and S. T. Acton [141] in 2004 introduced a prominent application for coastline detection using the despeckling based on anisotropic diffusion.

The model of MAP filters in the spatial domain is the C-MAP filter, introduced in [27] in 1990 and exhaustively analyzed in [28] in 1993. This model supposes that the radar reflectivity and the speckle noise both follow Gamma distribution and solves the MAP equation. It is intended to reduce and eliminate the speckle noise while retaining edges, texture, shape features and homogeneous and heterogeneous region in the image. The dissimilar sizes of the filter affect the quality of processed SAR images. If the filter size is very small, then the speckle filtering procedure is not effective. If the filter size is very large, then the information of the image gets lost in the filtering method. A filter of size 7 × 7 gives the best trade-off.

Donoho, D.L. and I.M. Johnstone [77] in 1994 introduced a technique to recover a function of unknown smoothness from noisy data. The Sure Shrink technique was introduced that eliminates the noise by performing the operation of thresholding on empirical wavelet coefficients. The thresholding is adaptive: a threshold level is allocated to each dyadic resolution level by the principle of minimizing the Stein Unbiased Estimate of Risk (Sure) for threshold estimates.

Meer's filter [60] in 1994 considers a native neighborhood organized by three concentric sliding masks, 3 × 3, 5 × 5, and 7 × 7. A uniformity index is specified by C_g, calculated over each of the masks. The spatial average on the biggest mask satisfying a uniformity criterion,

explained by thresholding its C_g, is specified as output. If this type of mask is not present, then Kuan's LLMMSE estimate on the innermost 3 × 3 mask is allocated to the center pixel. This filter is efficient in restoring and preserving point objects, linear features, and edges. It has the meritorious capability of shrinking its mask size. The performance of this filter is better on point objects and linear features than Lee's refined filter which, still, is better on linear edges.

H. Guo, J. E. Odegard, M. Lang, R. A. Gopinath, I. W. Selesnick, and C. S. Burrus [75] in 1994 introduced a novel despeckling method based on wavelet thresholding of the log-transformed speckled images. The computational cost of the method is low and it reduces the speckle noise while preserving the fine details image. Both soft and hard thresholding methods are considered.

D.L. Donoho [104] in 1995 proposed the method for reconstructing an unknown function f from noisy data by giving the classical hard and soft thresholding method. The work presented in the [104] is one of the pioneers works in the field of image denoising. The reconstruction process is stated in the wavelet domain by translating all the experimental wavelet coefficients.

Gagnon [34] in 1997 proposed a wavelet-based despeckling method grounded on Symmetric Daubechies. The speckled wavelet coefficients are modified by the shrinkage rule and restores the filtered image from it. The concept of elliptical soft thresholding method is used. The speckled image is directed to log transform followed by N level transform and then its covariance and mean is evaluated. Then inverse wavelet transform and exponential transformation are performed. The method reduces the speckle noise efficiently, but the computational load is increased.

B. Aiazzi [42] in 1998 applied an adaptive smoothing filter to the different resolutions of the Laplacian pyramid of a speckled SAR image. For real speckled SAR images, each layer is regarded by Signal to Noise Ratio (SNR) that rises as the resolution gets reduced. The hypothetical based theoretical framework is established for SAR image-dependent speckle noise models. A rational Laplacian pyramid is engaged to deal with multiplicative speckle noise. The experimental results are shown on gray-level SAR images degraded by real and simulated noise. Later improved by B. Aiazzi [43] in 1998, here ratio Laplacian pyramid (RLP) is presented to match the SAR image-dependent nature of speckle noise. Local statistics filtering is applied to the different spatial resolutions of the RLP of a speckled

image. In addition, the estimation of the local statistics driving the filter is more accurate thanks to the multiresolution framework. This filter is aimed at speckle reduction while smoothing the homogeneous regions and preserving point targets, edges, and linear features. A compromise, however, should be arranged on textured areas. In this work, A complete procedure is set up, and a general formulation, in which the variance of speckle is theoretically derived at each resolution, is developed.

E. Hervet [125] in 1998 presented a detailed investigational assessment of representative filters from both groups i.e. spatially adaptive filters and wavelet methods. Here the spatially adaptive statistical filters produce improved speckle noise reduction and preservation of details than wavelet-based methods. Bu the wavelet-based methods have certain benefits related to statistical filters which are not spatially adaptive.

The bilateral filter, originally familiarized by C. Tomasi and R. Manduchi [144] in 1998 for grayscale images, which is extended in recent times in the field of despeckling of SAR images by W. G. Zhang, Q. Zhang, and C. S. Yang [145] in 2011. A bilateral filter is a non-linear, smoothing, fine detail (edge, line and texture preservation) preservation method, which reduces noise for degraded images. It substitutes the intensity of each and every pixel with a weighted average of intensity values from nearby pixels. The adaptive version of bilateral filter appropriate for despeckling of SAR images is proposed by the G.-T. Li, C.-L. Wang, P.- P. Huang, and W.-D. Yu [56] in 2013, the spatial weighting is a Gaussian function, whose duration rest on the local coefficient of variation, equivalent to the enhanced Frost filter.

J. R. Sveinsson and J. A. Benediktsson [126] in 2003 presented a SAR image despeckling method based on two wavelet transformations. First, a DWT grounded on oversampled filter banks is used. This oversampled DWT is called a double-density DWT (DD-DWT). Second, a DWT based on two dual real wavelet trees is applied. The despeckling technique offered demonstrates the abundant potential for speckle removal and, later, can deliver decent detection performance for SAR-based recognition.

S. Solbo and T. Eltoft [127] in 2004 introduced the homomorphic wavelet maximum a posteriori filter and a wavelet-based statistical speckle filter comparable to the renowned /spl Gamma/-MAP filter. The log transform is applied to make the speckle noise additive in nature and statistically free of the radar cross-section. Additional, it is proposed to practice the normal inverse Gaussian distribution as a statistical model for the wavelet coefficients of

both the reflectance image and the speckled image. The speckle noise eliminated by the homomorphic /spl Gamma/-WMAP filter has information nearer to the theoretic model than the speckle contribution removed with the other filters. The wavelet despeckling method based on Bayesian shrinkage preserves the edge details is proposed by Dai M [35]. The speckle-free wavelet coefficients are projected from a Bayesian wavelet shrinkage factor. Edge details are obtained using an improved ratio edge detector. This acquired information is later used in the despeckling procedure to retain edges.

M. Mastriani, A. E. Giraldez [66] in 2004 introduced an enhanced directional smoothing (EDS) algorithm for edge-preserving filtering of SAR images. The EDS eliminates speckle noise from SAR images without distorting or disturbing edges. This new filtering method is proved effective by associating it to well-known speckle noise deduction methods on SAR images. The EDS algorithm delivers greater performance in assessment to the classical filters in terms of smoothing homogeneous areas and preserving the fine details i.e. edges and features. The efficiency of the method inspires the likelihood of using the method in a number of ultrasound and radar applications. Besides, the method is computationally effective and can considerably reduce the speckle noise while preserving the resolution of the original image.

M. I. H. Bhuiyan, M. O. Ahmad, and M. N. S. Swam [128] in 2005 introduced a new homomorphic Bayesian wavelet-based minimum mean absolute error filter for despeckling of SAR images. The logarithmically transformed reflectance image's wavelet coefficients and the speckled SAR image are modeled using a Cauchy prior and an additive white Gaussian noise distribution, respectively. These prototypes are later used to develop a Bayesian minimum mean absolute error estimator. The experimental results are tested on the classic speckle-free image degraded with synthetic speckle noise and a real speckled SAR image, and the consequences demonstrates that this method has a performance that is higher to that of the other prevailing approaches in terms of the PSNR, smoothness in the homogeneous regions and the visual appearances of the despeckled image. Later this work was enhanced by M. I. H. Bhuiyan, M. O. Ahmad, and M. N. S. Swam in the year 2007 by introducing a new spatially adaptive wavelet-based Bayesian method for despeckling of the SAR images. The wavelet coefficients of the logarithmically transformed reflectance and speckle noise are modeled using the zero-location Cauchy and zero-mean Gaussian distributions, respectively.

A. Buades, B. Coll, J.-M. Morel [78] in 2005 proposed a new measure, 'method noise', to estimate and relate the performance of digital image denoising approaches. In this paper, firstly the method noise is computed and analyzed to various denoising procedures, namely the local smoothing filters. Secondly, a new nonlocal means (NL-means) algorithm is proposed which is grounded on nonlocal averaging of all pixels in the image. Finally, the NL-means algorithm and the local smoothing filters are experimentally compared.

Achim [29] in 2006 suggested an adaptive MAP estimator with a heavy-tailed Rayleigh signal model. The multiplicative nature of speckle noise is transformed into additive by implementing the log transform. Here the real and imaginary part is presumed to be described by the alpha-stable family of distribution. There is another statistical theory that depends on the Mellin transform, is used to estimate the model parameters from noisy interpretations.

Sparse models are at the foundation of compressed sensing suggested by D. L. Donoho [153] in 2006, which is the depiction of signals with a number of samples at a sub-Nyquist rate. A new signal depiction model has lately become very prevalent and has fascinated the attention of scholars who are functioning in the arena of image restoration which is distorted by additive noise as well as in several other areas. Recently, some despeckling methods based on the compressed sensing paradigm and sparse representations have appeared [154]–[156].

J.-S. Lee, J.-H. Wen, T. L. Ainsworth, K.-S. Chen, and A. J. Chen [142] in 2009 extended and advance the Lee sigma filter [143] by eliminating its drawbacks i.e. blurring effect, disappointing solid reflected targets, and biased estimation. The bias difficulty is resolved by redefining the sigma range based on the probability density function of speckle noise. To resolve the difficulties of blurring effects and disappointing solid reflected scatterers, a target signature preservation method is established.

Wu [37] in 2010 proposed a method that performs an amalgamation of wavelet and curvelet soft thresholding method and then calculates the variance between the obtained two images. This method is proficient enough to suppress the speckle noise efficiently and preserves the fine details of the image. The major drawback is it produces blurriness. In the same year, J. Jennifer Ranjani and S. J. Thiruvengadam [32] proposed a DTCWT based despeckling of SAR image that considers the major requirements of the wavelet coefficients across various scales. The DTCWT has the benefit of better directional selectivity, approximate shift invariance, and perfect reconstruction over DWT. The wavelet coefficients of DTCWT in each and every sub-band are prototyped with a bivariate Cauchy PDF which takes into

account the statistical dependence among the wavelet coefficients. The 2-D Mellin transform derives the dispersion parameter of the bivariate Cauchy prior to the noisy observations. This method is quicker and operative when equated with other earlier methods of experimental integration.

V.R.Vijaykumar [31] in 2012 proposed a dual-tree complex wavelet transform (DTCWT) based despeckling algorithm for SAR images that work for the interscale and intrascale requirements of DTCWT. A multivariate Cauchy PDF is in a job to implement the interscale and intrascale dependence of the wavelet coefficients in each sub-band. This method uses mean and directional median values of the neighborhood mask for estimating the interscale and intrascale dependency vector of wavelet coefficients. The 2-D Mellin transform derives the dispersion parameter of the multivariate Cauchy prior. In the same year, R. Tao, H. Wan, and Y. Wang [130] introduced a novel Contourlet-based regularization technique to eliminate speckle noise without introducing artifacts. The elimination of speckle noise is significant and structures of the scene are well preserved. The experimental results prove such dominance on real SAR images. In 2012, F. Argenti, T. Bianchi, A. Lapini, and L. Alparone [131] introduced a SAR image despeckling technique using undecimated wavelet transform and the MAP criterion. The MAP solution is grounded on the hypothesis that wavelet coefficients have an identified scattering. The computational cost is reduced which was the major drawback of using the GG distribution. In 2012, H. Chen, Y. Zhang, H. Wang, and C. Ding [132] introduced a stationary-wavelet-based despeckling algorithm based on the two-sided generalized gamma distribution model. The model has low computational cost and decent quantitative values. It preserves the structural details and also reduces the speckle noise effectively.

Sara Parrilli [73] in 2012 presented a despeckling method based on non-local filtering and wavelet shrinkage using probabilistic similarity measure. The results are with consistent PSNR values that show better texture preservation and speckle reduction. Also, the technique has the capacity of better smoothing in the homogeneous areas. The other effective non-local filtering based Bayesian framework is presented in the [138] which is tested on both the ultrasound [139] as well as SAR images [140]. This work presents the effectiveness of non-local mean filtering in the domain of despeckling.

T. Teuber and A. Lang [146] in 2012 proposed an original similarity quantity and nonlocal filters for images degraded by multiplicative noise. The measured filters are simplifications

of the nonlocal means filter of Buades [78], which is well recognized for eliminating additive Gaussian noise. At last, the restoration outcomes for coherent images degraded by multiplicative Gamma and Rayleigh noise are offered to validate the decent performance of these nonlocal filters. D. Gragnaniello, G. Poggi, and L. Verdoliva [147] in 2012 deliver some vision into the perspective of classification-based nonlocal filtering by executing simulation tests in a well-ordered atmosphere. Then suggests a novel kind of the SAR-BM3D despeckling method in which each and every pixel is first classified as uniform or not, and then filtered with class-adapted factors. While outcomes on real SAR images are still doubtful, there is previously some important improvement in particular areas that validate the attention towards this methodology.

Christy [38] in 2013 put forward an improvement to the principal Non-Local Means Filtering (NLMF) Method. A discontinuity adaptive Non-Local Means Filtering (DA-NLMF) is proposed that implements a discontinuity adaptive weighting function that preserves the edges and other fine details better than the basic Non-Local Means. This DA-NLMF is used as resourceful post-processing process along with Importance Sampling Unscented Kalman Filter (ISUKF) for SAR image despeckling. This combination of (ISUKF and DANLMF) provides efficient despeckling result. In the same year, Heng-Chao Li [89] proposed a new Bayesian multiscale technique for speckle reduction technique for SAR images in the non-homomorphic agenda. In order to handle multiplicative speckle noise, linear decomposition is used for speckle contribution. Later in SWT, a two-sided general Gamma distribution is familiarized as an earlier to handle the heavy-tailed nature of wavelet coefficients of the speckle-free reflectivity. The used shrinkage rule performs thresholding on the diagonal component of the image which causes the horizontal and vertical component to be unfiltered so there is a high scope for improvement in the denoising process.

Sethunadh and T. Thomas [90] in 2014 introduced a new adaptive SAR image despeckling procedure in the spatial domain by using statistical interscale dependency of the directionlet transform coefficients; the work is highly efficient in preserving the high textured region. Lei Zhu [91] in 2014 introduced a recognized detail-preserving anisotropic diffusion (IDPAD) for despeckling speckled SAR image that undergoes from reduced despeckling presentation mainly at the edges and serious blocking artifacts in uniform areas.

David de la Mata-Moya, Alvaro Diaz-Soria, Jaime Martin-de-Nicolas, Maria-Pilar Jarabo-Amores, Victor Manuel Pelaez [76] in 2014 introduced a SAR image despeckling technique

grounded on Empirical Mode Decomposition. The work calculates a new threshold value with a sliding mask to preserve the fine details i.e. edges and removing the speckle noise. The outcomes display an acceptable despeckling avoiding an over-smoothing in the whole image.

Bin Xu, Yi Cui, Zenghui Li, Bin Zuo, Jian Yang and Jianshe Song [74] in 2015 proposed despeckling method grounded on patch ordering and transform-domain filtering. The log transform with bias correction is implemented on SAR image to transform the nature of speckle from multiplicative to the additive. The proposed technique has very robust speckle reduction capability and execution time of the planned method is also suitable for applied applications of SAR image processing.

Yao Zhao, Jianguo Liu, Bingchen Zhang, Wen Hong and Yirong Wu [72] in 2015 proposed a dual-formulation-based Adaptive Total Variation (ATV) regularization method which is implemented to explain the Total Variation Regularization. The parameter adaptation of the Total Variation regularization is accomplished grounded on the noise level assessed via wavelets. The work presented shows a great advancement than the previous standard total variation method in terms of speckle reduction in the homogeneous areas and detail preservation in the heterogeneous areas, but still, sometimes the generation of blocky artifacts is found. Some of the variational based despeckling works are grounded on total variation regularization are discussed in [133]-[137].

Abdourrahmane Mahamane Atto [39] in 2016 presented a paper that provides statistical characteristics of wavelet operators when the thought model can be realized as the product of a deterministic piecewise regular function (signal) and a stationary random field (noise). This multiplicative observation model is analyzed in two standard frameworks, (1) direct wavelet transform of the model (2) log transform of the model prior to wavelet decomposition.

Diego Gragnaniello [40] in 2016 proposed a new approach to synthetic aperture radar (SAR) despeckling, based on the arrangement of multiple alternative estimates of the same data. They have given a dependable pixel-wise characterization of the image; one can take gain of this diversity by selecting the most suitable combination of estimators for each image region. Following this example, they improved a simple algorithm where only two state-of-the-art despeckling tools, characterized by complementary properties, are linearly joined.

2.4 Conclusion

The chapter critically analyses the published work on the SAR image despeckling. The literature is assessed, analyzed and compared theoretically. It is concluded that the Bayesian approaches in the transform domain and non-Bayesian approaches perform better than the Bayesian approaches in the spatial domain during the process of despeckling. The non-Bayesian approaches are the efficient but complex approaches and the computational cost is also high. The Bayesian approaches in transform domain deliver the most optimal techniques in terms of details preservation, speckle reduction, and computational cost.

3. RELATED THEORIES

3.1 Background

The chapter discusses the methods and techniques that are related to the HMN-AD, HMN-DSF and HMN-CF i.e. DWT, homomorphic filtering using natural log and exponential operations, wavelet thresholding using Bayesian and Bivariate shrinkage rule, anisotropic diffusion, median filter, Wiener filter, method noise. The chapter also analyses the effect of speckle noise on the SAR images. Various quality assessment parameters required for the

despeckling method are also discussed for both with and without reference indexes. The dual nature of MSE is also discussed in the chapter.

3.2 Wavelet Transform

The wavelet transform is related to the Fourier transform and much more similar to the windowed Fourier transform with a totally dissimilar merit utility. The principal difference between Fourier and wavelet transform is that the Fourier transform decomposes the image into the functions that are localized in Fourier space i.e. sines and cosines while the wavelet transform practices those functions which are confined to both the real and Fourier space. Generally, the wavelet transform can be expressed by Eq. (3.1).

$$F(a,b) = \int_{-\infty}^{\infty} f(x)\Psi^{*}_{(a,b)}(x)dx \quad \text{.....(3.1)}$$

here the * is the complex conjugate symbol, Ψ is the wavelet function, a and b are the input denoting scaling factor and time respectively. Wavelets are mostly used in image compression and denoising. Wavelet is a quickly decaying wave-like oscillation that has zero mean, unlike sinusoidal waves which extend to infinity. A wavelet survives for a finite period of time. The wavelet comes in different sizes and shapes. Some are Morlet, Daubechies, Coiflets, Bi-orthogonal, Haar, Mexican Hat, and Symlets. An availability of wide range of wavelet is the key strength of data analysis.

3.2.1 Concept of Wavelet Transform

A. Scaling

Scaling states to the procedure of stretching and shrinking the image or signal in time that can be stated using Eq. (3.2).

$$\Psi\left(\frac{t}{s}\right)s > 0 \quad \text{.....(3.2)}$$

here s denotes scaling factor. It is a positive value that resembles to how much a signal scaled in time. The scale factor is inversely proportional to frequency.

In wavelet, there is a reciprocal relationship between scale and frequency to the constant of proportionality (COP). This COP is called as the center frequency of the wavelet because, unlike the sine wave, the wavelet has a bandpass characteristic in the frequency domain. Mathematically the equivalent frequency is calculated by Eq. (3.3).

$$F_{eq} = \frac{C_f}{s\ \delta t} \quad \text{.....(3.3)}$$

here C_f denotes center frequency of the wavelet, s denotes wavelet scale, and δt denotes sampling interval. By scaling a wavelet by the factor by 2, it results in reducing the equivalent frequency by an octave is shown in Table 3.1.

Table 3.1 Relation between wavelet scale and equivalent frequency in the wavelet transform

Wavelet Scale	2	4	8	16
Equivalent Frequency(F_{eq})	$F_{eq}/2$	$F_{eq}/4$	$F_{eq}/8$	$F_{eq}/16$

A larger scale factor results to the stretched wavelet which corresponds to the lower frequency while small-scale factor results to the shrunk wavelet which corresponds to the higher frequency. Hence this helps in capturing the abrupt changes more efficiently. It is possible to construct different scales that inversely correspond to the equivalent frequency as mentioned earlier.

B. Shifting

Shifting a wavelet means delaying and advancing the onset of the wavelet along with the length of the signal.

$$\varnothing(t-k) \quad \text{.....(3.4)}$$

A shifted wavelet is represented using above notation means; the wavelet is moved and centered at k. The shifting and scaling process of the DWT is shown in Figure 3.1.

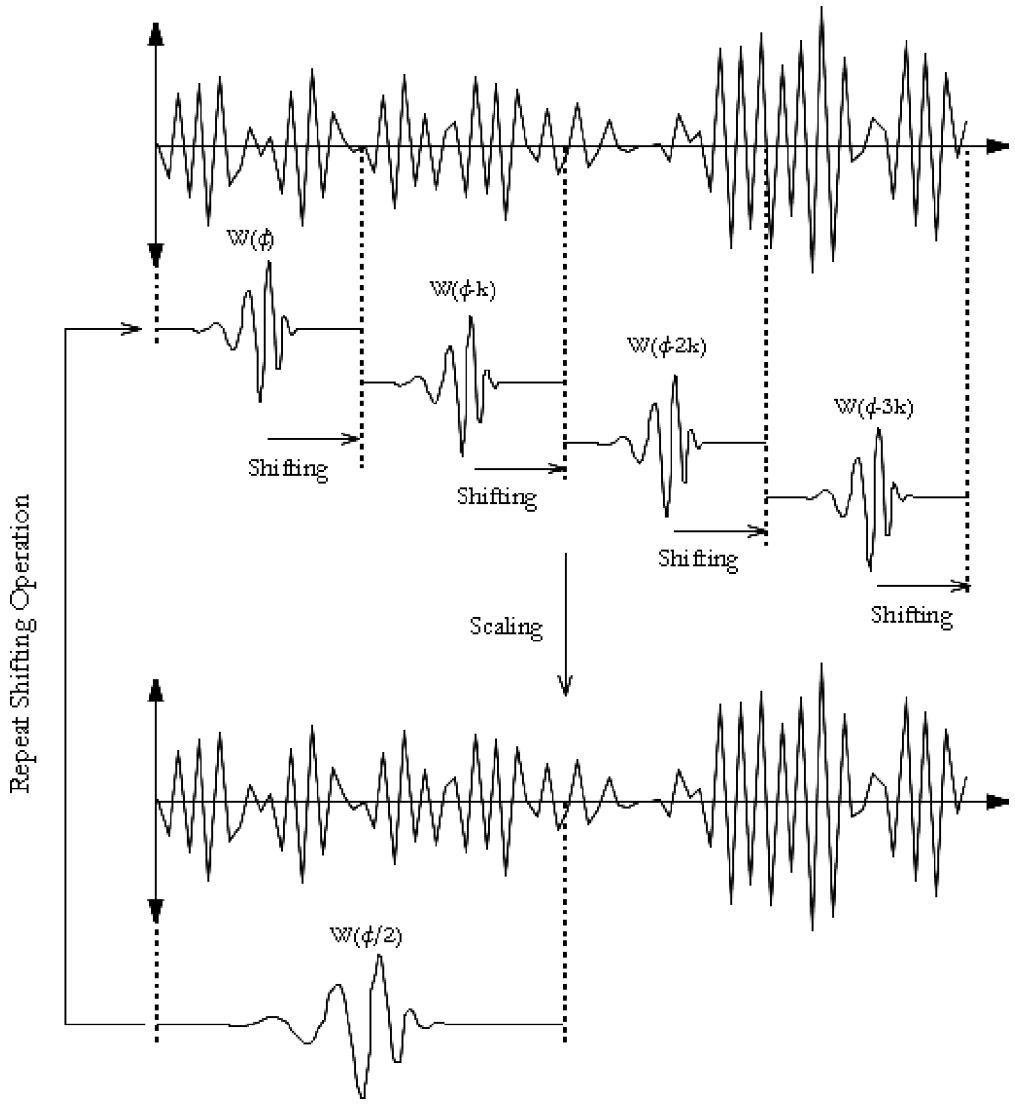

Figure 3.1 Scaling and Shifting process of DWT [105]

3.3 Types of Wavelet Transform

3.3.1. Discrete Wavelet Transform

Wavelets are mainly used in image compression and denoising. The DWT transforms the image from the spatial to the frequency domain [34], [47]. In the proposed methods, the 2D-DWT is applied to analyze the low and high-frequency component in the image. 2D-DWT corresponds to multi-resolution approximation expressions. The wavelet function is analyzed in Figure 3.2.

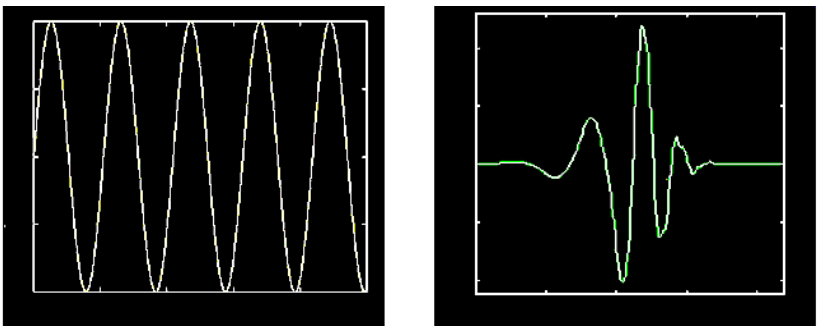

Figure 3.2 Comparison of sine wave and daubechies 5 wavelet [105]

In 1976 scientists Croiser, Esteban, and Galand established a technique to decompose the discrete-time signals that sited the foundation for DWT. Few other researchers named Crochiere, Weber, and Flanagan did the similar work of coding the speech signals in the same year. The title of their study is sub-band coding. In 1983, a technique associated to subband coding was explained by Burt and called that technique as pyramidal coding that is also acknowledged as multi-resolution analysis.

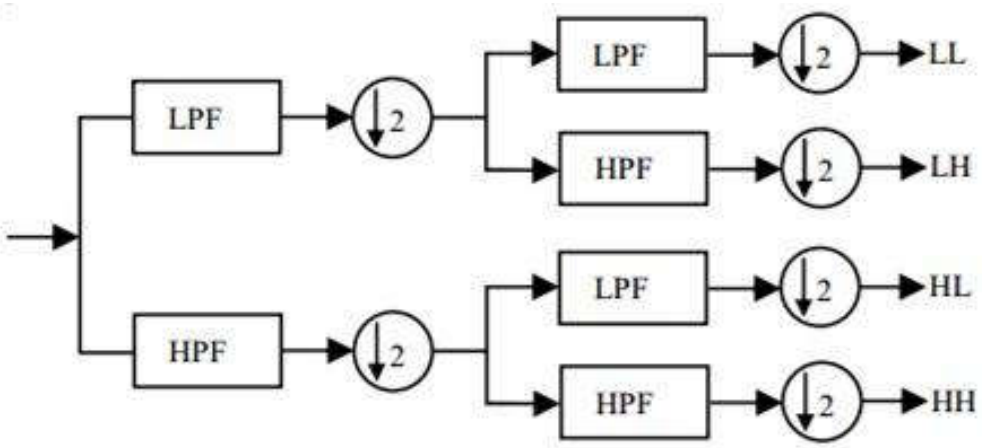

Figure 3.3 Wavelet decomposition by filter banks [106]

A low pass and high pass filter are selected in such a way the that they exactly halve the frequency range among themselves. This filter pair is known as analysis filter pair. The low pass filter is implemented at each row to obtain the low-frequency components [107]. The low pass filter is a half-band filter and output data comprise of frequencies in the first half of the original frequency range [129]. Now for the same row of data, high pass filter is implemented, and the high-frequency components can be parted similarly and located on the side of low pass components [107]. The method is implemented on all the rows. The DWT decomposition employed using filter bank is shown in Figure 3.3.

Next stage is to implement filtering at every column of the intermediary data. On applying 2D-DWT on the image at level one, it transforms the image into four subband i.e. LL (Approximate Image), HL (Horizontal Noisy Coefficients), LH (Vertical Noisy Coefficients), and HH (Diagonal Noisy Coefficients) [107]. In order to obtain the two-level decomposition, once again 2D-DWT is applied on the LL subband and it is further decomposed in the same way, thus generating additional sub-bands. This wavelet decomposition can be performed up to any level. Thus resultant is pyramidal decomposition as shown below in Figure 3.4 for single level decomposition and Figure 3.5 for two-level decomposition [107]. In Figure 3.4, the decomposed subbands are represented by X_n, where X denotes specific decomposed subband and n denotes the level of decomposition, for example LL_2 is aproximate component of the image at decomposition level 2.

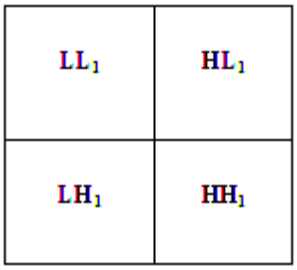

Figure 3.4 Single level decomposition

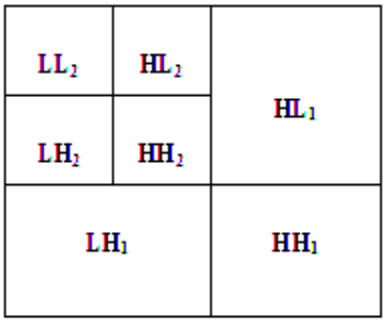

Figure 3.5 Two level decomposition

Same as the forward transformation to separate the image data into different classes, a reverse transformation is used to reunite the dissimilar classes of data into a restored image. A pair of high and low pass filter is in use here too. Such filter pair is identified as Synthesis Filter pair. This filtering process is just reverse as it is initiated from the highest level, implement the filter initially column wise and later row-wise, and this continues until this process reaches the first level. The DWT reconstruction employed using filter bank is shown in Figure 3.6.

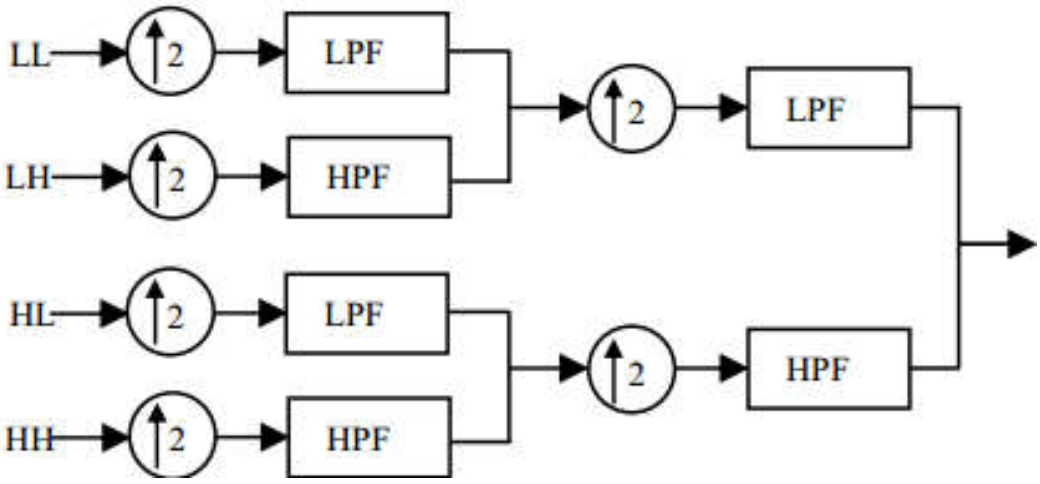

Figure 3.6 Wavelet reconstruction using filter banks [106]

The only drawback of 2D-DWT is that on applying DWT on the image, at every level it reduces the size of the image to half of the previous level size as shown in Figure 3.7. This causes loss of information.

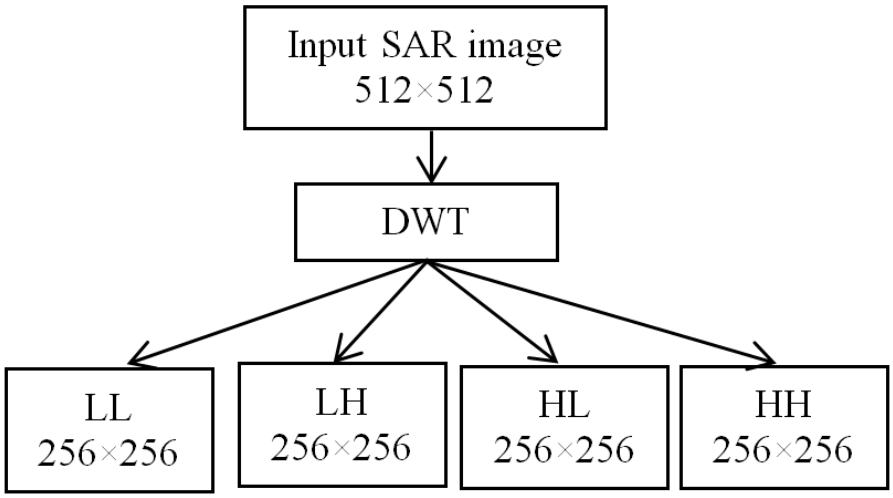

Figure 3.7 Frequency band decomposition using DWT

3.3.2 Continuous Wavelet Transform

Continuous wavelet transform (CoWT) is an execution of the wavelet transform using random scales and almost random wavelets. The wavelets here used in CoWT are not orthogonal and highly correlated data are obtained by this transform. This transform can also be used for the discrete time series, with the restriction that the least wavelet translations must be identical to the data sampling. This is at times called as the Discrete-Time Continuous

Wavelet Transform (DT-CoWT) and it is one of the most used methods of calculating CoWT in real-time and practical applications.

According to standards, CoWT works by using directly the characterization of the wavelet transform, i.e. here a convolution of the image with the scaled wavelet is calculated. For each and every scale, an array is obtained of the identical length A as the image has. By using B randomly selected scales we attain a field A×B that signifies the time-frequency plane directly. The procedure used for this calculation can be based on a direct convolution or on a convolution by means of multiplication in Fourier space (this is sometimes called Fast Wavelet Transform (FWT)).

The optimal selection of the wavelet that is used for time-frequency breakdown is the most significant thing. Through this optimal selection, we can guide the time and frequency resolution of the outcome. The chief features of wavelet transform can't be changed by this way (low frequencies have decent frequency and corrupt time resolution where high frequencies have a decent time and corrupt frequency resolution), but it can someway upturn the full frequency of full-time resolution. This is directly proportional to the width of the used wavelet in real and Fourier space. If the Morlet wavelet is used for instance (real part – damped cosine function), then high-frequency resolution can be expected as such a wavelet is exactly localized in frequencies. In opposing, using Derivative of Gaussian (DOG) wavelet will result in decent time localization, but poor frequency resolution.

3.4 Importance of DWT over other Wavelet Transforms

DWT is one of the mostly used wavelet transforms and it delivers an effective outcome in image denoising due to localization in both frequency and time domain and multi-resolution analysis. There are various forms of the wavelet transform, out of them, the complex wavelet transform (CWT), DWT and stationary wavelet transform (SWT) are the predominant wavelet transforms used in image denoising. CWT and SWT are the extended versions of DWT. The CWT is a complex-valued extension to the traditional DWT. It is a 2D wavelet transform that delivers multiresolution, sparse illustration, and useful description of the structure of an image [108]. The SWT [33] is a wavelet transform procedure aimed to improve the DWT by overcoming the lack of translation-invariance. The translation-invariance is accomplished by eliminating the downsamplers and upsamplers in the DWT and upsampling the filter coefficients by a factor of 2(j-1) in the jth level of the procedure [41]-

[43], [109]. Despite the existence of these extended versions, the DWT has the capability to outperform CWT and SWT. The results using DWT can be enhanced by incorporating the concept of method noise at detailed and approximate components.

The DWT holds the time and frequency information. DWT shows the more flexibility than other transforms. The DWT breaks the data into four components which makes the analysis of data easier. The DWT is less complex than SWT and CWT. The theory of DWT is far easy than SWT and CWT due to the vast availability of literature. The result interpretation of DWT results is easier than SWT and CWT. The implementation is also easier than SWT and CWT.

Even though the working of the CoWT by the computer system is facilitated by the discretized continuous wavelet transform but still it is not treated as a real discrete transform. In actuality, the wavelet series is just a experimented form of CoWT. In terms of image restoration, the information provided by it is very redundant. This redundancy causes wastage of resources and time. On the other hand, the computational cost of DWT is far less than CoWT as it offers adequate statistical data both for analysis and synthesis of the reference image.

The implementation of DWT is easier and efficient than CoWT. The main application of CoWT is filtering of time localized frequency components while that of DWT is image/ signal denoising and compression. The immediate time and frequency analysis of the signal is obtained by CoWT.

3.5 Homomorphic Filtering in Wavelet Transform

The homomorphic filtering is one of the most used techniques for multiplicative noise model. It uses natural log and exponential function for its operation. This method converts the multiplicative nature of speckle noise into additive nature. Later this nature transformation way helps in using the additive noise model for SAR image filtering. It is normally used for fixing and improving the non-homogeneous illumination in the SAR images. According to the illumination-reflectance model, the intensity value of the pixel is dependent on the light reflected by the point on the object and is equal to the product of the illumination of the scene and the reflectance of the objects in the scene, i.e.

$$X(a,b) = Y(a,b) \times Z(a,b) \quad \text{.....(3.5)}$$

where X is the image, Y is the illumination of the scene, and Z is the reflectance of the scene. Reflectance Z rises from the characteristics of the scene entities themselves, but illumination Y outcomes from the lighting surroundings at the time of image acquisition. To recompense the non-uniform illumination, the significant point is to eliminate the illumination module Y and preserve the reflectance module Z. If the illumination is considered as the noise signal (which is needed to be eliminated), this model is alike to the multiplicative noise model.

Illumination characteristically differs gradually across the image as related to reflectance which can change quite shortly at object edges. This dissimilarity is vital for sorting out the illumination module from the reflectance module [52]. In homomorphic filtering, the multiplicative modules are transformed into additive modules by applying the log domain using the formulas shown in Eq. 3.6.

$$\ln\left(X(a,b)\right) = \ln\left(Y(a,b)Z(a,b)\right)$$

$$\ln\left(X(a,b)\right) = \ln\left(Y(a,b)\right) + \left(Z(a,b)\right) \quad \text{.....(3.6)}$$

Then we use a high-pass filter in the log domain to remove the low-frequency illumination component while preserving the high-frequency reflectance component.

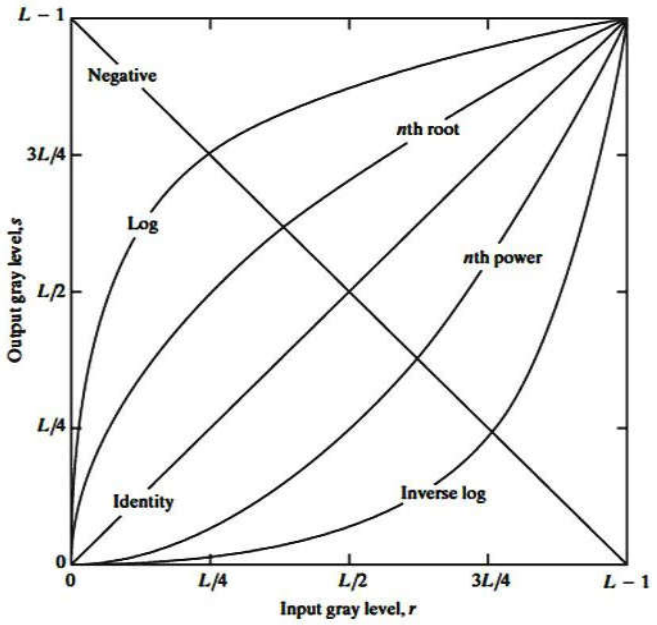

Figure 3.8 Gray-level transformation operations used for image enhancement [109]

The log transformation curvature is shown in Figure 3.8. The Eq. 3.7 shows the log transformation of the image.

$$s = c \times \log 1 + r \quad \text{.....(3.7)}$$

In the Eq. 3.7, c denotes a constant, and it is supposed that r ≥ 0. r is a input image's intensity value, and s is a output image's intensity value. The value i.e. 1 is taken into account in Eq. 3.7 in order to handle the situation when input image's intensity value is 0. In this case the log(0) becomes infinity. Therefore to make minimum value at least 1, the value 1 is added. The value of c in Eq. 3.7 adjusts the image enhancement as per needed by the researcher. The signal dependent and signal independent homomorphic models in respect of spatial domain are shown in Figure 3.9. The practical implementation of log and exponential operation on real SAR data is shown in the Figure 3.10.

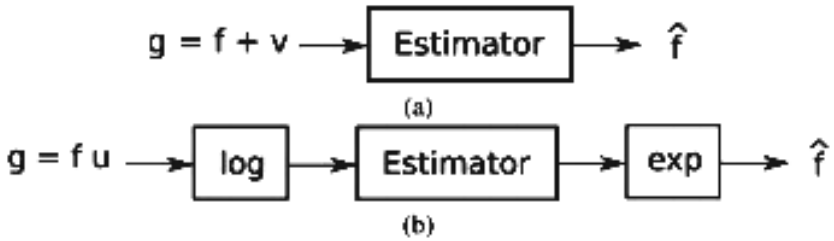

Figure 3.9 Additive models used in despeckling procedures [103]: (a) signal-dependent: spatial domain (b) signal-independent: spatial domain.

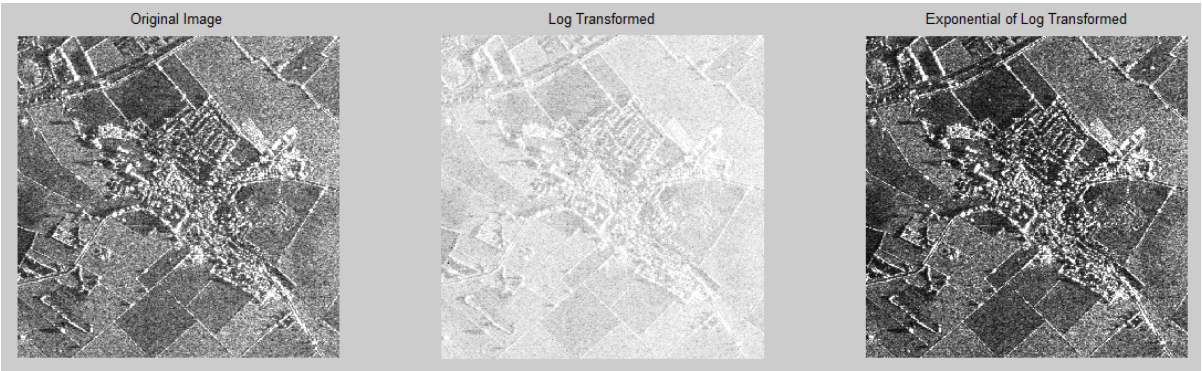

Figure 3.10 Applying log and exponential transform to the reference SAR image.

3.6 Despeckling SAR Images using Wavelet Transform

3.6.1 Analysis and Effect of Speckle-Noise on SAR Images

Noise plays a vital role in the field of image restoration. There are different kinds of noise that corrupt the image. Reducing noise from the satellite images is one of the major challenges. The kind of granular pattern present in the radar coherent image is called as the speckle noise [151]. The speckle noise is mainly found in the SAR image and ultrasound images. The speckle noise is a common phenomenon in all coherent imaging systems like a laser, acoustic and SAR imagery.

Speckle noise is an undesirable effect [150]. The source of this type of noise is caused due to random interference between the coherent returns issued from the so many scatterers present on an earth surface, on the scale of a wavelength of the incident radar wave. Thus reducing such noise from the image is turned out to be a most critical step [149]. In general, speckle noise is the grainy salt-and-pepper pattern present in radar imagery. Also speckle noise can be understood as a granular 'noise' that inherently exists in and degrades the quality of the medical ultrasound, SAR, active radar, and optical coherence tomography images. The effects of speckle noise are far adverse than any other kind of noise due to its multiplicative in nature. Due to which its denoising is more challenging task. This sub-section analyses the effects of speckle noise on SAR image at different noise variances i.e. σ = 5; 10; 15; 20; 25; 30; 35; 40; 45; 50 [150].

The Figure 3.11 depicts the SAR image at different noise variance levels ranging from (5-50)%. The quality degradation of the SAR image due to speckle noise is analyzed using the performance parameters such as PSNR and SSIM in the Table 3.2. This degradation is graphically analyzed in Figure 3.12 and 3.13 using PSNR and SSIM respectively.

Table 3.2 PSNR and SSIM values of SAR images at different noise variances i.e. σ = 5; 10; 15; 20; 25; 30; 35; 40; 45; 50

Noise variance (σ)	PSNR	SSIM
5	25.1471	0.6275
10	25.1620	0.6283
15	20.3862	0.3756
20	19.1516	0.3149
25	18.1897	0.2708

30	17.3828	0.2390
35	16.7366	0.2147
40	16.1876	0.1957
45	15.7469	0.1818
50	15.3763	0.1686

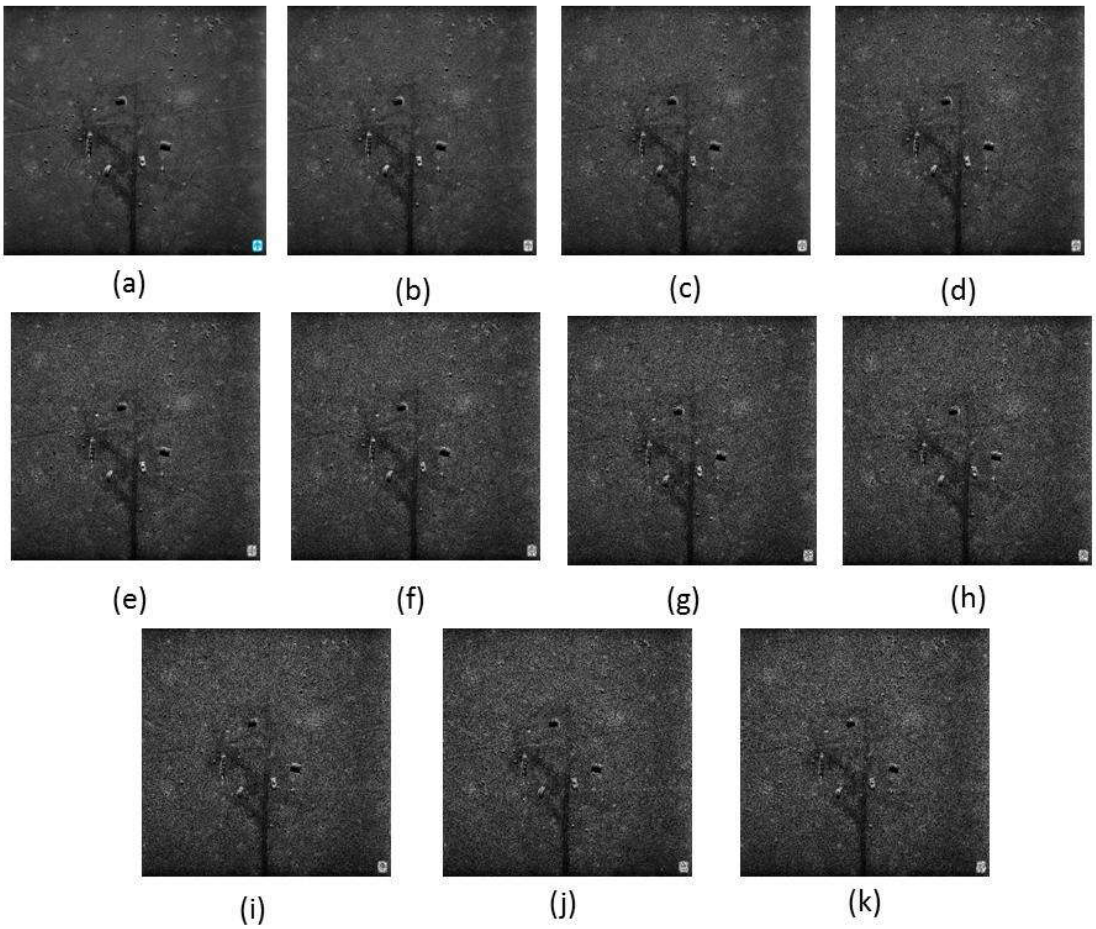

Figure 3.11 SAR images at different noise variances (a) Reference SAR image (b) σ = 5% (c) σ = 10% (d) σ = 15% (e) σ = 20% (f) σ = 25% (g) σ = 30% (h) σ = 35% (i) σ = 40% (j) σ = 45% (k) σ = 50%

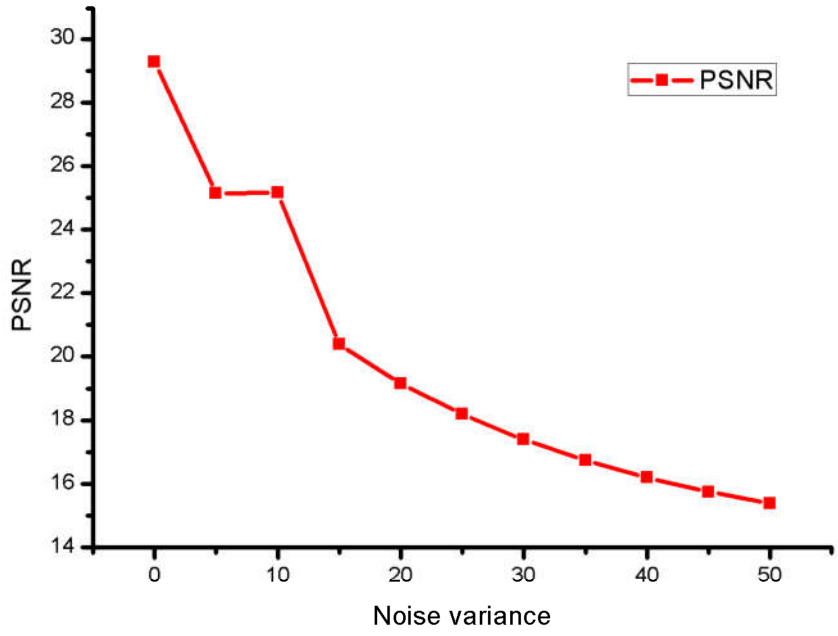

Figure 3.12 PSNR of speckled SAR image at different noise variances

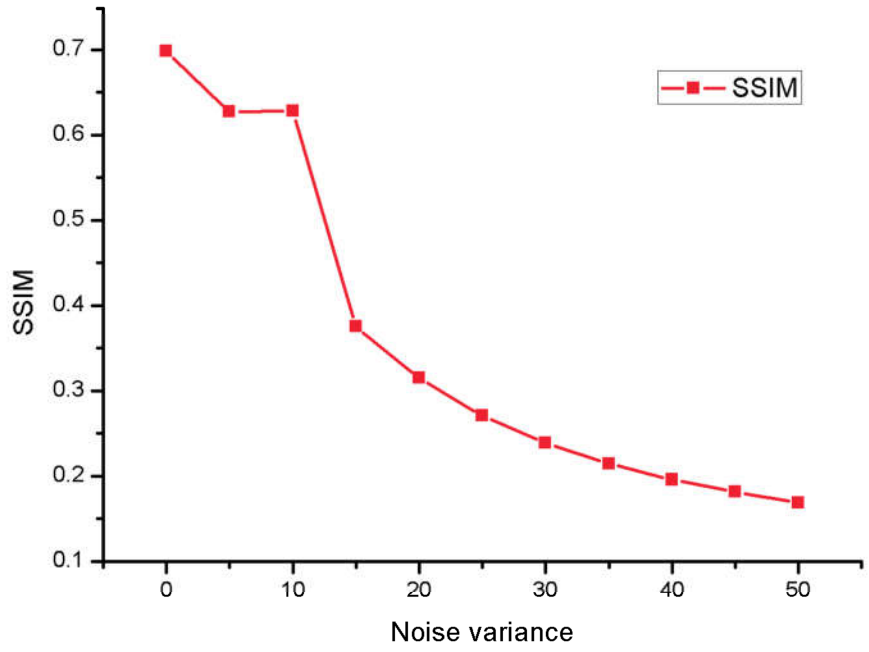

Figure 3.13 SSIM of speckled SAR image at different noise variances

Since Radar images are formed by the coherent interaction of the transmitted microwave with the targets. So it suffers from the adverse effects of speckle noise that arises from the

consistent summation of the signals from ground scatterers loosely distributed randomly within each pixel. A SAR image appears noisier than an optical image. Reducing speckle noise completely from the speckled SAR image is an impossible task and as the noise part increases, the probability to achieve the original reference image decreases [152]. The intensity of each and every pixel represents the microwave backscattered relative to that area on the ground which depends on a variety of factors: shape, sizes, types and orientations of the scatterers in the target area; moisture content of the target area; polarisation and frequency of the radar pulses; as well as the incident angles of the radar beam.

3.6.2 Wavelet Despeckling

The Figure 3.14 shows the detailed despeckling procedure using wavelet transform. The SAR images are already influenced by speckle noise i.e. SAR image are speckled in nature. Since the speckle noise is multiplicative in nature. Therefore homomorphic filtering is applied to deal with multiplicative nature of speckle noise. The wavelet transform is applied on the log-transformed speckled SAR image. The wavelet thresholding has following steps.

Step 1: Perform DWT on input speckled SAR image to obtain approximate and detail parts.
Step 2: Perform the despeckling using following steps:

i. Estimate noise variance.

ii. Calculate threshold.

iii. Apply thresholding on detail parts.

Step 3: Apply inverse DWT to obtain final despeckled SAR image.

Before applying DWT on SAR image, there are certain points to be taken care of. First of all, wavelet family basis is needed to be chosen for every decomposition layer like db2, haar etc. Secondly, the decomposition level is needed to be decided. Although in image denoising, the image can be decomposed up to any level, but it is observed in most of the cases that the better denoising results are obtained from level 3 to 5.

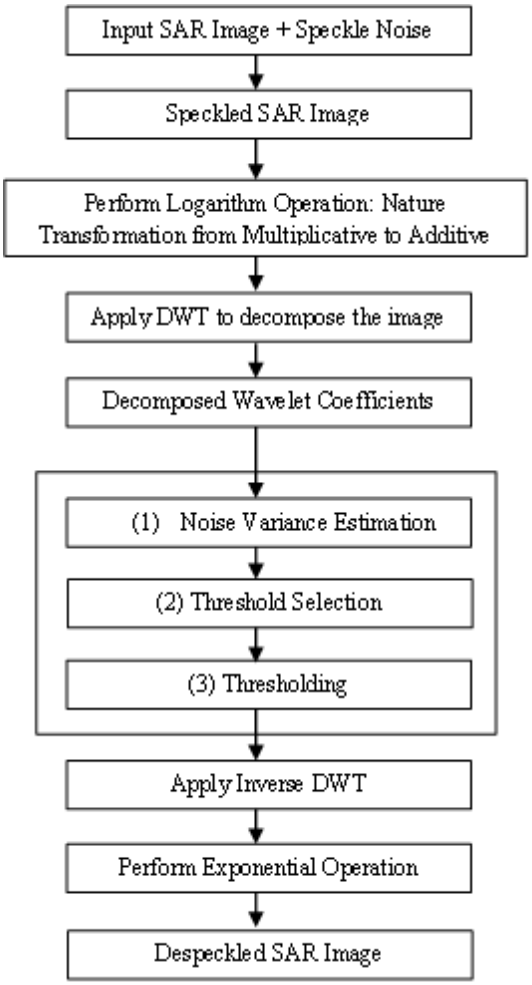

Figure 3.14 Image despeckling procedure using DWT [110] [111]

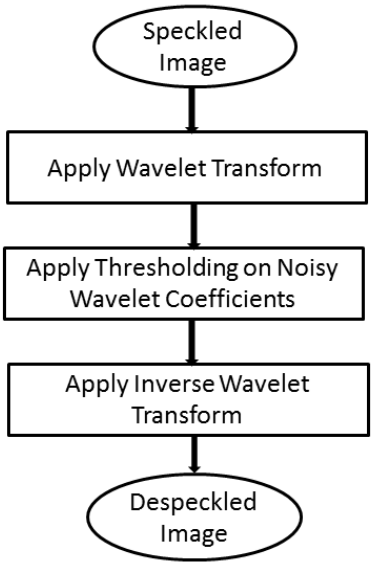

Figure 3.15 Basic block diagram of wavelet-based denoising

Figure 3.15 shows the basic block diagram of wavelet-based SAR image. It includes three elementary stages: the first stage is to apply the wavelet transform on the input speckled SAR image, the second stage implements the wavelet thresholding method on wavelet coefficients of the input image, and the last stage is to apply inverse wavelet transform. The resultant provides the despeckled SAR image.

The brief introduction of wavelet shrinkage rule, thresholding value and wavelet thresholding is given below:

A. Wavelet Shrinkage

The wavelet shrinkage is an important phase of wavelet-based SAR image despeckling process. It involves two major steps, first is selection of threshold value and second is selection of thresholding method. The selection of threshold value is crucial task. The despeckling method selects the optimal threshold value. The optimal threshold value is selected in three ways shown in Figure 3.16. The thresholding is performed by soft and hard thresholding method using the optimal threshold value.

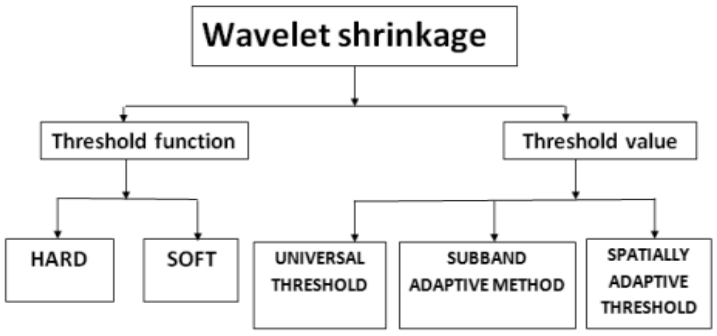

Figure 3.16 Block diagram of threshold process and its different methods [112]

B. Thresholding Value

The selection of threshold value is one of the important and critical tasks in wavelet despeckling method. The threshold value separates the speckled coefficients from the detailed coefficients. The detailed coefficients hold the major information of the image thus used for the image restoration. The threshold value is selected by three different ways as shown in Figure 3.16 i.e. universal threshold, subband adaptive threshold, and spatially adaptive threshold. The threshold value is exclusively selected for all wavelet coefficients in universal threshold [21], [112]. The threshold value is selected distinctly for each detailed subband in subband adaptive thresholding [112], [113]. In spatially adaptive threshold way, the selected threshold value is different for each detailed wavelet coefficient [25], [112], [113].

C. Wavelet Thresholding

According to the literature available in wavelet-based SAR image despeckling, it is observed that small threshold value preserves the fine details of the image. But such threshold is not sufficient to remove the speckle noise completely. The large threshold value can remove the speckle noise competently, but here the fine details of the image get destroyed. Therefore selecting a threshold value is one of the most important steps in wavelet thresholding.

- **Visu Shrink**

This wavelet thresholding technique was invented by Donoho and Johnstone [77], [114]. It uses the universal threshold method for threshold selection purpose. It is described by Eq. 3.8.

$$T_u = \sigma_n^2 \sqrt{2 \log N} \quad \text{.....(3.8)}$$

The artifacts are generated during the despeckling process [115], [116]. An estimate of the noise level σ_n in Eq. 3.8 is grounded on the median absolute deviation given by [117] in the Eq. 3.9.

$$\sigma_n^2 = \left[\frac{median\left(HH_1(n,m) \right)}{0.6745} \right]^2 \quad \text{.....(3.9)}$$

where n and m signify the pixel indexes of the wavelet decomposed diagonal subband of the first level decomposition i.e. HH_1. The despeckled SAR images are excessively sharp image that eliminates most of the coefficients.

- **Sure Shrink**

This wavelet thresholding method combines the Stein's Unbiased Risk Estimator (SURE) method and universal threshold [117]. A distinctive threshold value is evaluated for each subband that is well-matched to the SAR images with sharp discontinuities. This shrinkage rule demonstrates efficient despeckling and promises low MSE values [115]. In Sure Shrink, the soft threshold is expressed as,

$$T_S = min\left(T, \sigma_n^2 \sqrt{2logN} \right) \quad \text{.....(3.10)}$$

Here, T represents the value that minimizes the SURE.

- **Bayes Shrink**

It is a thresholding method that is grounded on the hypothesis of wavelet coefficients that are verified as random variables with general Gaussian distribution (GGD) within each sub-band. Under this condition, in order to minimize the Bayesian risk, the value is calculated using estimated threshold [104], [115].

The threshold λ is evaluated using below equation,

$$\lambda = \left(\frac{\sigma_n^{\ 2}}{\sigma_Y} \right) \quad \text{.....(3.11)}$$

The noise variance is estimated using robust median estimation method (Abramovitch et al. 1998) as follows:

$$\sigma_n^2 = \left[\frac{median\left(\left| X\left(x,y\right) \right| \right)}{0.6754} \right]^2 \quad \text{.....(3.12)}$$

where, $X(x,y) \in LH_L$, $X(x,y) \in HL_L$ and $X(x,y) \in HH_L$, and L is decomposition level. The standard Bayesian shrinkage rule works on the HH_L, but in the proposed research work i.e. HMN-AD, HMN-DSF and HMN-CF, it is applied to all the detail components (LH_L, HL_L, HH_L). The standard deviation of noise less image (σ_Y) is calculated using:

$$\sigma_Y^2 = max\left(\sigma_X^2 - \sigma_n^2, 0 \right) \quad \text{.....(3.13)}$$

where, $\sigma_X^2 = \frac{1}{c}\sum_{i=1}^{c} X_i^2$, and c is the patch size of the input image.

The Bayes Shrink displays better despeckling results when GGD is supposed [103], [148]. The coefficients are processed in the thresholding operation that describes the procedure used to differentiate between the detailed and speckled coefficients. The thresholding can be done either by hard and soft thresholding as shown in Figure 3.17 [75], [104], [118].

Hard thresholding sets any coefficient less than or equal to the threshold to zero [119].

$$Y(A,\lambda)=\begin{cases} A\ for\ all\ |A|>\lambda \\ 0\ otherwise \end{cases} \quad \text{.....(3.14)}$$

The proposed method uses soft thresholding. It is equated as:

$$\hat{Y}:=\begin{cases} 0 & if\ |X|\le\lambda \\ sign(X)(|X|-\lambda) & if\ |X|>\lambda \end{cases} \quad \text{.....(3.15)}$$

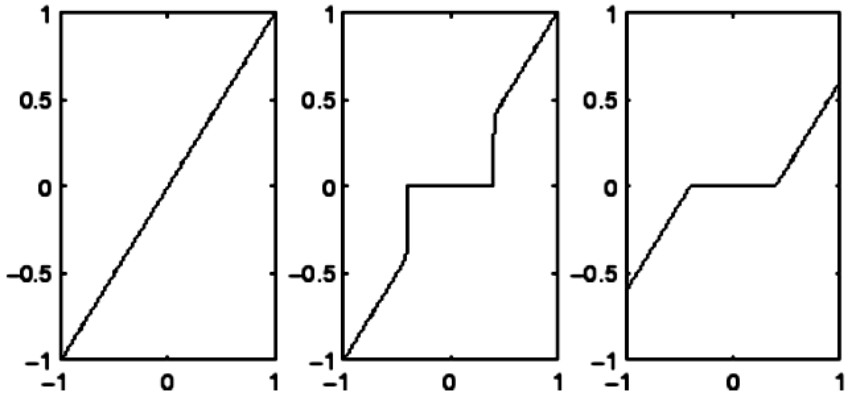

Figure 3.17 (a) Original signal (b) Hard threshold signal (c) Soft threshold signal [120]

D. Wavelet families

There are large numbers of wavelet families that can be used for both continuous and discrete analysis [124]. Some of them are 'haar'-Haar wavelet, 'db'-Daubechies wavelets, 'meyr'-Meyer wavelet, 'gaus'-Gaussian wavelets, 'shan'-Shannon wavelets, etc. [121]. In the thesis, the research work is performed using Daubechies (db2) wavelets as Daubechies wavelets are the most admired wavelets in the field of image denoising [122], [123].

3.6.3 Wavelet Thresholding using Bivariate Shrinkage Rule

To despeckle the high-frequency coefficients, a Bivariate shrinkage function is performed using adaptive thresholding. Suppose, b_{2p} signifies the parent of b_{1p} (b_{2p} is the wavelet coefficient at the identical location as the p^{th} wavelet coefficient b_{1p}, but at the next coarser scale). Then

$$a_{1p} = b_{1p} + n_{1p}$$

$$a_p = b_p + n_p \quad \text{.....(3.16)}$$

where, a_{1p} and a_{2p} are speckled wavelet coefficients, b_{1p} and b_{2p} are speckle less wavelet coefficients and n_{1p} and n_{2p} are additive noise coefficients. Eq. 3.16 can be re-written as:

$$a_p = b_p + n_p \quad \text{.....(3.17)}$$

where, $b_p = (b_{1p}, b_{2p})$, $a_p = (a_{1p}, a_{2p})$ and $n_p = (n_{1p}, n_{2p})$. To despeckle the high-frequency coefficients, Bivariate shrinkage rule [23] can be conveyed as:

$$\hat{b}_{1p} = \frac{\left(\sqrt{a_{1p}^2 + a_{2p}^2} - \lambda_p\right)_+}{\sqrt{a_{1p}^2 + a_{2p}^2}} . a_{1p} \quad \text{.....(3.18)}$$

The function $(z)_+$ is well-defined as:

$$(z)_+ := \begin{cases} 0, & if \quad z < 0 \\ z, & if \quad z > 0 \end{cases} \quad \text{.....(3.19)}$$

The term λ_p in Eq. 3.18 is the threshold for the p^{th} coefficient, calculated as:

$$\lambda_p = \frac{\sqrt{3}\sigma_n^2}{\sigma_p} \quad \text{.....(3.20)}$$

To calculate the noise variance σ_n^2 from the noisy wavelet coefficients, a robust median estimator is used from the finest scale wavelet coefficients (LH, HL and HH subbands) stated in the Eq. 3.12 and marginal variance of σ_p^2 for each wavelet coefficient can be estimated as:

$$\hat{\sigma}_p^2 = \left(\hat{\sigma}_{ap}^2 - \sigma_n^2\right)_+ \quad \text{.....(3.21)}$$

where, $\hat{\sigma}_{ap}^2$ is the marginal variance for noisy coefficients of a_{1p} and a_{2p}. Since, a_{1p} and a_{2p} are modeled as zero mean, $\hat{\sigma}_{ap}^2$ can be estimated as:

$$\hat{\sigma}_{ap}^2 = \frac{1}{|S(p)|} \sum_{a_i \in S(p)} a_i^2 \quad \text{.....(3.22)}$$

where, $|S(p)|$ is the size of the neighborhood S(p).

3.7 Anisotropic Diffusion

Noise occurrence and its restoration is a common and universal problem in the image processing. The fine details of the image are degraded by this noise such as edges and objects that holds the important information of the image. There are various methods and filters available that provides smoothening of the degraded image. These methods and filters are based on the diffusion of the pixel values. Diffusion can be either isotropic or anisotropic diffusion. In isotropic, there is a diffusion of pixel values all across the image due to which blurring occurs as it performs the averaging all across the image regardless of any edge or object. It simply averages the image due to which the pixels at edge and objects get mixed up. Here diffusion is same in every direction regardless of boundaries in the image. In the case of anisotropic diffusion, diffusion varies with the direction. It tries to average the image only at either side of the edge, object or boundary. It smooths the correct object. This is achieved by the evaluating the gradient of the image [44] which is also called as edge stopping function. The basic equation of anisotropic diffusion is,

$$\frac{\partial I(x,y,t)}{\partial t} = div\left[g\left(\| \nabla \mathrm{I}(\mathrm{x},\mathrm{y},\mathrm{t}) \|\right) \nabla I(x,y,t) \right] \quad \text{.....(3.23)}$$

here, $I(x,y,0)$ is original image, $\nabla \mathrm{I}(\mathrm{x},\mathrm{y},\mathrm{t})$ is the gradient of the image at time t, t is the time parameter and g(·) is the conductance function that controls the conduction as a function of gradient. The conductance function is selected to satisfy $\lim_{x\to 0} g(x) = 1$, so that the diffusion of pixel values is maximum within the homogenous regions and $\lim_{x\to 0} g(x) = 0$, so that the diffusion of pixel values gets stopped across the edges. In other words if conductance function is low, then small intensity gradients are capable enough to block conduction and hence diffusion across step edges and if it is large then it decreases the impact of intensity gradients on conduction. Perona and Malik [45] proposed two function,

$$g_1(x) = exp\left[-\left(\frac{x}{K} \right)^2 \right] \quad \text{.....(3.24)}$$

and,

$$g_2(x) = \frac{1}{1+\left(\frac{x}{K} \right)^2} \quad \text{.....(3.25)}$$

where K is the gradient magnitude threshold parameter that controls the speed of the diffusion. Diffusion Eq. 3.24 provides preferential treatment for high contrast edges over low contrast ones while the diffusion Eq. 3.25 supports wide regions over smaller ones.

Anisotropic diffusion filtering is an iterative process. It is extremely sensitive to the number of iterations. Choosing the time parameter T is vital, since misjudging it may result in blurring the true edges and boundaries, while undervaluing it may leave unfiltered noise artifacts. The correct choice of conductance function and gradient thresholding parameters may lead to higher PSNR values. The slope of the reduction of PSNR values will be low, keeping the diffused image close to the original one. It is noticed that PSNR value is always maximized in a specific iteration, which is the ideal time to terminate the process.

3.8 Directional Smoothing Filter

In the despeckling of SAR images, there is a great possibility of loss of image information, predominantly edges. During the process of smoothing, DSF is used to protect the edges from blurring [9], [10]. Applying DSF on an image is a parameter sensitive process as shown in Figure 3.18. The outcome changes as the parameter changes. The filtering caused by DSF depends upon two parameters: size of the mask and type of block processing applied. The proposed method i.e. HMN-DSF uses the mask of 3 × 3 size. HMN-DSF is experimentally performed on this mask using block processing in a non-overlapping fashion. The non-overlapping fashion prevents the filtering from over smoothing. The HMN-DSF is also experimentally tested on different mask sizes, but the best result is obtained at smallest mask size. The spatial average $v(m,n,\theta)$ is estimated in many directions as

$$v(m,n,\theta)=\frac{1}{N_\theta}\sum_{(k,l)\in w_\theta}\sum y(m-k,n-l) \quad \text{.....(3.26)}$$

And a direction θ^* is calculated such that the Eq. 3.27 is minimum

$$\left|y(m,n)-v(m,n,\theta^k)\right| \quad \text{.....(3.27)}$$

Then the below Eq. 3.28 gives the required result

$$v(m,n)=v(m,n,\theta^k) \quad \text{.....(3.28)}$$

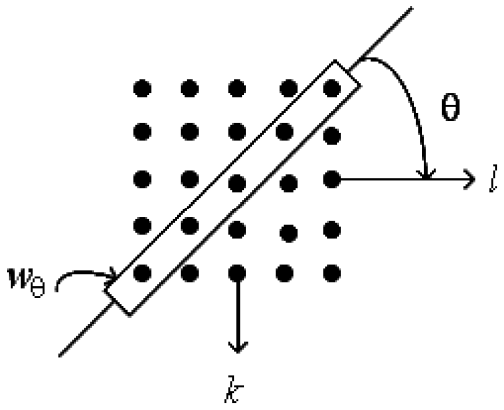

Figure 3.18 Directional smoothing [53]

3.9 Median Filter

The median filter is a nonlinear smoothing method. It is used to eliminate salt and pepper and impulsive noise from an image. This kind of filter is basically used as a classical pre-processing step to improve the outcomes of future image processing and denoising steps i.e. edge detection, noise reduction on an image [158]. Median filtering preserves the fine details of the image and removes the random noise. It has wide applications in image as well as in signal processing [158]. The median filter is slightly like the mean filter which is used to eliminate the noise from the image or signal. However, the results of the median filter are far better than the mean filter of preserving significant detail in the image [157].

The median filter studies each and every pixel in the image and looks at its neighboring pixels to judge whether or not it is representative of its surroundings. As an alternative of merely substituting the pixel value with the mean of nearby pixel values, it substitutes it with the median of those values [157].

The median is computed primarily by arranging all the pixel values from the nearby neighborhood into mathematical order and then substituting the pixel being measured with the central pixel value. If the neighborhood pixels under consideration contain an even number of pixels, the average of the two middle pixel values is used. Figure 3.19 illustrates an example calculation [157]. The median filter is formulated as,

$$y[m,n] = median\{x[i,j],(i,j) \in w\} \quad (3.29)$$

where, w is a neighborhood mask defined by the user, centered around location $[m,n]$ in the image.

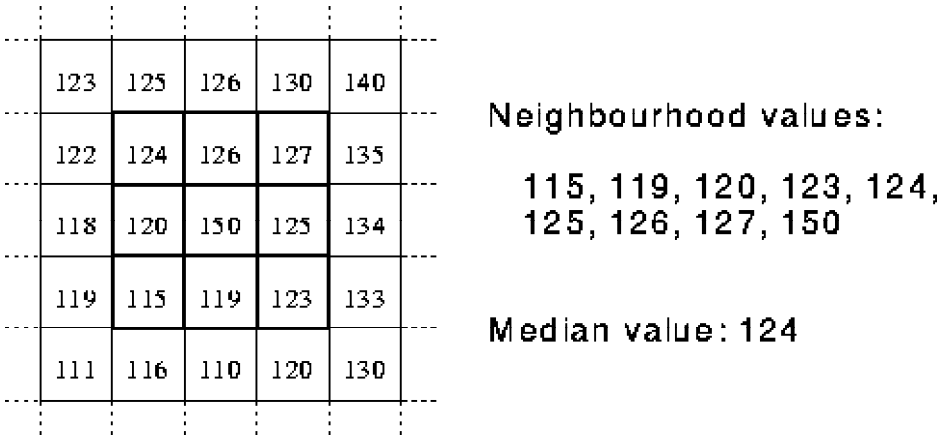

Figure 3.19 Computing the median value of a pixel neighborhood. The intensity value of central pixel 150 is somewhat to be regarded with suspicion of the nearby pixels and is substituted with the median value: 124. A 3×3 square neighborhood is castoff here [157]

3.10 Wiener Filter

The Wiener filter is used for reducing the additive noise in the image. It is based on Fourier iteration. It takes less computational time for filtering the image. It is mainly used for de-blurring [48]. The Wiener filter is used in both spatial and frequency domain filtering. It is more effective in the frequency domain. The disadvantage of Wiener filter is that it cannot reconstruct the image to its original form. It only reduces noise up to a limited extent. It can be used to filter the frequency components but can only suppress noise and is unable to reconstruct the frequency components which are degraded by the noise [49]. The Wiener filtering reduces the overall MSE in the procedure of inverse filtering and noise smoothing. The Wiener filtering is a linear approximation of the original image. The approach is based on a stochastic framework [50].

$$W(f_1,f_2)=\frac{H^*(f_1,f_2)S_{xx}(f_1,f_2)}{\left|H(f_1,f_2)\right|^2 S_{xx}(f_1,f_2)+S_{\eta\eta}(f_1,f_2)}) \quad (3.30)$$

3.11 Method Noise

This section explains the concept, use, implementation and effectiveness of method noise in the field of SAR image despeckling. The method noise has the capability to enhance the performance of any despeckling method. It is easy and efficient way of enhancing the results. The difference between noisy image and denoised image contains some residual image information that is due to the inefficiency of the denoising method. The comparison of

despeckling results of some well-known despeckling methods in two different cases i.e. with and without the use of method noise is presented in the Table 3.3. The despeckling results will be compared on the basis of PSNR and SSIM. The concept of method noise is not restricted to only classical and medical images. It has vast usages and applications. It can also be used in the despeckling methods.

The despeckling method depends on the filtering constraint 'f'. This constraint calculates the degree of filtering applied to the image. For most of the despeckling methods, the constraint f depends on an approximation of the noise variance. There are various ways of applying method noise but in most of the literature the concept of method noise is implemented of a post-processing step i.e. it is used after the filtering is performed. It enhances the result and improves the quality of the denoised image. Method noise is simple and effective concept that is easy to understand and implement.

Let D is the noisy image and after denoising E is obtained as the final denoised image. Now mathematically E1 is evaluated by Eq. 3.31,

$$E1 = D - E \quad \text{.....(3.31)}$$

Now E1 contains the residual image information, so further any denoising technique can be applied to E1 like thresholding or any filtering method. After denoising E1, let say E2 is achieved. Then Eq. 3.32 is executed to obtain the resultant denoised image, E3 that contains the lowest noise. The Fig 3.20 and 3.21 describe the step by step procedure of using method noise.

$$E3 = E2 + E \quad \text{.....(3.32)}$$

The Figure 3.20 shows the specific model of method noise application based on the wavelet transform. The Figure 3.21 shows the general model of method noise application. It depicts how any filtering technique can be easily incorporated with the concept of method noise. Here the residual component or unfiltered component can be filtered using any despeckling method. The method noise thresholding is applied to the unfiltered component of the image.

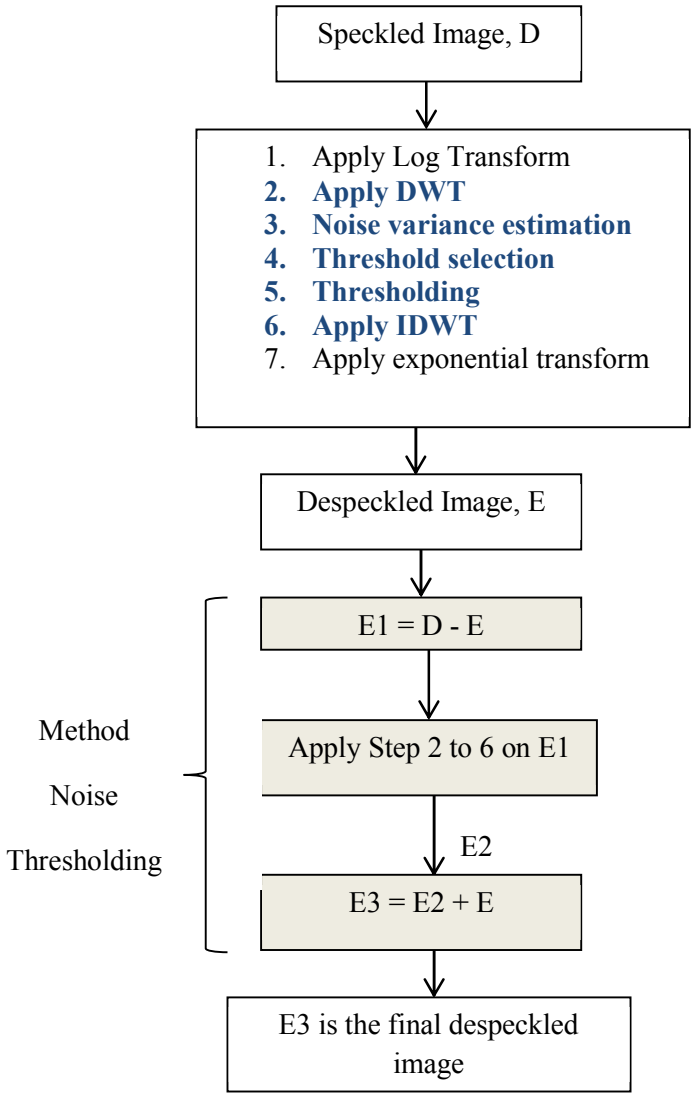

Figure 3.20 Wavelet-based despeckling using method noise thresholding

Method noise is a robust and adaptive way of improving a degraded image. It is a 100% working method. It may be any standard or custom filter that can be applied directly on the method noise. The thresholding can also be performed on the method noise, but it is experimentally observed that use of thresholding in method noise is more efficient than any other denoising method. It is observed that the application of method noise with wavelet transform is more efficient than other methods as shown in Table 3.3.

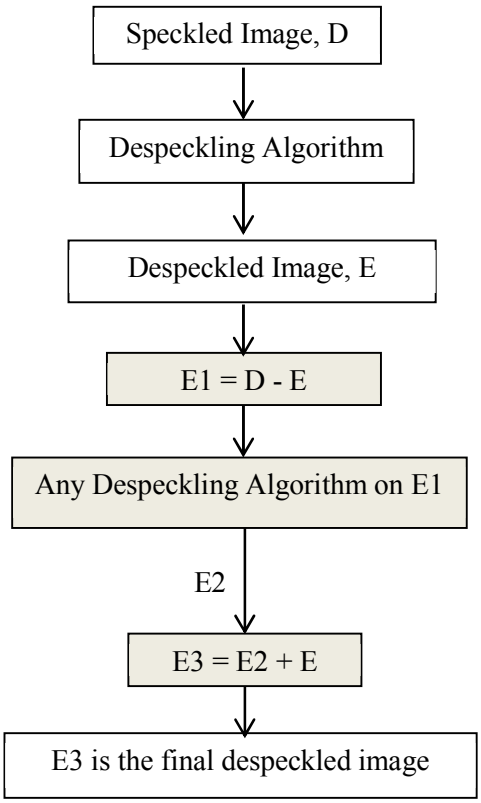

Figure 3.21 General model of method noise filtering.

The experimental results is shown using both the cases i.e. with and without method noise. The validity and efficiency of the despeckling method using method noise is shown on real SAR image. The real speckled SAR image at $\sigma = 20$ is shown in Figure 3.22.

During the experiment the compared method resizes the SAR images to 512×512 images for the faster execution of method. It uses db2 type wavelet basis during the DWT operation. The method noise is incorporated to the standard methods and filters as the post-processing step. The despeckled SAR images shown in Figure 3.23(a) and 3.23(b) are obtained by db2 based DWT thresholding using Bayesian shrinkage rule with and without method noise.

Figure 3.22 Reference speckled SAR image

The performance metrics used to assess the quality of the despeckled SAR image are PSNR and SSIM. The mathematical aspect of these metrics is available in [51]. The high value of PSNR depicts better image quality and in SSIM, the value tending towards 1 indicates the good image quality and tending towards 0 indicates bad image quality. The quantitative results are shown in Table 3.3 using various standard despeckling filters and methods. The comparison is made using Frost, homomorphic Frost, Kuan, homomorphic Kuan, Lee, homomorphic Lee, Kuwahara, Mean, Median, Hard and Soft thresholding, Universal threshold, Visu threshold and Bayesian thresholding strategies.

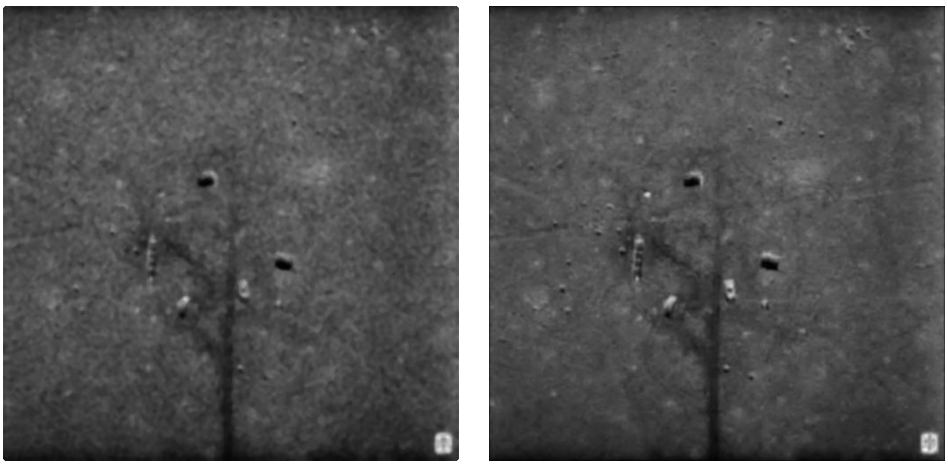

(a) **(b)**

Figure 3.23 Despeckled images (a) without method noise (b) with method noise

The efficiency of method noise can be analyzed by the visual appearance of the despeckled SAR image shown in Fig 3.23(b). In Fig 3.23, it can be observed that the despeckled image in Fig 3.23(b) is better than the despeckled image in Fig 3.23(a). The speckle content is reduced

and edges are preserved using method noise. The preservation of fine details in the non-uniform regions and smoothness in the uniform region is well maintained. Table 3.3 shows the quantitative analysis of despeckling techniques with and without method noise using PSNR and SSIM values.

Table 3.3 Performance evaluation of despeckling techniques with and without method noise using PSNR and SSIM

	S. no	Techniques	PSNR		SSIM	
			w/o method noise	with method noise	w/o method noise	with method noise
Speckled SAR Image Fig 3(b). $\sigma = 20$	1	Frost	18.5679	19.0001	0.7006	0.8025
	2	Homomorphic Frost	18.5031	19.5238	0.7309	0.7993
	3	Kuan	18.9513	20.8937	0.7892	0.8002
	4	Homomorphic Kuan	18.1243	18.9937	0.7911	0.8258
	5	Lee	18.4526	19.0023	0.7872	0.8235
	6	Homomorphic Lee	18.8039	18.9790	0.7095	0.7925
	7	Kuwahara	19.6609	20.9008	0.8974	0.9002
	8	Mean	16.0001	16.9909	0.7931	0.8632
	9	Median	16.9278	18.2973	0.8002	0.8403
	10	Soft Thresholding	19.7049	20.7395	0.8901	0.9567
	11	Hard Thresholding	18.8419	19.5637	0.8193	0.8881
	12	Universal Threshold	17.4019	18.6792	0.8991	0.9006
	13	Visu Threshold	16.0002	16.9835	0.8031	0.8563
	14	Bayesian Threshold	19.9509	21.2386	0.9181	0.9500

Figure 3.24 and 3.25 plots the PSNR and SSIM values of compared despeckling techniques with and without use of method noise using quantitative values. In Figure 3.24 and 3.25, it can

be observed that PSNR and SSIM values of the techniques with method noise are higher than techniques without method noise. This shows the validity and effectiveness of method noise.

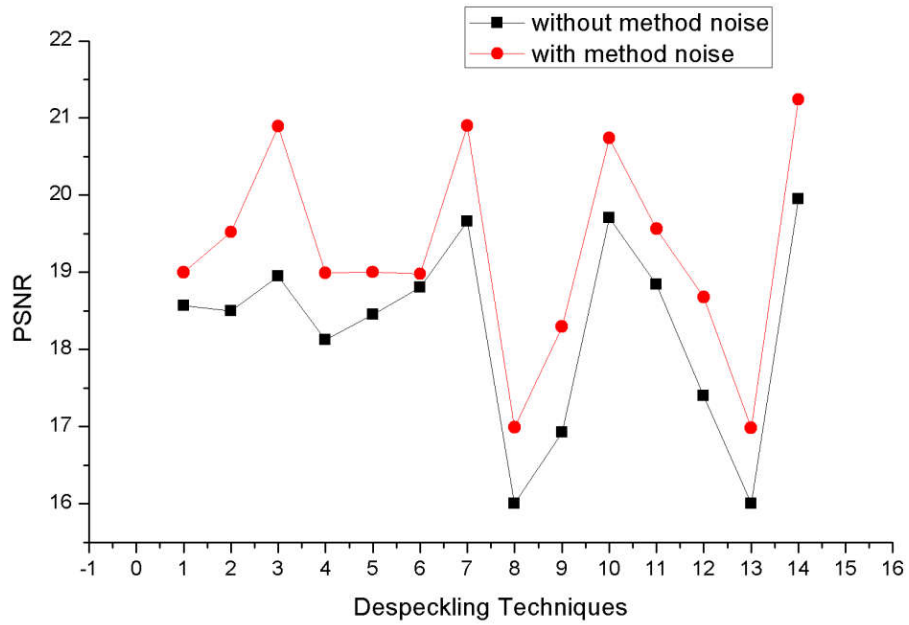

Figure 3.24 Plotting PSNR of all despeckling techniques with and without method noise.

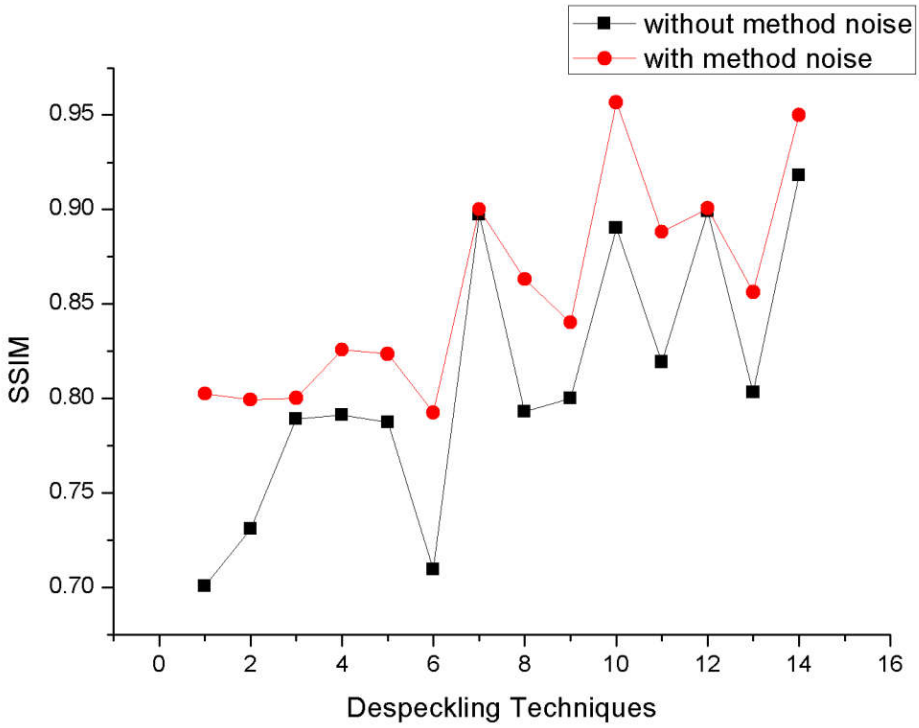

Figure 3.25 Plotting SSIM of all despeckling techniques with and without method noise.

The experimental analysis of using method noise on the real speckled SAR image validates the effectiveness of method noise in despeckling method that enhances the visual appearance of the despeckled image and also preserves the fine details in the heterogeneous areas.

3.12 Quality Assessment of Despeckling Methods

In SAR image despeckling, the utmost thought-provoking job is the speckle noise reduction by preserving the fine details of the image. The most evident concern in this field is the speckle-free reflectivity that is unidentified as the ground truth is unknown. Another significant matter is the relationship between quality and reliability of despeckled SAR images. The other despeckling outlines i.e. feature and reliability of originality of despeckled SAR images is calculated by analyzing the degradation in the homogeneous regions, i.e. reduction of speckle noise and preservation of fine details in heterogeneous areas.

Visual inspection of despeckled SAR image is one methodology for the assessment of quality of the image. It allows the detection of the main human naked eye visible features that best describes the nature of the despeckling procedures. It includes edge and point target preservation capability, blurriness, and structural and blocky artifacts that are not identified by objective and direct measurements. The visual assessment has a limitation of not allowing either quantitative assessment among the performances of different despeckling methods to be made or the bias introduced by the filter to be effectively estimated. To overcome these restrictions of visual investigation, several other performance metrics have been proposed for the assessment of the despeckling techniques. These quantitative metrics are divided in two segments: with–reference and without–reference indexes [36]. The performance of the proposed methods is assessed by these metrics. There are also other ways available for evaluating the performance of any despeckling algorithm like performance percentage calculation using confusion matrix [85]-[88] and quantitative values [55] of despeckled image. In the thesis, the performance percentage is calculated of HMN-AD by analyzing the quantitative values of the despeckled image in chapter 5.

There is an infinite literature available in the field of image denoising and despeckling in the presence of the reference image. In this case the author has complete information about the image. In the case of with-reference index, the image researchers can easily compare their despeckling results with the reference images. It creates the opportunity to enhance the results as the previous statistical details are available. In this case, there are many metrics available for edge detection, preservation of edge and texture, preservation of smoothness in

homogeneous and non-homogeneous areas. Here, the information of the despeckled image is compared with the reference SAR image using all perspectives into account.

In the case of without-reference index, the knowledge of original image information is unknown. This is completely based on arithmetical theories on the image model, as the image model is powerfully reliant on the unit of scene heterogeneity, a controlled choice of the homogeneous areas may be required for the computation of specific index.

3.12.1 With–Reference Indexes

A numerous literature is available for calculating the performance of the despeckled SAR image in the case of with-reference index [29], [51]-[53]. The quantitative metrics used under this category uses the information of the reference SAR image. These metrics uses two parameters: first is the reference SAR image and second is the despeckled SAR image. Here, the information of the despeckled SAR image is compared with the reference SAR image. The performance evaluation measures under this category are Mean square error (MSE), Structural Similarity Index Measurement (SSIM), Signal to Noise Ratio (SNR), Peak Signal to Noise Ratio (PSNR), Energy Signal-to-Noise Ratio (ESNR), Universal Image Quality Index (UIQI), Feature Similarity Index Metric (FSIM) [57], Edge Correlation (EC) [58], [59] and Pratt's Figure Of Merit (FOM) [60]. Some of the experimented metrics in the thesis are discussed below:

MSE [54] is a performance measure that evaluates the average squared difference between the despeckled SAR image and reference SAR image. It assesses the overall despeckled SAR image. It fails to evaluate the small specific details of the image.

$$MSE = \frac{1}{N}\sum_{j=0}^{N-1}\left(X - Y\right)^2 \quad \text{.....(3.33)}$$

where X and Y are the despeckled and reference images respectively.

The SSIM is used to estimate the similarity between despeckled image and reference image. It depends upon three factors, luminance, contrast and structure [55]. The SSIM is a multiplicative mixture of the three terms.

$$SSIM\left(a,b\right) = \frac{\left(2\mu_a\mu_b + P_1\right)\left(2\sigma_{ab} + P_2\right)}{\left(\mu_a^2 + \mu_b^2 + P_1\right)\left(\sigma_a^2 + \sigma_b^2 + P_2\right)} \quad \text{.....(3.34)}$$

where, μ_a, μ_b, σ_a, σ_b and σ_{ab} are the local means, standard deviation and cross variance for images *x; y*. $P1 = (0.01 * L)^2$ and $P2 = (0.03 * L)^2$, where L is the specified dynamic range value. The range of SSIM varies from 0 to 1 according to the literature [56].

The SNR is a quantitative metric used to measure the sensitivity of an imaging system.

$$SNR = 10.log_{10}\left[\frac{Var[g]}{MSE}\right] \quad \text{.....(3.35)}$$

where $Var[g]$ is reference image variance.

PSNR is one of the mostly used performances metric in the field of denoising. The high value of PSNR indicates better results. PSNR is computed by:

$$10\log_{10}\left(\frac{255\times 255}{MSE}\right) \quad \text{.....(3.36)}$$

The UIQI is defined by three components. The defined components are degree of linear correlation, the closeness of mean luminance and similarity of contrast in images. The range of the three components is in [0, 1]. Therefore, the final range of the UIQI is in between [0, 1]. The UIQI value that tends toward 1 indicates better image quality and those that tends towards 0 indicates the low image quality.

$$Q = \frac{\sigma_{xy}}{\sigma_x\sigma_y} \bullet \frac{2\overline{xy}}{(\overline{x})^2 + (\overline{y})^2} \bullet \frac{2\sigma_x\sigma_y}{\sigma_x^2 + \sigma_y^2} \quad \text{.....(3.37)}$$

3.12.2 Without–Reference Indexes

The performance metrics under the without-reference index does not depend upon the real SAR data. These metrics depend upon the arithmetical SAR data model as well as on core resolutions on the level of features like heterogeneity and homogeneity of the image. These metrics are concentrated on the statistics of the arrangement of the pixel values of the real speckled SAR image and assessed by Ratio Images, Coefficient of Variation (CV), Equivalent Number of Looks (ENL), Target–to–Clutter Ratio (TCR) [64], [65] and Noise Variance (NV). Some of the used metrics in the thesis are discussed below:

The ENL [61] is a performance assessment metric of despeckled SAR image, that analyzes the factor of smoothening during the image formation and post-processing operation. This metric depends upon the minimal number of looks that gets increased after the despeckling of SAR

image. It is calculated over the homogenous area and is defined as the ratio between the mean (μ) squared to the variance (σ).

$$ENL = \left(\frac{\mu}{\sigma}\right)^2 \quad \text{.....(3.38)}$$

The Ratio Image is the metric that contains the significant information both in homogeneous and non-homogeneous areas, defined as the pixel–by–pixel ratio among the speckled SAR ($a(m)$) and the despeckled SAR image ($\hat{b}(m)$) [62].

$$R(m) = \frac{a(m)}{\hat{b}(m)} \quad \text{.....(3.39)}$$

The CV [63] is used to assess the texture of the heterogeneous areas of the despeckled SAR image and is a statistical parameter defined as the ratio of standard deviation and means value and expressed as a percentage.

$$CV = \left(\frac{Standard\ deviation}{Mean}\right) \times 100 \quad \text{.....(3.40)}$$

The NV is used to show the amount of speckle content that currently exist in the image [66]. The smaller value of the NV indicates the reduction of speckle noise in the image. It necessarily doesn't depend upon the intensity of the image [66]. The NV is calculated using below formula:

$$\sigma^2 = \frac{1}{N}\sum_{j=0}^{N-1} u_j^2 \quad \text{.....(3.41)}$$

where N is the size of the image.

3.13 Quantitative Dual Nature Analysis of MSE in SAR Image Despeckling

The despeckling of SAR images is a critical task. There are certain quantitative metrics that analyses the quality of despeckled SAR image. This section statistically analyses the dual and diverse nature of MSE in despeckling method. This dual and diverse nature of MSE is examined in two different cases. Case 1: when the reference SAR image is available (with-reference index). Case 2: when reference SAR image is not available (without-reference index). In both the cases, the comparative statistics of the MSE is different. In case 1, the MSE should be as low as possible for better image quality. In case 2, MSE must be high for

significant speckle reduction. This analysis will show the dual and diverse behavior of MSE as a performance metric in both the cases. MSE is a valuable metric in despeckling.

Case 1: When reference SAR image is available (with-reference index).

MSE and PSNR are the two performance evaluation metrics for assessing the image quality. MSE denotes the cumulative squared difference between despeckled and reference SAR image. PSNR depicts the maximum error possible [51]. The low MSE value indicates low error and high-quality image.

$$MSE = \frac{1}{M \times N} \sum_{M,N} \left[I_1(m,n) - I_2(m,n) \right]^2 \quad \text{.....(3.42)}$$

m, n are rows and column of the input SAR image.

$$PSNR = 10 \log_{10} \left(\frac{R^2}{MSE} \right) \quad \text{.....(3.43)}$$

R is the maximum pixel value of the input SAR image. The PSNR should be comparatively high for the best image quality results.

According to the Eq. 3.43,

$$PSNR \propto \frac{1}{MSE}$$

PSNR is inversely proportional to MSE. When the PSNR value is high then the MSE value is low and low MSE value denotes better image quality results. It concludes that in case 1, MSE must be comparatively low among other filtering techniques for best despeckling results [92].

Theoretically, MSE is the average squared difference between reference SAR image and despeckled SAR image. If this cumulative difference is large, then the final despeckled SAR image is different from reference SAR image that represents bad despeckling results. If the cumulative difference is small, then the pixel statistics of the despeckled image is close to reference image that represents efficient despeckling results.

Case 2: When reference SAR image is not available (without-reference index).

In case 2, MSE indicates the average squared difference between despeckled and real speckled SAR image. The comparatively small MSE value shows the smaller difference

between despeckled and real speckled SAR image that denotes less reduction of speckle noise i.e. weak algorithm. The comparatively high MSE value indicates the greater difference despeckled and real speckled SAR image that means that there is a significant speckle reduction [66]. In case 2, it is extremely necessary to be very careful with the edge and region preservation while analyzing the MSE value.

Table 3.4 MSE value comparison of A5 with other filtering techniques for best quantitative results in two different cases: case 1 and case 2. σ = speckle noise variance.

Filtering Techniques	MSE	
	CASE 1 (At σ = 20)	CASE 2
A1	B1	C1
A2	B2	C2
A3	B3	C3
A4	B4	C4
A5	**B5**	**C5**

Let say, A5 is the proposed technique that is compared with the four other techniques [A1, A2, A3 and A4] on the basis of MSE metric.

According to statistical study of MSE, the performance of the A5 is best for the following results,

$$CASE\ 1\text{: } [B5] < [B1, B2, B3, B4]$$

$$CASE\ 2\text{: } [C5] > [C1, C2, C3, C4]$$

For the best despeckling results of the A5 method, the MSE value i.e. B5 must be minimum in the case 1 and the MSE value i.e. C5 must be maximum in the case 2 [55] as shown in Table 3.4.

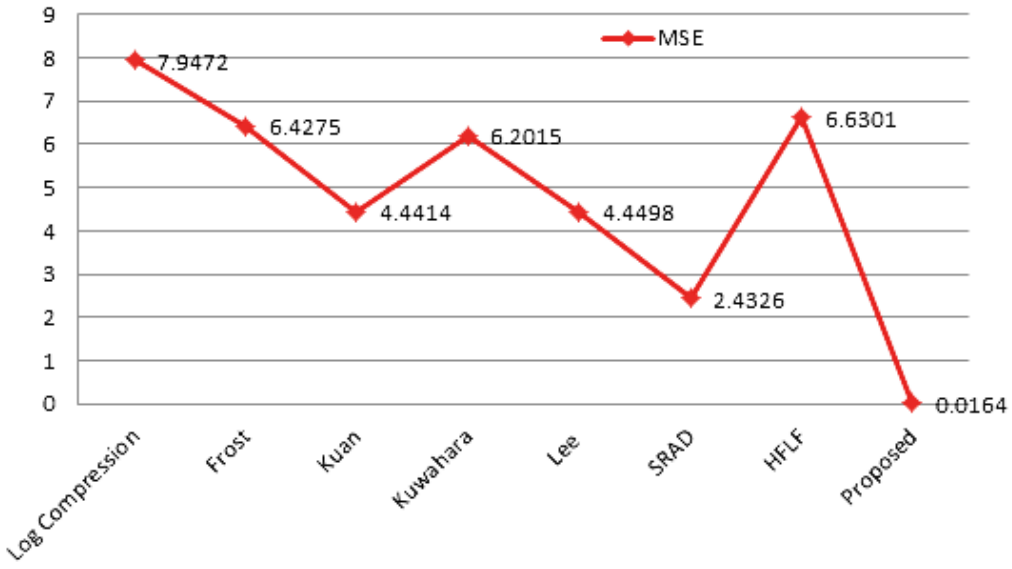

Figure 3.26 MSE results of the article [3].

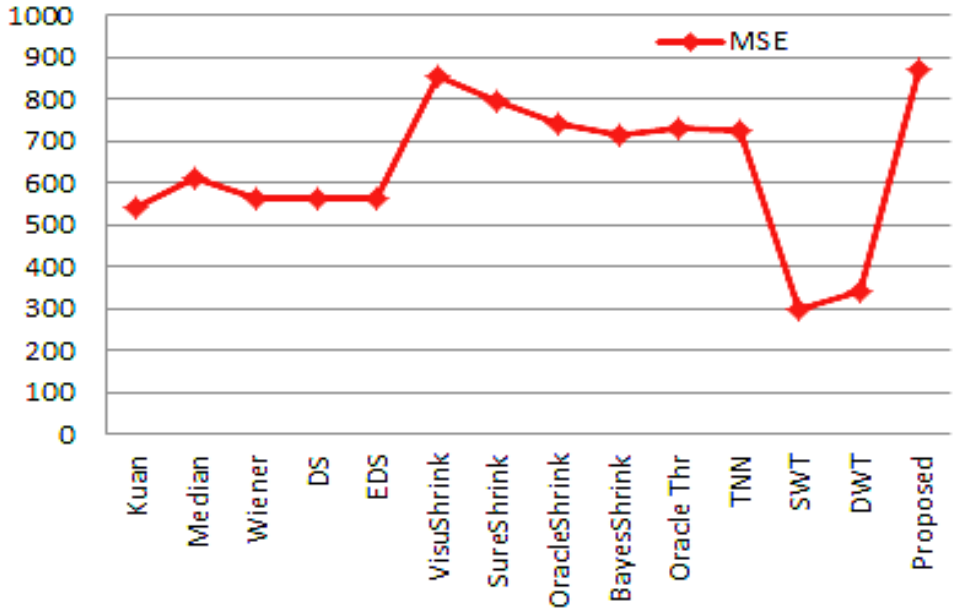

Figure 3.27 MSE results of the article [6].

This study of MSE metric is experimented on two articles of despeckling i.e. [3] and [6]. The above experimental analysis verifies the dual nature of MSE metric. In Figure 3.26, the best despeckling results are obtained at minimum MSE values in the case of with reference indexes while in Figure 3.27 the best results are obtained at maximum MSE values in the case of without reference indexes.

There are certain specified performance metrics for with-reference and without-reference indexes, out of them; MSE is experimentally observed to be the only metric to be used for

performance evaluation in both the cases. MSE is a valuable metric. Its dual nature in different situations validates the importance of its use. This study clears the air of confusion of using MSE in the case of without-reference indexes. Its diversity is the real strength. It can be easily used in either case.

3.14 Conclusion

This chapter discusses all the methodology related to proposed methods i.e. HMN-AD, HMN-DSF and HMN-CF. Various quantitative metrics related to SAR image despeckling are discussed. On intelligently applying the method noise in DWT, the despeckling results can be enhanced and it can outperform the despeckling results with SWT and CoWT. The effect of speckle noise on SAR images is analyzed. The effect of speckle noise are adverse than other types of noise due to its multiplicative nature that is handled by the homomorphic filtering. The concept, use and various perspectives of method noise and its implementation is also discussed. The concept of method noise is 100% working method in SAR image despeckling. It has the capability to enhance the results of any denoising or despeckling method. Lastly, it verifies the dual nature of quantitative measure i.e. MSE in two different scenarios i.e. with and without-reference indexes.

4. PROPOSED METHODOLOGY

4.1 Background

All the proposed SAR image despeckling methods i.e. HMN-AD, HMN-DSF and HMN-CF are discussed in this section. The proposed methodology is grounded on db2 based 2D-DWT. The concept of method noise is intelligently incorporated in the proposed methods. The HMN-AD and HMN-DSF are based on global filtering and HMN-CF is based on local filtering. The concept of fusion is used in HMN-CF. The proposed methods are easily analyzed by flowchart. All the despeckling methods are briefly summarized. The switching from HMN-AD to HMN-DSF and HMN-DSF to HMN-CF is also discussed at the last of each section of proposed methods. The role and importance of related methodology and flow of proposed method is discussed in the summary section.

4.2 A New Homomorphic SAR Image Despeckling using Method Noise Thresholding and Anisotropic Diffusion (HMN-AD)

4.2.1 Algorithm of HMN-AD

Input: Speckled SAR Image, S.

Output: Despeckled SAR image, $D_{ESupdated}$.

Step 1: Apply iterative anisotropic diffusion/filtering on S.

a) Initiate the parameters, g(*) and K.
b) Compute Perona-Malik diffusion Eq. 3.25 using required parameters.
c) **for** i = 1 to n; i = No. of iterations, **do**
    i. solve the standard Eq. 3.23 of anisotropic diffusion.
    ii. Update the values.

    end for

d) Resultant image is S_{ad}.

Step 2: Apply log transformation, S_l.

Step 3: for j = 1 to 3; j = level of decomposition, **do**

a) Apply DWT on S_l.
b) Decomposition into 4 subbands, approximate part (a1, a2, a3) and detail part (b1 c1 d1), (b2 c2 d2), (b3 c3 d3).
c) Apply 2D median filtering on a2 and a3 subbands using 3*3 neighborhood mask using Eq. 3.29.
d) Apply 2D adaptive Wiener filtering on a1 subbands using 3*3 neighborhood mask using Eq. 3.30.
e) Perform thresholding on the detailed part (b1 c1 d1), (b2 c2 d2), (b3 c3 d3) using following step:
    i. Estimate noise variance using Eq. 3.12.
    ii. Threshold calculation using Eq. 3.11.

iii. Apply soft thresholding using Eq. 3.13 and Eq. 3.15.

end for

Step 4: Apply inverse DWT.

Step 7: Apply exponential transform, S_e.

Step 5: $S - S_e$.

Step 6: for i = 1 to 3, i = level of decomposition, **do**

a) Apply db2 based 2D-DWT on S - Se.
b) Decomposition into two sub-bands, approximate subband (a11, a22, a33) and a detailed subband (b11, c11, d11), (b22, c22, d22) and (b33, c33, d33).
c) Apply wavelet thresholding on detailed diagonal part (b11, c11, d11), (b22, c22, d22) and (b33, c33, d33) of (S-Se) using below steps:
    i. Noise variance estimation using Eq. 3.12.
    ii. Threshold calculation using Eq. 3.11.
    iii. Apply soft thresholding using Eq. 3.13 and 3.15.

    end for

d) Apply inverse DWT, the resultant image is H.
e) Add H and S_e to get D_{ES}, as $D_{ES} = H + Se$.

Step 8: Final output despeckled SAR image, $D_{ESupdated}$.

4.2.2 Flowchart of HMN-AD

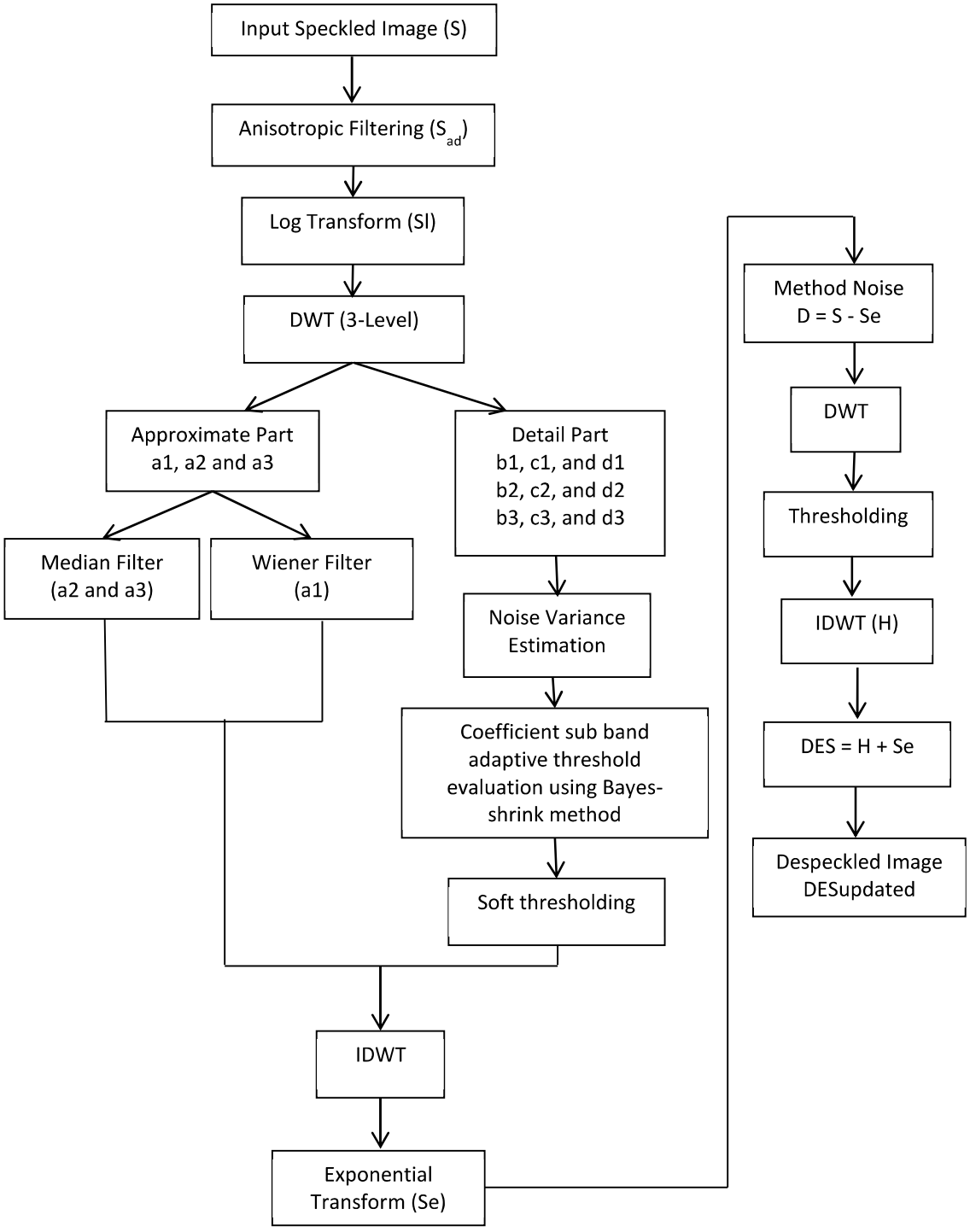

Figure 4.1 Flowchart of HMN-AD.

4.2.3 Summary of HMN-AD

The proposed approach i.e. HMN-AD is based on the homomorphic filtering in the wavelet domain as shown in Figure 4.1. The despeckling methods that are based on homomorphic filtering are more adaptive and robust than other methods [34], [67]. The linear, non-linear filters and non-Bayesian methods can easily be incorporated in the homomorphic filtering methods. This despeckling technique proposes a new hybrid method based on the Bayesian approach in a transform domain (homomorphic filtering using wavelet) and non-Bayesian approach (anisotropic diffusion). There is no such despeckling method available that can assure full noise removal. There is always a scope for enhancement in this field. The HMN-AD is efficient in despeckling the simulated as well as real speckled SAR images.

The speckle noise is multiplicative in nature. Therefore most of the literature related to wavelet transforms implement the homomorphic filtering that applies the log and exponential operations to deal with the multiplicative nature of the speckle noise. The non-Bayesian approach works directly over the speckled image without modifying their nature. The HMN-AD implements anisotropic diffusion directly on the speckled SAR image iteratively. This operation is followed by the homomorphic filtering based on wavelet transform using a linear and non-linear filter.

The anisotropic diffusion is efficient in preserving edges, but slightly inefficient in preserving the smoothness in the homogeneous regions. It is observed in the experimental testing that after applying anisotropic diffusion on the speckled SAR image, there is still presence of speckle content in the image and the smoothness is also bit lost in the homogeneous areas. In order to handle this situation, homomorphic filtering using 2D-DWT based on modified Bayesian shrinkage rule using method noise thresholding is proposed. This operation reduces the speckle content without disturbing the fine details of the image. The log transform converts the multiplicative nature of speckle noise into additive nature. Now, 2D-DWT is applied and it decomposes the image into two components: approximate (a1, a2, a3) and detail components (b1 c1 d1), (b2 c2 d2), (b3 c3 d3). The approximate part is the residual part while, the detailed component comprises of the vertical, horizontal and diagonal part. The decomposition is performed up to level 3. The HMN-AD is experimented from decomposition level 1 to 7. It is observed that in the field of image restoration the better denoising results are obtained at decomposition level 3 to 5 in terms of detail preservation and computational cost. So the final decomposition is set at level 3 in HMN-AD. The

approximate and detailed components are separately processed. The 2D adaptive Wiener filtering is applied on the (a1) subband using 3×3 neighborhood mask. The 2D median filtering is applied on the (a2) and (a3) subbands using 3×3 neighborhood mask. The detailed components are thresholded using modified Bayesian shrinkage rule. In the standard Bayesian shrinkage rule, the thresholding is usually applied to the diagonal part of the detailed component. But in HMN-AD, the thresholding is applied to all the detailed components i.e. vertical, horizontal and diagonal. The soft thresholding is applied after noise variance estimation and threshold calculation. After these operations, the approximate and detailed parts are directed to the IDWT followed by anti-log operation i.e. exponential operation.

The HMN-AD is a three-layered approach. The first layer is applying anisotropic diffusion, second is applying wavelet thresholding using modified Bayesian shrinkage rule and linear and non-linear filters and third layer is applying method noise thresholding. After the second layer, method noise thresholding is applied. The output image of the second layer is subtracted from the input speckled SAR image. The resultant is the residual part and directed to the 2D-DWT. Again wavelet decomposition is set to level 3 and now wavelet thresholding using modified Bayesian shrinkage rule is applied on the high-frequency component of the residual part. Later IDWT is applied. And the resultant image is added to the output image of the second layer (wavelet thresholding). This resultant is the final despeckled output SAR image.

As it may appear that there may be over smoothing due to multi-layered approach. But the HMN-AD has the potential for the best speckle reduction and detail preservation. The first layer preserves edges and other fine details of the image that are significant for the better interpretation of the image. The prime advantage of wavelet thresholding is that they in spite of having uneven shape are able to flawlessly restructure functions with linear and higher order polynomial shapes. As a consequence, wavelets are capable enough to despeckle the SAR images in comparison to traditional methods. The method noise thresholding is applied to restore the unfiltered edges. Method noise thresholding is highly effective method for enhancing the despeckled results. It recover the fine details of the image. An efficient and intelligent use of method noise can enhance the results.

This three-layered hybrid combination presents high image quality with good visual appearance. The computational cost of this method is highly efficient. The concept of method

noise is implemented as the post-processing operation. It enhances the quantitative results as well as the visual quality of the image. During the experimental testing of HMN-AD it is observed that the use of method noise thresholding as the post-processing step enhances the quality of the despeckled image. If the concept of method noise is applied more intelligently and in more robust way, then it can give much better results. The results of this technique persuade to go for designing a new despeckling method i.e. HMN-DSF with more intelligent use of method noise using DSF for better edge preservation.

4.3 A New Homomorphic SAR Image Despeckling using Directional Smoothing Filter and Method Noise Thresholding (HMN-DSF)

4.3.1 Algorithm of HMN-DSF

Input: Speckled SAR image

Output: Despeckled SAR image

1. Read input speckled SAR image.
2. Apply log transformation, S.
3. **for** i = 1 to 3, i = level of decomposition, **do**
    - **A.** Apply db2 based 2D-DWT on S.
    - **B.** Decomposition into two subbands, approximate sub-band A_i = (LL1, LL2, LL3) and detailed sub-band D_i = (LH1, HL1, HH1), (LH2, HL2, HH2) and (LH3, HL3, HH3).
    - **C.** Apply DSF followed by method noise thresholding (step(b-d)) on approximate subbands using following steps:
        - **a.** Apply DSF on A_i using mask [3×3] using Eq. 3.26, 3.27 and 3.28, L'.
        - **b.** $A_i - L'$.
        - **c.** Apply wavelet thresholding on the ($A_i - L'$) using below steps:
            - **i.** Noise variance estimation using Eq. 3.12.
            - **ii.** Threshold calculation using Eq. 3.11.
            - **iii.** Apply soft thresholding using Eq. 3.13 and 3.15. The resultant image is L''.
        - **d.** L'' + L'.

D. Apply wavelet thresholding followed by method noise thresholding (step(b-d)) on detailed subbands using following steps:

a. Apply wavelet thresholding on D_i using below steps:

i. Noise variance estimation using Eq. 3.12.

ii. Threshold calculation using Eq. 3.11.

iii. Apply soft thresholding using Eq. 3.13 and 3.15. The resultant image is H'.

b. $D_i - H'$.

c. Apply wavelet thresholding on $(D_i - H')$ using below steps:

i. Noise variance estimation using Eq. 3.12.

ii. Threshold calculation using Eq. 3.11.

iii. Apply soft thresholding using Eq. 3.13 and 3.15. The resultant image is H''.

d. H'' + H'.

end for

4. Apply inverse DWT, S'.
5. S - S'.
6. **for** i = 1 to 3, i = level of decomposition, **do**

A. Apply db2 based 2D-DWT on S - S'.

B. Decomposition into two subbands, approximate subband (LL11, LL22, LL3) and a detailed subband (LH11, HL11, HH11), (LH22, HL22, HH22) and (LH33, HL33, HH33).

C. Apply wavelet thresholding on detailed diagonal part (HH11, HH22, HH33) of (S – S') using below steps:

a. Noise variance estimation using Eq. 3.12.

b. Threshold calculation using Eq. 3.11.

c. Apply soft thresholding using Eq. 3.13 and 3.15.

end for

7. Apply inverse DWT, the resultant image is S''.
8. S'' + S'.
9. Apply exponential transform on (S'' + S').
10. Final output despeckled SAR image, S'''.

4.3.2 Flowchart of HMN-DSF

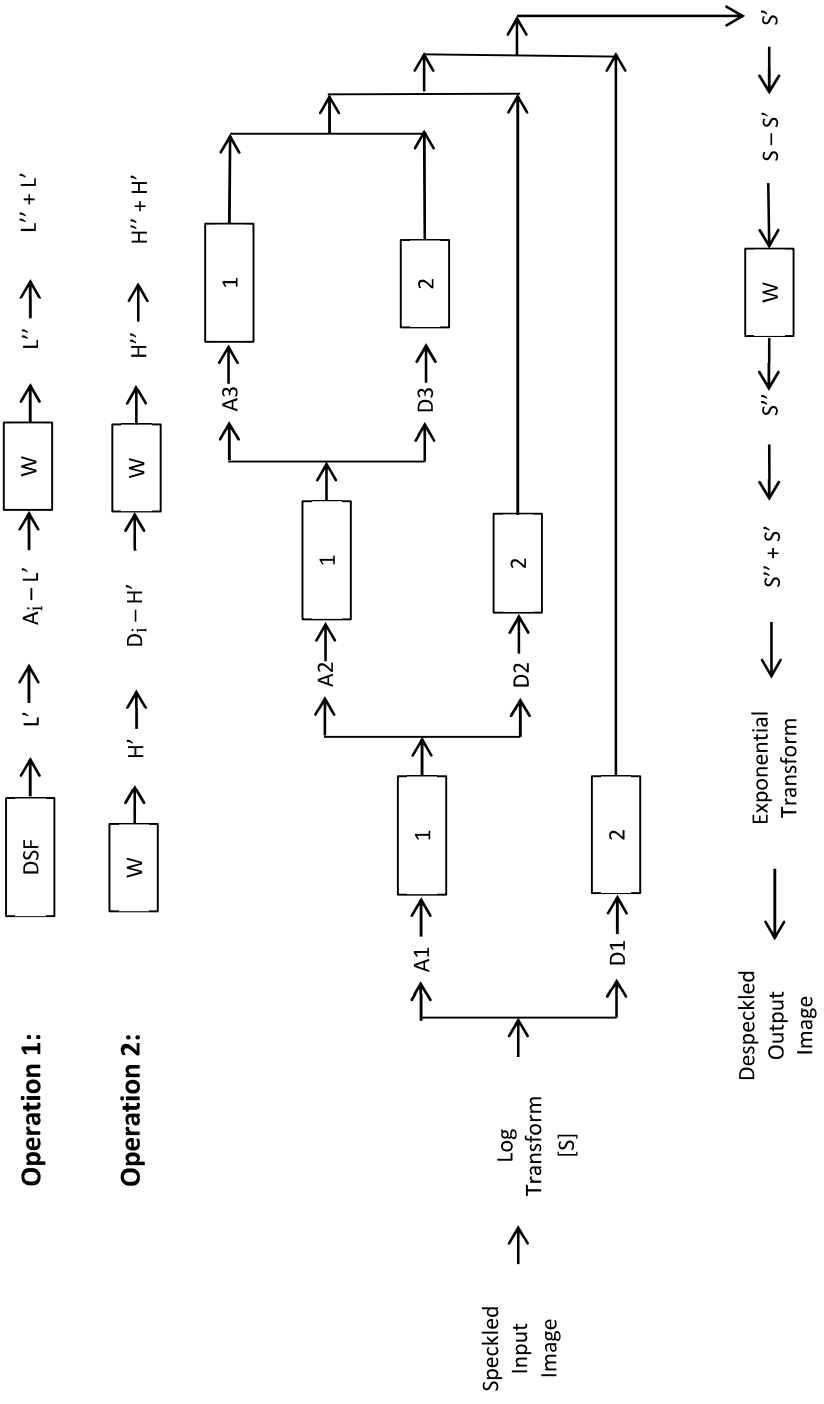

Figure 4.2 Flowchart of HMN-DSF

4.3.3 Summary of HMN-DSF

The approach is focused on despeckling the simulated [68], [69] as well as real speckled SAR images. It uses a bit complex but efficient method to remove the speckle noise. The HMN-DSF uses a wavelet-based hybrid combination of DSF, wavelet thresholding and method noise thresholding. The core idea of HMN-DSF is to implement the concept of method noise intelligently. The method noise is an adaptive concept. It can be incorporated in any despeckling technique. An intelligent use of method noise can enhance the result efficiently [93]-[96]. In the previous literature [93]-[96], the concept of method noise is mainly used as the post-processing step. In HMN-DSF, a new application of method noise is proposed that processes the low and high-frequency subband of the image after DWT decomposition as shown in Figure 4.2. In Figure 4.2, flowchart of HMN-DSF is shown where db2 based 2D-DWT based decomposition is performed up to level 3, that decomposes the image into approximate (A1, A2, and A3) and detailed part (D1, D2, and D3). The approximate part is directed to operation 1 and the detailed part is directed to operation 2. Operation 1 = DSF followed by method noise thresholding. Operation 2 = wavelet thresholding followed by method noise thresholding. 'i' in Ai denotes the level of wavelet decomposition. The DSF is applied on the approximate component followed by method noise thresholding and the detailed component is directed to wavelet thresholding followed by method noise thresholding. The HMN-DSF is developed with the intention to improve the despeckling results in terms of fine detail preservation, especially edges. The multiplicative nature of speckle noise is handled by homomorphic filtering [92].

On DWT decomposition, the approximate part of the image contains lot of information. Since HMN-DSF works up to three level of decomposition. So DSF is applied three times to the approximate part till the third level of decomposition. The method noise thresholding follows DSF to restore the remaining degraded information after DSF. The approximate part contains the maximum information that is actually degraded. The DSF performs the block-wise smoothing. This operation does not guarantee the complete speckle reduction of the approximate part. The unfiltered part of the approximate component is directed to the method noise thresholding that efficiently preserves the edges and other fine details. The concept of method noise thresholding is introduced to process the remaining unfiltered parts. Its main application is fine detail preservation especially edges.

The difference between the speckled image and the despeckled image shows the noise removed by the algorithm that is called as method noise [93]-[96]. Let say, D is the noisy image. Let denoising technique 'T' is applied on D. E is obtained as the final denoised image. Now mathematically F is evaluated by, $F = D - E$. F contains the residual noisy part, so further any denoising method can be applied to it like thresholding technique or some filter. After denoising F, let say E1 is achieved. Then $E2 = E + E1$ is performed to get the resultant denoised image, which contains the minimum noise, 'E2'.

Since the HMN-DSF works up to three level of decomposition hence the approximate parts are denoted as A1, A2, and A3. Therefore, A_i represents the approximate component, where 'i' is the decomposition level. The wavelet thresholding is represented by 'W'. The DSF followed by method noise thresholding is shown in the below equations,

Apply DSF on the approximate part(A_i),

$$L' = DSF\left(A_i\right) \quad \text{.....(4.1)}$$

$$L_{up} = A_i - L' \quad \text{.....(4.2)}$$

Now, apply wavelet thresholding (W) on the L_{up},

$$L'' = W\left(L_{up}\right) \quad \text{.....(4.3)}$$

$$L_{updated} = L'' + L' \quad \text{.....(4.4)}$$

The $L_{updated}$ at the third level of decomposition contains the optimal noise free approximate component.

The HMN-DSF works on the universal threshold where the threshold value is exclusively chosen for all wavelet coefficients [67], [103]. The HMN-DSF is experimented from 1 to 7 decomposition level. The best results are obtained at the third level of DWT decomposition in terms of speckle reduction, detail preservation and computational cost. HMN-DSF is also tested at several wavelet families that are proven to be specifically valuable in DWT. The tested wavelet families are 'haar', 'db', 'sym', 'coif', 'bior', 'rbio', 'meyr' etc. The comparative result of the HMN-DSF at these wavelet families is shown in the result section. The best results are obtained at 'db2'. Since the noise is uniformly distributed in simulated SAR images, then both the global thresholding and block processing give better results. The HMN-

DSF implements global thresholding due to better computational cost. The same procedure is experimented on the real SAR images and the obtained results are good as in the first case. Since the speckle distribution is unknown in the real speckled SAR images, still HMN-DSF works fine in this case. This is due to the efficient and intelligent use of method noise thresholding.

In the field image denoising, the complete denoising is not possible but the maximal restoration of the information is possible. After DWT decomposition, image is decomposed into approximate and detailed components. The approximate component contains the low-frequency components. The detailed component contains the high-frequency components. The detailed component contains the information related to the edges while the approximate component contains the other information including edges information such as information related to homogeneous and heterogeneous regions. Since the detailed component contains the edge information, therefore, a dual thresholding is performed using the concept of method noise to restore the maximum information as much as possible.

The method noise thresholding plays an excellent role in restoring the remaining unfiltered edge components. In the previous literature, the method noise is used as the post-processing step. But the concept of method noise can be more intelligently used. The best use of method noise gives the best result. In order to obtain best results, the method noise thresholding is applied to the wavelet coefficients that deliver noise-free coefficients to the next level for further processing.

The combination advantage of DWT and method noise gives the best outcome as edges are preserved locally rather than globally. It is done by processing the wavelet coefficients in the 2D-DWT operation. The wavelet thresholding followed by method noise thresholding is applied to the detailed parts (horizontal, vertical and diagonal) that delivers the best outcome in terms of edge preservation. The detailed parts are represented as D1, D2, and D3, i.e. D_i, where 'i' denotes the level of wavelet decomposition.

Apply wavelet thresholding (W) on every detailed part(D_i),

$$H' = W\left(D_i\right) \quad \text{.....(4.5)}$$

$$H_{up} = D_i - H' \quad \text{.....(4.6)}$$

Now, again operation 'W' is applied on the H_{up},

$$H'' = W\left(H_{up}\right) \quad \text{.....(4.7)}$$

$$H_{updated} = H'' + H' \quad \text{.....(4.8)}$$

The $H_{updated}$ at the third level of decomposition contains the optimal noise free detailed components (horizontal, vertical and diagonal).

The standard use (as a post-processing step) of method noise in the HMN-AD presents the decent despeckling result. HMN-DSF concludes with a new idea of using method noise in the more intelligent way for better results. The HMN-DSF is completely based on the use of method noise. The method noise is used for fine detail preservation. The other filter used in this method is DSF which is also an edge-preserving filter. This method offers a new intelligent use of method noise in two different ways. In HMN-DSF, the method noise is used three times. Firstly, on the low-frequency components, secondly on the high-frequency components and lastly as a post-processing operation. This unique way of implementing the method noise enhances the despeckling result.

The HMN-AD and HMN-DSF works on global filtering. According to the literature available, the despeckling results using local filtering shows a better result than the global filtering. In HMN-AD and HMN-DSF, the decomposition level is manually set by experimenting the method from level 1-7. The optimal despeckling results are obtained at level 3. The computational cost of HMN-DSF is low. The use of local filtering i.e. blocks processing and automatic selection of decomposition level can enhance the despeckling results by preserving more information. This advancement lead to design a new despeckling method i.e. HMN-CF.

4.4 A New Homomorphic SAR Image Despeckling using Correlation based Fusion and Method Noise Thresholding (HMN-CF)

4.4.1 Algorithm of HMN-CF

Step 1: The speckled SAR image is multiplicative in nature. Natural log transform is applied to convert this multiplicative nature to the additive. Let the speckled SAR image is S.

Step 2: *Entropy-based Wavelet Decomposition to n-level*

The db2 based 2D-DWT is applied to the log-transformed speckled SAR image up to level n depending on the measurement of texture using entropy parameter for best results. The entropy metric (E') is used for automatic selection of decomposition level which is an arithmetical parameter of measuring the uncertainty of pixel values that can be used to illustrate the texture of the input image [159].

On the every next decomposition level (n), E' is evaluated for the parent and child node. The higher value of E' of parent node than the child node indicates the presence of information in the image that requires next decomposition for detail preservation. This process continues until the above condition fails. This process of setting the decomposition level gives the best outcome in terms of detail preservation. E' is formulated as,

$$E' = -\sum_i P_i Log_2 P_i \quad \text{.....(4.9)}$$

The entropy-based wavelet decomposition level is decided by following steps:

A: Firstly apply 2D-DWT on the image and set the maximum number of levels.

B: Perform decomposition into four components (LL, LH, HL, HH) for each level.

C: Compute the entropy of each component (LL, LH, HL, HH) for each layer using Eq. 4.9 and then calculate average entropy value (AEV) for each layer using Eq. 4.10,

$$AEV = \left(\frac{E'(LL) + E'(LH) + E'(HL) + E'(HH)}{4} \right) \quad \text{.....(4.10)}$$

D: In top-down approach manner, check the AEV,

i. if (AEV (parent node) > AEV (child node)), then go for next decomposition level.

ii. Otherwise, remove the remaining child nodes.

E: Finish the procedure, if there is no node to decompose.

Step 3: The dual thresholding (Bayesian (**A.**) and Bivariate (**B.**) shrinkage) is applied in parallel on the detailed part. The improved detailed parts of both thresholding are later fused to get more enhanced results.

A. For each decomposition level, apply wavelet thresholding using Bayesian shrinkage rule on the detailed part (HL, LH, HH).

i. Noise variance estimation using Eq. 3.12.

ii. Threshold calculation using Eq. 3.11.

iii. Apply soft thresholding using Eq. 3.13 and 3.15, resultant detailed parts are (HL', LH', HH').

B. For each decomposition level, apply wavelet thresholding using bivariate shrinkage rule on the detailed part (HL, LH, HH).

i. Calculate local noise variance σ_n^2 using Eq. 3.12.

ii. For each coefficient of each high pass subbands

a) Compute $\hat{\sigma}_{ap}^2$ using Eq. 3.22

b) Compute $\hat{\sigma}_p^2$ using Eq. 3.21

c) Compute the threshold λ_p using Eq. 3.20

d) Estimate each coefficient using Eq. 3.18

e) Restore the value in $a_{1p.}$ The resultant detailed parts are (HL'', LH,'' HH'').

Step 4: *Locally correlation based fusion.*

The obtained high-frequency coefficients (HL', LH', HH') and (HL'', LH,'' HH'') after two different parallel thresholding methods are fused using local correlation based approach. Firstly, the threshold value is calculated by this way: the non-overlapping block-wise correlation coefficients (CC) are calculated from these high-frequency coefficients (HL', LH', HH') and (HL'', LH,'' HH'') using 3 × 3 mask size. The average of all the CC is evaluated and is decided as the threshold value. In the proposed work, the evaluated threshold value is denoted as *T*. The CC [24] is evaluated using the below Eq. 4.11:

$$CC = \frac{\sum_m \sum_n \left(A_{mn} - \bar{A}\right)\left(B_{mn} - \bar{B}\right)}{\sqrt{\left(\sum_m \sum_n \left(A_{mn} - \bar{A}\right)^2\right)\left(\left(\sum_m \sum_n \left(B_{mn} - \bar{B}\right)^2\right)\right)}} \quad \text{.....(4.11)}$$

where, $\bar{A}$ = mean2(A), and $\bar{B}$ = mean2(B). The m and n represents the source images. mean2(A) = $A_l^X(i,j)$ and mean2(B) = $B_l^Y(i,j)$. $A_l^X(i,j)$ and $B_l^Y(i,j)$ are mean values of their respective high frequencies subbands. 2D-DWT is applied upto l-level of decomposition over the source images X and Y. (i,j) represents the pixel coordinates. The value of CC lies between [-1 to 1] range, where '1' specifies a strong positive relationship, '-1' specifies a strong negative relationship. A CC of '0' specifies no relationship at all.

In the local correlation based fusion strategy of obtained high-frequency coefficients (HL', LH', HH') and (HL'', LH,'' HH''), a non-overlapping block-wise CC are calculated from these high frequencies using 5 × 5 mask size using Eq. 4.11. Here, the acquired CC is compared with the threshold value (T). If the CC value is less than or equal to the T, then the maximum operation is executed. In maximum operation, fusion is implemented by choosing the largest values from both of the transformed images. Or else, the average operation is applied, which calculates the average value using both of the transformed images to perform fusion. Local correlation-based fusion strategy is given as follows:

$$A_l^{new} = \begin{cases} \max\left(A_l^X, B_l^Y\right) & if\ (\mathrm{CC} \le T) \\ \mathrm{avg}\left(A_l^X, B_l^Y\right) & otherwise \end{cases} \quad \text{.....(4.12)}$$

In the Eq. 4.12, the operations "max" and "avg" stand for maximum and average values, respectively, and A_l^{new} for the fused coefficients (HL^{new}, LH^{new}, HH^{new}).

Theoretically, when $(\mathrm{CC} \le T)$, this means that the similarity rate between the detailed despeckled components is less, so "max" operation is used to take the best despeckled component between the two that helps to preserve the edges. When $(\mathrm{CC} > T)$, this means the similarity rate between the detailed despeckled components is more and both the components are almost equivalent, so it is better to average them. On the experimental note, the detailed despeckled components are experimentally tested and fused using 'max' and 'avg' operations and on the basis of experimental evaluation, it is observed this formulation i.e. Eq. 4.12 delivers the best result.

Step 5: Apply inverse DWT using low-frequency coefficient (LL) and fused high-frequency coefficients (HL^{new}, LH^{new}, HH^{new}) to get the despeckled SAR image, D.

Step 6: *Apply method noise thresholding.*

Perform (S - D) operation. Now apply 2D-DWT on (S - D) up to n-level of decomposition using step 2. The detailed part is filtered using Bayesian thresholding method. After performing this step, the output image S'. Now perform addition operation i.e. (S' + D). The final step is to perform an exponential operation on (S' + D). The output image is the despeckled SAR image, S''.

4.4.2 Flowchart of HMN-CF

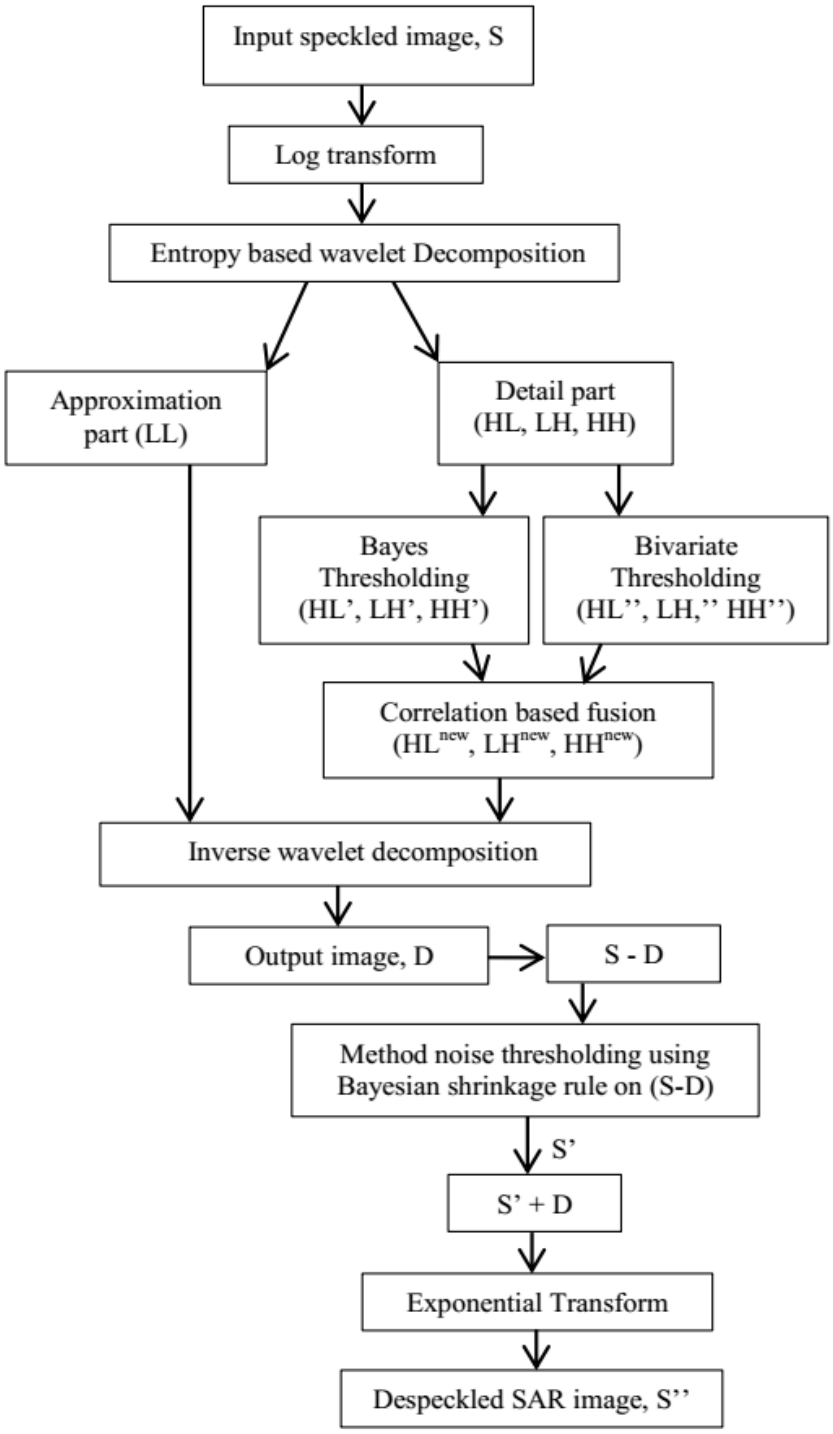

Figure 4.3 Flowchart of HMN-CF

4.4.3 Summary of HMN-CF

The proposed despeckling technique i.e. HMN-CF is experimented on the simulated speckled SAR image and real speckled SAR image. The quantitative despeckling results are shown using with-reference indexes case. The quality of despeckled image is visually analyzed based on certain parameters. These parameters are preservation of edges and corners, preservation of smoothness in the homogeneous regions and preservation of fine details in heterogeneous region. The designed despeckling method grounded on four major steps: the decomposition level is automatically set using entropy metric, the detailed components are thresholded using two different shrinkage rules that executes in parallel i.e. Bayesian and Bivariate shrinkage rules, the two enhanced output detailed components are fused using local correlation strategy and finally method noise thresholding is applied as the post-processing as shown in Figure 4.3.

In HMN-AD and HMN-DSF, the decomposition is set at level 3 for optimal results and low computational cost. The HMN-CF proposes an automatic setting of decomposition level using entropy metric based on texture feature analysis. This is an information preserving method applied for wavelet decomposition using entropy factor that checks the availability of information left at each decomposition level in the form texture analysis.

After wavelet decomposition, the image is transformed into two components i.e. approximate and detailed component. The detailed components consist of the vertical, horizontal and diagonal part. The detailed part contains the fine details of the image like edges etc. The Bayesian and Bivariate shrinkage rule are executed in parallel on the same detailed component of the image. This operation provides two enhanced detailed components. These two enhanced detailed components are fused using local correlation based strategy. This fusion strategy is based on the correlation coefficient, selection of threshold value, max and average operation.

The last step of this despeckling method is method noise thresholding that is implemented as post-processing step of the despeckled image. Its use is explained in the summary sub-section of HMN-AD. The method noise thresholding is applied as the post-processing step that results to a more enhanced and sharp despeckled image. The main advantage of method noise is the preservation of fine detail like edges.

4.5 Conclusion

The chapter discusses the HMN-AD, HMN-DSF and HMN-CF in detail. Each section of the proposed method comprises of three sub-sections i.e. algorithm, flowchart and summary of the proposed method. The proposed methods are grounded on wavelet transform using method noise thresholding. It implements global as well as local filtering. The concept of method noise and fusion enhances the despeckling results.

5. EXPERIMENTAL RESULTS AND DISCUSSION

5.1 Background

This chapter discusses the experimental results of HMN-AD, HMN-DSF and HMN-CF with their validation using hypothesis testing by paired T-test. The experimental results are analyzed and discussed in detail. The proposed methods are experimented on real SAR data and simulated speckled classical images. The performance of the HMN-AD, HMN-DSF and HMN-CF is tested by assessing the visual quality of the despeckled image and by using quantitative metrics like SNR, PSNR, ENL, CV, and SSIM etc. The performance of the proposed methods is compared with some of the traditional and non-traditional methods. The quantitative values are shown in tabular as well as in graphical form for easy understanding of the results. The proposed methods are also compared on the basis of their computational cost. In the final section, the proposed methods are compared among themselves on the basis of visual quality, quantitative measure and computational cost.

5.2 Result and Analysis of HMN-AD: A New Homomorphic SAR Image Despeckling using Method Noise Thresholding and Anisotropic Diffusion

This section displays the experimental result with their performance aspect on simulated as well as on real SAR images. Figure 5.1 shows speckled SAR image dataset at $\sigma = 20$. The proposed method i.e. HMN-AD is experimented at different noise variance levels i.e. ($\sigma \in 4$; 10; 20; 30; 40). The despeckled results of HMN-AD and other compared methods are shown in Figure 5.2 - 5.9, that are experimented at $\sigma = 20$.

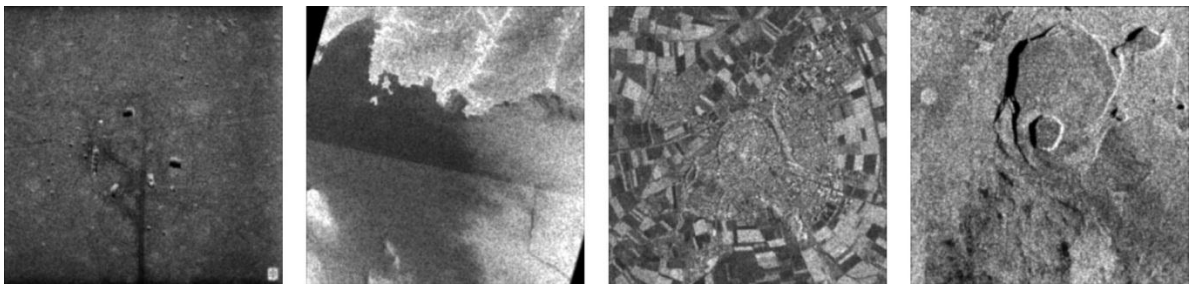

(a) (b) (c) (d)

Figure 5.1 Speckled SAR image data set $\sigma = 20$.

The experimental testing is performed on the speckled SAR images of size 512×512. It helps in comparing and verifying the performance of HMN-AD for qualitative and quantitative evaluation on a specific system. All experiment results are evaluated in MATLAB version =

8.3, name = R2014a on Intel(R) Core(TM) i5-2410 M CPU @ 2.30 GHz, 4 GB RAM and 64-bit operating system. The system configuration is necessary to note down as the execution time of the HMN-AD will be compared to the other despeckling techniques on the same system [51]. During the experiment, the window size is fixed at 3 × 3. The no. of iteration 'I' is not fixed. I is tested from (1 - 10) and despeckling results are displayed at best iteration number.

In order to validate the HMN-AD, the experimental result are compared with the result of well-known standard filters and techniques, such as log compression filtering method [80], Frost filter [25], Kuan filter [81], Kuwahara filter [82], Lee filter [21], SRAD (Speckle Reduction using Anisotropic Diffusion) [83], and HFLF (Homomorphic Filtering with Log Function) [80]. The code of SRAD [83] is taken from Image Despeckle Filtering Toolbox of [80] available on the MathWorks website [84]. Anisotropic total variation and diffusion delivers best results in terms of high visual quality and edge preservation [21], [79]. The required parameters are 'I', window size and lambda (time step). I is the common parameter used in all the compared work, the window size is fixed at 3 × 3, used in [82] and lambda [0.00 – 0.25] is used in [83]. All the parameters are changed and measured for values of best results except for window size. The experimental results are shown at noise variance $\sigma = 20$ in Figure 5.2 – 5.9.

5.2.1 Performance Evaluation

In order to measure the performance of the any despeckling method in the case of with-reference indexes, some of the commonly used metrics are, Root Mean Square Error (RMSE), Signal to Noise Ratio (SNR), Peak Signal to Noise Ratio (PSNR), Energy Signal-to-Noise Ratio (ESNR), Structural Similarity Index Measure (SSIM), Edge Correlation (EC) index and Pratts Figure Of Merit (FOM) etc [36]. Among these performance measures, PSNR, SSIM, RMSE and Universal Image Quality Index (UIQI) are used to assess the quantitative performance of the HMN-AD.

5.2.2 Experimental Evaluation and Comparison

Figures 5.2 – 5.9 shows the despeckling result of log compression filtering, Fost filter, Kuan filter, Kuwahara filter, Lee filter, SRAD, HFLF and HMN-AD respectively. There are certain measures for analysing the quality of despeckled SAR image through their visual appearance

such as, (i) presence of the artifacts (ii) edge preservation (iii) visibility of low contrast objects (iv) texture preservation (v) smoothness in the homogeneous regions and (vi) preservation of fine details in the heterogeneous region, but there is no such mathematical formula or specific process available to do so.

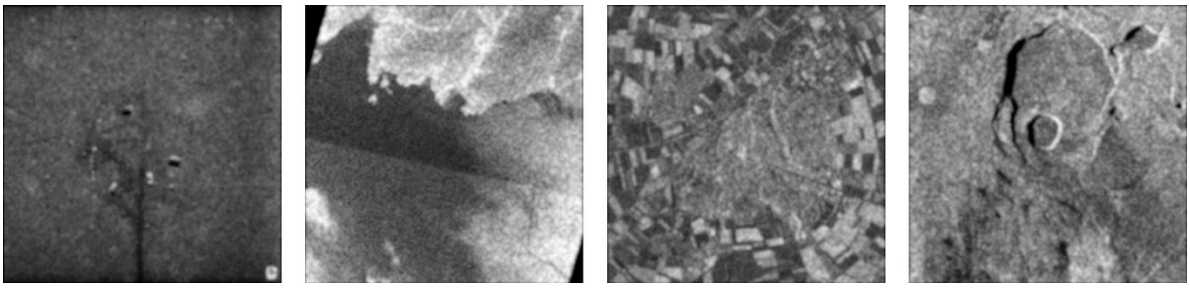

Figure 5.2 Results of Log compression filtering

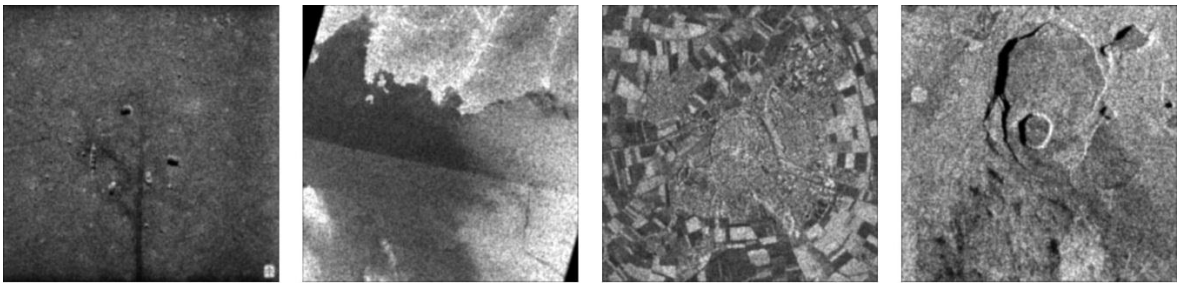

Figure 5.3 Results of Frost filter.

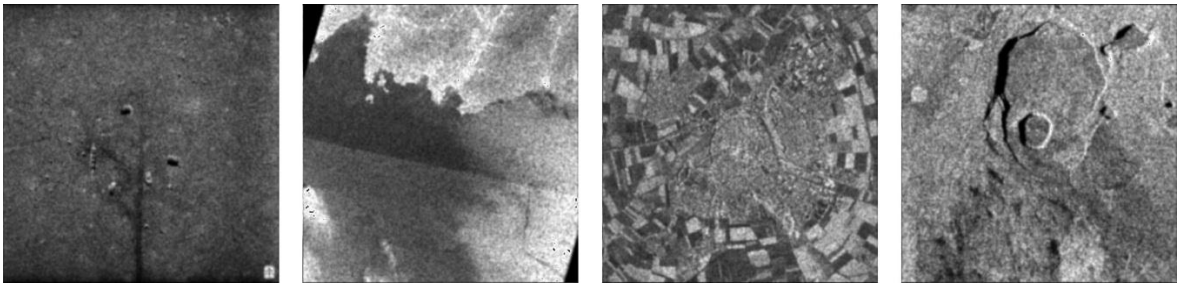

Figure 5.4 Results of Kuan filter

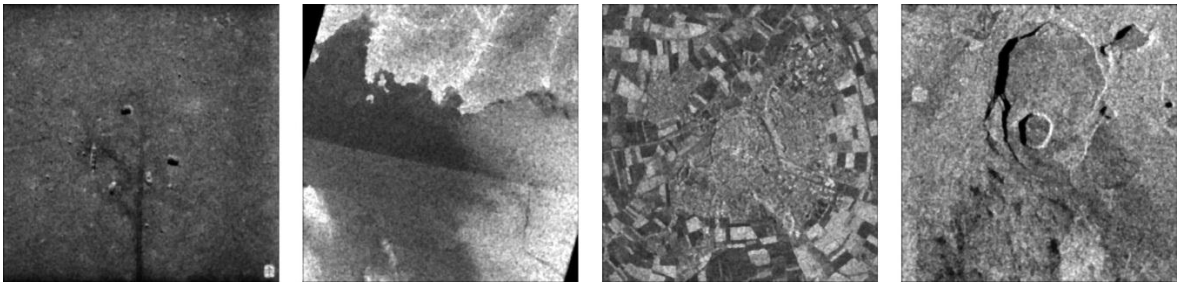

Figure 5.5 Results of Kuwahara filter.

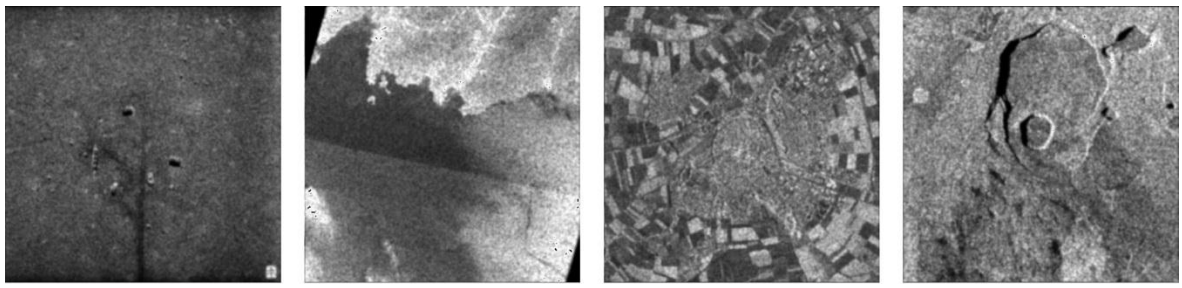

Figure 5.6 Results of Lee filter.

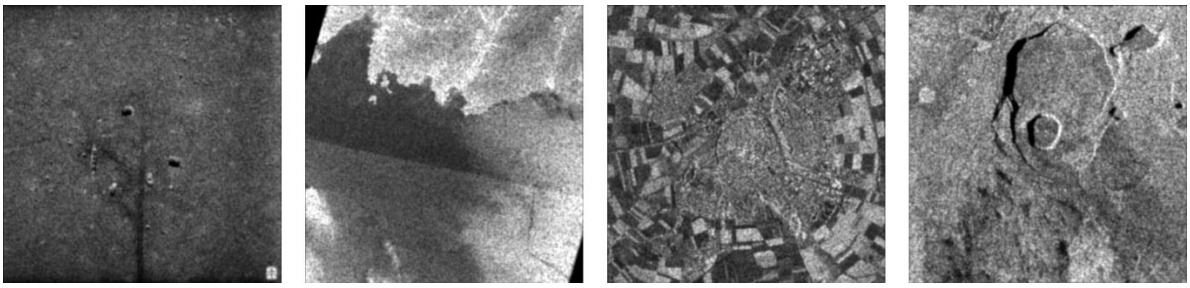

Figure 5.7 Results of SRAD.

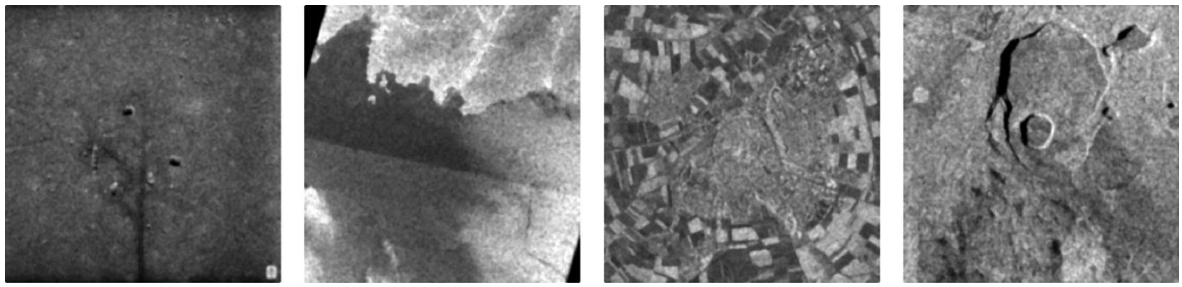

Figure 5.8 Results of HFLF.

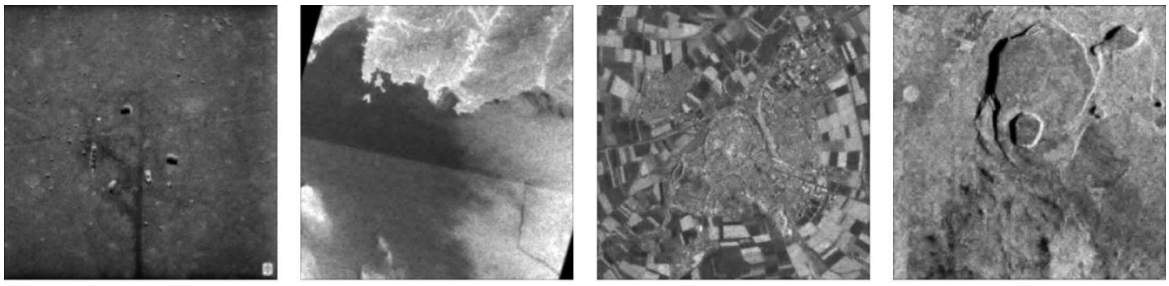

Figure 5.9 Results of HMN-AD

In terms of texture and edge preservation Kuan, Kuwahara and SRAD filter show the better results, fine details are preserved properly and not over-smoothed over the homogeneous areas. In the SAR4 image, the edges are well preserved by Kuan, Kuwahara and SRAD filter. The log compression and HFLF does not show good despeckling results as edges get distorted especially in the SAR1 image. The proper smoothing is not performed and the presence of speckle content can be observed in the despeckled images of log compression and

HFLF on zooming the image. The Frost filter performs better than lee filter, although the results of both methods are satisfactory but still there is a blurriness which can be seen in SAR1 and SAR2 image, but in rest two images, their results are better.

The Figure 5.2 – 5.9 shows the despeckling result in the simulated SAR image at $\sigma = 20$. The Figure 5.26 shows the despeckling results on the real speckled SAR image. The speckle distribution behavior in case of simulated SAR image is known but in real speckled SAR images, it is unknown. Therefore it is a tricky task to despeckle the real speckled SAR image as the speckle distribution is unknown.

On analyzing the despeckling results of HMN-AD in the SAR1 image, fine details and texture are well preserved, details are not blurred and smoothness is maintained in the homogeneous areas without the inclusion of any artifacts. In the SAR2 image, edges are well preserved and the visual appearance of the SAR3 and SAR4 image is best among all methods in respect of all parameters. The results of HMN-AD on SAR2 image shows that it can be used in various applications like wave forecasting, marine climatology, regional ice monitoring, and ship detection in the coastal regions, while the results of the SAR1, SAR3, and SAR4 of earth's land terrain area shows that it can also be used in field of agricultural and tropical forest monitoring.

The performance metrics (PSNR, SSIM, UIQI, and RMSE) are evaluated at different noise variances shown in Tables 5.1 – 5.4. The best results are shown in bold. On comparing Table 5.1 – 5.5, it is clear that the results of the HMN-AD are better than the standard despeckling methods. Table 5.1 and 5.2, shows a comparative table of various despeckling methods including a HMN-AD based on PSNR and UIQI respectively, while Table 5.3 and 5.4, based on UIQI and RMSE respectively. The results of Kuan and Kuwahara filters show the good performance results in terms of visual appearance of the image, but still, presence of artifacts and slight disturbance in edges can be seen there.

Table 5.1 PSNR of despeckled SAR images

		PSNR				
Image	Noise Variance	4	10	20	30	40
SAR1	Log Compression	36.647	36.0538	34.9534	33.9844	33.1368
	Frost	43.112	41.4352	39.0494	36.8906	34.9803
	Kuan	42.4187	41.3284	38.6061	37.3362	**37.1907**
	Kuwahara	40.4171	39.4169	37.7651	36.4102	35.2912
	Lee	42.4187	41.1534	39.0061	37.3362	34.1907
	SRAD	43.2369	40.9462	38.4532	37.9469	35.4101
	HFLF	38.5577	37.9848	36.7265	35.6321	34.7107
	HMN-AD	**43.7758**	**41.601**	**39.9001**	**38.4579**	36.6709
SAR2	Log Compression	36.1302	34.8258	32.9989	31.665	30.5224
	Frost	41.9545	38.2017	33.7232	31.5344	30.0437
	Kuan	33.5174	33.4021	32.7725	32.1921	31.4272
	Kuwahara	35.468	34.4955	32.9353	31.9244	30.8737
	Lee	35.7995	35.5979	34.5047	33.667	32.6689
	SRAD	40.4123	39.4624	35.0432	33.9467	32.1256
	HFLF	34.6708	33.7066	32.3736	31.3879	30.517
	HMN-AD	**42.7729**	**40.7504**	**37.0465**	**34.9169**	**32.8688**
SAR3	Log Compression	32.1007	31.5781	30.3034	29.8619	29.2327
	Frost	**41.1252**	36.4462	34.1957	32.0019	30.8811
	Kuan	36.125	35.4573	33.8029	34.1759	31.0092
	Kuwahara	33.9882	33.4617	32.0788	31.6396	30.9167
	Lee	38.125	36.4763	34.1123	33.9769	30.1694
	SRAD	29.0049	29.4843	32.2613	30.5044	30.2244
	HFLF	34.7756	34.0279	32.4083	31.8244	30.9849
	HMN-AD	39.2991	**36.9472**	**34.3189**	**34.9939**	**31.1602**
SAR4	Log Compression	31.8743	31.8187	30.1481	29.2254	28.4631
	Frost	36.8249	32.2271	31.1902	30.0011	29.0040
	Kuan	32.6358	34.4218	31.5743	29.9742	28.9994
	Kuwahara	32.9419	32.3182	31.2995	30.0035	29.0091
	Lee	33.6358	33.1421	31.5743	29.3073	28.9461
	SRAD	31.1452	31.0094	30.4683	28.4321	26.4414
	HFLF	32.6814	31.1111	31.0843	30.0037	29.5014
	HMN-AD	**36.9001**	**33.3331**	**31.9939**	**30.0272**	**29.9536**

Table 5.2 SSIM of despeckled SAR images

Image	Noise Variance	SSIM				
		4	10	20	30	40
SAR1	Log Compression	0.7186	0.7186	0.7106	0.7981	0.7589
	Frost	0.9676	0.9472	0.9296	0.8761	0.8247
	Kuan	0.9404	0.9414	**0.9597**	0.9117	0.9205
	Kuwahara	0.9443	0.9282	0.9008	0.8756	0.8539
	Lee	0.9304	0.936	0.9297	0.9151	0.9005
	SRAD	0.9642	0.9543	0.8962	0.9001	0.8911
	HFLF	0.9470	0.9276	0.8914	0.8573	0.8277
	HMN-AD	**0.9725**	**0.9691**	0.9358	**0.9229**	**0.9209**
SAR2	Log Compression	0.9215	0.9016	0.8456	0.8035	0.7752
	Frost	0.9605	0.9202	0.8272	0.7562	0.7102
	Kuan	0.9643	0.9270	0.9167	0.8901	0.8850
	Kuwahara	0.9405	0.9070	0.8638	0.8334	0.8113
	Lee	0.9644	0.9371	0.9248	0.8946	0.8851
	SRAD	0.9423	0.9231	0.9142	0.8991	0.8712
	HFLF	0.9495	0.9021	0.8449	0.8016	0.7723
	HMN-AD	**0.9749**	**0.9489**	**0.9252**	**0.9001**	**0.8914**
SAR3	Log Compression	0.8246	0.8274	0.7849	0.7512	0.7132
	Frost	0.9797	0.9344	0.8804	0.8258	0.7769
	Kuan	0.9260	0.9311	0.9150	0.8964	0.8864
	Kuwahara	0.9110	0.8965	0.8702	0.8498	0.8328
	Lee	0.9460	0.9211	0.9149	0.8925	0.8164
	SRAD	0.8848	0.9263	**0.9846**	0.8964	0.8764
	HFLF	0.9245	0.9009	0.8639	0.8325	0.8059
	HMN-AD	**0.9808**	**0.9377**	0.9211	**0.9085**	**0.8957**
SAR4	Log Compression	0.7946	0.7640	0.7177	0.6787	0.6522
	Frost	0.8912	0.8783	0.8424	0.7692	0.7244
	Kuan	0.9002	0.9237	0.8295	0.7692	0.8504
	Kuwahara	0.8877	0.8713	0.8428	0.8147	0.8022
	Lee	**0.9254**	0.8759	0.8659	0.8564	0.8491
	SRAD	0.8843	0.8613	0.8015	0.7751	0.7561
	HFLF	0.8833	0.8592	0.8174	0.7837	0.7599
	HMN-AD	0.9040	**0.9244**	**0.8758**	**0.8655**	**0.8529**

Table 5.3 UIQI of despeckled SAR images.

Image	Noise Variance	UIQI				
		4	10	20	30	40
SAR1	Log Compression	0.7349	0.7009	0.6763	0.6505	0.6268
	Frost	0.9001	0.8743	0.8631	0.8319	0.7804
	Kuan	0.9051	0.886	0.8315	**0.9151**	0.8701
	Kuwahara	0.8620	0.8568	0.8419	0.8258	0.8133
	Lee	0.8916	0.8863	0.8531	0.8452	0.8562
	SRAD	0.9004	0.8464	0.8345	0.8311	0.8312
	HFLF	0.8296	0.8168	0.7921	0.7676	0.7492
	HMN-AD	**0.9060**	**0.8952**	**0.8761**	0.8656	**0.8758**
SAR2	Log Compression	0.8185	0.8447	0.8033	0.7704	0.7539
	Frost	0.8715	0.8264	0.8001	0.7328	0.7006
	Kuan	0.8115	**0.9243**	0.8003	0.8124	0.8148
	Kuwahara	0.8615	0.8447	0.8204	0.8008	0.7902
	Lee	0.8156	0.8248	0.8248	0.8348	0.8153
	SRAD	0.8123	0.8001	0.8002	0.8124	0.8227
	HFLF	0.8401	0.8036	0.7690	0.7411	0.7276
	HMN-AD	**0.8773**	0.8458	**0.8384**	**0.8399**	**0.8228**
SAR3	Log Compression	0.8021	0.7805	0.7524	0.7295	0.7132
	Frost	0.9074	0.8946	0.8838	0.8376	0.7962
	Kuan	0.8962	0.8896	0.8846	0.8766	0.8562
	Kuwahara	0.8856	0.8776	0.8617	0.8480	0.8372
	Lee	0.8664	0.8567	0.8434	0.8764	0.8264
	SRAD	0.8846	**0.9061**	0.8912	0.8641	0.8162
	HFLF	0.8919	0.8723	0.8467	0.8227	0.8055
	HMN-AD	**0.9079**	0.9016	**0.8921**	**0.8804**	**0.8737**
SAR4	Log Compression	0.7412	0.7193	0.6882	0.6611	0.6502
	Frost	0.8611	0.8179	0.8516	0.7893	0.7544
	Kuan	0.8512	**0.8934**	**0.9320**	0.7896	0.7942
	Kuwahara	0.8562	0.8145	0.8439	0.8261	0.8156
	Lee	0.8612	0.8611	0.8421	0.8166	0.7944
	SRAD	0.8441	0.8292	0.8041	0.7760	0.7599
	HFLF	0.8572	0.8390	0.8075	0.7833	0.7667
	HMN-AD	**0.8681**	0.8648	0.8521	**0.8457**	**0.8375**

Table 5.4 RMSE of despeckled SAR images.

Image	Noise Variance	RMSE				
		4	10	20	30	40
SAR1	Log Compression	5.2637	5.6803	6.4474	7.2083	7.9472
	Frost	1.2712	1.8153	3.6273	5.1585	6.4275
	Kuan	2.7083	2.8144	3.3632	3.8926	4.4414
	Kuwahara	3.4102	3.8566	4.6645	5.4519	6.2015
	Lee	2.7008	2.8144	3.3632	3.8926	4.4498
	SRAD	0.9041	1.2352	1.3256	1.7432	2.4326
	HFLF	4.2242	4.548	5.2569	5.9628	6.6301
	HMN-AD	**0.0072**	**0.0094**	**0.0127**	**0.0151**	**0.0164**
SAR2	Log Compression	5.6305	6.5428	8.0744	9.4146	10.7383
	Frost	2.0386	4.4358	7.4284	9.5572	11.3467
	Kuan	7.6065	7.7081	8.2877	8.8604	9.676
	Kuwahara	6.0766	6.7964	8.1337	9.1377	10.3127
	Lee	5.849	5.9868	6.7892	7.4766	8.3871
	SRAD	0.8461	1.2034	2.1234	2.9846	3.1456
	HFLF	6.6606	7.4426	8.6772	9.7198	10.745
	HMN-AD	**0.0072**	**0.0116**	**0.0157**	**0.0201**	**0.0227**
SAR3	Log Compression	8.954	9.5093	10.5374	11.5867	12.4573
	Frost	2.5165	4.0846	6.7316	8.6661	10.3039
	Kuan	4.4751	4.8327	5.5914	6.4037	7.1715
	Kuwahara	7.2052	7.6554	8.5894	9.4422	10.2617
	Lee	4.4751	4.8328	5.5945	6.4307	7.1715
	SRAD	12.7882	12.1016	8.4109	10.7605	6.1712
	HFLF	6.5805	7.1723	8.2697	9.2438	10.1815
	HMN-AD	**0.0153**	**0.0178**	**0.0215**	**0.0245**	**0.0277**
SAR4	Log Compression	9.1905	9.9473	11.2113	12.4678	13.3374
	Frost	2.9229	4.9625	7.8985	10.194	11.8836
	Kuan	4.2195	4.825	6.0026	10.195	7.7929
	Kuwahara	8.1275	8.7326	9.8193	10.9531	11.9014
	Lee	4.2195	4.8254	6.0026	6.9453	7.7929
	SRAD	2.2951	3.1375	3.9467	4.6742	5.9919
	HFLF	8.375	8.9423	10.0656	11.1012	12.0777
	HMN-AD	**0.0218**	**0.0241**	**0.0282**	**0.0315**	**0.0348**

On applying all the methods on the SAR1 image, it is observed that at noise variance level 40, Kuan filter shows the best results in terms of PSNR, while in rest of the noise variances, HMN-AD shows the best results. On SAR2 image, HMN-AD shows the best results in terms of PSNR and SSIM. On the SAR3 image, frost filter shows better results at low variance level i.e. 4 in terms of PSNR. SRAD shows better results at variance level 20 in terms of SSIM, while in rest cases in terms of PSNR and SSIM, HMN-AD shows the best results as depicted in Table 5.1 and 5.2. In the SAR1 image, Kuan filter shows good result at noise level 30 in terms of UIQI. In the SAR2 image, again Kuan filter shows good result at variance level 10 in terms of UIQI. In the SAR3 image, SRAD method shows better result at variance level 10 in terms of UIQI. In SAR4 image Kuan filter shows good result at noise variance level 10 and 20 in terms of UIQI. On comparing Kuan and HMN-AD in terms of UIQI, the HMN-AD is better in 80 percent of the cases while Kuan shows best results in almost all the rest cases. The results of the HMN-AD are far better than other methods in terms of RMSE. The RMSE value should be as low as possible and RMSE value of the HMN-AD is evaluated very low than others, thus PSNR also shows better results. For easy understanding and analysis, the PSNR value of the despeckled SAR images is graphically analyzed in the Figure 5.10 – 5.13. The SSIM value of the despeckled SAR images is graphically analyzed in the Figure 5.14 – 5.17. The UIQI value of the despeckled SAR images is graphically analyzed in the Figure 5.18 – 5.21. The RMSE value of the despeckled SAR images is graphically analyzed in the Figure 5.22 – 5.25.

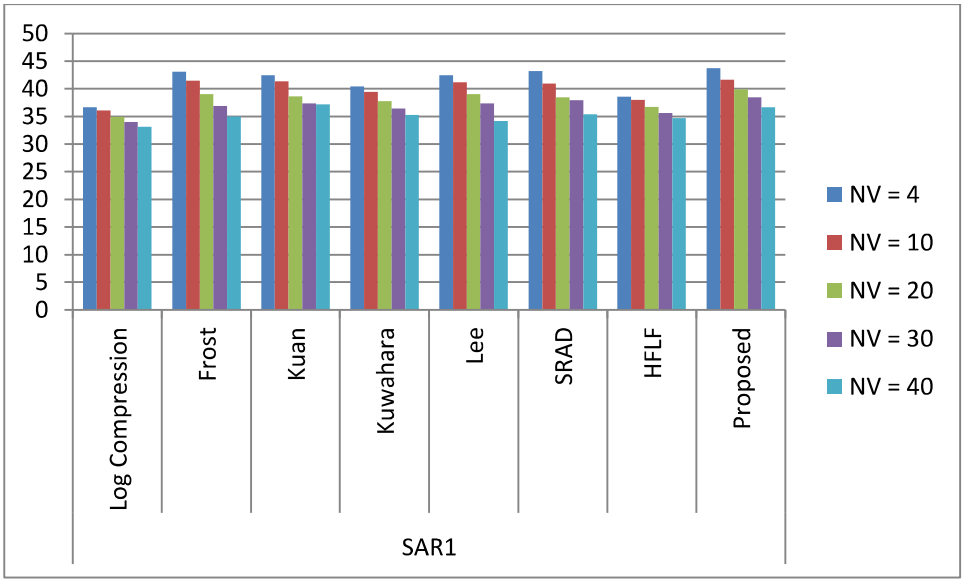

Figure 5.10 PSNR of despeckled SAR image 1

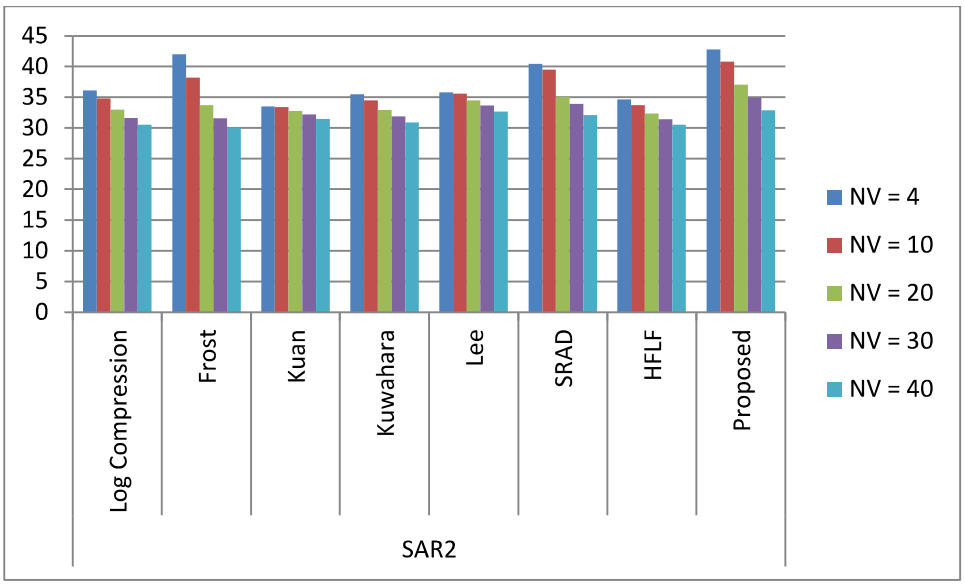

Figure 5.11 PSNR of despeckled SAR image 2

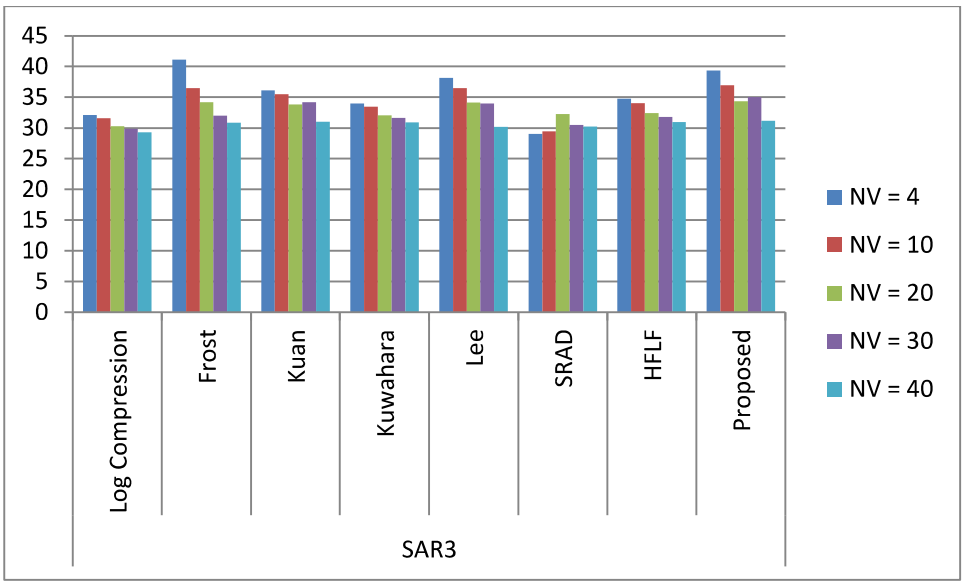

Figure 5.12 PSNR of despeckled SAR image 3

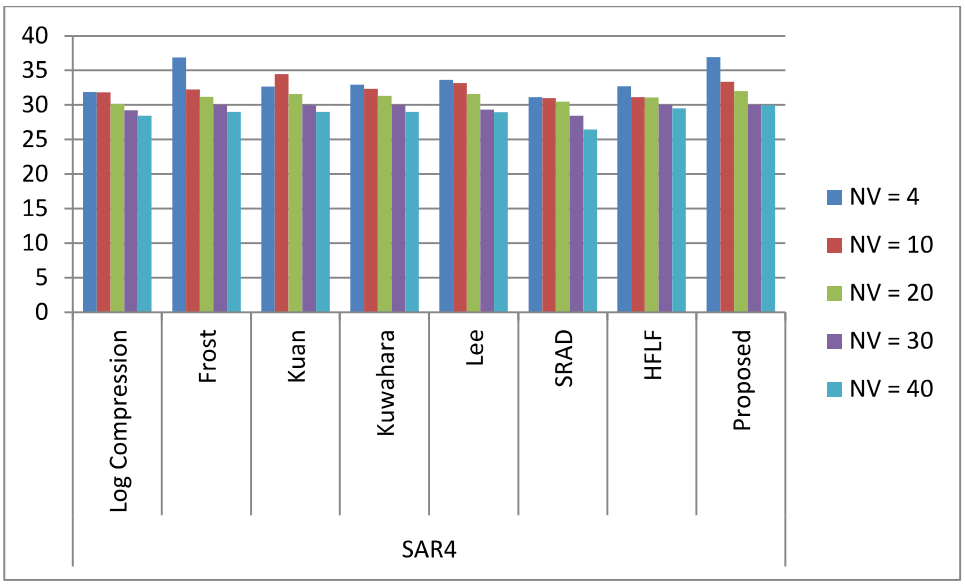

Figure 5.13 PSNR of despeckled SAR image 4

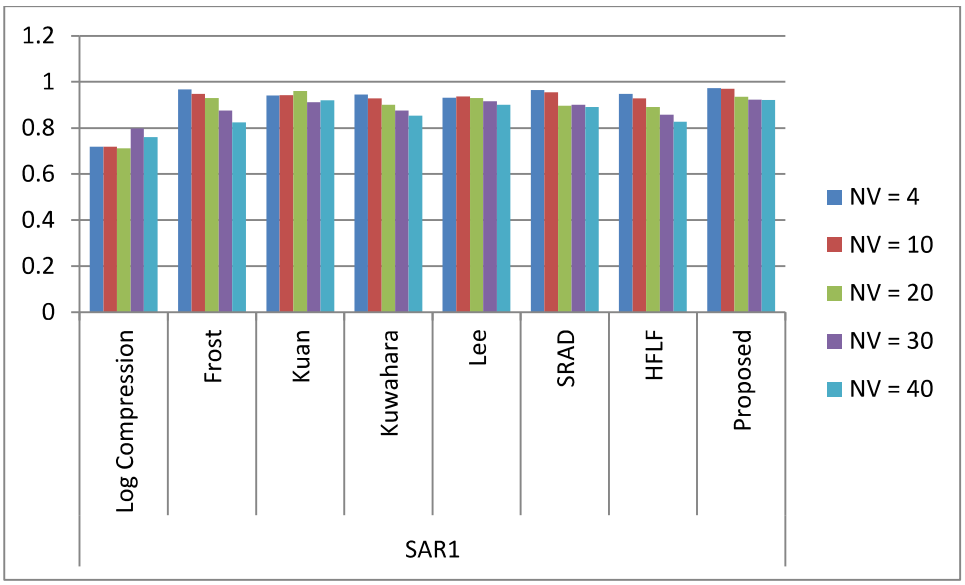

Figure 5.14 SSIM values of despeckled SAR image 1

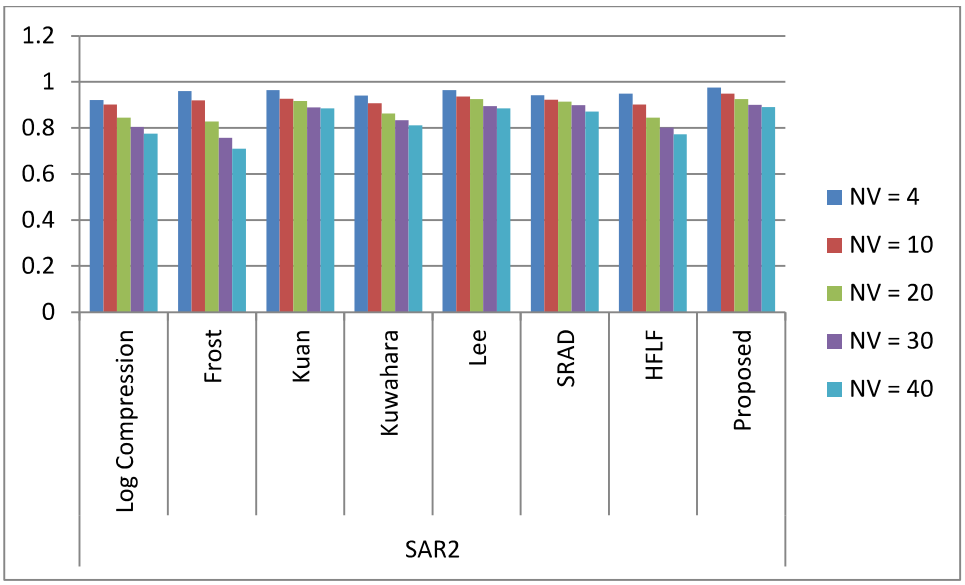

Figure 5.15 SSIM values of despeckled SAR image 2

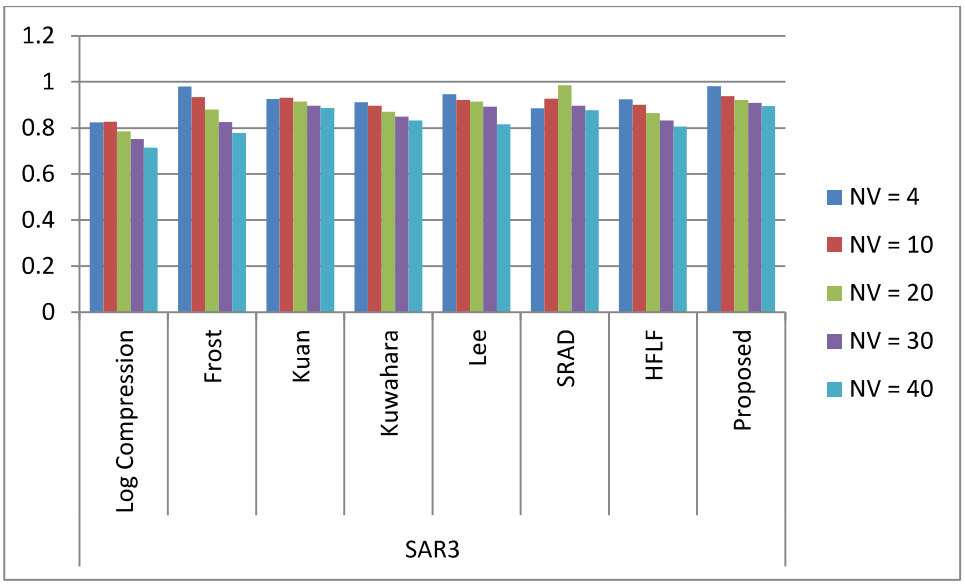

Figure 5.16 SSIM values of despeckled SAR image 3

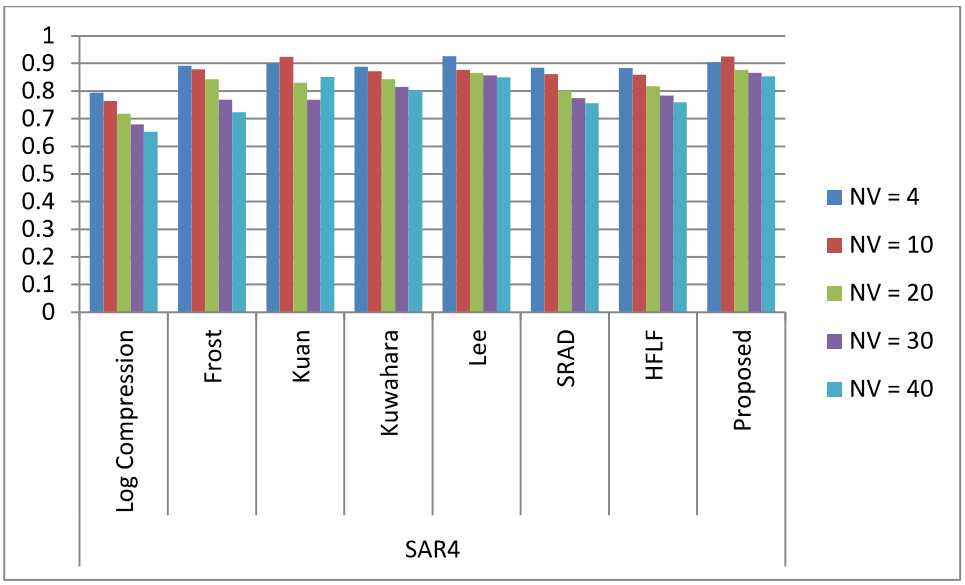

Figure 5.17 SSIM values of despeckled SAR image 4

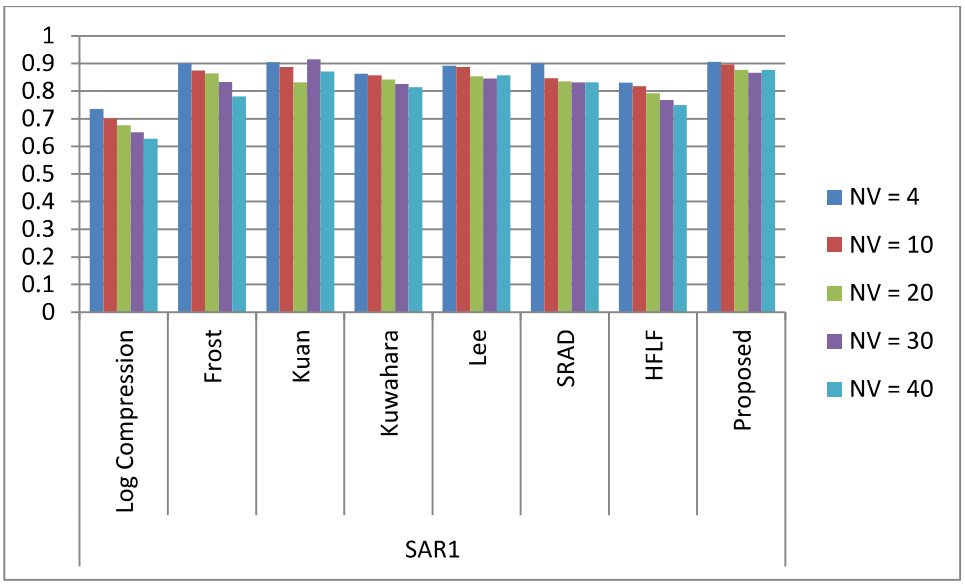

Figure 5.18 UIQI values of despeckled SAR image 1

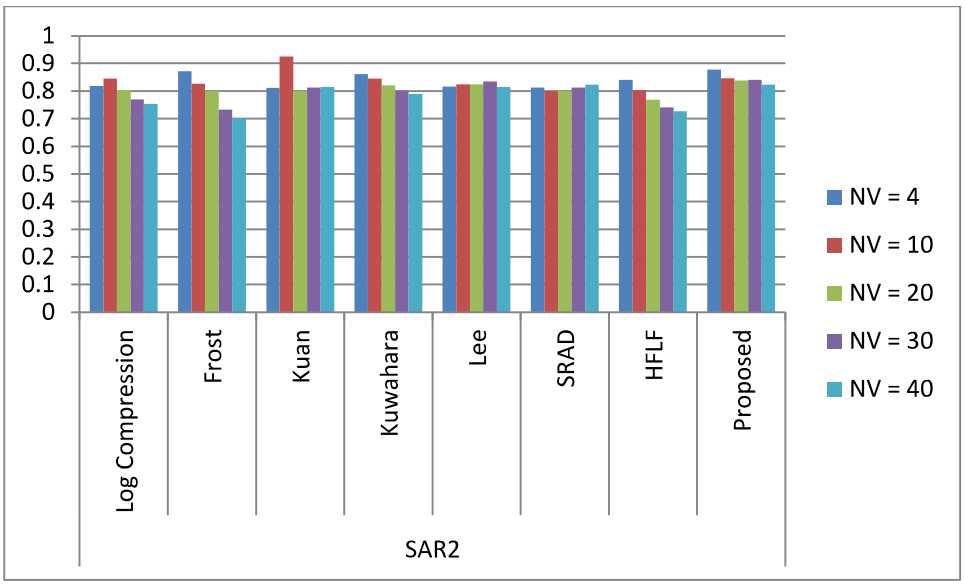

Figure 5.19 UIQI values of despeckled SAR image 2

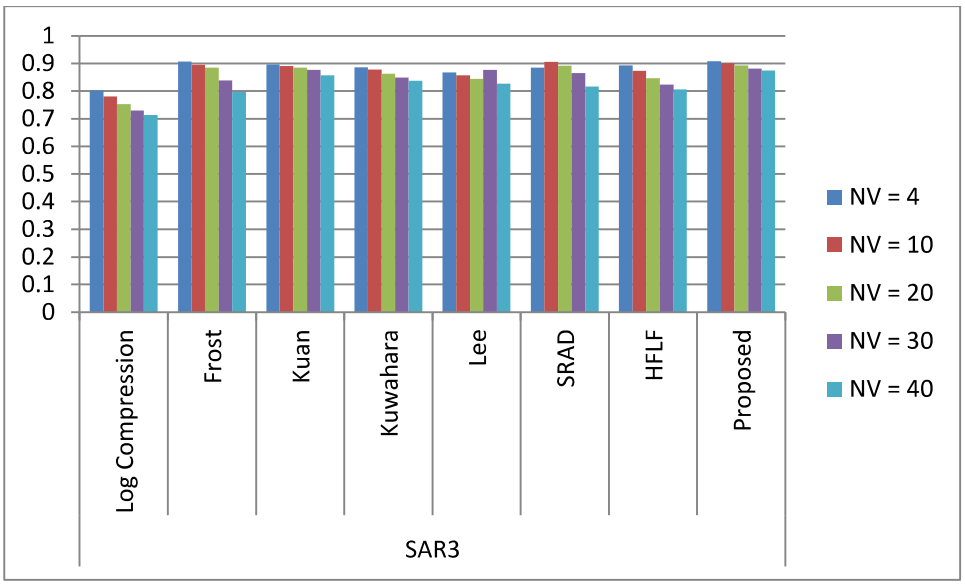

Figure 5.20 UIQI values of despeckled SAR image 3

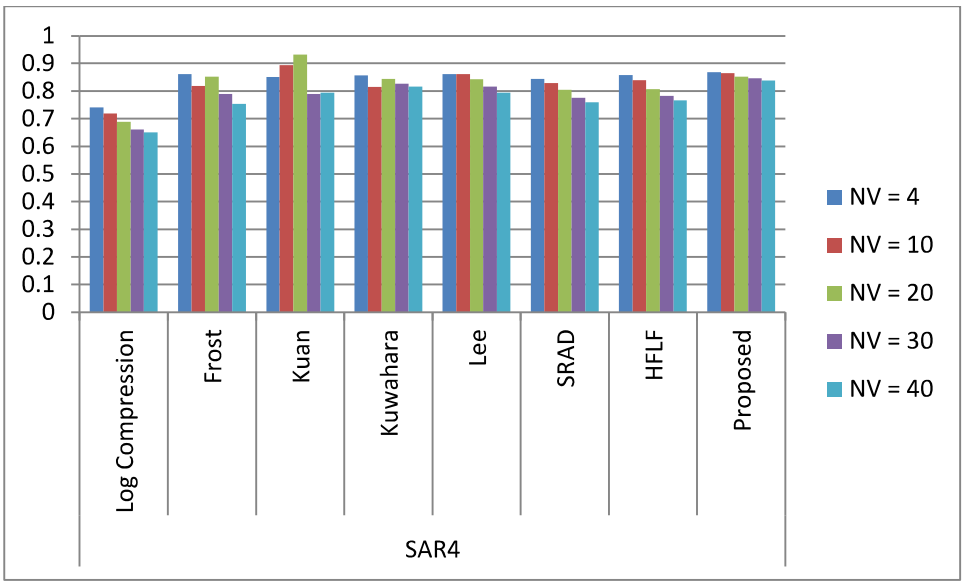

Figure 5.21 UIQI values of despeckled SAR image 4

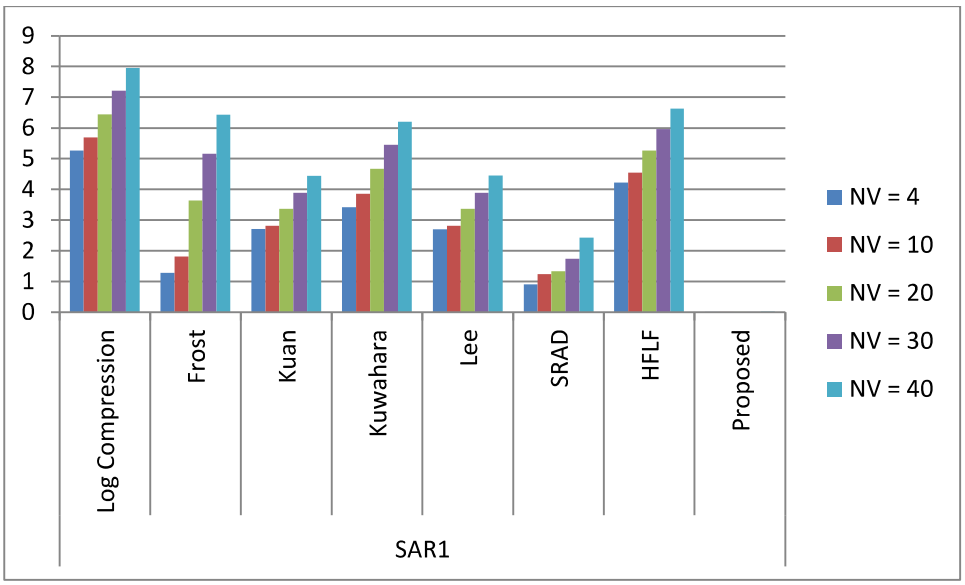

Figure 5.22 RMSE values of despeckled SAR image 1

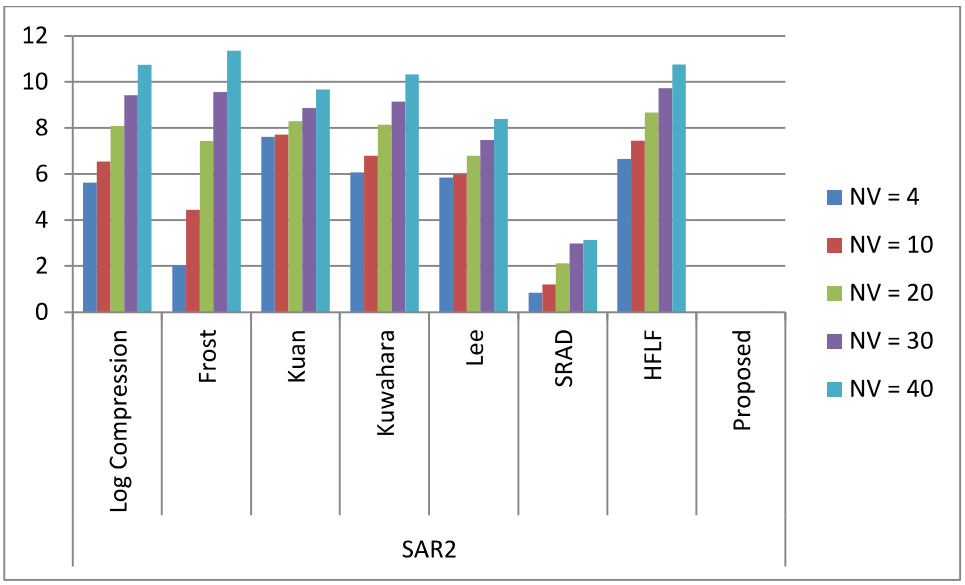

Figure 5.23 RMSE values of despeckled SAR image 2

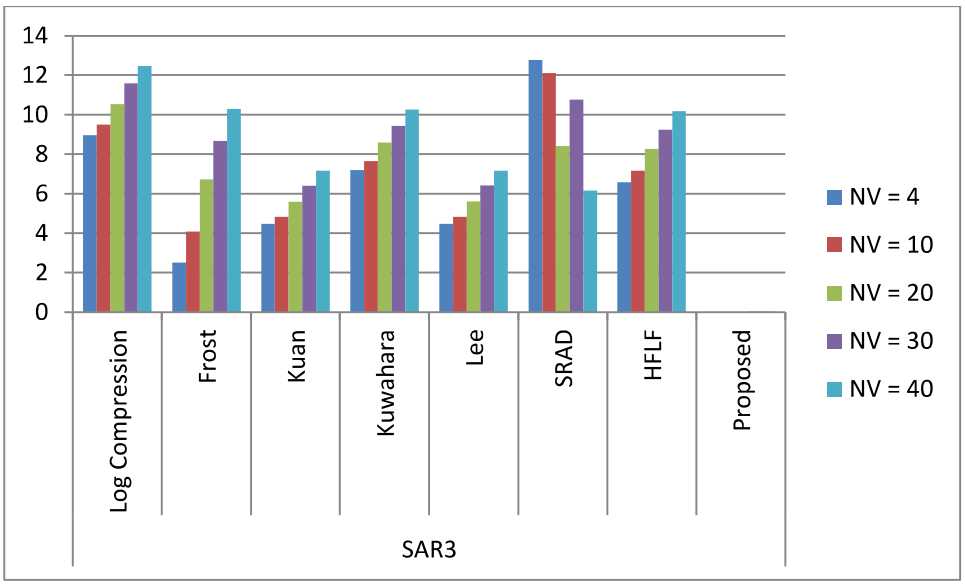

Figure 5.24 RMSE values of despeckled SAR image 3

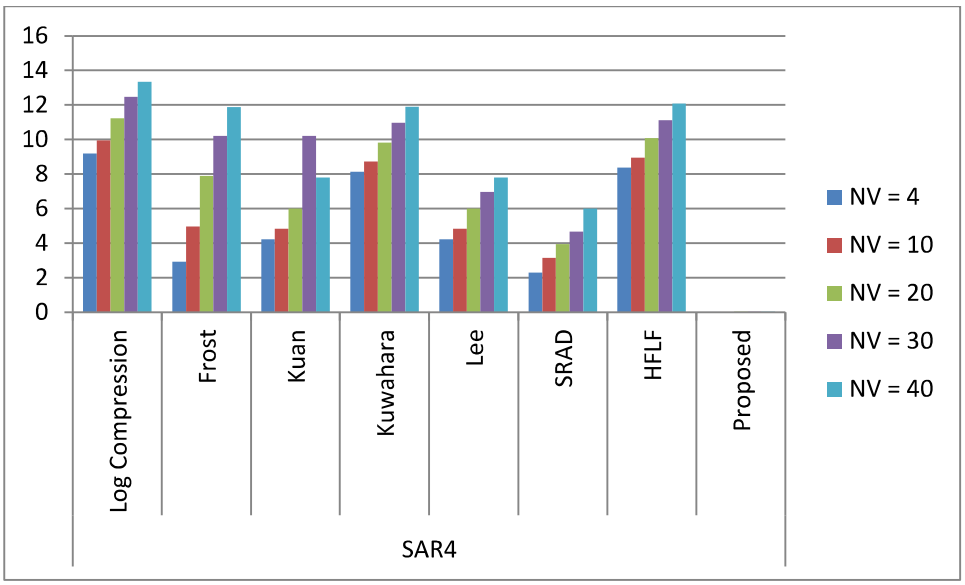

Figure 5.25 RMSE values of despeckled SAR image 4

The performance percentage of HMN-AD is evaluated by analyzing the quantitative values at different noise variance levels in Table 5.1 – 5.4. There are 20 cases each for every metrics. There are 4 metrics used for performance evaluation. Therefore there are total 80 cases, over which the HMN-AD is compared with other standard work. Out of 80 cases, the HMN-AD shows better results in 70 cases. So, the performance percentage of the HMN-AD is 87.50 %.

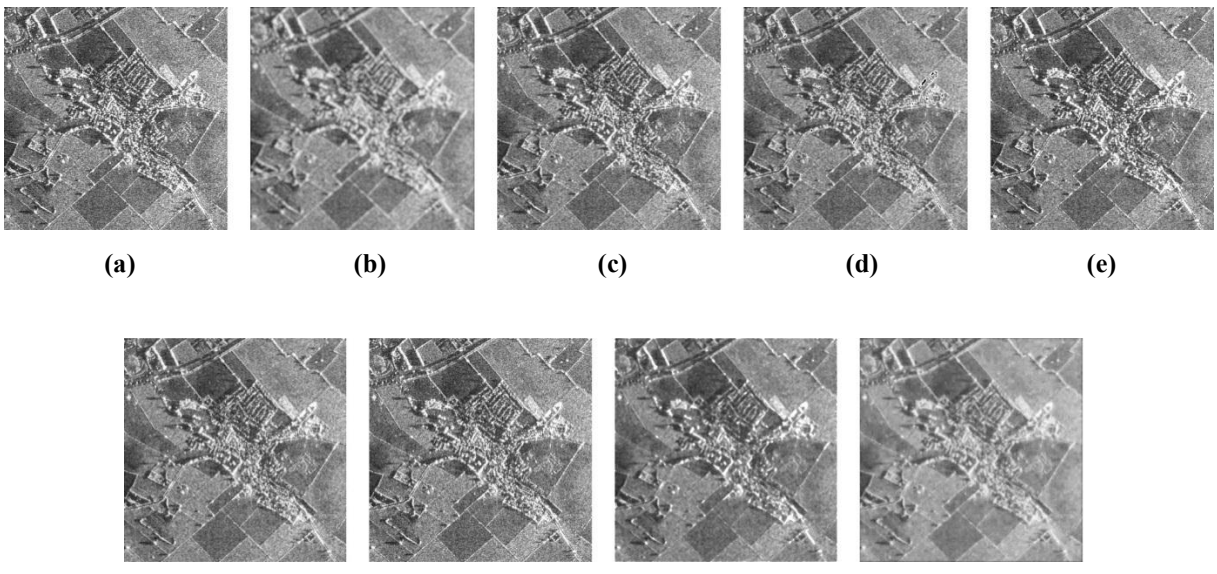

(a) **(b)** **(c)** **(d)** **(e)**

(f) **(g)** **(h)** **(i)**

Figure 5.26 Analysis on real speckled SAR image: (a) real speckled SAR image; (b) result of Log compression; (c) result of Frost; (d) result of Kuan; (e) result of Kuwahara; (f) result of Lee; (g) result of SRAD; (h) result of HFLF; and (i) result of HMN-AD.

Figure 5.26 shows the comparative result of HMN-AD with other standard works on real speckled SAR image. The visual quality of despeckled image of HMN-AD is better than other methods in terms of edge and texture preservation and smoothness in homogeneous areas. For critically analyzing the HMN-AD, Figure 5.27 shows the intensity profile of line on the SAR1 image. Figure 5.27 critically analyses and compares the HMN-AD with the standard despeckling methods. The accurate overlapping of two waves shows that HMN-AD delivers the best result. The method is further analyzed by plotting the histogram of the full reference image and despeckled image on the same plot in Figure 5.28. Again overlapping of two histograms is shown at different noise variances to check the impact of the HMN-AD. It can be observed that even at noise variance = 40, the HMN-AD shows descent despeckling result.

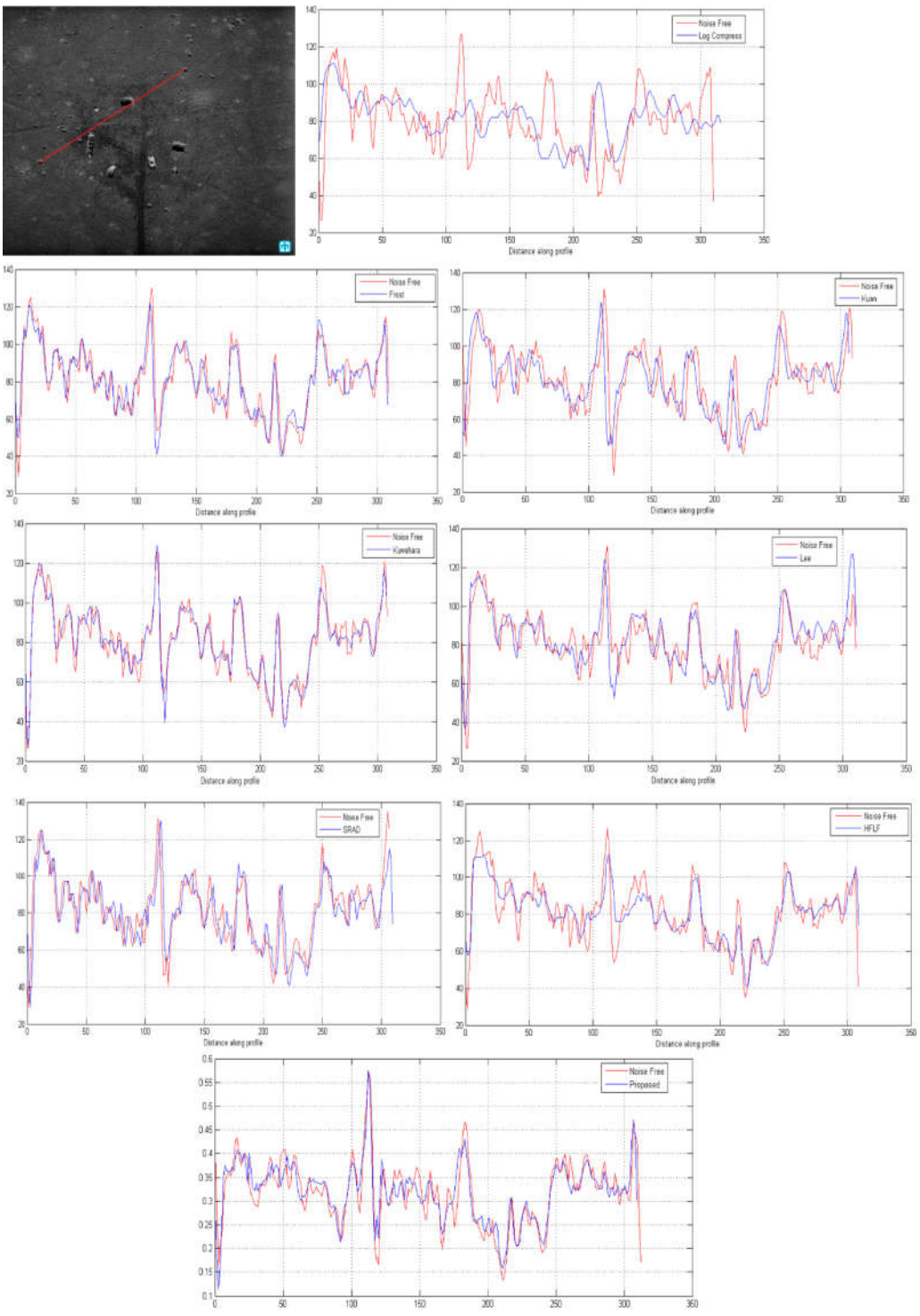

Figure 5.27 Intensity profile of a line on the SAR1 image. In each plot, the noise-free intensity profile is plotted in red and despeckled profile is plotted in blue.

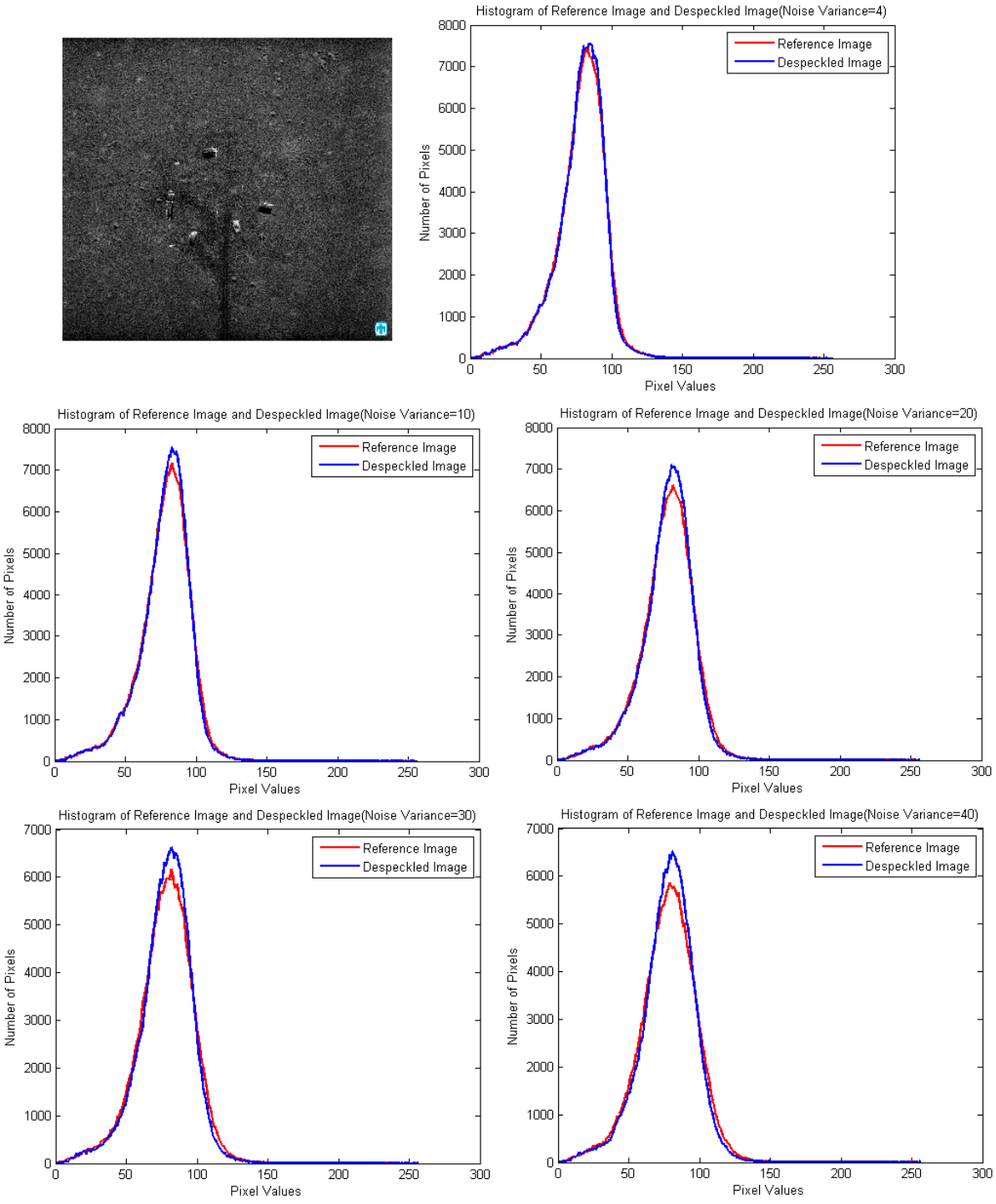

Figure 5.28 Histogram of the reference image and despeckled image at different noise variance level on the SAR2 image using the proposed method. In each plot, reference image is plotted in red and despeckled image is plotted in blue.

5.2.3 Execution Time Comparison

Apart from evaluating a despeckled image based on visual appearance and quantitative metrics, the computational time is also one important factor for performance evaluation. The computational time of the HMN-AD is shown in comparative Table 5.5 and graphically analyzed in Figure 5.29. It can be observed from the Table 5.5 that the HMN-AD takes comparatively less computational time than Frost, Kuan, Kuwahara, lee, and SRAD but slightly more time than Log compression and HFLF. Although the computational time is slightly more than Log compression and HFLF, still HMN-AD displays better results than these two. So, more execution time than Log compression and HFLF doesn't underrate the proposed method. The computational time of the algorithm depends upon the number of iteration involved in the execution. So, it is better to check the algorithm at a maximum number of iterations and then later resolve the issue by fixing the values of inner parameters to perform the proposed method iteratively. The results may be get changed by changing the inner parameter values of the proposed method.

Table 5.5 Execution time of different despeckling techniques

Despeckling Methods	Log compression	Frost	Kuan	Kuwahara	Lee	SRAD	HFLF	HMN-AD
Time (in seconds)	2.0034	17.5055	24.6968	25.0012	36.6120	4.1567	1.7898	3.2136

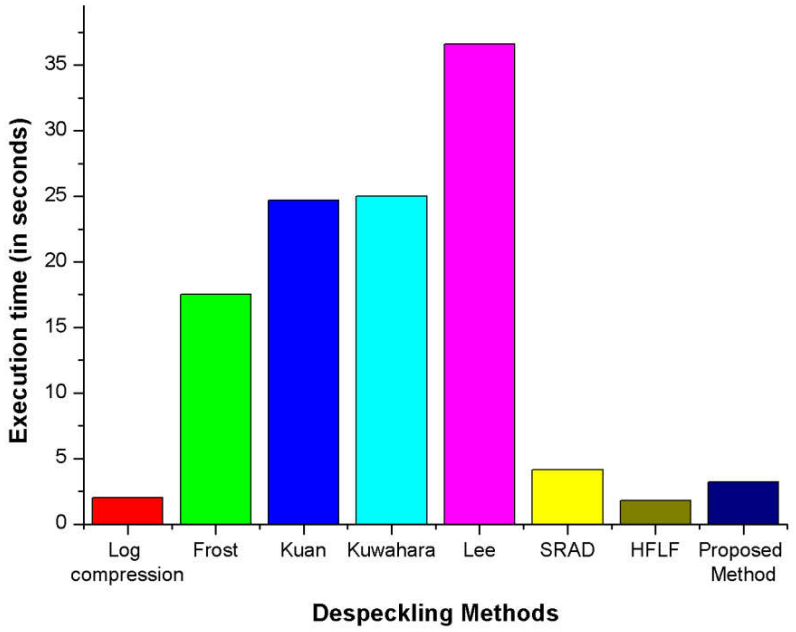

Figure 5.29 Execution time of different despeckling techniques (in seconds).

5.2.4 Validation of HMN-AD: Hypothesis Testing using Paired T-Test.

The proposed method i.e. HMN-AD is validated using paired T-test based on the defined hypothesis testing. The hypothesis testing can be performed by three different tests: Chi test, T-test, and Z-test. The HMN-AD is validated using T-test over 60 numbers of samples. The HMN-AD is experimented using different metrics like PSNR, SSIM, UIQI, and RMSE at different noise variances over four different SAR images. Based on the experimented results over the different SAR images as shown in Table 5.6 of dataset 1, the experimented sample data is collected and tested using hypothesis testing based on paired T-test.

There is total of 60 numbers of experimented sample data collected using the PSNR, SSIM, and UIQI at different noise variances (σ = 4, 10, 20, 30, 40). This data is collected by performing the experiment over four different SAR images. The RMSE values are not included in the results as MSE is the part of the PSNR. The related sample data is the quantitative values of the SAR image before and after despeckling. The level of significance is set to 5.

The following null and alternate hypothesis needs to be tested: The H_o denotes the null hypothesis and H_a denotes the alternate hypothesis.

$H_o: \mu_D = 0$ (There is no difference between SAR image before and after despeckling in terms of quality, i.e. “No despeckling”)

$H_a: \mu_D \neq 0$ (There is a difference between SAR image before and after despeckling in terms of quality, i.e. “Good despeckling”)

Table 5.6 Dataset 1

No. of Samples	Values before Despeckling (X_i)	Values after Despeckling(Y_i)	Difference ($D_i=X_i - Y_i$)
1.	25.1588	43.7758	-18.617
2.	22.1475	41.6010	-19.4535
3.	19.1526	39.9001	-20.7475
4.	17.3726	38.4579	-21.0853
5.	16.2027	36.6709	-20.4682
6.	16.5492	42.7729	-26.2237

7.	14.5746	40.7504	-26.1758
8.	12.1826	37.0465	-24.8639
9.	11.6207	34.9169	-23.2962
10.	11.5692	32.8688	-21.2996
11.	22.3314	39.2991	-16.9677
12.	14.4002	36.9472	-22.547
13.	15.4900	34.3189	-18.8289
14.	13.8670	34.9939	-21.1269
15.	12.7947	31.1602	-18.3655
16.	20.2091	36.9001	-16.691
17.	17.3042	33.3331	-16.0289
18.	14.4775	31.9939	-17.5164
19.	12.8544	30.1272	-17.2728
20.	11.7723	29.9536	-18.1813
21.	0.6281	0.9725	-0.3444
22.	0.4682	0.9691	-0.5009
23.	0.3144	0.9358	-0.6214
24.	0.2380	0.9229	-0.6849
25.	0.1950	0.9209	-0.7259
26.	0.3292	0.9749	-0.6457
27.	0.1875	0.9489	-0.7614
28.	0.1149	0.9252	-0.8103
29.	0.0863	0.9001	-0.8138
30.	0.0696	0.8914	-0.8218
31.	0.7058	0.9808	-0.275
32.	0.5311	0.9377	-0.4066
33.	0.3925	0.9211	-0.5286
34.	0.3112	0.9085	-0.5973
35.	0.2622	0.8957	-0.6335
36.	0.7895	0.9040	-0.1145
37.	0.6575	0.9244	-0.2669
38.	0.4959	0.8758	-0.3799

39.	0.3992	0.8655	-0.4663
40.	0.3364	0.8529	-0.5165
41.	0.6409	0.9060	-0.2651
42.	0.4305	0.8952	-0.4647
43.	0.2834	0.8761	-0.5927
44.	0.2118	0.8656	-0.6538
45.	0.1715	0.8758	-0.7043
46.	0.2134	0.8773	-0.6639
47.	0.1270	0.8458	-0.7188
48.	0.0812	0.8384	-0.7572
49.	0.0616	0.8399	-0.7783
50.	0.0511	0.8228	-0.7717
51.	0.6879	0.9079	-0.22
52.	0.5550	0.9016	-0.3466
53.	0.4195	0.8921	-0.4726
54.	0.3373	0.8804	-0.5431
55.	0.2862	0.8737	-0.5875
56.	0.7569	0.8681	-0.1112
57.	0.6724	0.8648	-0.1924
58.	0.5104	0.8521	-0.3417
59.	0.4109	0.8457	-0.4348
60.	0.3464	0.8375	-0.4911
n = 60			$\sum \mathrm{D_i} = 426.7842$

As calculated from the above sample data, the corresponding sample means are $\overline{X_i}$=5.6130 and $\overline{Y_i}$=12.7260 and the calculated sample standard deviation are s_1=7.8090 and s_2=17.0360. The mean of difference ($\overline{D}$) and standard deviation of difference (σ_{diff}) are calculated using below two equation respectively.

$$\overline{D} = \frac{\sum D_i}{n} = -7.1130$$

$$\sigma_{diff} = \sqrt{\frac{\sum D_i^2 - (\overline{D})^2 * n}{n-1}} = 9.5570$$

Depending on the information available, the significance level is $\alpha = 0.05$, and the degree of freedom (df) = n – 1 = 59.

Hence, it is found that the critical value for this two-tailed test is

$t_c = 2.001$, for $\alpha = 0.05$ and df = 59.

The rejection region for this two-tailed test is $R = \{ t : | t | > 2.001\}$.

The t-statistic is calculated as shown in the following formulation:

$$t = \frac{\overline{D}}{\sigma_{diff}/\sqrt{n}} = \frac{-7.113}{9.557/\sqrt{60}} = -5.765$$

Since it is observed that $| t | = 5.765 > t_c = 2.001$. It is concluded that the null hypothesis H_o is rejected. Therefore, there is enough evidence to claim that the difference of quantitative values before and after despeckling is considered to be extremely statistically significant, at the 0.05 significance level.

5.3 Result and Analysis of HMN-DSF: A New Homomorphic SAR Image Despeckling using Directional Smoothing Filter and Method Noise Thresholding

The proposed method i.e. HMN-DSF is experimented on simulated as well as real speckled SAR image. In simulated SAR image experiment, the speckle generation is performed through multiplicative speckle noise model. Here the speckle noise is uniformly distributed in the SAR image. The noise distribution in the real speckled SAR images is unknown. The concept despeckling of simulated speckled SAR images was discussed in [68], [69]. The purpose of showing result in the simulated SAR images is to test the effectiveness, validity and adaptive feature of the HMN-DSF in different situations at different noise variances. The reference SAR image at noise variance (σ) = 20 is shown in Figure 5.30 and real speckled SAR image is shown in Figure 5.35(a). The HMN-DSF is experimented at various noise variance levels i.e. (σ = 5; 10; 20; 30; 40). The Figure 5.31 shows the comparative experimental results of HMN-DSF at noise variance level, $\sigma = 20$.

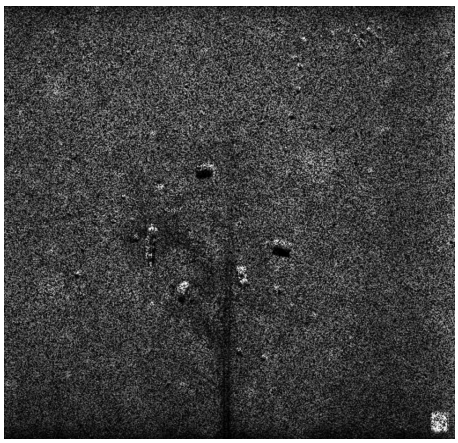

Figure 5.30 Reference speckled SAR image (σ = 20)

The experiment is performed on speckled SAR image at size 512 × 512 to validate the efficiency of the HMN-DSF for the quantitative and qualitative evaluation. It also helps in advancing the computational complexity of the HMN-DSF. The standard filters and techniques used for comparison are Frost filter, homomorphic Frost filter, Kuan filter, homomorphic Kuan filter, Refined-Lee filter, homomorphic Refined-Lee filter, Kuwahara filter, Median filter, SRAD, soft thresholding, hard thresholding, universal thresholding, visu thresholding, Bayesian thresholding, Bivariate Cauchy based MAP (BCMAP) [32], Multivariate Cauchy MAP (MCMAP) [31], ATV [72], H-BM3D [73], H-PPB [73], coarse filtering [74], DSF, NLM filter and refined filtering [74]. The window size used in DSF is fixed at [3×3] in a non-overlapping fashion.

5.3.1 Performance Evaluation

The HMN-DSF despeckle the SAR image in both the cases: with and without reference indexes. In order to overcome the restrictions of the visual evaluation, numerous other objective performance measures have been suggested in the literature for the quality assessment of the despeckling filters [66], [36]. They are mainly divided into two classes: with and without reference indexes [36]. In the first case (with-reference indexes) it is believed that the actual reflectivity (information) or ground truth is known and the performance of the despeckled image is evaluated by comparing it with the reference image. In the second case (without-reference indexes), the whole knowledge of true reflectivity (ground truth) is not known. The performance metrics used in the case of without-reference indexes are based on the statistical model of multiplicative SAR noise model and the degree of heterogeneity of the underlying scene. The performance metrics used in the first case are PSNR, SSIM and UIQI, while in the second case, the metrics used are Equivalent Numbers

of Looks (ENL), Noise Variance (NV), Coefficient of Variation (CV) and Mean-squared Error (MSE).

5.3.2 Experimental Evaluation and Comparison

Case 1: With-Reference Indexes

Figures 5.31(a-x), shows the comparative despeckling result of Frost filter, homomorphic Frost filter, Kuan filter, homomorphic Kuan filter, Refined-Lee filter, homomorphic Refined-Lee filter, Kuwahara filter, Median filter, SRAD, soft thresholding, hard thresholding, universal thresholding, Visu thresholding, Bayesian thresholding, BCMAP, MCMAP, ATV [72], H-BM3D [73], H-PPB [73], coarse filtering [74], refined filtering [74], DSF, NLM filter and HMN-DSF respectively. There are some specific parameters for analyzing the quality of despeckled SAR image through their visual appearances such as (i) presence of the artifacts; (ii) edge preservation; (iii) visibility of low contrast objects (iv) texture preservation and (v) preservation of smoothness in homogeneous and non-homogeneous regions. The performance metrics like PSNR, SSIM and UIQI are evaluated at different noise variances shown in Table 5.7, 5.8 and 5.9 for simulated SAR images. The best quantitative values are specified in bold in Table 5.7, 5.8 and 5.9. Table 5.7, 5.8 and 5.9, shows the validation and effectiveness of HMN-DSF among best despeckling techniques. BCMAP, MCMAP, ATV, H-BM3D, H-PPB, coarse filtering and refined filtering that are advanced works in the field of SAR image despeckling and on comparing the HMN-DSF with these work, it shows better results in terms of overall texture preservation. The PSNR value of the despeckled SAR images is graphically analyzed in the Figure 5.32. The SSIM value of the despeckled SAR images is graphically analyzed in the Figure 5.33.

(a) **(b)** **(c)**

(d) **(e)** **(f)**

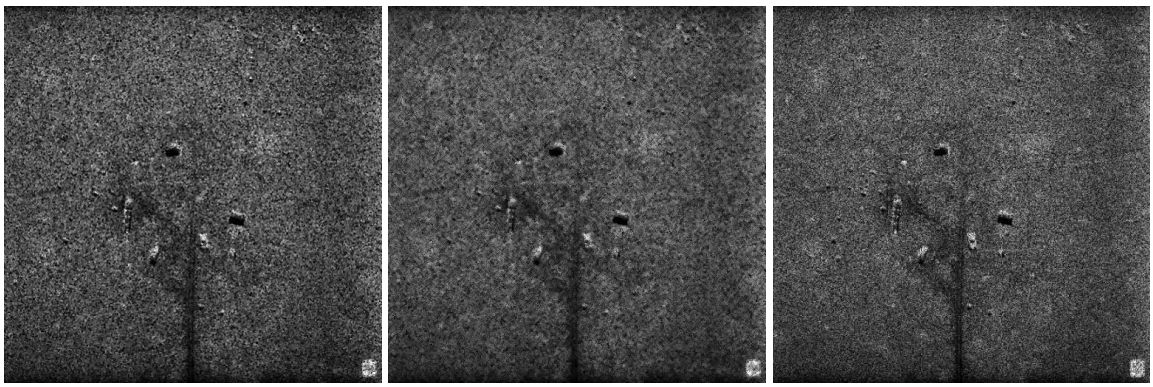

(g) **(h)** **(i)**

(j) **(k)** **(l)**

(m)

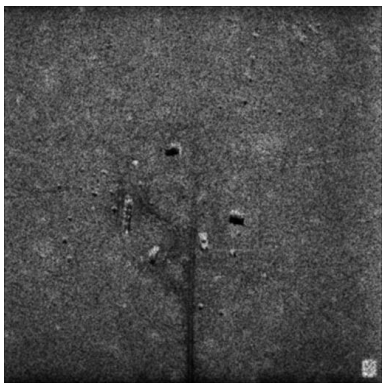

(n)

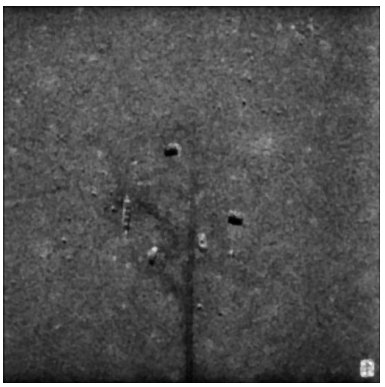

(o)

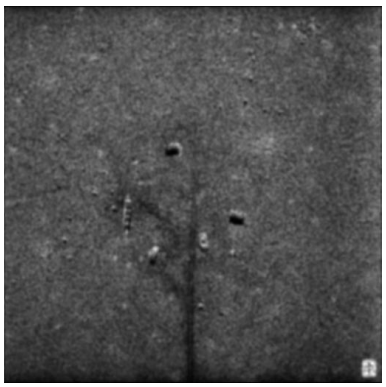

(p)

(q)

(r)

(s)

(t)

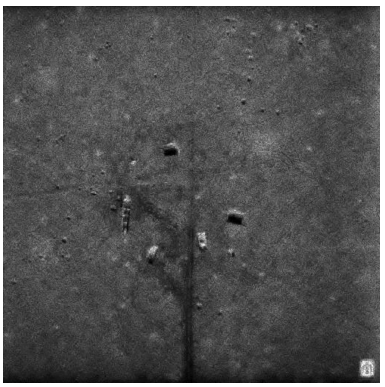

(u)

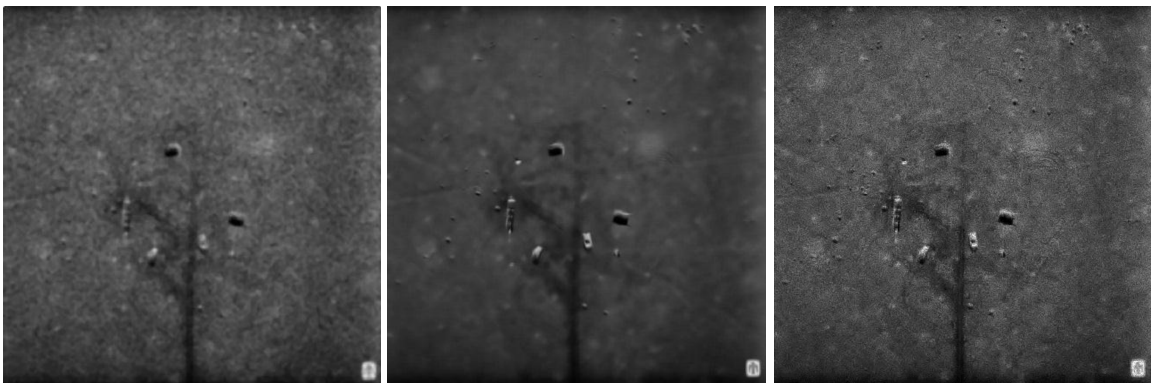

(v) (w) (x)

Figure 5.31 Results of despeckling algorithm on simulated SAR Image (a) result of Frost filter (b) result of homomorphic Frost filter (c) result of Kuan filter (d) result of homomorphic Kuan filter (e) result of Refined-Lee filter (f) result of homomorphic Refined-Lee filter (g) result of Kuwahara filter (h) result of Median filter (i) result of SRAD (j) result of Soft thresholding (k) result of Hard thresholding (l) result of Universal thresholding (m) result of Visu thresholding (n) result of Bayesian thresholding (o) result of BCMAP (p) result of MCMAP (q) result of ATV (r) result of H-BM3D (s) result of H-PPB (t) result of Coarse filtering (u) result of Refined filtering (v) result of DSF (w) result of NLM filter (x) result of HMN-DSF

Out of all compared methods, BCMAP, MCMAP, ATV, H-BM3D, H-PPB, coarse filtering and refined filtering are close to HMN-DSF. The Bayesian thresholding, soft thresholding, and SRAD also show decent performance in terms of quantitative analysis. ATV and refined filtering preserve the edges better. In terms of PSNR, at lesser speckled images, the refined filtering shows the better results in terms no artifact generation and texture preservation mainly at σ = 5 and 10. Coarse filtering and H-PPB shows better results and preserves the texture and generate no artifacts at σ = 30. In the case of average and highly speckled images, HMN-DSF shows the best result and maintains the smoothness and generates no artifacts. The edges are well preserved by the HMN-DSF that can be visually analyzed in Figure 5.31(x). In terms of SSIM, HMN-DSF shows the better result in lesser speckled and average speckled SAR images specifically at σ =5, 20 and 30. The low contrast objects can be easily identified in the despeckling results of the HMN-DSF; fine details are well preserved that validates the effectiveness of HMN-DSF. At σ =10 and 40, ATV and refined filtering show the better performance respectively. The quantitative and qualitative results of these two methods are close to the HMN-DSF. The preservation of the low contrast objects and object

structure preservation is also seen in the results of ATV and refined filtering. The DSF and NLM filter also shows the decent result in terms of speckle reduction and smoothness in the homogeneous region.

In terms of UIQI, the HMN-DSF depicts the best correlation between despeckled and reference SAR image. At σ = 10, 30 and 40, the HMN-DSF outperforms all the other compared methods, even at other noise variances the results are fairly good. Refined filtering at lesser noise σ =5, shows the better despeckling result and H-PPB at σ = 20, shows the better result. The DSF and NLM also give competitive results in terms of UIQI. The structure preservation at the high contrast areas is high. The UIQI value of the despeckled SAR images is graphically analyzed in the Figure 5.34.

On comparing the HMN-DSF with other 23 conventional and non-conventional despeckling methods, the visual appearance of BCMAP, MCMAP, ATV, H-BM3D, H-PPB, coarse filtering and refined filtering are close to the HMN-DSF. But on zooming the image and analyzing the fine details, it is observed that the despeckling results of HMN-DSF are best among all other compared methods. The smoothness over the uniform and non-uniform areas in the image is well preserved. The object structure and edges are preserved in the resultant despeckled images of HMN-DSF.

Table 5.7 PSNR of despeckled SAR images

		PSNR				
Image	Noise Variance	5	10	20	30	40
Speckled SAR Image Figure 5.30. [σ = 20]	Frost	41.7888	39.3939	38.5937	32.5930	30.2976
	Homomorphic Frost	42.0275	40.2180	39.6021	34.2973	31.2846
	Kuan	40.9711	37.8980	35.0001	33.9137	32.9697
	Homomorphic Kuan	41.9948	39.3363	39.6590	34.2500	31.2307
	Refined-Lee [24]	41.8732	40.1240	39.2569	38.8891	34.8952
	Homomorphic Refined-Lee	41.9593	40.0071	38.4587	37.0725	34.0097
	Kuwahara	41.7584	38.3298	36.2381	35.6002	33.2657
	Median	40.7524	37.2035	35.6350	33.56987	32.3263
	SRAD	43.9562	42.2837	38.5671	36.5687	34.1259
	DWT with Soft Thresholding [75]	42.5338	41.2973	40.1121	37.9189	34.9299
	DWT with Hard Thresholding [75]	40.0021	38.2819	38.1120	36.2917	33.2657
	Universal Threshold [76]	41.9351	40.5639	38.5637	37.2614	30.2973
	Visu Threshold [77]	42.9482	40.2910	39.2310	37.2858	32.2310
	DWT with Bayesian Threshold	43.0115	42.2927	39.6308	37.2350	35.0023
	BCMAP [32]	43.2897	42.1121	39.8029	37.9580	34.2698
	MCMAP [31]	44.3290	42.3197	39.9898	39.2581	34.8896
	ATV [72]	45.4259	42.3333	40.3891	38.5690	34.5297
	H-BM3D [73]	44.1898	42.2158	40.5894	38.1555	34.2361
	H-PPB [73]	44.2954	42.1567	40.3258	40.2582	34.9597
	Coarse filtering [74]	44.3791	42.1012	40.7939	**40.3230**	34.1595
	Refined filtering [74]	**44.5734**	**43.6427**	40.3281	39.2589	34.3267
	DSF [66]	42.2358	42.1258	42.0279	41.8598	34.2879
	NLM filter [76]	43.2679	41.2589	39.5105	39.0005	34.1289
	HMN-DSF	44.5715	42.3764	**40.9403**	40.0023	**35.0193**

Table 5.8 SSIM of despeckled SAR images

		SSIM				
Image	Noise Variance	5	10	20	30	40
Speckled SAR Image Figure 5.30. [σ = 20]	Frost	0.8481	0.8085	0.7714	0.7011	0.6859
	Homomorphic Frost	0.8601	0.8200	0.7982	0.7819	0.7008
	Kuan	0.8330	0.7989	0.7989	0.7012	0.6592
	Homomorphic Kuan	0.8491	0.8123	0.8025	0.7706	0.7149
	Refined-Lee [24]	0.8783	0.8681	0.8302	0.8059	0.7994
	Homomorphic Refined-Lee	0.8421	0.8158	0.8005	0.7901	0.7795
	Kuwahara	0.8671	0.8437	0.8025	0.7878	0.7253
	Median	0.8520	0.8312	0.8147	0.7898	0.6197
	SRAD	0.9562	0.9359	0.8989	0.9001	0.8107
	DWT with Soft Thresholding [75]	0.9141	0.9108	0.8828	0.8858	0.8817
	DWT with Hard Thresholding [75]	0.8230	0.7985	0.7710	0.7485	0.7194
	Universal Threshold [76]	0.8761	0.8561	0.8181	0.7892	0.7529
	Visu Threshold [77]	0.9104	0.8952	0.8587	0.8320	0.8028
	DWT with Bayesian Threshold	0.9382	0.9257	0.8981	0.8567	0.8753
	BCMAP [32]	0.9701	0.9411	0.9001	0.9194	0.9093
	MCMAP [31]	0.9858	0.9251	0.9217	0.9027	0.9025
	ATV [72]	0.9723	**0.9510**	0.9123	0.9090	0.9117
	H-BM3D [73]	0.9849	0.9368	0.9258	0.9164	0.9057
	H-PPB [73]	0.9528	0.9267	0.9158	0.9151	0.9005
	Coarse filtering [74]	0.9552	0.9441	0.9112	0.9012	0.9087
	Refined filtering [74]	0.9689	0.9399	0.9078	0.9111	**0.9257**
	DSF [66]	0.9457	0.9258	0.8965	0.8874	0.8659
	NLM filter [76]	0.9359	0.9021	0.8859	0.8879	0.8698
	HMN-DSF	**0.9958**	0.9487	**0.9261**	**0.9220**	0.9119

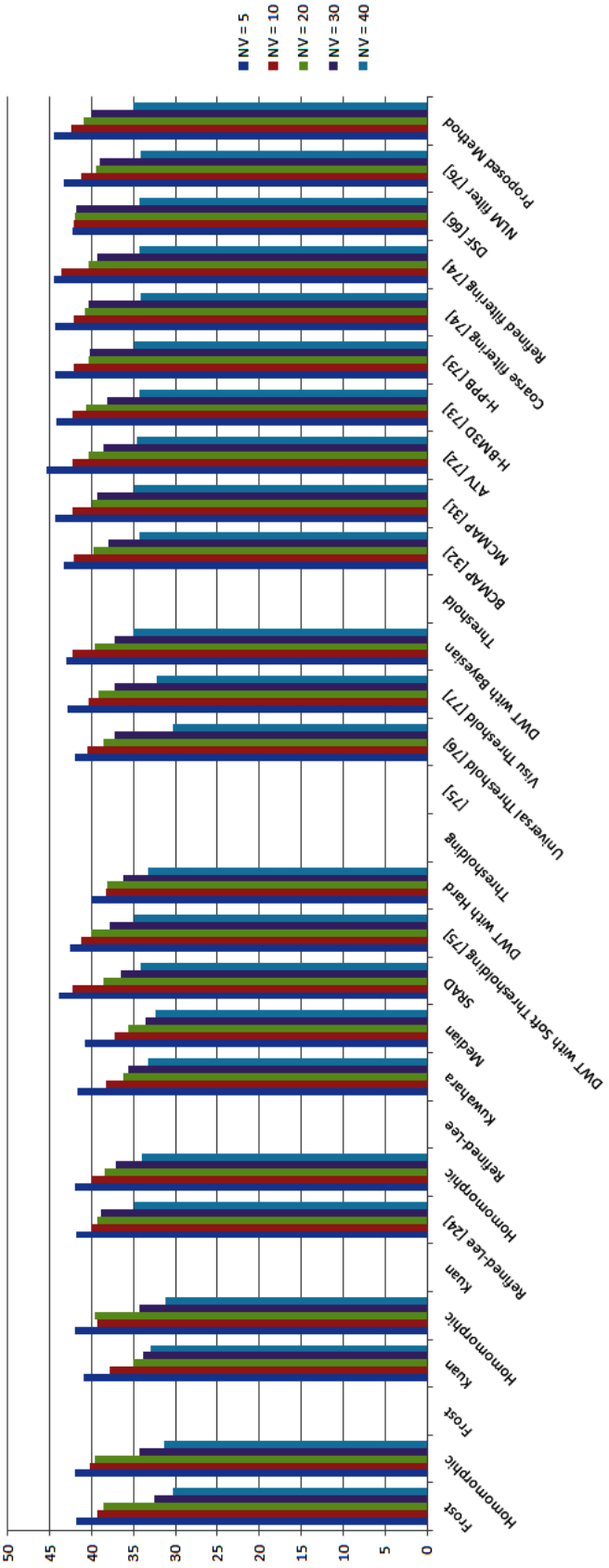

Figure 5.32 Performance evaluation using PSNR

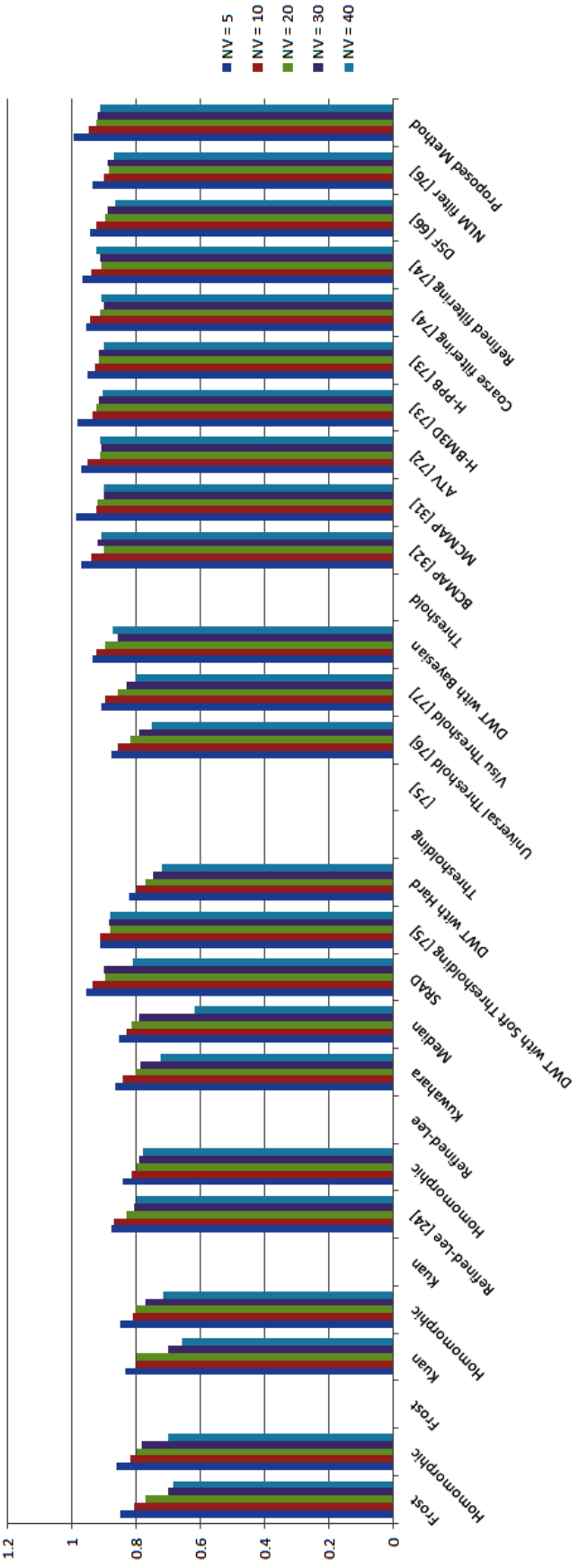

Figure 5.33 Performance evaluation using SSIM

Table 5.9 UIQI of despeckled SAR images

		UIQI				
Image	Noise Variance	5	10	20	30	40
Speckled SAR Image Figure 4(b). [σ = 20]	Frost	0.7174	0.7199	0.6901	0.6644	0.6987
	Homomorphic Frost	0.6919	0.7213	0.7004	0.6859	0.6589
	Kuan	0.7250	0.7249	0.7211	0.6859	0.7147
	Homomorphic Kuan	0.7191	0.7093	0.6991	0.6591	0.6684
	Refined-Lee [24]	0.8717	0.8359	0.8019	0.7812	0.7089
	Homomorphic Refined-Lee	0.8821	0.8431	0.8232	0.8081	0.7948
	Kuwahara	0.8191	0.8016	0.7757	0.7161	0.6874
	Median	0.7813	0.7691	0.7522	0.7491	0.7149
	SRAD	0.7952	0.7901	0.7599	0.8603	0.8127
	DWT with Soft Thresholding [75]	0.8492	0.8693	0.8362	0.8123	0.7548
	DWT with Hard Thresholding [75]	0.7730	0.7959	0.7569	0.7341	0.6984
	Universal Threshold [76]	0.7952	0.8042	0.7951	0.7802	0.7328
	Visu Threshold [77]	0.8111	0.8041	0.7962	0.7760	0.7713
	DWT with Bayesian Threshold	0.8991	0.8662	0.8831	0.8204	0.7981
	BCMAP [32]	0.9102	0.8723	0.8565	0.8250	0.8020
	MCMAP [31]	0.9139	0.8851	0.8599	0.8425	0.8101
	ATV [72]	0.9217	0.9028	0.8758	0.8494	0.8058
	H-BM3D [73]	0.9198	0.8987	0.8657	0.8359	0.8100
	H-PPB [73]	0.9115	0.9014	**0.8797**	0.8258	0.7989
	Coarse filtering [74]	0.9356	0.8965	0.8754	0.8420	0.8029
	Refined filtering [74]	**0.9489**	0.8999	0.8870	0.8367	0.8057
	DSF [66]	0.9345	0.9019	0.8441	0.8001	0.7948
	NLM filter [78]	0.9256	0.8875	0.8551	0.8350	0.8056
	HMN-DSF	0.9438	**0.9065**	0.8872	**0.8591**	**0.8134**

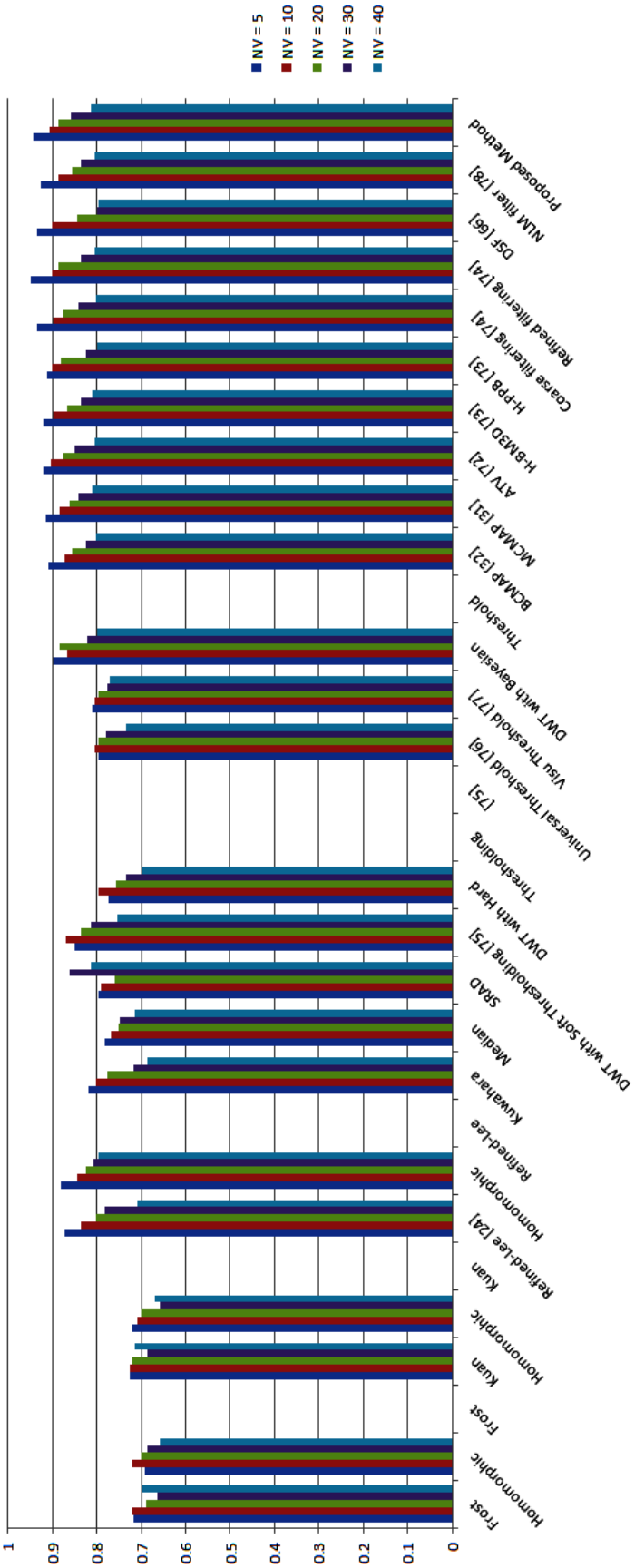

Figure 5.34 Performance evaluation using UIQI

Case 2: Without-Reference Indexes

The quantitative despeckling results shown in Table 5.10 shows that the performance of HMN-DSF on real speckled SAR images. It performs better than most of the compared traditional and non-traditional methods. The CV metric investigates the introduction of the artifacts and poor preservation of the details. The CV of HMN-DSF is 33.0083 and of reference real speckled SAR image is 32.6373. There is no big difference between them; hence there is no poor preservation of details but a bit introduction of the artifacts that is almost negligible. The CV of BCMAP, MCMAP, ATV, H-BM3D, H-PPB, coarse filtering and refined filtering are 33.9510, 34.2325, 34.1919, 34.4837, 34.9180, 34.3672 and 34.7653 respectively. These values clearly indicate the small difference between them and CV of reference SAR image, which shows their effective results too. But on the ground of visual appearance, the HMN-DSF shows the better despeckling results. Refined-Lee, SRAD, and Bayesian thresholding also show descent quantitative CV result. On evaluating NV, it is calculated that the non-traditional methods work far better than the standard filters which can be visualized by looking at the smoothness in the homogeneous and non-homogeneous areas of the image. The NV of real speckled SAR image is 7.2567 and that of despeckled SAR image of the proposed method is 0.3915, which represents an excellent noise reduction. Only refined filtering shows better NV than HMN-DSF i.e. 0.3838. The NV of BCMAP, MCMAP, ATV, H-BM3D, H-PPB and coarse filtering are 0.9025, 0.5632, 0.4561, 0.4125, 0.4672 and 0.4009 respectively and are decent results too.

(a) **(b)** **(c)**

(d) **(e)** **(f)**

(g) **(h)** **(i)**

(j) **(k)** **(l)**

(m) **(n)** **(o)**

(p) **(q)** **(r)**

(s) **(t)** **(u)**

(v) **(w)** **(x)**

(y)

Figure 5.35 Results of despeckling algorithm (a) Real speckled SAR image (b) result of Frost filter (c) result of homomorphic Frost filter (d) result of Kuan filter (e) result of homomorphic Kuan filter; (f) result of Refined-Lee filter (g) result of homomorphic Refined-Lee filter (h) result of Kuwahara filter (i) result of Median filter (j) result of SRAD (k) result of Soft thresholding (l) result of Hard thresholding (m) result of Universal thresholding (n) result of Visu thresholding (o) result of Bayesian thresholding (p) result of BCMAP (q) result of MCMAP (r) result of ATV (s) result of H-BM3D (t) result of H-PPB (u) result of Coarse filtering (v) result of Refined filtering (w) result of DSF (x) result of NLM filter (y) result of HMN-DSF.

In terms of ENL values, it is observed that HMN-DSF shows comparative better results that can also be visually analyzed in Figure 5.35 as the smoothness in homogeneous areas is somewhat proportional to the speckle reduction in the image. High ENL value (2.5657) of HMN-DSF depicts descent smoothness in the homogeneous areas. Since the SAR image has both homogeneous and non-homogeneous regions, so the ENL is evaluated using block processing in a non-overlapping fashion. The despeckled SAR image is divided into multiple

blocks of 25 × 25. ENL is evaluated for each and every block using Eq. 3.38 and then average of all ENL's is calculated. Other methods like Frost, homomorphic Frost, homomorphic Kuan, Refined-Lee, homomorphic Refined-Lee, Kuwahara, median, SRAD, soft thresholding, universal thresholding, Visu and Bayesian thresholding, BCMAP, MCMAP, ATV, H-BM3D, H-PPB, coarse filtering and refined filtering evaluates ENL ranging from {2-3} which shows nice quantitative values.

MSE is one performance evaluation metric used in both the cases with and without reference image. Here MSE is used in the case of without reference indexes. It evaluates the average difference between real speckled SAR image and despeckled SAR image. Here in this case, the high MSE values correspond to high image quality. In the case 1: with-reference indexes, low MSE values correspond to high image quality. The MSE is inversely proportional to the PSNR. On analyzing the Table 5.10, MSE of the HMN-DSF is 991.1201. There are three other methods that show high MSE values i.e. refined filtering (997.9037), MCMAP (1001.0281) and Kuwahara (1079.3087). All other methods having low MSE value depicts the minimum speckle reduction. While comparing on the basis of MSE, it is very necessary to take special care of edges, texture, and structure of the objects. The despeckling results of NLM show better results in the terms of visual appearance. Also, the speckle reduction and smoothness are also well preserved in the despeckled images. The despeckling results of DSF are also satisfactory. In the case of MSE, the Kuwahara filter shows the highest MSE depicting the best result, but when looking at the visual results and other performance measure's value it is observed that the HMN-DSF is better than the Kuwahara filter. Figure 5.40 (c) and 5.40 (d) shows the intensity profile of the specified line on SAR image 1 and 2 shown in 5.40 (a) and 5.40 (b) before and after despeckling respectively. The overlapping of the plot in 5.40 (c) denotes the better results of HMN-DSF. The NV value of the despeckled SAR images is graphically analyzed in the Figure 5.36. The MSE value of the despeckled SAR images is graphically analyzed in the Figure 5.37. The ENL value of the despeckled SAR images is graphically analyzed in the Figure 5.38. The CV value of the despeckled SAR images is graphically analyzed in the Figure 5.39.

Table 5.10 Performance assessment parameters vs. filtering methods

S. No.	Filtering methods	Performance assessment parameters			
		NV	MSE	ENL	CV
a.	Real speckled SAR image	7.2567	-	1.8055	32.6373
b.	Frost	6.3378	841.8739	2.3461	34.9981
c.	Homomorphic Frost	6.2341	825.8911	2.3981	34.5671
d.	Kuan	6.0981	913.8233	1.9091	36.2341
e.	Homomorphic Kuan	5.9912	908.2391	2.3323	36.1101
f.	Refined-Lee [24]	5.0002	689.0156	2.5058	31.9958
g.	Homomorphic Refined-Lee	4.9851	701.1219	2.5091	30.0017
h.	Kuwahara	6.7743	**1079.3087**	2.4156	36.6391
i.	Median	5.9123	625.601	2.1001	29.7629
j.	SRAD	5.2134	795.2331	2.1089	33.4568
k.	DWT with Soft Thresholding [75]	3.1251	635.2523	2.2509	34.6291
l.	DWT with Hard Thresholding[75]	4.9824	680.2001	1.9128	34.9981
m.	Universal Threshold [76]	4.9671	699.8975	2.0191	35.7294
n.	Visu Threshold [77]	4.997	681.1221	2.1741	35.7912
o.	DWT with Bayesian Threshold	3.8926	617.2301	2.1791	33.9891
p.	BCMAP [32]	0.9025	980.1683	2.4281	33.9510
q.	MCMAP [31]	0.5632	1001.0281	2.5601	34.2325
r.	ATV [72]	0.4561	984.0909	2.5229	34.1919
s.	H-BM3D [73]	0.4125	899.9462	2.5119	34.4837
t.	H-PPB [73]	0.4672	958.9826	2.2361	34.9180
u.	Coarse filtering [74]	0.4009	957.8947	2.4345	34.3672
v.	Refined filtering [74]	0.4038	997.9037	2.5465	34.7653
w	DSF [66]	0.4084	890.2846	2.4928	35.9696
x.	NLM filter [78]	0.4001	925.6580	2.5028	34.0819
y.	HMN-DSF	**0.3915**	991.1201	**2.5657**	**33.0083**

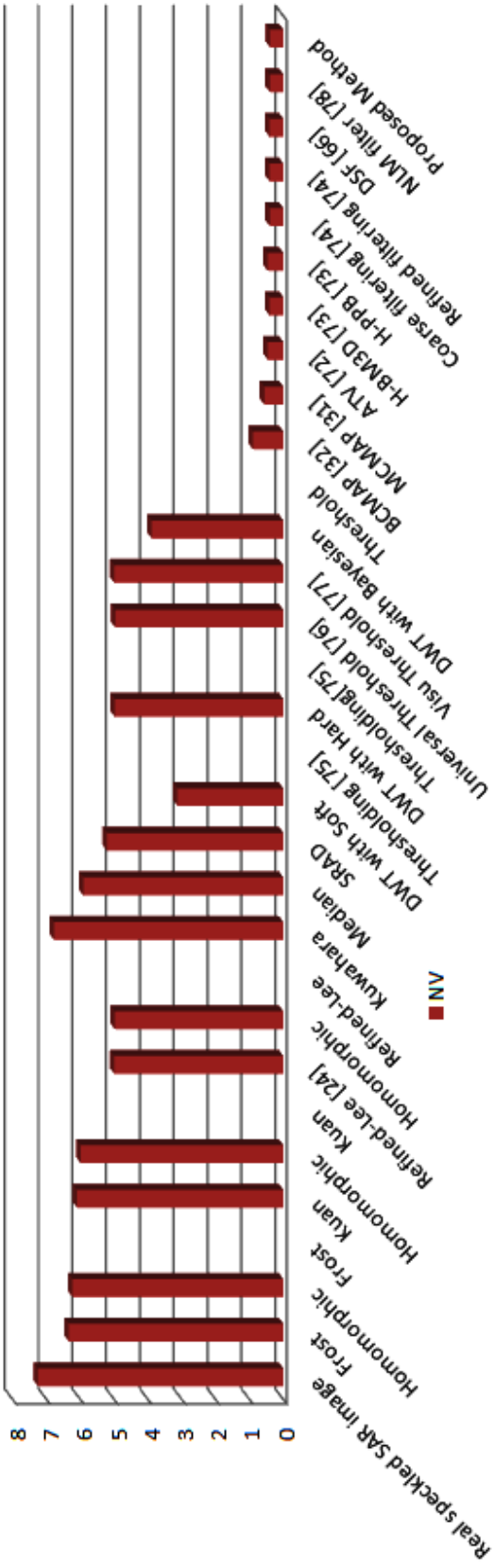

Figure 5.36 Performance assessment using noise variance

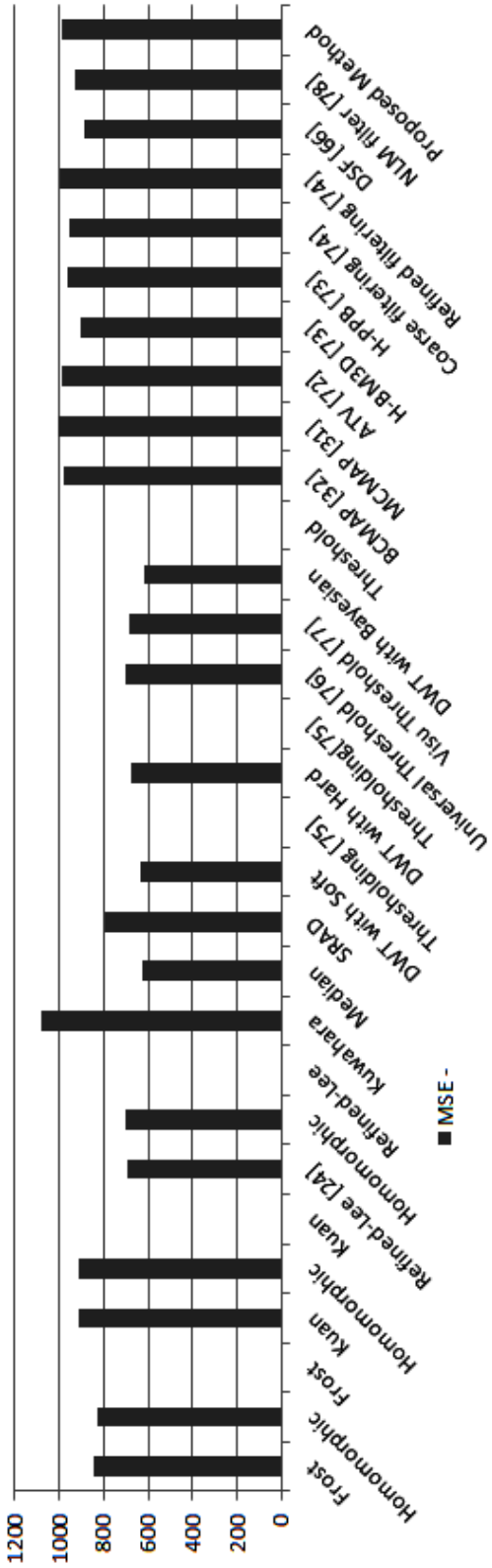

Figure 5.37 Performance assessment using MSE

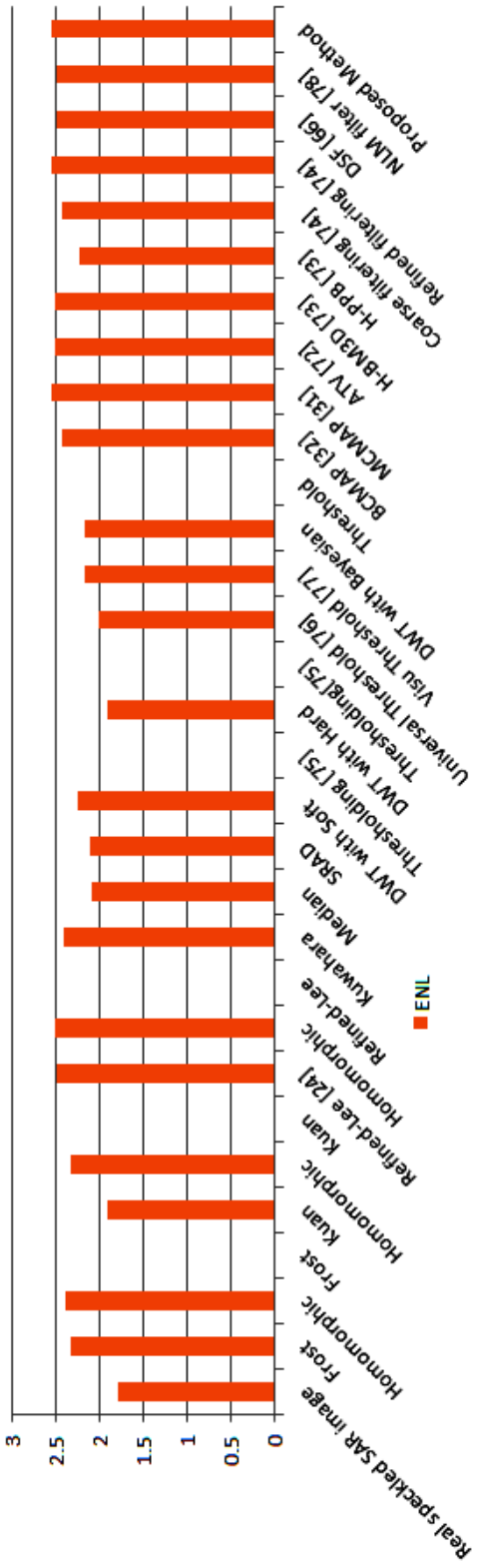

Figure 5.38 Performance assessment using ENL

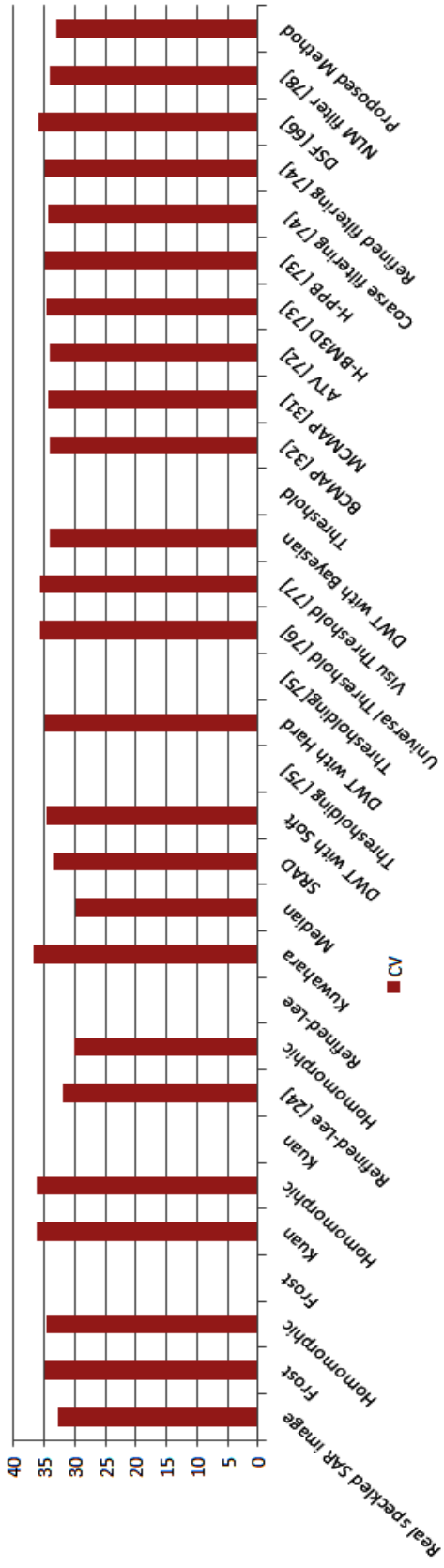

Figure 5.39 Performance assessment using CV

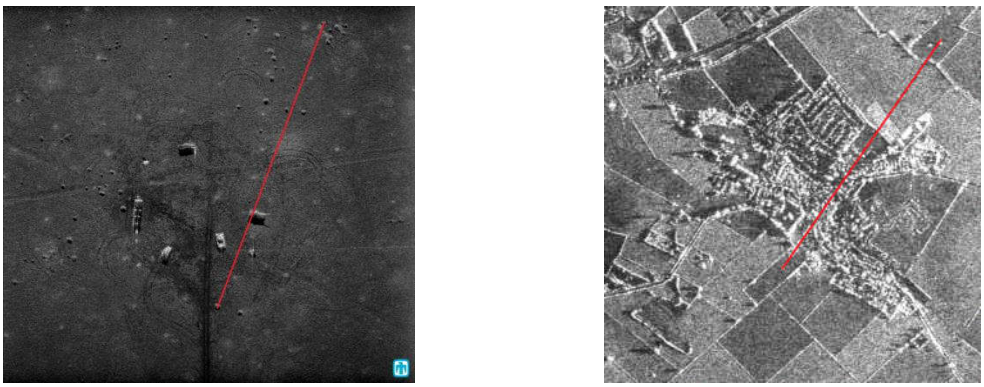

(a) **(b)**

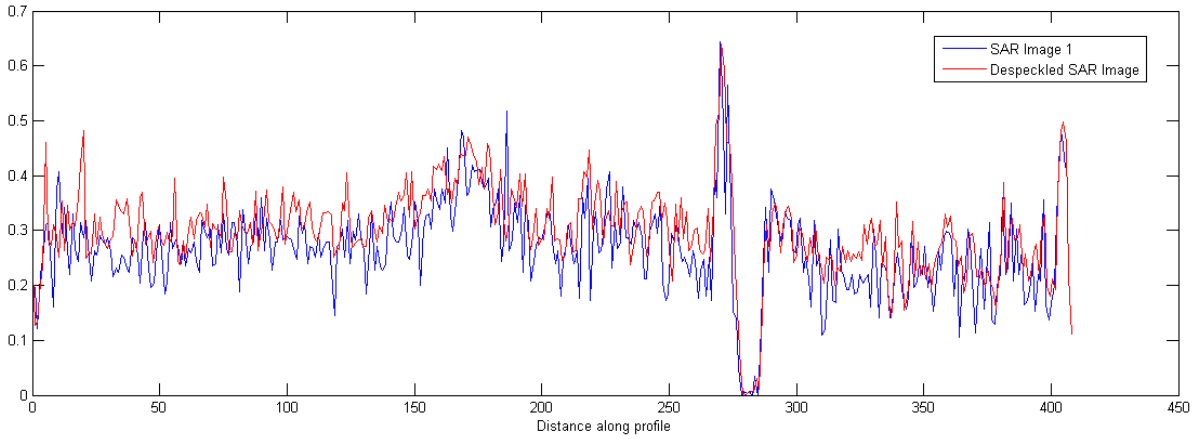

(c)

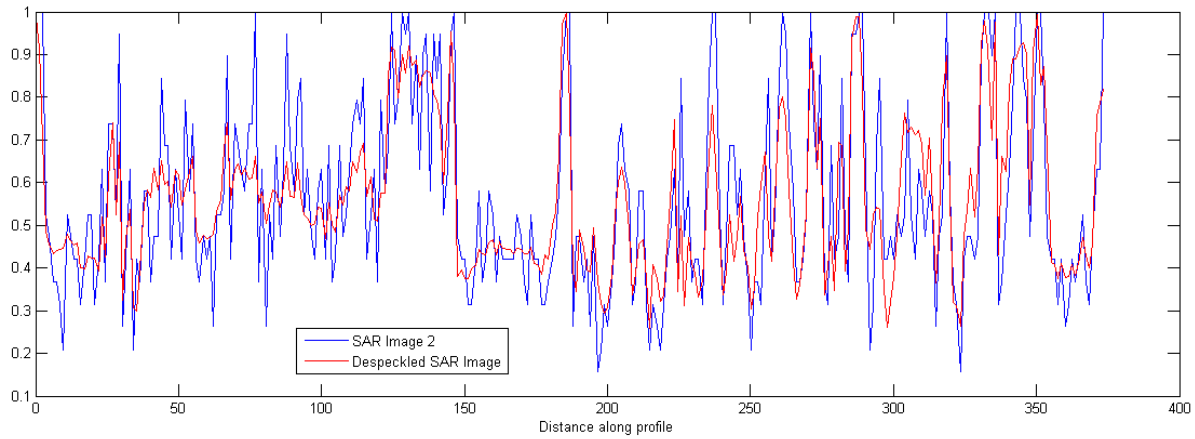

(d)

Figure 5.40 Plotting the line profile of SAR image 1 and SAR image 2 with their despeckled results using intensity profile

Table 5.11 Preservation of mean values before and after despeckling of SAR images in simulated SAR image (at σ = 5; 10; 20; 30; 40) and in real speckled SAR images

Result of simulated SAR image				
	Mean of reference SAR image	Mean of simulated SAR image before despeckling at different noise variances (σ)		Mean of despeckled SAR image
SAR Image 1	60.0354	σ	Mean	
		5	59.9881	60.0658
		10	59.9781	60.0205
		20	59.9226	60.0794
		30	59.9124	60.0056
		40	59.9090	60.1015

Result of real speckled SAR image		
	Mean (before despeckling)	Mean (after despeckling)
SAR Image 2	132.1021	131.3164

Table 5.11 depicts the preservation of mean values in both the cases: simulated SAR images at different noise variances and real speckled SAR image before and after despeckling. An efficient image denoising method retains the mean value of the image after denoising. This concept similarly applies to the SAR image despeckling. The Table 5.11 shows the preservation of mean values before and after despeckling using HMN-DSF. The values in the Table 5.11 shows well preservation of the mean values which validates accurate filtering as the mean values before and after filtering are almost same in both the cases.

5.3.3 Experimental Results on Standard Digital Images

This sub-section experiment the HMN-DSF on the standard classical images shown in Figure 5.41 through speckle simulation process in order to check the effectiveness and strength of despeckling method. It is done by experimenting the method on the 'Lena', 'Boat' and 'Baboon' through speckle simulation process. These results are shown in Figure 5.43. The despeckled results obtained by the HMN-DS are experimented at σ = 25 shown in Figure

5.42. The histogram is plotted for the speckled and despeckled classical images in the Figure 5.44.

(a) **(b)** **(c)**

Figure 5.41 Speckle-free classical images

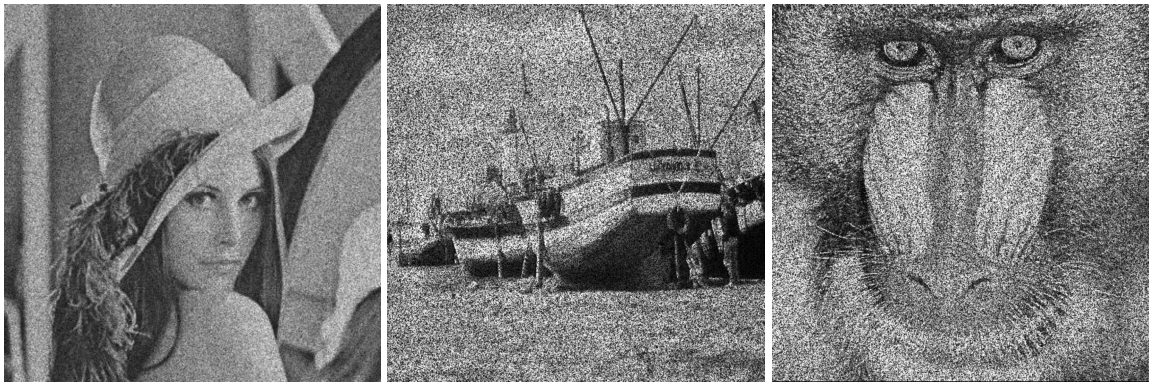

(a) **(b)** **(c)**

Figure 5.42 Speckled classical images at σ = 25

(a) **(b)** **(c)**

Figure 5.43 Despeckled classical images

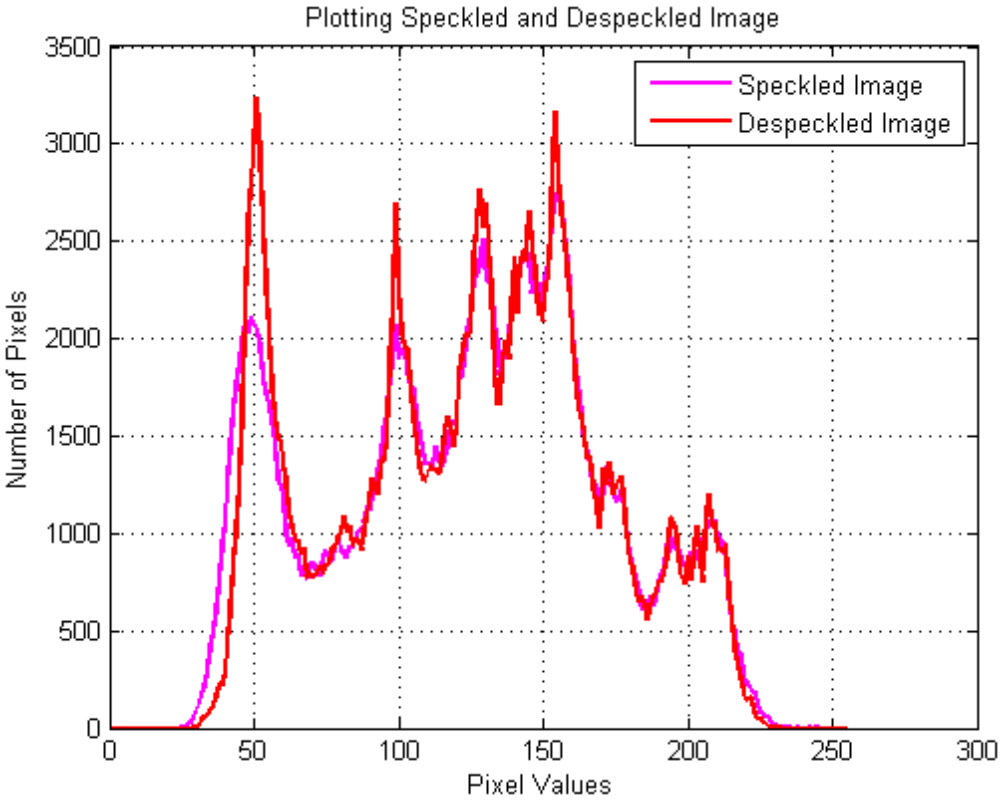
Plotting Speckled and Despeckled Image
Speckled Image
Despeckled Image
Number of Pixels
Pixel Values
0
500
1000
1500
2000
2500
3000
3500
0
50
100
150
200
250
300

(a)

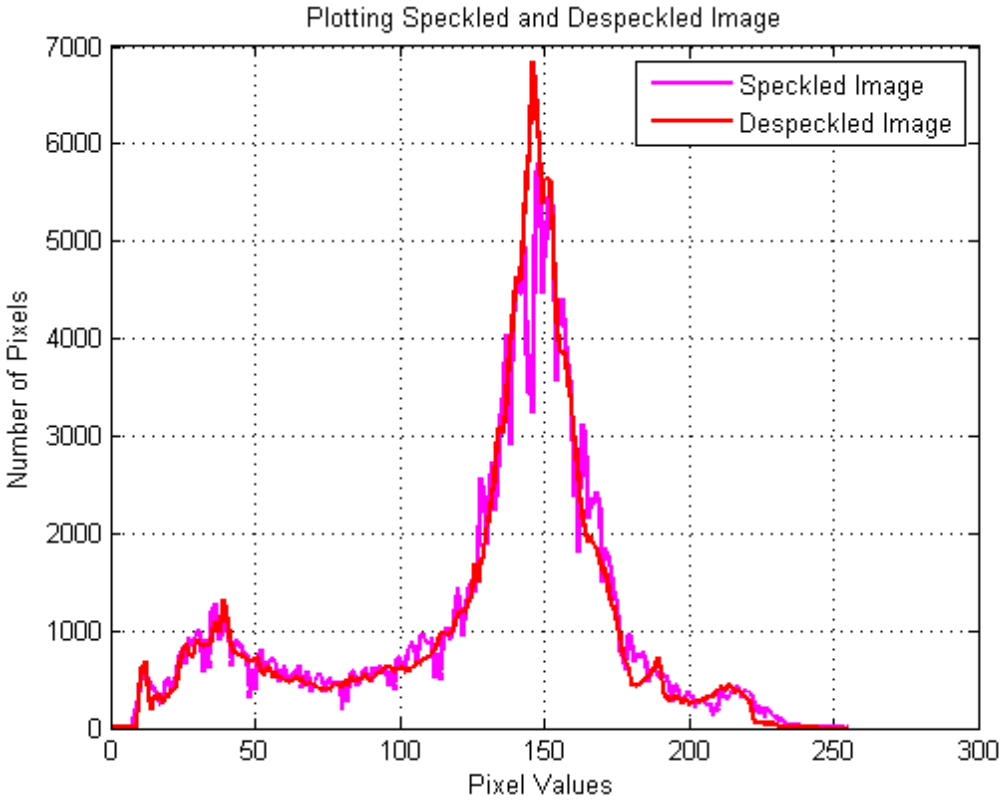
Plotting Speckled and Despeckled Image
Speckled Image
Despeckled Image
Number of Pixels
Pixel Values
0
1000
2000
3000
4000
5000
6000
7000
0
50
100
150
200
250
300

(b)

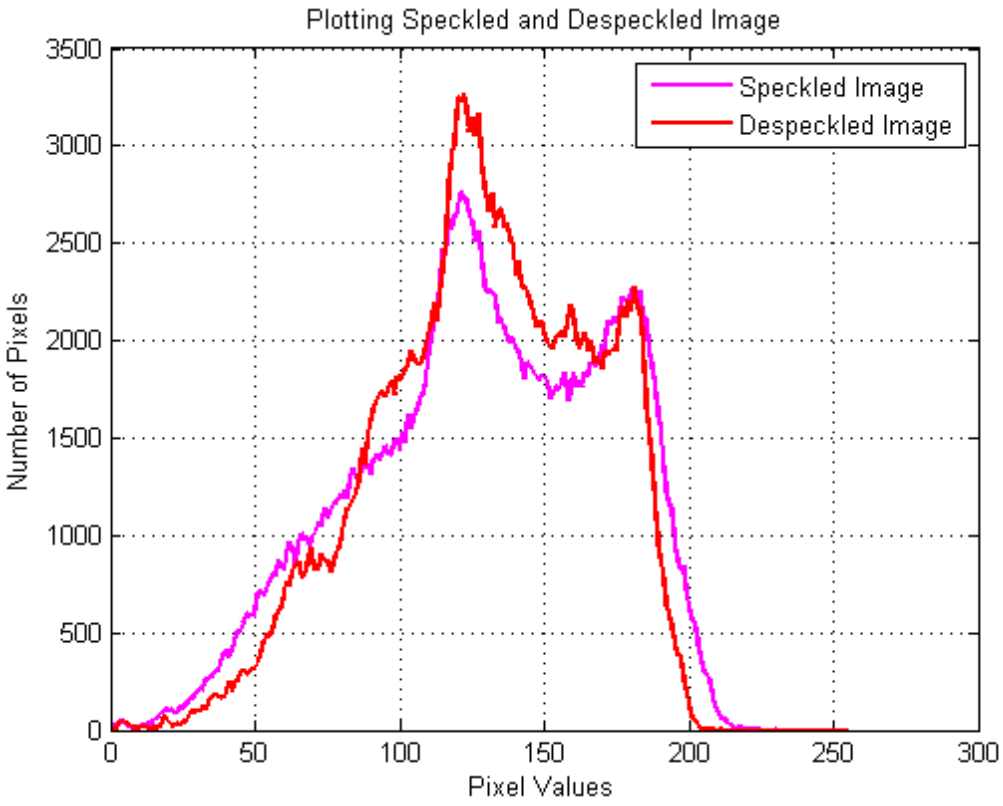

(c)

Figure 5.44 Comparison by plotting a histogram of speckled and despeckled classical images using HMN-DSF at σ = 25 (a) Lena (b) Boat (c) Baboon

5.3.4 Experimental Results over other Wavelet Families and Transforms

The HMN-DSF specifically works on ‘db2’ wavelet family for best results, although the HMN-DSF is tested on several wavelet families that are proven to be specifically valuable in DWT. The tested wavelet families are 'haar', 'db', 'sym', 'coif', 'bior', 'rbio', 'meyr' etc. The comparative analysis of the HMN-DSF at these wavelet families demonstrates the effectiveness of ’db2’ over other wavelet families. The zoomed despeckling results of HMN-DSF with different wavelet families are shown in Figure 5.45. The experiment is performed at noise variance (σ = 20) and visually analyzed on the zoomed part. Table 5.12 shows the performance of HMN-DSF using different wavelet families.

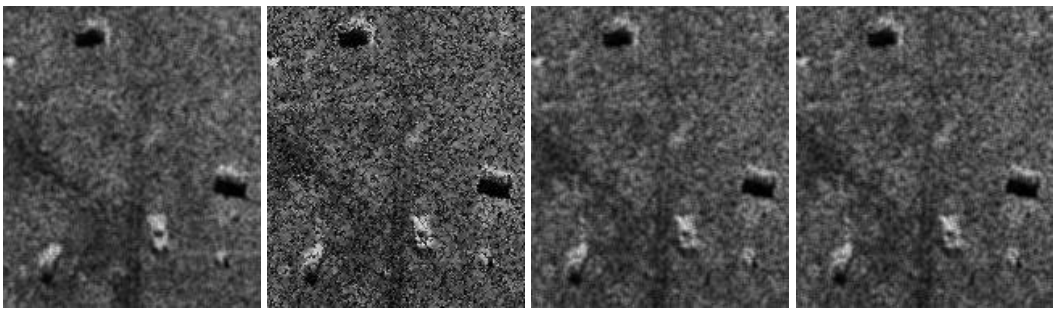

(a) **(b)** **(c)** **(d)**

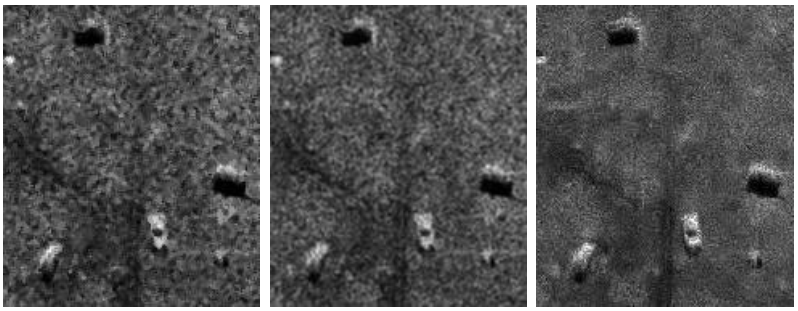

(e) **(f)** **(g)**

Figure 5.45 Result of HMN-DSF at different wavelet families (a) haar (b) sym4 (c) coif3 (d) bior4.4 (e) rbio2.6 (f) meyr (g) db2

Table 5.12 Performance evaluation of HMN-DSF at various wavelet families

Wavelet family	haar	sym4	coif3	bior4.4	rbio2.6	Meyr	**db2**
PSNR	37.2970	32.4689	33.2028	34.2597	35.2598	37.2323	**40.9403**
SSIM	0.8898	0.7585	0.7981	0.8101	0.8569	0.8968	**0.9261**

The DWT is one of the widely used and accepted transform in the real-time applications among other wavelet transforms [97]. The two main reasons behind its wide use are its simplicity and low computational time. The CoWT and SWT [98] are the advanced versions of DWT, but they are complex and take much time in execution [99]-[103]. The HMN-DSF proposes advancement in the methodology of DWT by merging the concept of method noise thresholding in it. The HMN-DSF advances DWT by enhancing the filtering operation on the approximate and detailed part of the image during DWT operation using method noise thresholding. The comparative analysis of these three wavelet transform validates the effectiveness of DWT over CoWT and SWT. The computational results are evaluated at noise variance ($\sigma = 20$).

The despeckling results of HMN-DSF are compared with the standard despeckling techniques using SWT and CoWT . The intelligent use of method noise using DWT has enhanced the despeckling results. The computational cost, PSNR, and SSIM using DWT show the better performance than the CoWT and SWT. The UIQI parameter using SWT shows a better result than the DWT. Apart from visual results and quantitative result, there are many other parameters due to which the DWT is preferred over SWT which is considered as advanced transform than the DWT. The DWT holds the time and frequency information. DWT shows the more flexibility than other transforms. The DWT breaks the data into four components which makes the analysis of data easier. The DWT is less complex than SWT and CoWT. The result interpretation of DWT results is easier than SWT and CoWT. The implementation is also easier than SWT and CoWT. These are the few reasons which motivate to use DWT over SWT and CoWT. Figure 5.46 and Table 5.13 shows the effectiveness of DWT over SWT and CoWT in terms of visual appearance and objective quantitative measures respectively.

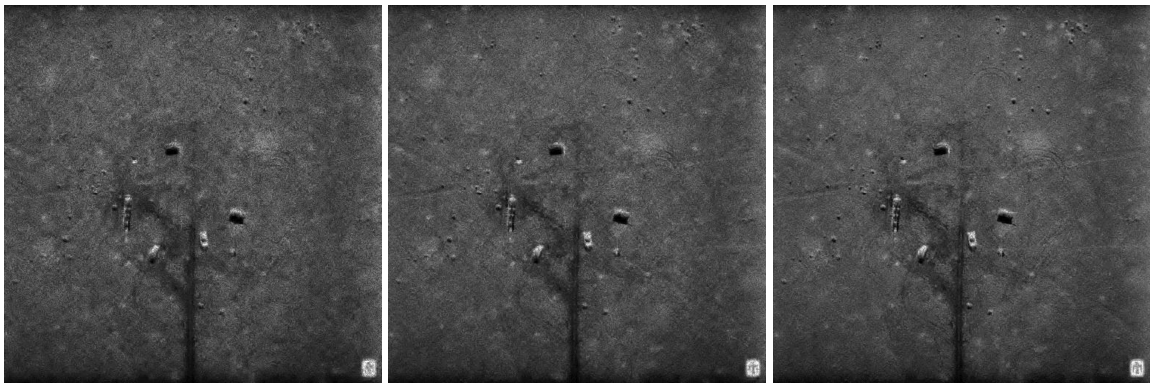

(a) **(b)** **(c)**

Figure 5.46 Comparative analysis (a) CoWT using wavelet thresholding (b) SWT using wavelet thresholding (c) DWT using wavelet thresholding (HMN-DSF)

Table 5.13 Comparative analysis of different wavelet transforms

Wavelet transform	PSNR	SSIM	UIQI	Execution time (in seconds)
CoWT	38.5820	0.8856	0.9014	34
SWT	40.1102	0.9157	**0.9299**	42
DWT	**40.9403**	**0.9261**	0.9145	**6**

5.3.5 Execution Time Comparison

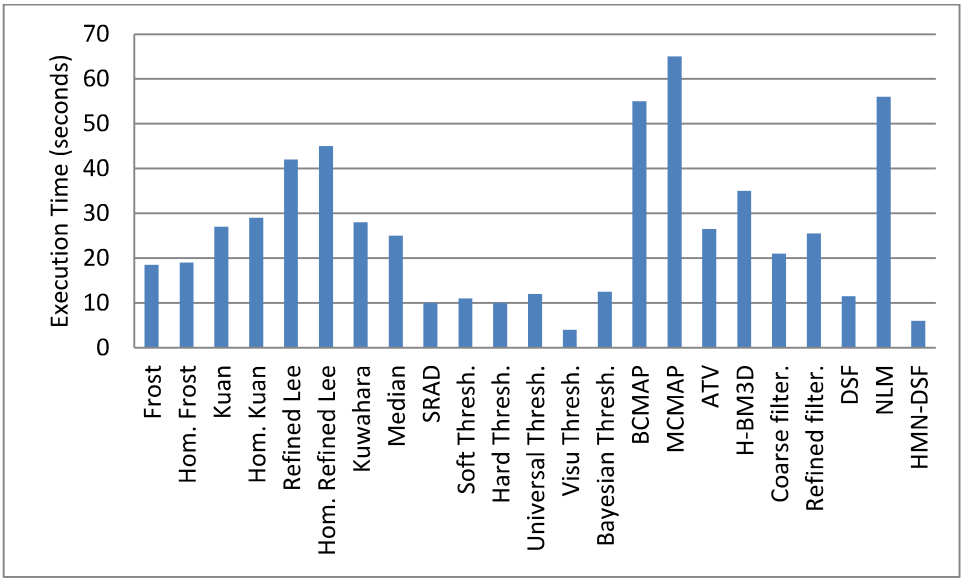

Figure 5.47 Computational time of different despeckling techniques (in seconds)

All the experimental results are evaluated on the system with MATLAB version=8.3, name=R2014a on Intel(R) Core(TM) i5-2410M CPU @ 2.30 GHz, 4GB RAM and 64-bit operating system. It is necessary to note down system configuration in order to match the processing time of the HMN-DSF with other methods as shown in Figure 5.47. The execution time of HMN-DSF is around 6-7 seconds. It is faster than most of the compared methods. The Visu thresholding method shows better processing time but it lacks behind in performance. Bayesian, universal, soft thresholding and SRAD also shows decent processing time, out of which universal thresholding lacks in performance, rest three techniques shows good result. The NLM is an effective filter but has high computational cost. It can be said computationally that the HMN-DSF is the faster than others. The high visual quality of despeckled images and low computational cost validates the high performance of the HMN-DSF.

5.3.6 Validation of HMN-DSF: Hypothesis Testing using Paired T-test.

The HMN-DSF is validated using T-test over 18 numbers of samples. The HMN-DSF is experimented using different metrics like PSNR, SSIM, UIQI, NV, ENL and CV values at different noise variances over two different SAR images i.e. simulated SAR image (PSNR, SSIM, UIQI) and real speckled SAR image (NV, ENL, CV). Based on the experimented

results over the different SAR images as shown in Table 5.14, the experimented sample data is collected and tested using hypothesis testing based on paired T-test.

There is total of 18 numbers of experimented sample data collected using the PSNR, SSIM, UIQI, NV, ENL, and CV at different noise variances (σ = 5, 10, 20, 30, 40). This data is collected by performing the experiment over two different SAR images, i.e. simulated SAR image (PSNR, SSIM, UIQI) and real speckled SAR image (NV, ENL, CV). The related sample data is the quantitative values of the SAR image before and after despeckling. The level of significance is set to 5.

The following null and alternate hypothesis needs to be tested: The H_o denotes the null hypothesis and H_a denotes the alternate hypothesis.

$H_o: \mu_D = 0$ (There is no difference between SAR image before and after despeckling in terms of quality, i.e. "No despeckling")

$H_a: \mu_D \neq 0$ (There is a difference between SAR image before and after despeckling in terms of quality, i.e. "Good despeckling")

Table 5.14 Dataset 2

No. of Samples	Values before Despeckling (X_i)	Values after Despeckling(Y_i)	Difference ($D_i=X_i - Y_i$)
1.	25.1588	44.5715	-19.4127
2.	22.1475	42.3764	-20.2289
3.	19.1526	40.9403	-21.7877
4.	17.3726	40.0023	-22.6297
5.	16.2027	35.0193	-18.8166
6.	0.6281	0.9958	-0.3677
7.	0.4682	0.9487	-0.4805
8.	0.3144	0.9261	-0.6117
9.	0.2380	0.9220	-0.684
10.	0.1950	0.9119	-0.7169
11.	0.6409	0.9438	-0.3029
12.	0.4305	0.9065	-0.476
13.	0.2834	0.8872	-0.6038
14.	0.2118	0.8591	-0.6473
15.	0.1715	0.8134	-0.6419

16.	7.2567	0.3915	6.8652
17.	1.8055	2.5657	-0.7602
18.	32.6373	33.0083	-0.371
n = 18			$\sum \mathrm{D_i} = 116.4047$

As calculated from the above sample data, the corresponding sample means are $\overline{X_i}$=8.073 and $\overline{Y_i}$=13.777 and the calculated sample standard deviation are s_1=10.858 and s_2=18.744. The mean of difference ($\overline{D}$) and standard deviation of difference (σ_{diff}) are calculated using below two equation respectively.

$$\overline{D} = \frac{\sum D_i}{n} = -5.704$$

$$\sigma_{diff} = \sqrt{\frac{\sum D_i^2 - (\overline{D})^2 * n}{n-1}} = 9.678$$

Depending on the information available, the significance level is α = 0.05, and the degree of freedom (df) = n – 1 = 17.

Hence, it is found that the critical value for this two-tailed test is

t_c = 2.11, for α = 0.05 and df = 17.

The rejection region for this two-tailed test is R = { t : | t | > 2.11}.

The t-statistic is calculated as shown in the following formulation:

$$t = \frac{\overline{D}}{\sigma_{diff}/\sqrt{n}} = \frac{-5.704}{9.678/\sqrt{18}} = -2.501$$

Since it is observed that | t | = 2.501 > t_c =2.11, It is concluded that the null hypothesis H_o is rejected. Therefore, there is enough evidence to claim that the difference of quantitative values before and after despeckling is considered to be extremely statistically significant, at the 0.05 significance level.

5.4 Result and Analysis of HMN-CF: A New Homomorphic SAR Image Despeckling using Correlation based Fusion and Method Noise Thresholding

This section discusses the experimental despeckling result of HMN-CF on simulated as well as real speckled SAR images. The dataset of speckled SAR image at noise variance $\sigma = 25$ is shown in the Figure 5.48. The despeckling results are tested at various noise variance level i.e. ($\sigma = 5$; 10; 20; 30; 40). The size of input speckled SAR image is fixed at 512 × 512 in order to evaluate the performance of the HMN-CF for the quantitative and qualitative assessment.

The proposed method i.e. HMN-CF is a multi-step procedure that contains various changeable parameters that are user sensitive. The HMN-CF is grounded on db2 based 2D-DWT and the level of decomposition is automatically set by using entropy metric based on the texture analysis of image. Here the detailed component is filtered using two parallel processing shrinkage rule i.e. Bivariate and modified Bayesian shrinkage rule. The Bivariate and modified Bayesian shrinkage rule are applied in parallel on the detailed component of speckled SAR image after DWT decomposition. The 3 × 3 mask is used for selecting the threshold value during the fusion process and 5 × 5 mask is used for comparing the two enhanced detailed components during the fusion process. The soft thresholding using Bayesian shrinkage rule is applied in the method noise thresholding step.

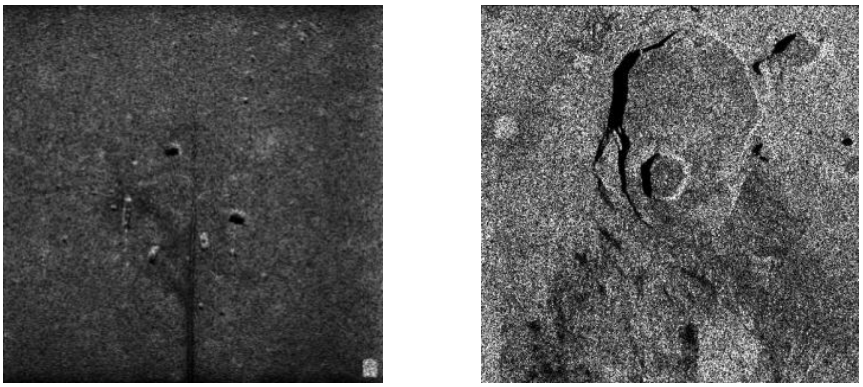

(a) **(b)**

Figure 5.48 Speckled SAR images ($\sigma = 25$)

In order to validate the HMN-CF, the despeckling results of HMN-CF are compared with the results of well-known despeckling techniques such as ATV [72], BayesWS-HAW [89], Bivariate thresholding [90] and IDPAD [91]. In this section the results of HMN-CF are shown on three different kinds of SAR images shown in the Figure 5.48 and 5.61.

5.4.1 Performance Evaluation Metrics

The experimental results of HMN-CF are performed on simulated as well as on real speckled SAR image. In case of simulated SAR images, the performance of the HMN-CF is evaluated using quantitative metrics like PSNR, SNR and SSIM. In case of real speckled SAR images, the performance of HMN-CF is analyzed by visual appearance of the despeckled SAR image. The HMN-CF is also compared on the basis of computational time.

5.4.2 Experimental Evaluation and Comparison

The comparative despeckling results of HMN-CF on simulated speckled SAR images at noise variance, $\sigma = 25$ are shown in the Figure 5.49 – 5.53. There are certain parameters that analyses the quality of despeckled SAR image. These parameters depend on the visual appearance of the despeckled SAR image. These parameters are (i) occurrence of the artifacts; (ii) edge preservation; (iii) visibility of low contrast objects and (iv) texture and structure preservation (v) smoothness in the homogeneous region and, (vi) preservation of fine details in heterogeneous region. Since there is no such scientific principle available to do so, therefore the analysis is done by analyzing the visual appearance of the despeckled SAR image. The decomposition level of HMN-CF is decided by the entropy metric based on the texture analysis. In HMN-CF, the decomposition level is different for different SAR images.

The Bivariate thresholding and IDPAD show decent despeckling results. The results of ATV method appear over smooth and minor details are lost. The results of Bayesian (BayesWS-HAW) also show some loss of information and the output images appear quite blurred. The HMN-CF overcomes all the compared methods in terms of edge, texture preservation. In terms of artifact generation in the despeckled results, it is seen that there is no occurrence of artifacts in the HMN-CF. Blocky artifacts can be seen in the despeckling results of BayWS-HAW. The ATV, Bivariate and IDPAD don't generate any artifacts. The structure of the objects observed in the despeckled image of HMN-CF is well preserved. The SAR images are low contrast images and speckle noise distorts the overall texture of the image. The proposed method is capable of preserving the low contrast objects in the SAR image.

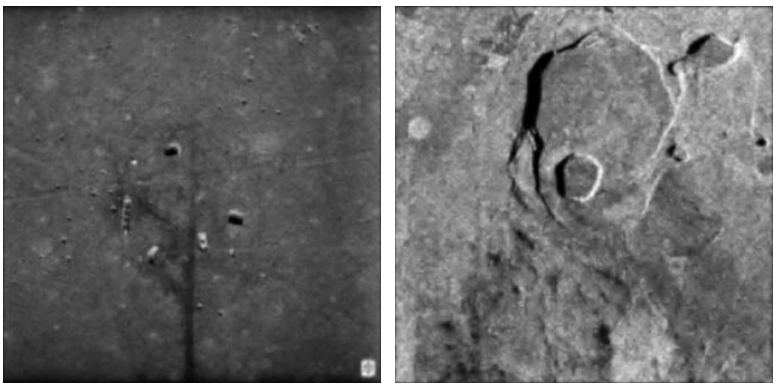

(a) **(b)**

Figure 5.49 Results of ATV

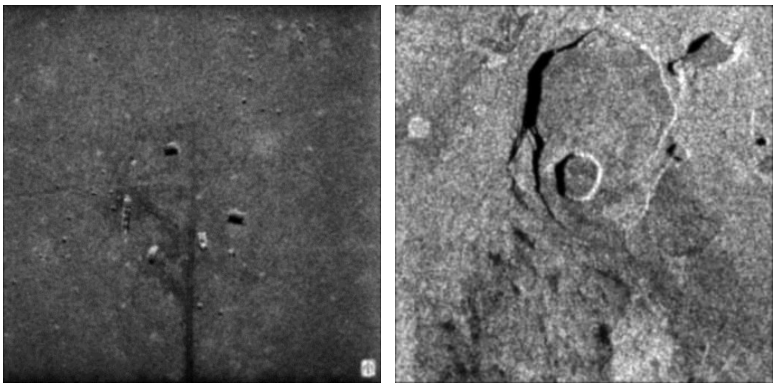

(a) **(b)**

Figure 5.50 Results of BayesWS-HAW

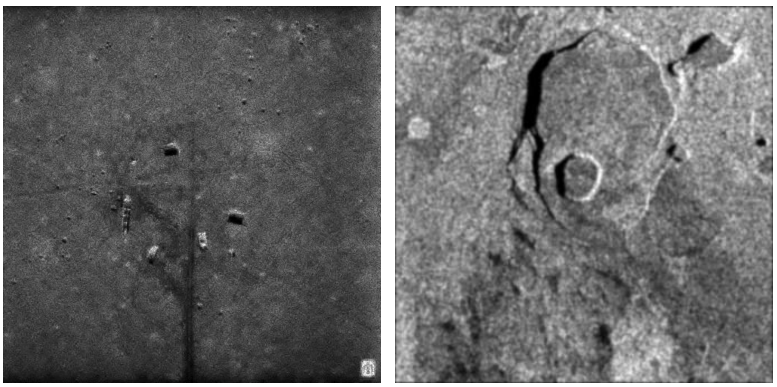

(a) **(b)**

Figure 5.51 Results of Bivariate thresholding

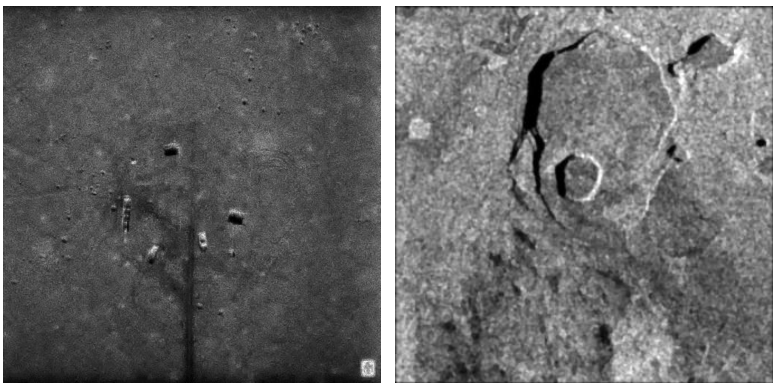

(a) **(b)**

Figure 5.52 Results of IDPAD

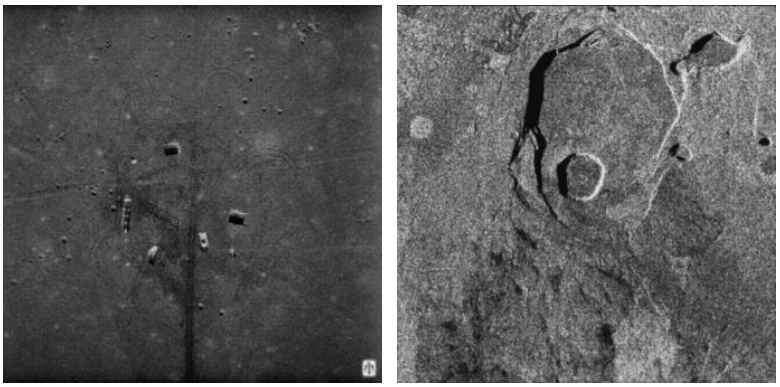

(a) **(b)**

Figure 5.53 Results of the HMN-CF

On analyzing the small details by zooming the despeckled images, the HMN-CF shows the best preservation of the detail. The HMN-CF utilizes meritorious attributes of both Bayesian and Bivariate shrinkage methods, as it is observed that corners and edge details are well preserved and even the smoothness over the homogeneous areas is well maintained. The fusion strategy of high-frequency coefficients is the core of the proposed method as it provides the best enhancement of the high-frequency coefficients on the basis of local correlation. In order to select the best threshold value, a mask of 3 × 3 is taken that decides on the basis of correlation coefficients. The method is tested on the 5 × 5, 7 × 7 and 9 × 9 masks. As the mask size increases the despeckled image quality degrades, this shows the importance of the threshold value in this method. The average and max operation depends on the threshold value. Hence the fusion strategy depends on the threshold value. The wavelet decomposition level is set using the entropy factor. The decomposition is performed till the level n^{th} until the entropy value of level n is approximately equal to the level n-1.

Table 5.15 PSNR of despeckled SAR images

		Before Despeckling	After Despeckling				
Image	σ	Default PSNR Values	ATV [26]	BayesWS-HAW[27]	Bivariate Thresholding [28]	IDPAD [29]	Proposed Method
SAR Image 1	5	25.1588	44.6736	43.2879	43.9918	44.8527	**48.8954**
	10	22.1475	44.5672	43.2341	42.7834	44.4261	**45.1272**
	20	19.1526	44.6732	42.5641	41.5642	43.7659	**44.8522**
	30	17.3726	43.2431	42.9867	41.4451	43.0909	**43.7231**
	40	16.2027	42.1101	41.6739	40.0934	41.6452	**42.6387**
SAR Image 2	5	20.2091	46.5643	43.3923	44.1983	46.1131	**46.7341**
	10	17.3042	45.6294	42.4562	43.8563	**45.9321**	45.7563
	20	14.4775	45.0095	42.2231	43.1951	44.0774	**45.1247**
	30	12.8544	44.6719	42.2495	42.6443	44.2341	**44.7684**
	40	11.7723	44.0035	41.0941	42.0902	43.7675	**44.1191**

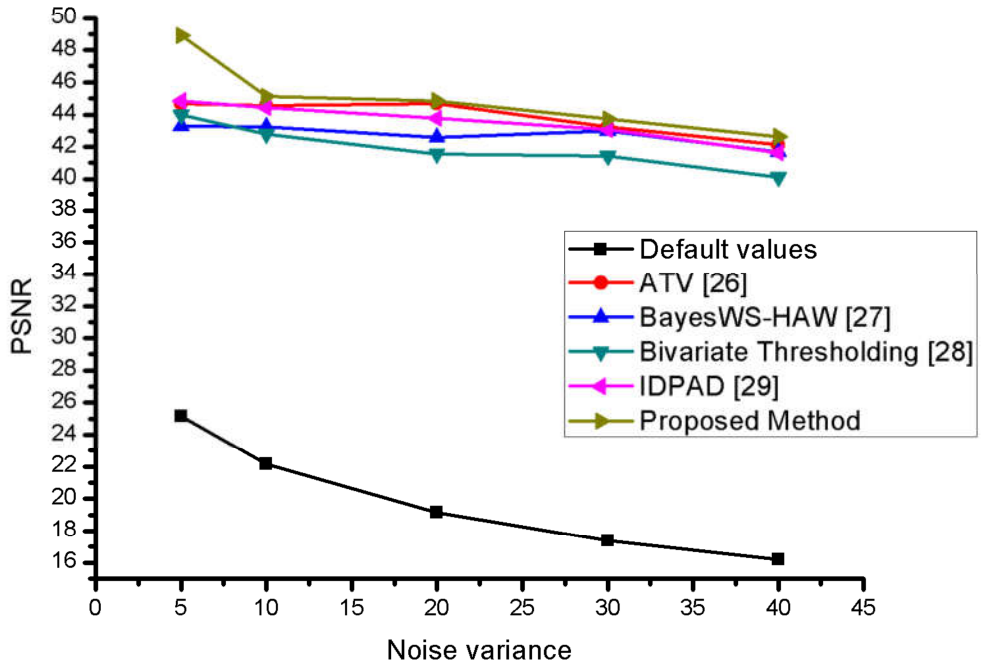

Figure 5.54 PSNR of SAR image 1

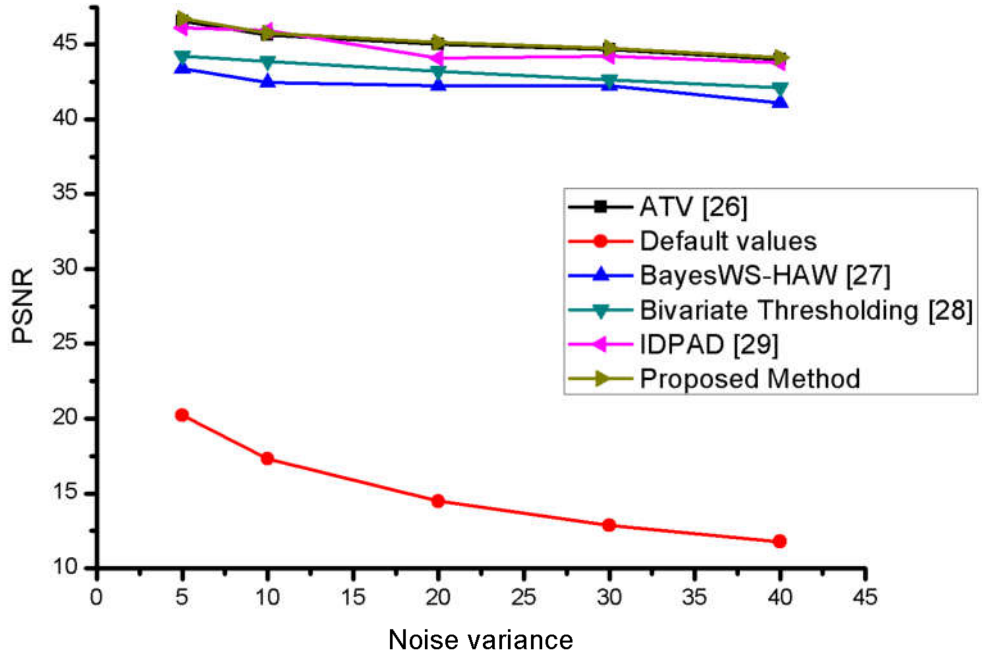

Figure 5.55 PSNR of SAR image 2

Table 5.16 SSIM of despeckled SAR images

		Before Despeckling	After Despeckling				
Image	σ	Default SSIM Values	ATV [26]	BayesWS-HAW[27]	Bivariate Thresholding [28]	IDPAD [29]	Proposed Method
SAR Image 1	5	0.6281	0.9878	0.9543	0.9673	0.9784	**0.9989**
	10	0.4682	0.9564	0.9432	0.9564	0.9453	**0.9647**
	20	0.3144	0.9153	0.9274	0.9241	0.9213	**0.9389**
	30	0.2380	0.9057	0.9094	0.9075	0.9091	**0.9182**
	40	0.1950	0.8954	0.8971	0.8745	0.8875	**0.8973**
SAR Image 2	5	0.7895	0.9785	0.9674	0.9666	0.9817	**0.9853**
	10	0.6575	0.9666	0.9561	0.9654	0.9563	**0.9756**
	20	0.4959	0.9514	0.9153	0.9482	0.9063	**0.9541**
	30	0.3992	**0.9219**	0.9085	0.9131	0.9063	0.9191
	40	0.3364	0.8974	0.8751	0.8821	0.8874	**0.9093**

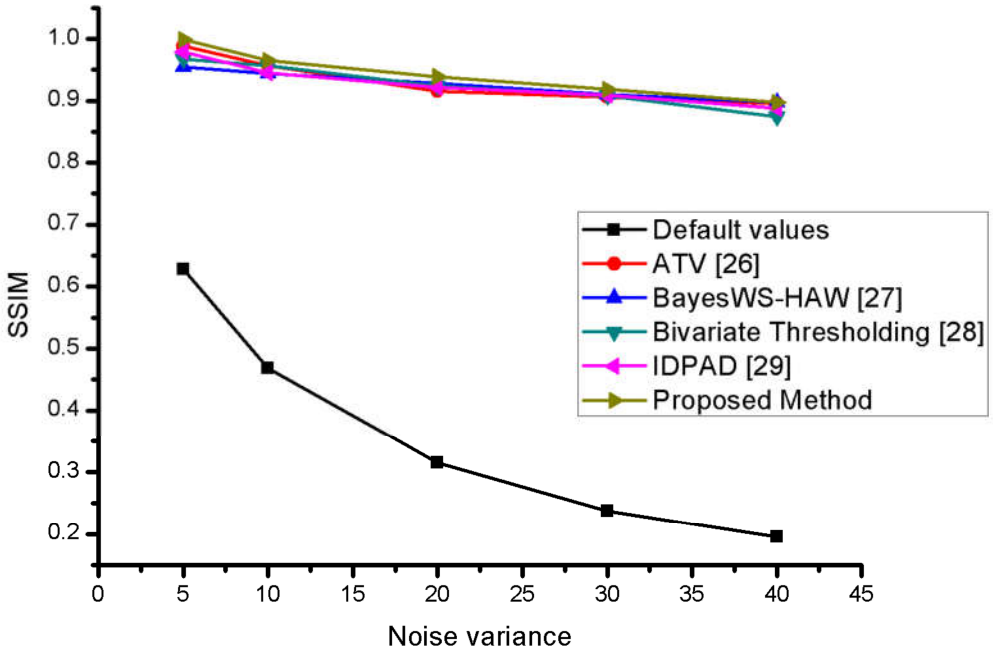

Figure 5.56 SSIM of SAR image 1

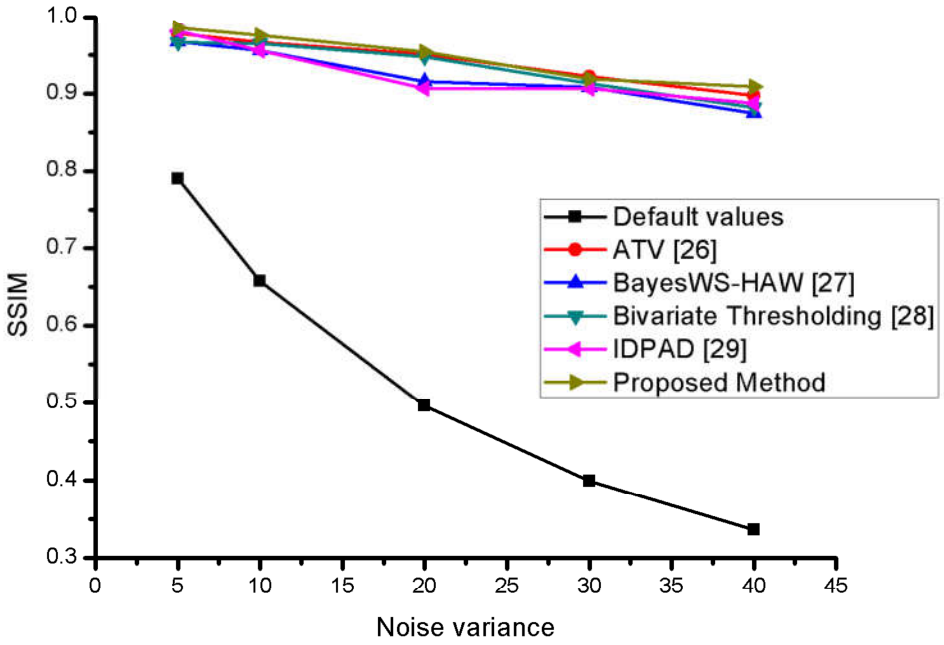

Figure 5.57 SSIM of SAR image 2

Table 5.17 SNR of despeckled SAR images

		Before Despeckling	After Despeckling				
Image	σ	Default SNR Values	ATV [26]	BayesWS-HAW [27]	Bivariate Thresholding [28]	IDPAD [29]	Proposed Method
SAR Image 1	5	20.4960	24.1256	25.0068	23.5674	24.0019	**25.3430**
	10	19.2512	23.4561	**24.9989**	23.1258	24.2985	24.3198
	20	17.4705	23.0258	23.9898	22.9478	**24.3333**	24.1021
	30	16.2215	22.5689	23.0258	22.0201	23.0589	**23.1230**
	40	15.2771	22.0145	22.9157	21.5698	22.9971	**23.0090**
SAR Image 2	5	13.7497	21.2365	22.3495	21.2598	23.0989	**23.1964**
	10	13.0248	22.3598	22.1254	21.0547	22.9589	**23.0101**
	20	11.9114	21.1211	21.2864	20.3256	22.5646	**22.9184**
	30	11.0817	20.1254	21.0597	20.0201	22.0358	**22.1614**
	40	10.4375	20.0032	20.7613	20.5632	21.9898	**22.1009**

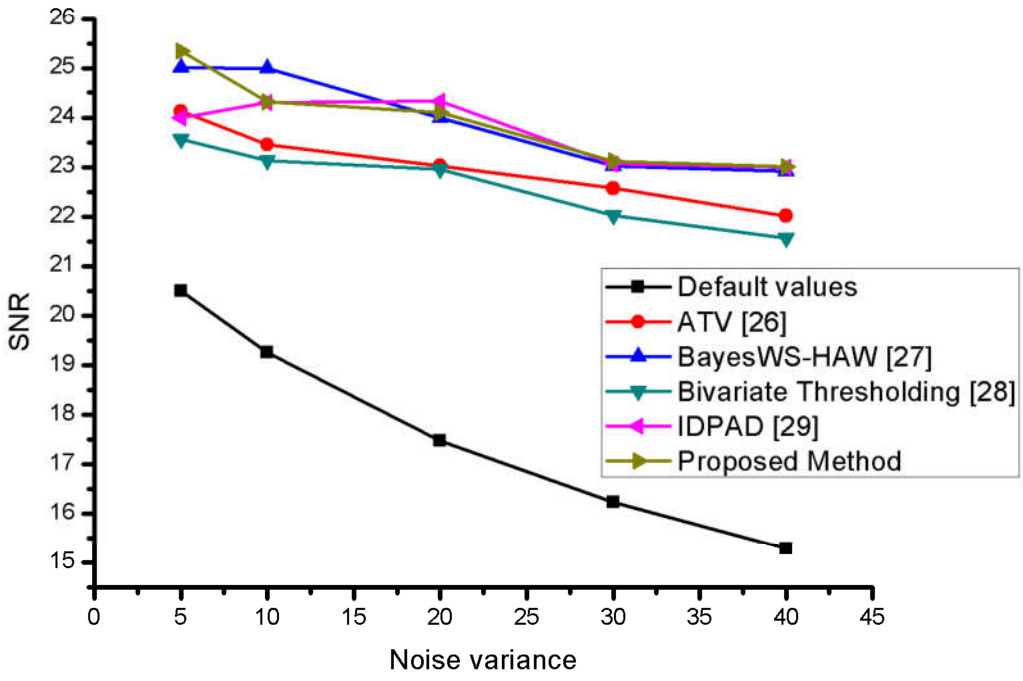

Figure 5.58 SNR of SAR image 1

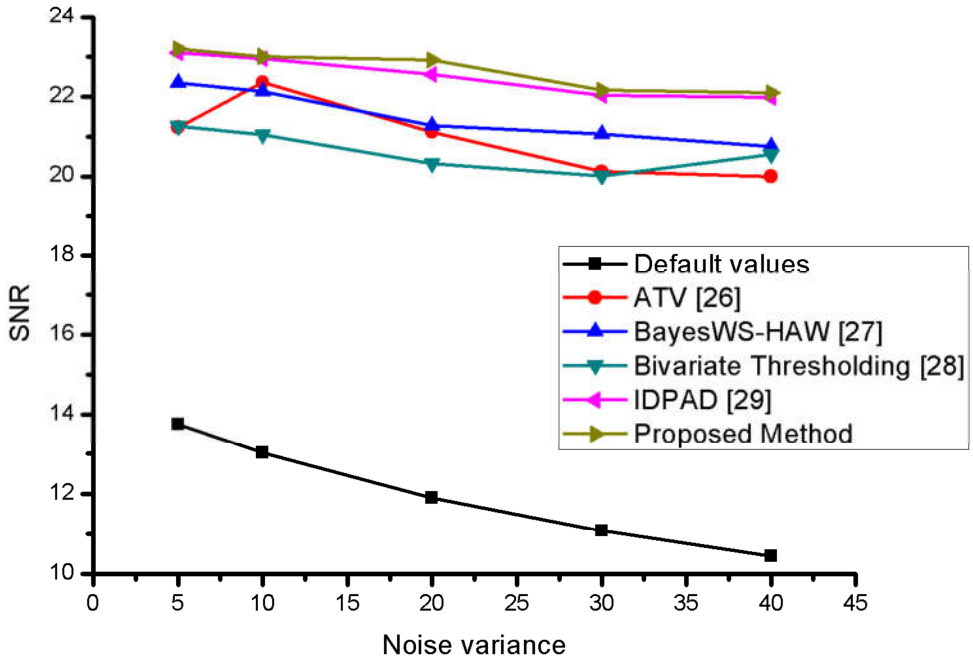

Figure 5.59 SNR of SAR image 2

Table 5.15, 5.16 and 5.17 shows the comparative analysis of HMN-CF with respect to other existing methods in terms of PSNR, SSIM and SNR. The best quantitative results are denoted in bold. The despeckling results displayed in 5.15, 5.16 and 5.17 shows the superiority of the HMN-CF among other existing methods. In Table 5.15, the PSNR of the HMN-CF shows the best results among the compared method. The IDPAD method at $\sigma = 10$ in SAR image 2 shows the best result among all methods but still, the overall texture of the HMN-CF is better than IDPAD at $\sigma = 10$. In Table 5.16, The SSIM of the HMN-CF also shows the best result among all compared methods. The ATV method at $\sigma = 30$ in SAR image 2 shows the better result but on zooming the output image it is seen that the small detail parts are lost and overall structure of the image is slightly distorted. The method based on anisotropic diffusion (IDPAD) shows better result in terms of texture and edge preservation. In Table 5.17, the results of the HMN-CF are compared on the basis of SNR values. All the SNR quantitative values show the better performance than the other compared methods. Only two methods i.e. BayesWS-HAW and IDPAD show better results than the HMN-CF at $\sigma = 10$ and 20 respectively. The Table 5.15, 5.16 and 5.17 shows the quantitative analysis of the despeckling methods before and after despeckling. It helps in understanding the effectiveness and strength of the despeckling methods at different noise variances. The PSNR value of the despeckled

SAR image 1 and 2 are graphically analyzed in the Figure 5.54 and 5.55. The SSIM value of the despeckled SAR image 1 and 2 are graphically analyzed in the Figure 5.56 and 5.57. The SNR value of the despeckled SAR image 1 and 2 are graphically analyzed in the Figure 5.58 and 5.59.

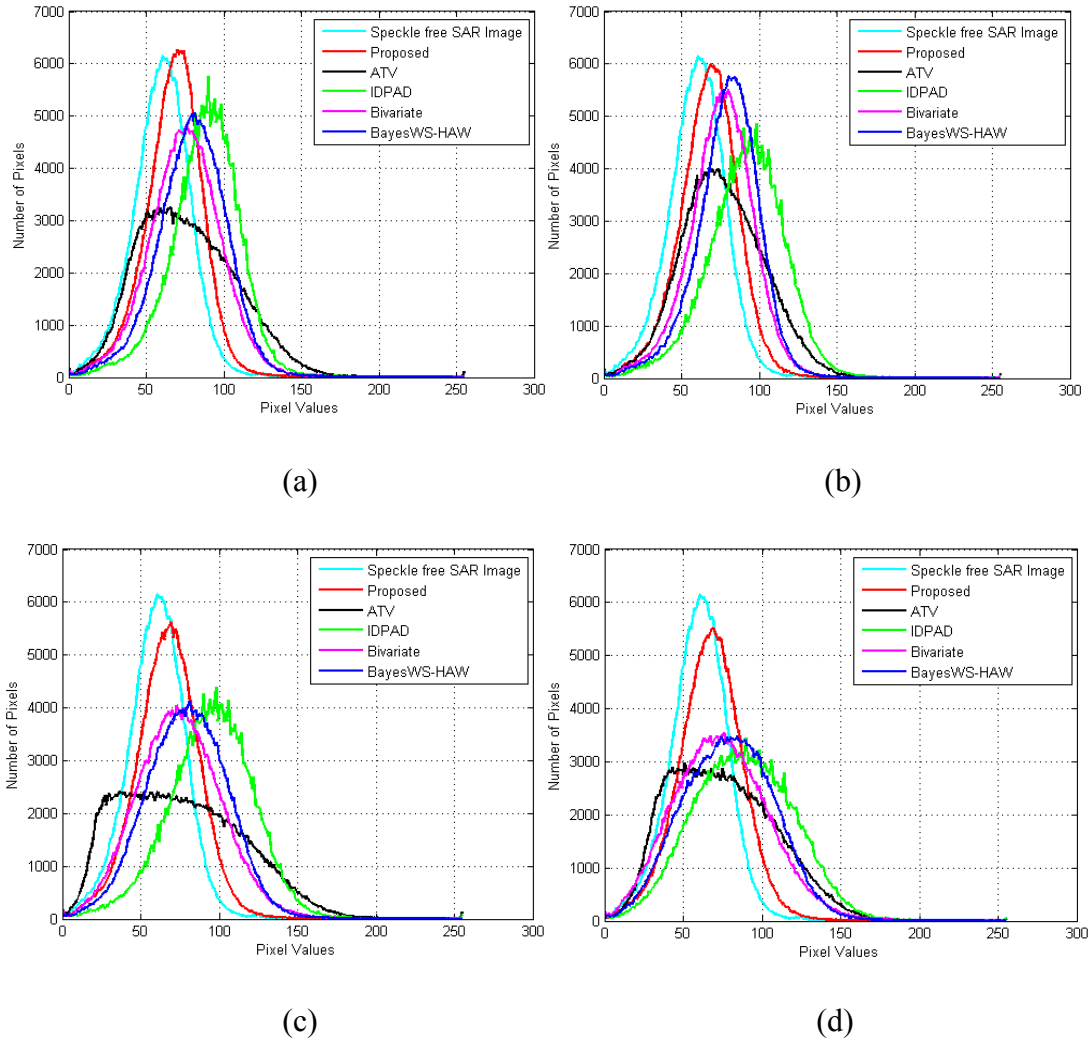

Figure 5.60 Plotting reference SAR image and results of proposed method (HMN-CF), ATV, IDPAD, Bivariate and BayesWS-HAW methods using histogram at (a) σ = 10 (b) σ = 20 (c) σ = 30 (d) σ = 40.

The Figure 5.60 shows the comparative analysis of the despeckled results of despeckling methods at various noise variance levels i.e. (σ = 10, 20, 30, 40). The plot is generated using histogram. It depicts the similarity and closeness of the despeckling output result with the reference SAR image. The plot closer to the reference SAR image shows the best result. It can be observed that the HMN-CF is close to the reference SAR image. This indicates the best despeckling results of HMN-CF.

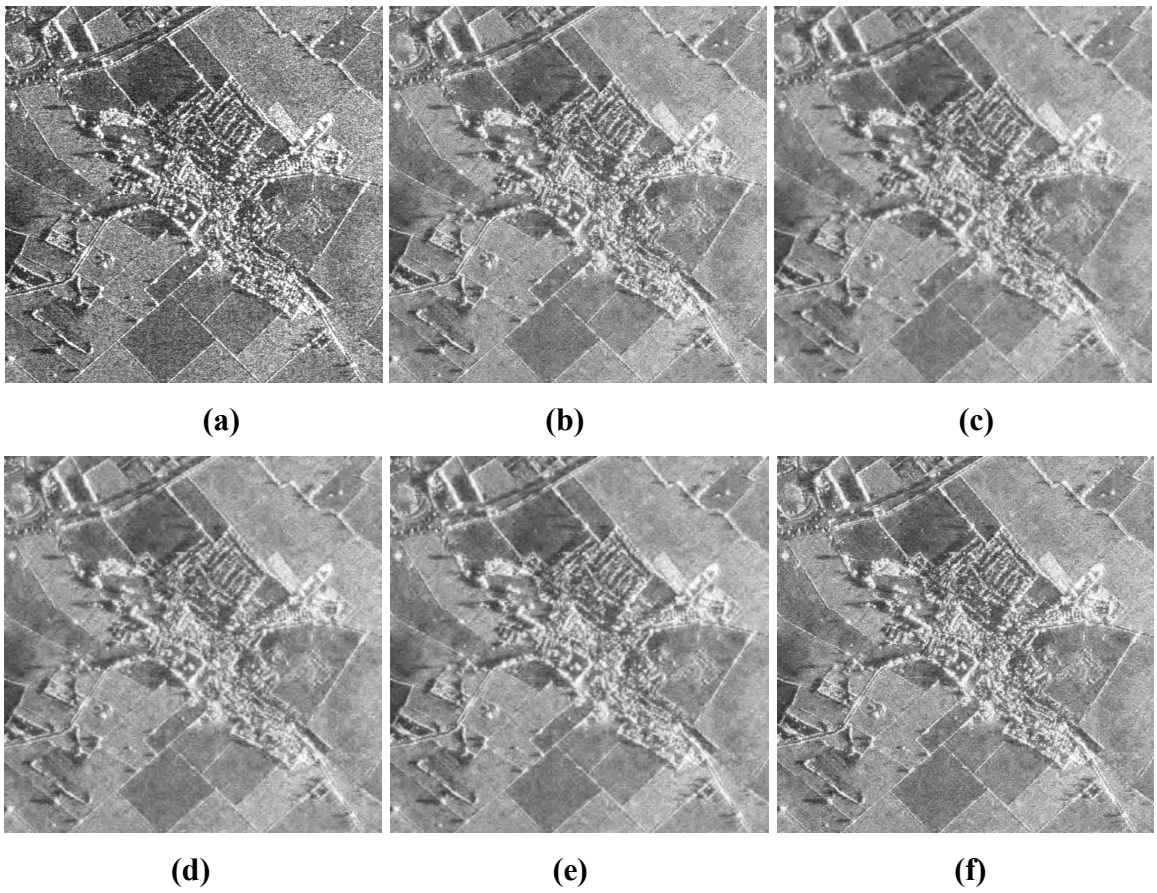

Figure 5.61 Results of the despeckling algorithm on real SAR images (a) real speckled SAR image (b) results of ATV (c) results of BayesWS-HAW (d) results of Bivariate thresholding (e) results of IDPAD (f) results of the HMN-CF

The HMN-CF is experimented on the both simulated and real speckled SAR image. The visual results of the despeckling methods on the real speckled SAR images are shown in Figure 5.61 and analyzed in Figure 5.62 and 5.63. The detail preservation can be analyzed by concentrating on the important features of the image. In Figure 5.62 and 5.63, the despeckling results of the HMN-CF are shown in terms of edge and texture preservation. The smoothness in the homogeneous region and detail preservation in the heterogeneous areas is better achieved by HMN-CF and analyzed by zooming the specific parts of the image as shown in Figure 5.63.

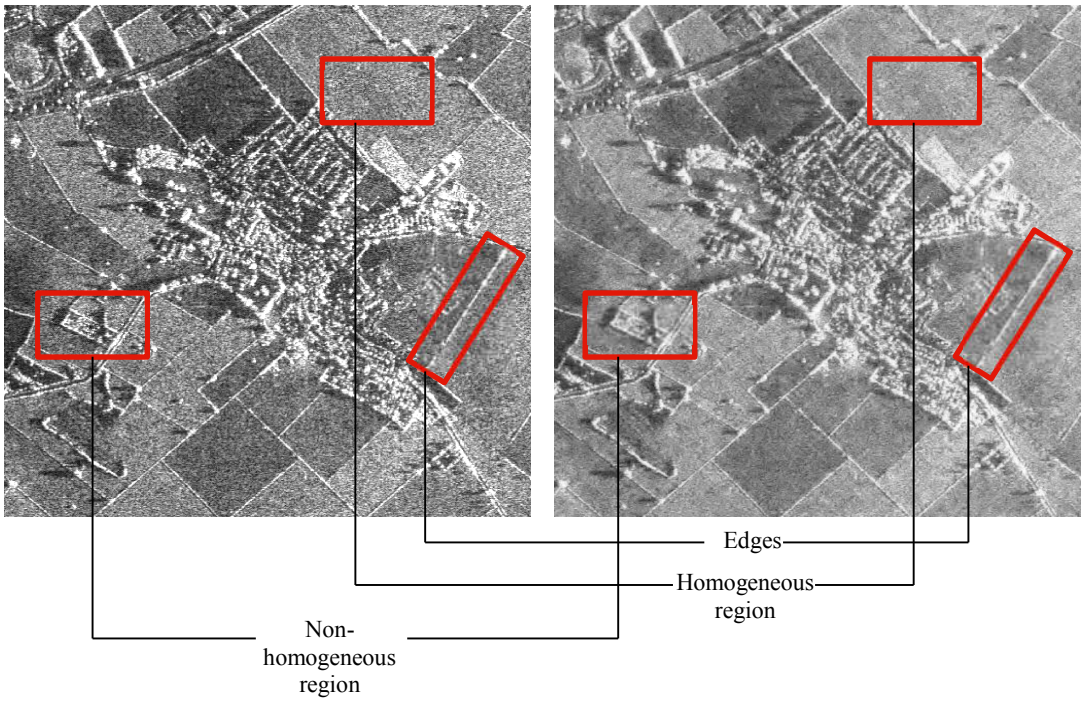

Figure 5.62 Analysis of speckle reduction and detail preservation in the HMN-CF

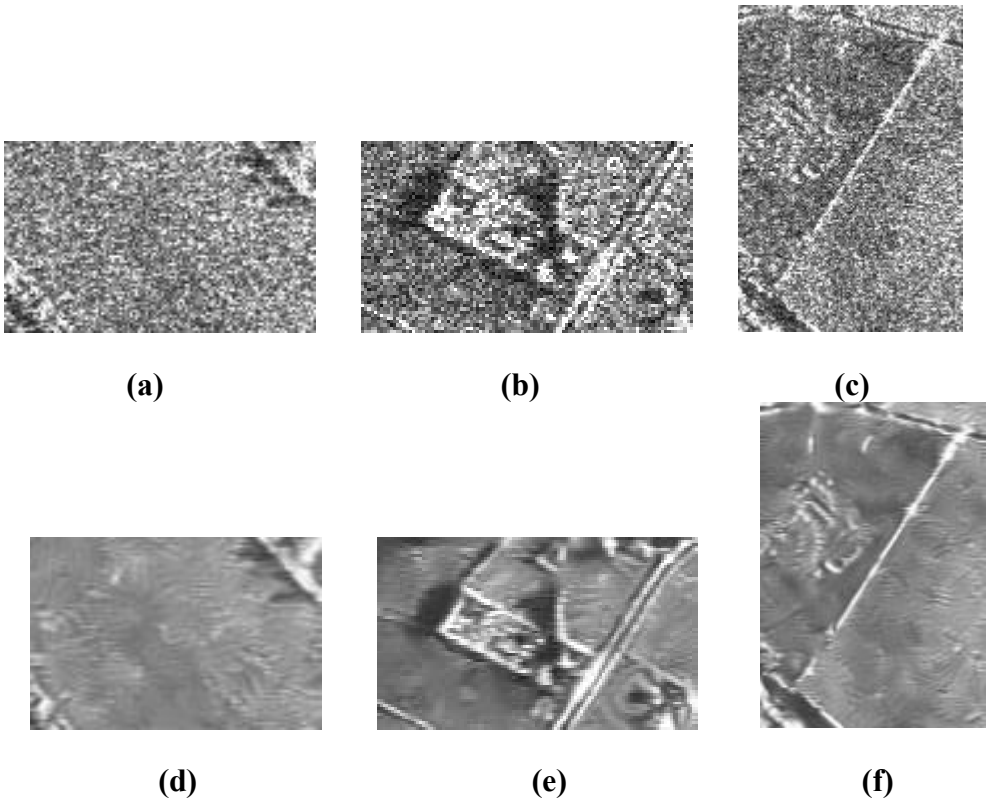

Figure 5.63 Analysis of zoomed part of the despeckled SAR image 3 using HMN-CF assessing the detail preservation like edge preservation, smoothness in the homogeneous region, texture preservation in the heterogeneous region and speckle reduction

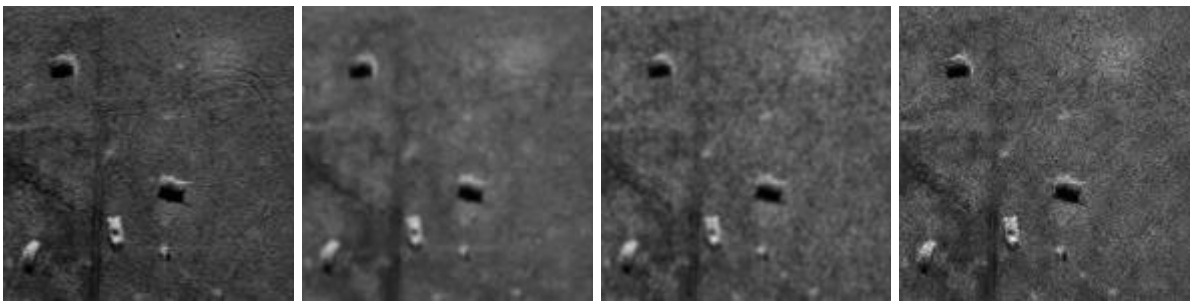

(a) **(b)** **(c)** **(d)**

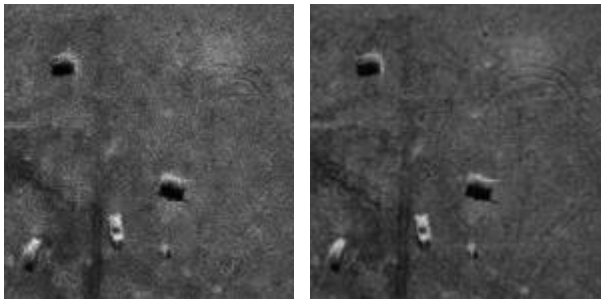

(e) **(f)**

Figure 5.64 Results of zoomed areas of SAR image 1 using different despeckling algorithm (a) reference SAR image (b) results of ATV (c) results of BayesWS-HAW (d) results of Bivariate thresholding (e) results of IDPAD (f) results of the HMN-CF

The smoothness of the homogeneous region, preservation of edge, point scatterers and textured region are assessed in Figure 5.64. On comparing the zoomed-in despeckling result of despeckling methods i.e. Figure 5.64(b-f); it is observed that the HMN-CF (Figure 5.64(f)) shows the best preservation of details in the despeckled SAR image as a comparison to other methods (Figure 5.64(b-e)). The Figure 5.64(a) shows the reference zoomed-in SAR image. On visual inspection, the Figure 5.64(f) shows that it is the most similar image to Figure 5.66(a). This validates the best speckle reduction and detail preservation in the HMN-CF.

5.4.3 Analysis of Locally Correlated Detailed Subband

The resultant high-frequency subbands of Bayesian and Bivariate shrinkage methods are fused using local correlation based strategy. Table 5.18 shows the degree of similarity i.e. correlation between the despeckled detailed subbands of Bayesian and Bivariate shrinkage methods at various noise variances (σ = 5, 10, 20, 30, 40).

Let, at σ = 20, the despeckled detailed subbands of Bayesian and Bivariate shrinkage rule are (HL', LH', HH') and (HL'', LH,'' HH'') respectively, the CC is calculated using Eq. 4.11.

At σ = 20,

$$CC(LH', LH'') = 0.8759,$$

$$CC(HL', HL'') = 0.8598,$$

$$CC(HH', HH'') = 0.8479.$$

Similarly, the correlation of rest of the subbands is evaluated. This analysis determines the degree of similarity between these two subbands. Based on this correlation similarity factor, the local correlation based fusion strategy is designed using which these two high-frequency coefficients are fused.

Table 5.18 Correlation values between detailed subbands at various noise levels

Noise variance	LH subband	HL subband	HH subband
σ = 5	0.9527	0.9658	09758
σ = 10	0.9159	0.9158	0.9258
σ = 20	0.8759	0.8598	0.8479
σ = 30	0.8143	0.8258	0.8157
σ = 40	0.7589	0.7656	0.7458

The HMN-CF uses local correlation based fusion strategy. Here the local filtering is applied based on the fusion strategy which is grounded on the correlation coefficients of the selected masks.

5.4.4 Execution Time Comparison

The experiment is performed on following system configuration: MATLAB version = 8.3, name = R2014a on Intel(R) Core(TM) i5-2410 M CPU @ 2.30 GHz, 4 GB RAM and 64-bit operating system. The system configuration is essential to note down for the comparative evaluation of the execution time of the proposed method. The HMN-CF is computationally

costly due to two main reasons. First, the selection of the threshold value takes time as a mask of 3 × 3 is run over the two different enhanced detailed components. A non-overlapping block processing is done for the calculation of threshold value. The second reason for high cost is a fusion of two enhanced detailed component using a mask of 5 × 5 by defined local correlation based strategy. The local block processing is always time-consuming. But the results are better than global block processing in most of the case.

Table 5.19 Execution time of various despeckling techniques

Despeckling methods	Execution time (in seconds)
ATV	**27.2658**
BayesWS-HAW	28.1673
Bivariate Thresholding	75.2697
IDPAD	55.2366
HMN-CF	73.561

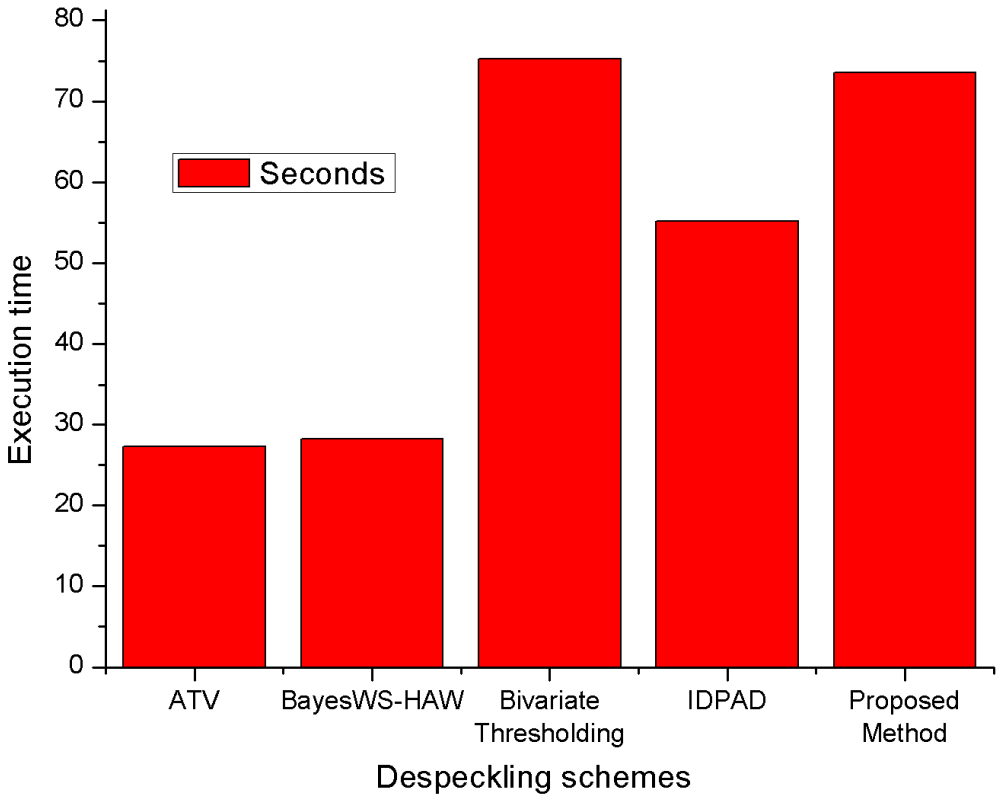

Figure 5.65 Graphical comparative computational cost analysis

Therefore the selection of threshold value and fusion strategy are the two main reasons for the high computational cost of HMN-CF as shown in Table 5.19 and analyzed in Figure 5.65. But the despeckling result of HMN-CF is better than the compared methods. Therefore the demerit of high computation cost can be ignored against better visual and quantitative results.

5.4.5 Validation of HMN-CF: Hypothesis Testing using Paired T-test.

The HMN-CF is validated using T-test over 30 numbers of samples as shown in Table 5.20. The HMN-CF is experimented using different metrics like PSNR, SSIM and SNR values at different noise variances over two different SAR images. Based on the experimented results over the different SAR images, the experimented sample data is collected and tested using hypothesis testing based on paired T-test.

There is total of 30 numbers of experimented sample data collected using the PSNR, SSIM, and SNR at different noise variances (σ = 5, 10, 20, 30, 40). This data is collected by performing the experiment over two different SAR images. The related sample data is the quantitative values of the SAR image before and after despeckling. The level of significance is set to 5.

The following null and alternate hypothesis needs to be tested: The H_o denotes the null hypothesis and H_a denotes the alternate hypothesis.

$H_o: \mu_D = 0$ (There is no difference between SAR image before and after despeckling in terms of quality, i.e. “No despeckling”).

$H_a: \mu_D \neq 0$ (There is a difference between SAR image before and after despeckling in terms of quality, i.e. “Good despeckling”).

Table 5.20 Dataset 3

No. of Samples	Values before Despeckling (X_i)	Values after Despeckling(Y_i)	Difference ($D_i=X_i - Y_i$)
1.	25.1588	48.8954	-23.7366
2.	22.1475	45.1272	-22.9797
3.	19.1526	44.8522	-25.6996
4.	17.3726	43.7231	-26.3505
5.	16.2027	42.6387	-26.436

6.	20.2091	46.7341	-26.525
7.	17.3042	45.7563	-28.4521
8.	14.4775	45.1247	-30.6472
9.	12.8544	44.7684	-31.914
10.	11.7723	44.1191	-32.3468
11.	0.6281	0.9989	-0.3708
12.	0.4682	0.9647	-0.4965
13.	0.3144	0.9389	-0.6245
14.	0.2380	0.9182	-0.6802
15.	0.1950	0.8973	-0.7023
16.	0.7895	0.9853	-0.1958
17.	0.6575	0.9756	-0.3181
18.	0.4959	0.9541	-0.4582
19.	0.3992	0.9191	-0.5199
20.	0.3364	0.9093	-0.5729
21.	20.4960	25.3430	-4.847
22.	19.2512	24.3198	-5.0686
23.	17.4705	24.1021	-6.6316
24.	16.2215	23.1230	-6.9015
25.	15.2771	23.0090	-7.7319
26.	13.7497	23.1964	-9.4467
27.	13.0248	23.0101	-9.9853
28.	11.9114	22.9184	-11.007
29.	11.0817	22.1614	-11.0797
30.	10.4375	22.1009	-11.6634
n = 30			$\sum \mathrm{D_i} = 364.3894$

As calculated from the above sample data, the corresponding sample means are $\overline{X_i}$=11.003 and $\overline{Y_i}$=23.149 and the calculated sample standard deviation are s_1=8.244 and s_2=18.398. The mean of difference ($\overline{D}$) and standard deviation of difference (σ_{diff}) are calculated using below two equation respectively.

$$\overline{D} = \frac{\sum D_i}{n} = -12.146$$

$$\sigma_{diff} = \sqrt{\frac{\sum D_i^2 - (\overline{D})^2 * n}{n-1}} = 11.757$$

Depending on the information available, the significance level is α = 0.05, and the degree of freedom (df) = n – 1 = 29.

Hence, it is found that the critical value for this two-tailed test is

$t_c = 2.045$, for α = 0.05 and df = 29.

The rejection region for this two-tailed test is R = { t : | t | > 2.045}.

The t-statistic is calculated as shown in the following formulation:

$$t = \frac{\overline{D}}{\sigma_{diff}/\sqrt{n}} = \frac{-12.146}{11.757/\sqrt{30}} = -5.659$$

Since it is observed that | t | = 5.659 > t_c = 2.045, It is concluded that the null hypothesis H_o is rejected. Therefore, there is enough evidence to claim that the difference of quantitative values before and after despeckling is considered to be extremely statistically significant, at the 0.05 significance level.

5.5 Comparison of HMN-AD, HMN-DSF and HMN-CF

The proposed methods i.e. HMN-AD, HMN-DSF and HMN-CF are experimented on simulated as well as real speckled SAR images. The performance of the HMN-AD, HMN-DSF and HMN-CF are evaluated in both cases i.e. with and without-reference indexes. This section compares the HMN-AD, HMN-DSF and HMN-CF on the basis of quantitative metrics used in with and without-reference index cases. The despeckling results of HMN-AD, HMN-DSF and HMN-CF are also analyzed by visual quality of the despeckled image and computational time.

5.5.1 Results (With-Reference Indexes)

In order to compare HMN-AD, HMN-DSF and HMN-CF in terms of performance evaluation, their experimental results are performed on simulated SAR image 1 as shown in Figure 5.66. In this case it is assumed that the actual reflectivity or actual ground truth is known. The experimental and quantitative results are computed with respect to the results of the reference SAR image 1. The quantitative measures used to evaluate the performance are

PSNR and SSIM. The PSNR measures the overall quality of the image and SSIM emphasis on the structure of the objects in the image.

Figure 5.66 SAR image 1

Table 5.21 PSNR values of HMN-AD, HMN-DSF and HMN-CF

		Before Despeckling	After Despeckling		
Image	σ	Default PSNR Values	HMN-AD	HMN-DSF	HMN-CF
SAR Image 1	5	25.1588	43.7059	44.5715	**48.8954**
	10	22.1475	41.6010	42.3764	**45.1272**
	20	19.1526	39.9001	40.9403	**44.8522**
	30	17.3726	38.4579	40.0023	**43.7231**
	40	16.2027	36.6709	35.0193	**42.6387**

Table 5.22 SSIM values of HMN-AD, HMN-DSF and HMN-CF

		Before Despeckling	After Despeckling		
Image	σ	Default SSIM Values	HMN-AD	HMN-DSF	HMN-CF
SAR Image 1	5	0.6281	0.9725	0.9958	**0.9989**
	10	0.4682	0.9691	0.9487	**0.9647**
	20	0.3144	0.9358	0.9261	**0.9389**
	30	0.2380	**0.9229**	0.9220	0.9182
	40	0.1950	**0.9209**	0.9119	0.8973

(a) **(b)** **(c)**

Figure 5.67 Results of HMN-AD, HMN-DSF and HMN-CF at σ = 25

After applying HMN-AD, HMN-DSF and HMN-CF on SAR image 1 at different noise variances ranging from (σ ≈ 1-50); it is observed that the HMN-CF performs best among all the three proposed methods. The observed PSNR and SSIM value denotes the best quantitative results of the HMN-CF as shown in the Table 5.21 and 5.22. The despeckling results shown in the Figure 5.67, Table 5.21 and 5.22 is experimented at the σ = 25. At high noise variances the HMN-AD shows better result than the other two methods in terms of structure preservation but on visually analyzing the Figure 5.67, it can be easily observed that the visual appearance of the Figure 5.67(c) is best among all in terms of edge, texture and structure preservation. The HMN-AD and HMN-DSF perform well in terms of detail preservation, but the HMN-CF is best among all.

The performance of the HMN-AD, HMN-DSF and HMN-CF are graphically shown in the Figure 5.68 and 5.69, that demonstrates the despeckling results at the σ = 25 before and after the despeckling process.

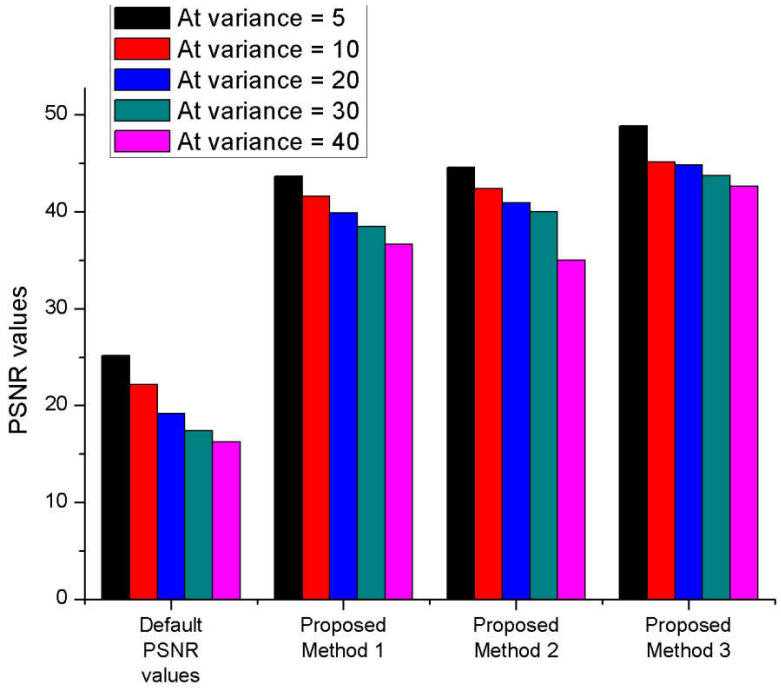

Figure 5.68 Plotting PSNR of HMN-AD, HMN-DSF and HMN-CF

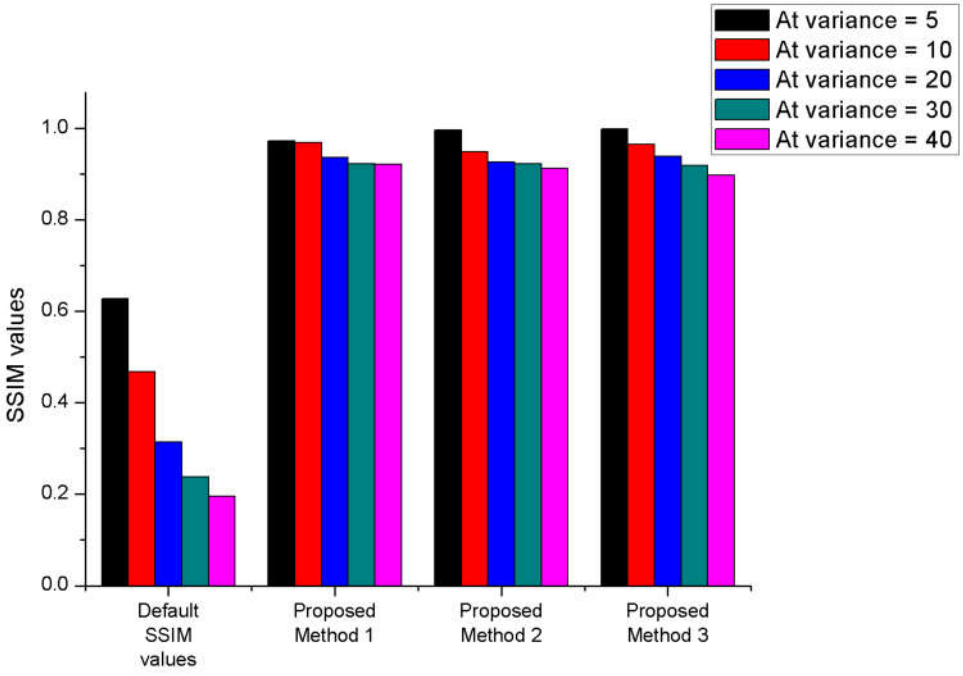

Figure 5.69 Plotting SSIM of HMN-AD, HMN-DSF and HMN-CF

5.5.2 Results (Without-Reference Indexes)

Figure 5.70 SAR image 2

The proposed methods i.e. HMN-AD, HMN-DSF and HMN-CF are experimented on real speckled SAR image 2 with the noise variance = 7.2567 as shown in Figure 5.70. The quantitative metrics used for performance evaluation are different from the metrics used in with-reference indexes case. Here the performance metrics are grounded on the multiplicative noise model i.e. NV and ENL.

Table 5.23 Noise Variance of HMN-AD, HMN-DSF and HMN-CF

	Before Despeckling	After Despeckling		
Image	Noise Variance	HMN-AD	HMN-DSF	HMN-CF
SAR Image 2	7.2567	0.5013	0.3915	**0.3591**

Table 5.24 ENL values of HMN-AD, HMN-DSF and HMN-CF

	Before Despeckling	After Despeckling		
Image	ENL	HMN-AD	HMN-DSF	HMN-CF
SAR Image 2	1.8055	2.4013	2.6657	**2.8612**

(a) **(b)** **(c)**

Figure 5.71 Results of HMN-AD, HMN-DSF and HMN-CF

The quantitative values of the despeckling results are shown in the Table 5.23 and 5.24. The NV of real speckled SAR image is calculated to 7.2567. After applying all three proposed methods, HMN-CF performs the best among all. The NV after despeckling using HMN-CF is calculated as 0.3591 that is lowest among all the three methods that demonstrate the lowest speckle content. The second metric used for performance evaluation is ENL. It evaluates the smoothness in the homogeneous areas of the image. The ENL of the HMN-CF is highest i.e. 2.8612. The results in the Figure 5.71, Table 5.23 and Table 5.24 concludes that the HMN-CF performs the best among all the three methods in terms of speckle reduction, deblurring and smoothness in the homogeneous regions. The NV values of HMN-AD, HMN-DSF and HMN-CF are graphically analyzed in the Figure 5.72. The ENL values of HMN-AD, HMN-DSF and HMN-CF are graphically analyzed in the Figure 5.73.

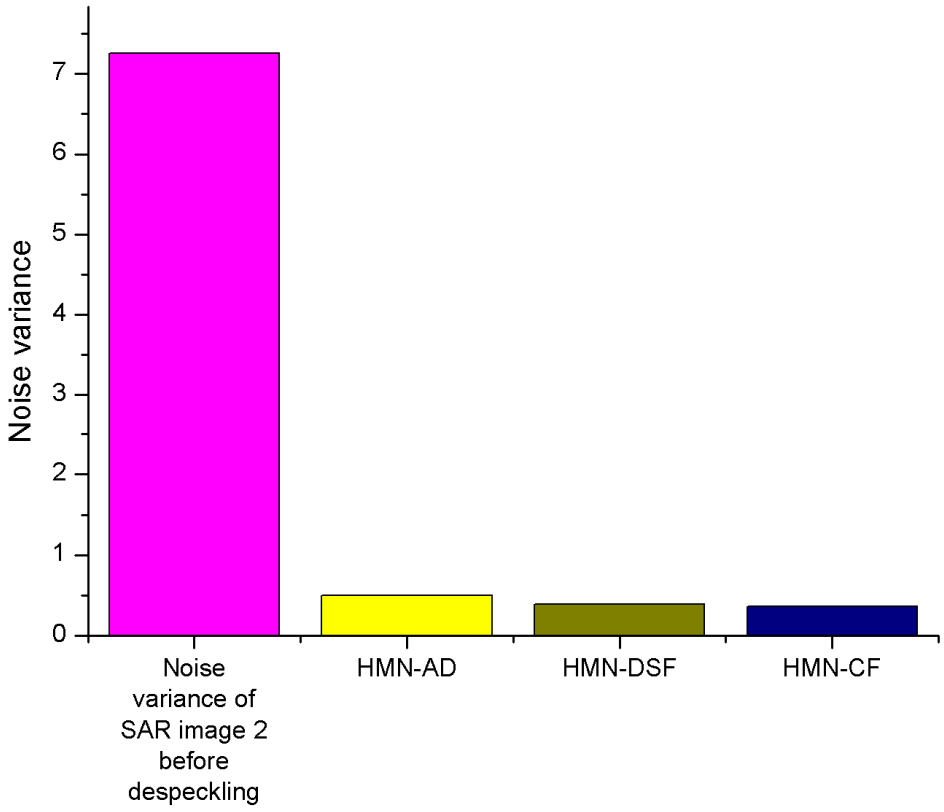

Figure 5.72 Plotting noise variance of HMN-AD, HMN-DSF and HMN-CF

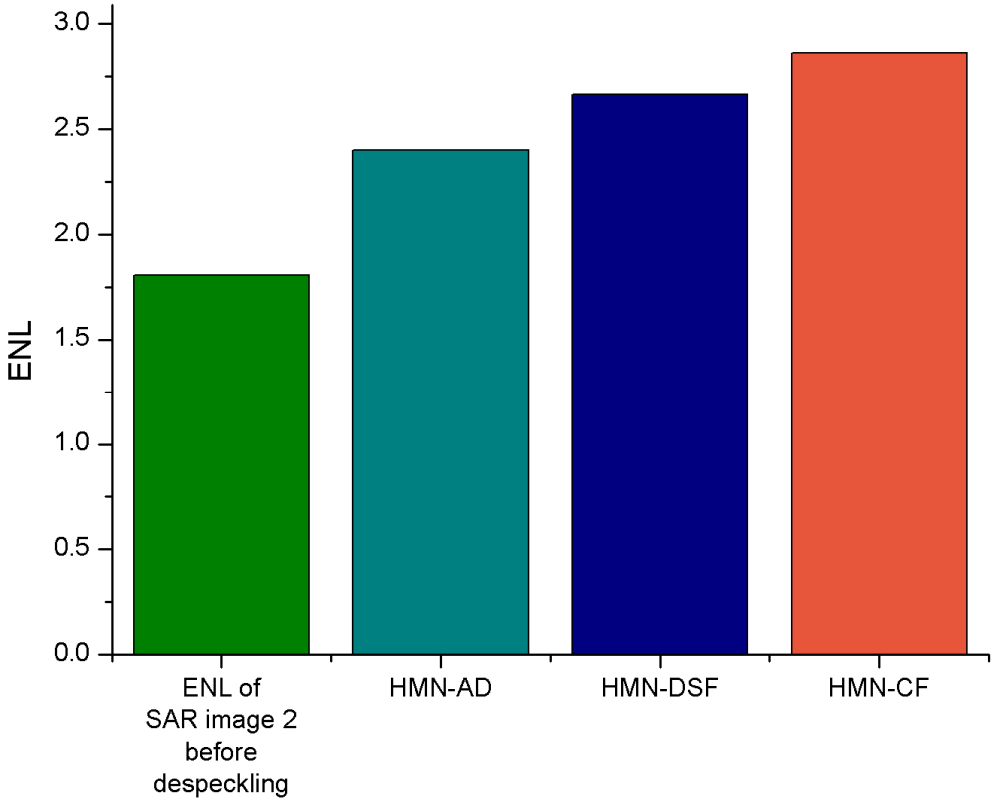

Figure 5.73 Plotting ENL of HMN-AD, HMN-DSF and HMN-CF

5.5.3 Execution Time Comparison

The visual quality and quantitative values of the HMN-CF is best among the proposed methods. But the computation cost of the HMN-CF is highest among them. The HMN-CF takes approximately 73 seconds to execute. This time is very large as a comparison to the time taken by the HMN-AD and HMN-DSF as shown in Table 5.25 and comparatively analyzed in Figure 5.74.

Table 5.25 Execution time of HMN-AD, HMN-DSF and HMN-CF

Despeckling method	Execution time (in seconds)
HMN-AD	3.2136
HMN-DSF	6.3219
HMN-CF	73.5610

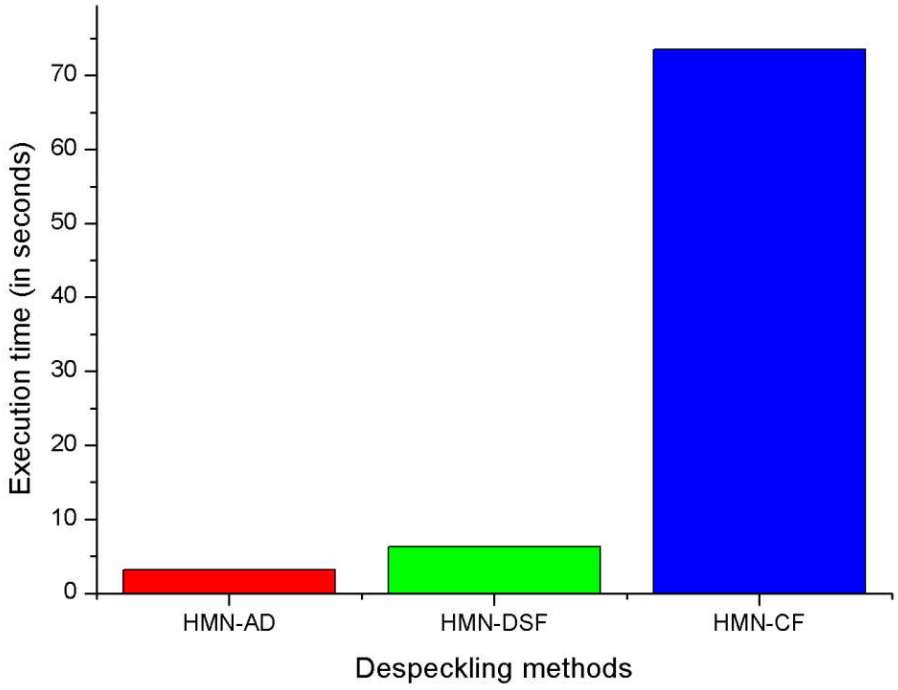

Figure 5.74 Plotting computational time of HMN-AD, HMN-DSF and HMN-CF

5.6 Conclusion

This chapter discusses the experimental results of HMN-AD, HMN-DSF and HMN-CF in detail and analyses in tabular and graphical form. The proposed methods are compared with some conventional and non-conventional methods. All the three proposed methods are analyzed using visual quality of the despeckled SAR image and quantitative measures like PSNR, SNR, and ENL etc. The HMN-AD, HMN-DSF and HMN-CF show better performance among the compared despeckling methods. Among the three proposed methods, the HMN-CF shows the best performance in terms of visual quality and quantitative measure. But this method is computationally costly. The HMN-AD is best in terms of computational cost. The HMN-DSF shows better visual results than HMN-AD but again it is slightly more costly than the HMN-AD.

6. CONCLUSION AND FUTURE SCOPE

6.1. Background

This chapter summarizes the thesis with the major finding and achievements of the research. Other analytical findings related to SAR image despeckling are also discussed. The transition from one method to another is highlighted. The possible future scope and directions are also discussed at the end of this chapter.

6.2 Major Findings

The main motive behind this thesis is to design and develop a speckle reduction technique for SAR images with better preservation of fine details like texture, edges and other features. The experimental results are performed on simulated SAR image at different noise variance level and on real speckled SAR images. The image denoising is one of the highly researched fields in the domain of image processing. The wavelet-based image denoising techniques that offer multiresolution analysis have established significant landmark in last few years. But due to the restriction of directional selectivity, the wavelet-based multi-resolution image restoration techniques cannot easily cater to the growing requirements of effective denoising with an edge and feature preservation. Despite this restriction of the wavelet transform, the proposed methods i.e. HMN-AD, HMN-DSF and HMN-CF based on the wavelet transform show better despeckling results than many of the other conventional and non-conventional methods by the intelligent use of method noise and local correlation based fusion strategy. The optical imaging, SAR imaging, medical imaging etc. are the major application fields that contain the

highest information and require detail preservation, image enhancement and denoising procedures. The thesis proposes three different despeckling techniques for SAR images. The proposed methods are based on wavelet transform using hybrid combination of Bayesian and non-Bayesian methods. The experimented result of proposed methods is compared with the traditional and non-traditional methods. In order to validate the proposed methods, the experiment is also performed on the optical images by simulation process. For more rigorous analysis of proposed methods, the speckle noise is added ranging from (σ = 5 to 50) in those SAR images where the noise variance is low. This tests the effectiveness and strength of the proposed methods at the higher noise level.

A new wavelet-based SAR image despeckling technique is proposed to reduce the speckle noise by preserving the fine details of the image using anisotropic diffusion and method noise thresholding i.e. HMN-AD. The part of the despeckled image that still contains the speckle noise i.e. unfiltered part of the image is processed again using method noise thresholding. The performance of the HMN-AD is assessed by visual appearance of the despeckled SAR image and with quantitative metrics such as PSNR, SSIM, UIQI, and RMSE. It is observed that the visual quality of the despeckled image of HMN-AD is better than the compared standard methods. The computational time of the HMN-AD is compared with some standard filters. The execution time of the HMN-AD is very low. The performance percentage of the HMN-AD is 87.50 % that is calculated by analyzing the comparative quantitative value of the performance metrics. The HMN-AD is implemented and tested on simulated SAR images at various noise variance levels as well as on real speckled SAR images. On critical comparative analysis, it can be said that HMN-AD eliminates the speckle noise efficiently and recovers the lost edges and structures in the SAR image. No blocky artifacts are generated during the despeckling process. The HMN-AD has the potential ability to be used in various practical applications of SAR images.

This HMN-AD is the hybrid combination of the Bayesian method in a transform domain (homomorphic filtering in wavelet domain) and non-Bayesian methods (anisotropic diffusion). This unique despeckling combination delivers high image quality with good visual appearance. The computational cost of HMN-AD is highly efficient. The method noise thresholding is implemented as the post-processing step. It enhances the quantitative results as well as the visual quality of the despeckled image. This hybrid combination and easy use of method noise can give such good results, then a way better and intelligent use of method

noise can give much better results. The results of HMN-AD motivate to go for designing of new proposed method i.e. HMN-DSF with more intelligent use of method noise.

A new wavelet-based homomorphic SAR image despeckling method has been proposed for eliminating the speckle noise using DSF and method noise thresholding i.e. HMN-DSF. The first step of this method is to decompose speckled SAR image using db2 based 2D-DWT into approximation and detailed component. The second step is to filter the approximate component using DSF followed by method noise thresholding and the third step is to filter the detailed component by wavelet thresholding followed by method noise thresholding. The detailed analysis is performed on the experimental results of the HMN-DSF and competitive comparison is done with 23 standard filters and advanced methods. It validates the best performance of the HMN-DSF over other conventional and non-conventional methods. The qualitative analysis of the despeckled SAR image is performed by analyzing the visual appearance and it is concluded that there is no presence of the artifacts after the despeckling process, the edges and texture are well preserved, the low contrast objects are visible and the smoothness in homogeneous and non-homogeneous region is well maintained. The execution time of HMN-DSF is low. The quantitative analysis is done using ENL, NV, CV, and MSE for real speckled SAR image and PSNR, SSIM and UIQI for simulated SAR image. The statistical results of the HMN-DSF are normalized and encouraging. On comparing with the 23 traditional and non-traditional filters, the proposed method gives a very competitive performance in terms of speckle noise removal, performance metrics and computational cost. The HMN-DSF has the capability to be used in the practical and real-time applications.

The basic implementation (as a post-processing step) of method noise in the HMN-AD shows the decent result. This concludes with the new idea of using the concept of method noise in the more intelligent way for best results. The HMN-DSF is entirely based on the use of method noise. The method noise is used for fine detail preservation like edges. Another filter used in HMN-DSF is DSF that is specifically used for edge preservation. HMN-DSF is an edge-preserving procedure. This method offers a new intelligent use of method noise in two different ways. The concept of method noise is used in three different ways. First is on the low-frequency components, secondly on the high-frequency components and lastly as a post-processing operation. This new way of implementing the method noise enhances the result. The HMN-AD and HMN-DSF operates on global filtering. According to the literature available, the despeckling results using local filtering shows a better result than the global

filtering. Also in the HMN-AD and HMN-DSF, the decomposition level is manually set by experimenting the methods from level 1-7 and the optimal results are obtained at level 3. The local filtering and automatic selection of decomposition level motivate to design a new despeckling method that leads to HMN-CF.

Here a new homomorphic SAR image despeckling method is proposed using local correlation based fusion in wavelet transform and method noise thresholding i.e. HMN-CF. The proposed method uses two different wavelet shrinkage rule in parallel i.e. Bayesian and Bivariate shrinkage rule for filtering the high-frequency coefficients. The Bayesian method smooths the homogenous region but it is sensitive to the edges. The Bivariate method analyses the dependence between the child coefficient and its parent coefficient and enhances the edge component of the image. The high-frequency coefficient components of both the shrinkage rules are fused using local correlation based strategy. After fusion of two improved high-frequency coefficient components, the despeckled image results into a higher quality image. Entropy-based wavelet decomposition decides the decomposition level of the wavelet transform based on the texture feature analysis. This automatic selection of decomposition level extracts the maximum information possible. The method noise thresholding is applied to process the unfiltered components of the image and to restore the remaining fine details of the image. This concept is capable of restoring the significant information like edges and corners which remain unfiltered in the initial stage of despeckling. The performance of the HMN-CF is assessed by the visual appearance of the despeckled SAR image and with the help of quantitative metrics like PSNR, SSIM, and SNR. From the critical comparative analysis, it can be said that HMN-CF preserves the edges and structure of the object in the SAR image. During this research, no visual artifacts are generated. Therefore HMN-CF has the potential ability to be used in various practical applications of SAR images.

The HMN-CF uses local correlation based fusion strategy. Here the local filtering is applied based on the fusion strategy which is grounded on the correlation coefficients of the selected masks. The HMN-CF selects wavelet decomposition level automatically on analyzing the texture of the speckled SAR image by entropy metric. The concept of method noise is used as a post-processing step. The visual appearance of the despeckled image in HMN-CF is better than the despeckled image obtained from the HMN-AD and HMN-DSF and the quantitative values of the metrics in HMN-CF shows better result than HMN-AD and HMN-DSF. But the computational cost of HMN-CF is a higher than HMN-AD and HMN-DSF.

6.3 Other Findings

The thesis stands upon three novel SAR image despeckling methods i.e. HMN-AD, HMN-DSF and HMN-CF. Their quantitative and qualitative results are better than many of the traditional and non-traditional methods. Apart from these despeckling techniques, the thesis concludes with two more analytical findings i.e. first is the intelligent use of method noise that can improve the result of any despeckling method and another is the performance metric i.e. MSE that can be used as a performance metric in both the cases i.e. with and without reference indexes.

6.3.1 Use of Method Noise in Despeckling of SAR Images

The concept of method noise is well known in the field of image denoising. In the past decade, there are many applications of method noise discussed in the literature especially in the field of classical imagery and medical imagery. The concept of method noise is still untouched in the field of SAR imagery. So before applying method noise on the proposed methods, it is experimentally tested on the traditional and non-traditional despeckling methods of SAR images as a post-processing step and obtained results are brilliant (discussed in chapter 3). It is a 100% working method. It is observed that the quality of the despeckled SAR image with method noise is better than without method noise. It is validated by analyzing the performance of the despeckled SAR images using qualitative parameters i.e. visual appearance and quantitative metrics i.e. PSNR and SSIM. On the basis this analysis, it is concluded that the concept of method noise is efficient in the despeckling process.

On analyzing the efficient results of various despeckling method with method noise, this concept is implemented in proposed methods i.e. HMN-AD, HMN-DSF and HMN-CF. In HMN-AD, the method noise is implemented as post-processing step and it enhances the result of the HMN-AD. On observing the better results of HMN-AD with method noise, it is again applied in the HMN-DSF in an intelligent manner. In HMN-DSF, the method noise is applied in three different ways. Firstly on the low-frequency coefficient, secondly on the high-frequency coefficient and lastly as the post-processing step. On analyzing the results it is observed that it's more intelligent use can enhance the results in terms of fine detail preservation. In HMN-DSF, the low-frequency coefficients are directed to the DSF followed by the method noise thresholding. The high-frequency coefficients are directed to the wavelet thresholding using Bayesian shrinkage rule followed by the method noise thresholding. Lastly it is used as the post-processing operation. It is an excellent tool to enhance the results

by preserving the fine details of the image mainly edges and corners. No blocky artifacts are generated due to method noise operation. It is concluded from the results of the HMN-DSF that, if the concept of method noise is used more efficiently and intelligently then, the results of any despeckling algorithm can be enhanced. The HMN-CF also uses the concept of method noise as the final post-processing step.

This is concluded from the experimental result of the proposed methods using method noise that, the use of method noise in SAR image despeckling can enhance the results more than it's without use. Method noise has the capability to enhance the quality of the despeckled image of any despeckling technique. It is an extremely effective tool in the field of despeckling.

6.3.2 Use of MSE in Despeckling

The experimental analysis of MSE in the cases i.e. with and without reference indexes verifies the dual nature of MSE metric in assessing the performance of the despeckled SAR image. In the case of with reference index, the best results are obtained at minimum MSE values i.e. when the actual reflectivity or the ground truth is known. In the case of without reference indexes, the best results are obtained at maximum MSE values i.e. when the actual reflectivity or the ground truth is unknown.

There is certain number of quantitative metrics used for assessing the quality of despeckled SAR image in two different cases of despeckling i.e. with and without- reference indexes, out of them; MSE is observed as the only metric to be used for performance evaluation in both the cases. In the case of with-reference index, the small MSE value of despeckled SAR image indicates the small difference between reference image and despeckled image, this means efficient despeckling. In the case of without-reference indexes, the high MSE value of despeckled SAR image indicates the efficient speckle reduction. During the analysis of MSE in this case, it is necessary to keep an eye on the quantitative values of other metrics. MSE is a valuable metric. Its dual nature in different situations validates the importance of its use. This thesis clears the air of confusion of using MSE in case of without reference indexes. It can be easily used in either case.

6.4 Future Scope

The research work presented in this thesis can be extended in many directions. There is never-ending scope of research in the field of SAR image despeckling because it is not possible to completely restore the degraded image to its original form. The proposed methods are grounded on the db2 based 2D-DWT. Here the applied transform in the proposed methods is DWT but the work is also tested on CWT and SWT. With the intelligent use of method noise, the results obtained with DWT are better than CWT and SWT. There are various other types of wavelet related transforms. The work can be extended using those transforms. Some of them are, fast wavelet transform, complex wavelet transform, undecimated wavelet transform where the downsampling is omitted, wavelet packet decomposition where the detailed coefficients are decomposed too, second generation wavelet transform, dual-tree complex wavelet transform, and there is a collection of a hundredth of wavelet names in-let and associated multiscale, directional, geometric, representations, from activelets to x-lets through bandelets, chirplets, contourlets, curvelets, noiselets, wedgelets, ridgelet, shearlet, chirplet etc.

The concept of method noise is used to enhance the quality of the image and preserve the fine details of the image. It has been used in the digital as well as medical images in the past but never used in the SAR imagery. The despeckling methods proposed in the thesis demonstrated three types of application of method noise using DWT. Those three application are on low and high-frequency coefficients and as a post-processing step. The method noise can also be used with the other advanced wavelet related transform. Even more intelligent use of method noise can be discovered and applied to other wavelet transforms using several ways.

The concept of image fusion can be used for the image enhancement purpose. The fusion strategy is developed and applied to two enhanced detailed components in the HMN-CF. After DWT decomposition, the detailed component are filtered by Bayesian shrinkage rule and Bivariate shrinkage rule in parallel. Their output is fused using local correlation based strategy. This strategy uses “max” and “avg” operation for fusion. In this scenario, there is a lot scope of work to be done in future. The “min” operation can also be introduced in the local correlation based strategy. Other shrinkage rules can be used. A new fusion strategy can be developed.

The wavelet family used in the HMN-AD, HMN-DSF and HMN-CF is Daubechies (db2). There are several other wavelet families that can be used and tested like Haar, Daubechies, Biorthogonal, Coiflets, Symlets, Morlet, Mexican Hat, Meyer, Other Real Wavelets: Reverse Biorthogonal, Gaussian derivatives family, FIR based approximation of the Meyer wavelet and Complex Wavelets: Gaussian derivatives, Morlet, Frequency B-Spline, Shannon. Few of them are used, tested and compared in the result section of HMN-DSF. There is an extensive option for spontaneously choosing the mother wavelet from the extensive range of wavelet family associated with the DWT.

In the HMN-AD and HMN-DSF, the wavelet decomposition level experiments from level 1 to 7. The optimal results are obtained at the level ranging from 3 to 5. In the HMN-CF, the decomposition level is automatically set by analyzing the texture of the image based on entropy metric. So there are other ways which can also automatically choose the wavelet decomposition level like, local range, MSE, contrast etc. The field of SAR image despeckling is never ending research field. There is always a scope improvement in this field.

6.5 Conclusion

The chapter concludes with all the achieved objectives of all the proposed methodologies i.e. HMN-AD, HMN-DSF and HMN-CF. It also discusses the merits and limitations of the proposed methods. It briefly describes the other findings like the use of method noise and use of MSE metric in with and without reference index cases. The future scope is also discussed in the last.

REFERENCES

[1] Translation Bureau. "Radar definition". Public Works and Government Services Canada, 2013.

[2] McGraw-Hill dictionary of scientific and technical terms / Daniel N. Lapedes, editor in chief. Lapedes, Daniel N. New York ; Montreal : McGraw-Hill,[xv], 1634, A26 p., 1976

[3] "ABBREVIATIONS and ACRONYMS". Navy dot MIL. United States Navy. Retrieved 9 August 2017.

[4] "Small and Short-Range Radar Systems". CRC Net Base. Retrieved 9 August 2017.

[5] Real Aperture Radar, Available at: http://wtlab.iis.u-tokyo.ac.jp/~wataru/lecture/rsgis/rsnote/cp4/cp4-2.htm

[6] What is Synthetic Aperture Radar (SAR)?, Sandia National Laboratories, Available at: http://www.sandia.gov/radar/what_is_sar/

[7] Synthetic Aperture Radar, Available at: http://wtlab.iis.u-tokyo.ac.jp/~wataru/lecture/rsgis/rsnote/cp4/cp4-3.htm

[8] Synthetic Aperture Radar (SAR), Available at: http://sar.ece.ubc.ca/SARintro/SAR.html

[9] Creating a SAR Image, Available at: http://www.pbs.org/wgbh/nova/spiesfly/rada_creating.html

[10] Cheney, Margaret. Introduction to Synthetic Aperture Radar (SAR) and SAR Interferometry. JPL. Available at: http://southport.jpl.nasa.gov/scienceapps/dixon/report2.html

[11] Synthetic Aperture Radar (SAR) Imagery, Sandia National Laboratories, Airborne ISR', Available at: http://www.sandia.gov/RADAR/imagery/

[12] Cheney, Margaret, “Problems in synthetic-aperture radar imaging”, Inverse Problems, Volume 25, (2009), Available at: http://hdl.handle.net/10945/43818

[13] M.S. Ranga Rao, P. R. Mahaptra, “Synthetic Aperture Radar: A Focus on Current Problems”, Defence Science Journal, Vol 47, No 4, pp. 517-536, DESIDOC, October 1997.

[14] T. TOUTIN, “Review article: Geometric processing of remote sensing images: models, algorithms and methods”, INT. J. REMOTE SENSING, VOL. 25, NO. 10, 1893–1924, 20 MAY, 2004.

[15] A. L. Choo, Y. K. Chan, and V. C. Koo, “Geometric Correction on SAR Imagery”, Progress In Electromagnetics Research Symposium Proceedings, KL, MALAYSIA, March 27-30, 2012.

[16] Alberto Moreira, Pau Prats-Iraola, Marwan Younis, Gerhard Krieger, Irena Hajnsek, And Konstantinos P. Papathanassiou, “A Tutorial on Synthetic Aperture Radar”, IEEE GEOSCIENCE AND REMOTE SENSING MAGAZINE, Digital Object Identifier: 10.1109/MGRS.2013.2248301, Date of publication: 17 April 2013.

[17] Birgir Bjorn Saevarsson,Johannes R.Sveinsson and Jon Atli Benediktsson, “Combined Wavelet and Curvelet Denoising of SAR Images” Proceedings of IEEE 2004.

[18] Dr. A. Bhattacharya, Speckle Filtering/ Speckle Statistics, (Slide courtesy Prof. E. Pottier and Prof. L. Ferro-Famil).

[19] Guozhong Chen,Xingzhao Liu, “Wavelet-Based Despeckling SAR Images Using Neighbouring Wavelet Coefficients.” Proceedings of IEEE 2005.

[20] F. Sarti, “Remote sensing and SAR images processing, Characterization and speckle filtering in radar images”, Available: https://earth.esa.int/c/document_library/get_file?folderId=226458&name=DLFE-2125.pdf.

[21] J.-S. Lee, “Digital image enhancement and noise filtering by use of local statistics,” IEEE Trans. Pattern Anal. Mach. Intell., vol. PAMI-2, no. 2, pp. 165–168, Feb. 1980.

[22] J.-S. Lee, “Speckle analysis and smoothing of synthetic aperture radar images,” Comput. Graph. Image Process., vol. 17, no. 1, pp. 24–32, Sept. 1981.

[23] J.-S. Lee, “Speckle suppression and analysis for synthetic aperture radar images,” Opt. Eng., vol. 25, no. 5, pp. 636–643, May 1986.

[24] J.-S. Lee, “Refined filtering of image noise using local statistics,” Comput. Graph. Image Process., vol. 15, no. 2, pp. 380–389, Apr. 1981.

[25] V.S.Frost et al, “A model for radar images and its application to adaptive digital filtering of multiplicative noise”, IEEE Trans. Pattern Anal. And Machine Intell.,vol. PAMI-4, pp.157-166. 1982.

[26] Kuan DT, Sawchuk AA, Strand TC, Chavel P, "Adaptive noise smoothing filter for images with signal dependent noise", IEEE Trans Pattern Anal Mach Intell., PAMI-7(2):165–77, Mar 1985.

[27] A. Lopès, E. Nezry, R. Touzi, and H. Laur, "Maximum a posteriori speckle filtering and first-order texture models in SAR images," in Proc. IEEE Int. Geoscience and Remote Sensing Symp. (IGARSS), pp. 2409–2412, 1990.

[28] A. Lopès, E. Nezry, R. Touzi, and H. Laur, "Structure detection and statistical adaptive speckle filtering in SAR images," Int. J. Remote Sensing, vol. 14, no. 9, pp. 1735–1758, June 1993.

[29] Achim A, Kuruoglu EE, Zerubia J. SAR image filtering based on the heavy-tailed Rayleigh model. IEEE Trans Image Process, 15(9):2686–93, Sep 2006.

[30] Bianchi T, Argenti F, Alparone L. Segmentation-based map despeckling of SAR images in the undecimated wavelet domain. IEEE Trans Geoscience and Remote Sensing. 46(9):2728–42, 2008.

[31] V.R.Vijaykumar, Anu Mathew, Baskar Rao, Santhanamari, "Dual Tree Complex Wavelet Transform Based SAR Image Despeckling", 4th International Conference on Intelligent and Advanced Systems (ICIAS2012), 2012.

[32] J. J. Ranjani and S. J. Thiruvengadam, "Dual tree complex wavelet transform based despeckling using interscale dependency," IEEE Trans. Geosci. Remote Sens., vol. 48, no. 6, pp. 2723–2731, Jun. 2010.

[33] A. Lopès, R. Touzi, and E. Nezry, "Adaptive speckle filters and scene heterogeneity," IEEE Trans. Geosci. Remote Sensing, vol. 28, no. 6, pp. 992–1000, Nov. 1990.

[34] Gagnon L, Jouan A. Speckle filtering of SAR images – a comparative study between a complex-wavelet-based and standard filter. Proc SPIE; pp. 80–91, 1997.

[35] Dai M, Peng C, Chan AK, Loguinov D. Bayesian wavelet shrinkage with edge detection for SAR image de-speckling, IEEE Trans Geo Sci Remote Sens.; 42(8):1642–8, Aug 2004.

[36] Fabrizio argenti, alessandro lapini, and luciano alparone, "A Tutorial on Speckle Reduction in Synthetic Aperture Radar Images", IEEE Geoscience and remote sensing magazine, September 2013.

[37] Wu J, Yan W, Bian H, Ni W. A despeckling algorithm combining curvelet and wavelet transforms of high resolution SAR images. Proc Computer Design and Applications. 1:302–5, 2010 June.

[38] Jojy C, Nair MS, Subrahmaniyam GRKS, Riji R. Discontinuity adaptive non-local means with importance sampling unsented Kalman filter for despeckling SA images. IEEE Transaction on selected topics in Applied Earth Observation And Remote Sensing.; 6(4), Aug 2013.

[39] Abdourrahmane Mahamane Atto, Emmanuel Trouvé, Jean-Marie Nicolas, and Thu Trang Lê, "Wavelet Operators and Multiplicative Observation Models—Application to SAR Image Time-Series Analysis", IEEE TRANSACTIONS ON GEOSCIENCE AND REMOTE SENSING, VOL. 54, NO. 11, NOVEMBER 2016.

[40] Diego Gragnaniello, Giovanni Poggi, Giuseppe Scarpa, Luisa Verdoliva, "SAR Image Despeckling by Soft Classification", Published in: IEEE Journal of Selected Topics in Applied Earth Observations and Remote Sensing (Volume: 9, Issue: 6, June 2016), Page(s): 2118 – 2130, Date of Publication: 27 May 2016.

[41] P. Meer, R.-H. Park, and K. Cho, "Multiresolution adaptive image smoothing," Graph. Models Image Process., vol. 56, no. 2, pp. 140–148, Mar. 1994.

[42] B. Aiazzi, L. Alparone, S. Baronti, and G. Borri, "Pyramid-based multiresolution adaptive filters for additive and multiplicative image noise," IEEE Trans. Circuits Syst. II, vol. 45, no. 8, pp. 1092–1097, Aug. 1998.

[43] B. Aiazzi, L. Alparone, and S. Baronti, "Multiresolution local-statistics speckle filtering based on a ratio Laplacian pyramid," IEEE Trans. Geosci. Remote Sensing, vol. 36, no. 5, pp. 1466–1476, Sept. 1998.

[44] David Jacobs, Introduction to Image Gradients, Class Notes for CMSC 426, Fall 2005.

[45] P. Perona, J. Malik, Scale space and edge detection using anisotropic diffusion, IEEE Transactions on Image Processing 12 (8), pp-629–639, (1990).

[46] Anil K.Jain, Fundamentals of Digital Image Processing first edition, Prentice Hall, Inc, 1989.

[47] Syed Musharaf Ali, Muhammad Younus Javed, and Naveed Sarfraz Khattak, "Wavelet-Based Despeckling of Synthetic Aperture Radar Images Using Adaptive and Mean Filters", World Academy of Science, Engineering and Technology

International Journal of Computer, Electrical, Automation, Control and Information Engineering Vol:1, No:7, 2007

[48] Wiener Filtering, Available at: http://www.owlnet.rice.edu/~elec539/Projects99/BACH/proj2/wiener.html

[49] The Wiener filter, Available at: http://homepages.inf.ed.ac.uk/rbf/CVonline/LOCAL_COPIES/VELDHUIZEN/node15.html

[50] Theory of Wiener Filtering, Available at: http://www.cs.tau.ac.il/~turkel/notes/wiener_theory.html

[51] Prabhishek Singh, Raj Shree, "A New Computationally Improved Homomorphic Despeckling Technique of SAR Images", IJARCS, Volume 8, No. 3, March-April 2017.

[52] H. Xie, L. E. Pierce, and F. T. Ulaby, "Statistical properties of logarithmically transformed speckle," IEEE Trans. Geosci. Remote Sensing, vol. 40, no. 3, pp. 721– 727, Mar. 2002.

[53] M. Walessa and M. Datcu, "Model-based despeckling and information extraction from SAR images," IEEE Trans. Geosci. Remote Sensing, vol. 38, no. 5, pp. 2258– 2269, Sept. 2000

[54] Measures of image quality, Available at: http://homepages.inf.ed.ac.uk/rbf/CVonline/LOCAL_COPIES/VELDHUIZEN/node18.html

[55] Singh, P., Shree, R. "A new homomorphic and method noise thresholding based despeckling of SAR image using anisotropic diffusion", Journal of King Saud University – Computer and Information Sciences, http://dx.doi.org/10.1016/j.jksuci.2017.06.006, 2017.

[56] G.-T. Li, C.-L. Wang, P.- P. Huang, and W.-D. Yu, "SAR image despeckling using a space-domain filter with alterable window", IEEE Geosci. Remote Sensing Lett., vol. 10, no. 2, pp. 263267, Mar. 2013.

[57] Lin Zhang, Lei Zhang, Xuanqin Mou and David Zhang, "FSIM: A Feature SIMilarity Index for Image Quality Assessment", IEEE Trans. Image Processing, vol. 20, no. 8, pp. 2378-2386, 2011.

[58] F. Sattar, L. Floreby, G. Salomonsson, and B. Lovstrom, "Image enhancement based on a nonlinear multiscale method," IEEE Trans. Image Process., vol. 6, no. 6, pp. 888– 895, June 1997

[59] A. Achim, P. Tsakalides, and A. Bezerianos, “SAR image denoising via Bayesian wavelet shrinkage based on heavy-tailed modeling,” IEEE Trans. Geosci. Remote Sensing, vol. 41, no. 8, pp. 1773–1784, Aug. 2003.

[60] Y. Yu and S. T. Acton, “Speckle reducing anisotropic diffusion,” IEEE Trans. Image Process., vol. 11, no. 11, pp. 1260–1270, Nov. 2002.

[61] Stian Normann Anfinsen, Anthony P. Doulgeris, TorbjØrn Eltoft, “Estimation of the Equivalent Number of Looks in Polarimetric Synthetic Aperture Radar Imagery”, IEEE Transactions on Geoscience and Remote Sensing (Volume: 47, Issue: 11), Page(s): 3795 – 3809, Nov. 2009.

[62] C. Oliver and S. Quegan, Understanding Synthetic Aperture Radar Images. Boston, MA: Artech House, 1998.

[63] R. D'Alvise, C. Moloney, G. Ramponi, “Statistical methods for the evaluation of the coefficient of variation in SAR images”, Geoscience and Remote Sensing Symposium, IGARSS '99 Proceedings. IEEE 1999 International, Date of Conference: 28 June-2 July 1999, DOI: 10.1109/IGARSS.1999.774595.

[64] G. R. Benitz, “High-definition vector imaging,” Lincoln Lab. J., vol. 10, no. 2, pp. 147–170, 1997.

[65] M. Çetin, W. C. Karl, and D. A. Castañon, “Evaluation of a regularized SAR imaging technique based on recognitionoriented features,” in Proc. SPIE Algorithms for Synthetic Aperture Radar Imagery VII, vol. 4053, pp. 40–51, 2000.

[66] M. Mastriani, A. E. Giraldez, “Enhanced Directional Smoothing Algorithm for Edge-Preserving Smoothing of Synthetic-Aperture Radar Images”, MEASUREMENT SCIENCE REVIEW, Volume 4, Section 3, 2004.

[67] Hervet, E., Fjrtoft, R., Marthon, P., Lops, A., Comparison of wavelet-based and statistical speckle filters. In: Proc. SPIE SAR Image Analysis, Modelling, and Techniques III, F. Posa, Ed., vol. 3497, p. 4354, 1998.

[68] Charles-Alban Deledalle, Lo¨ıc Denis, Florence Tupin, “Iterative Weighted Maximum Likelihood Denoising with Probabilistic Patch-Based Weights”, IEEE TRANSACTION ON IMAGE PROCESSING, VOL. 18, NO. 12, DECEMBER 2009.

[69] Michael J. Collins, Jeremy M. Allan, “Modeling and Simulation of SAR Image Texture”, IEEE TRANSACTIONS ON GEOSCIENCE AND REMOTE SENSING, VOL. 47, NO. 10, OCTOBER 2009.

[70] DATASET OF STANDARD [512X512] GRAYSCALE TEST IMAGES, Available at: http://decsai.ugr.es/cvg/CG/base.htm

[71] Test Images, Available at: http://decsai.ugr.es/cvg/dbimagenes/

[72] Yao Zhao, Jianguo Liu, Bingchen Zhang, Wen Hong, Yirong Wu: Adaptive Total Variation Regularization Based SAR Image Despeckling and Despeckling Evaluation Index. IEEE Trans. Geoscience and Remote Sensing 53(5): 2765-2774 (2015)

[73] Sara Parrilli, Mariana Poderico, Cesario Vincenzo Angelino, Luisa Verdoliva: A Nonlocal SAR Image Denoising Algorithm Based on LLMMSE Wavelet Shrinkage. IEEE Trans. Geoscience and Remote Sensing 50(2): 606-616 (2012)

[74] Bin Xu, Yi Cui, Zenghui Li, Bin Zuo, Jian Yang, Jianshe Song, "Patch Ordering-Based SAR Image Despeckling Via Transform-Domain Filtering", IEEE Journal of Selected Topics in Applied Earth Observations and Remote Sensing (Volume: 8, Issue: 4, April 2015), Page(s): 1682 – 1695, DOI: 10.1109/JSTARS.2014.2375359.

[75] H. Guo, J. E. Odegard, M. Lang, R. A. Gopinath, I. W. Selesnick, and C. S. Burrus, "Wavelet based speckle reduction with application to SAR based ATD/R," in Proc. IEEE Int. Conf. Image Processing (ICIP), 1994, vol. 1, pp. 75–79.

[76] David de la Mata-Moya, Alvaro Diaz-Soria, Jaime Martin-de-Nicolas, Maria-Pilar Jarabo-Amores, Victor Manuel Pelaez, "Spatially Adaptive Thresholding of the Empirical Mode Decomposition for Speckle Reduction Purposes", EUSAR 2014; 10th European Conference on Synthetic Aperture Radar; Proceedings of Date of Conference: 3-5 June 2014

[77] Donoho, D.L. and I.M. Johnstone, 1994. Adapting to unknown smoothness via wavelet shrinkage. J. Am. Stat. Assoc., 90: 1200-1224. DOl: 10.1080101621459.1995.10476626

[78] A. Buades, B. Coll, J.-M. Morel, "A non-local algorithm for image denoising", Computer Vision and Pattern Recognition, 2005. CVPR 2005. IEEE Computer Society Conference on, 20-25 June 2005

[79] Kumar, M., Diwakar, M. A new exponentially directional weighted function based CT image denoising using total variation. Journal of King Saud University Computer and Information Sciences (2017), http://dx.doi.org/10.1016/j.jksuci.2016.12.002

[80] Christos P. Loizou, Charoula Theofanous, Marios Pantziaris, Takis Kasparis, Despeckle filtering software toolbox for ultrasound imaging of the common carotid artery, computer methods and programs in biomedicine 114(2014), 109124.

[81] D.T.Kuan et al., Adaptive restoration of images with speckle, IEEE Trans. Acc. Speech and signal Proc. Vol. 35, no.3 pp.373-383, March 1987.

[82] M. Kuwahara. K. Hachimura, S. Eiho, and M. Kinoshita, Processing of RIangiocardiographic images, in Digital Processing of Biomedical Images, K. Preston Jr.and M. Onoe, Editors. New York: Plenum, 1976. pp. 187202

[83] Y. Yuand S. T. Acton, Speckle reducing anisotropic diffusion, IEEE Trans. Image Process., vol. 11, no. 11, pp. 12601270, Nov. 2002.

[84] Image Despeckle Filtering Toolbox, Mathworks website, Available: https://in.mathworks.com/matlabcentral/fileexchange/54044-image-despeckle-filtering-toolbox

[85] Semwal, Vijay Bhaskar, Manish Raj, and Gora Chand Nandi. Biometric gait identification based on a multilayer perceptron, Robotics and Autonomous Systems 65 (2015): 65-75.

[86] Semwal, Vijay Bhaskar, Kaushik Mondal, and G. C. Nandi., Robust and accurate feature selection for humanoid push recovery and classification: deep learning approach. Neural Computing and Applications (2015): 1-10.

[87] Singh, Umesh Kumar, Chanchala Joshi, and Neha Gaud. Measurement of Security Dangers in University Network. Measurement 155.1 (2016).

[88] Semwal, Vijay Bhaskar, et al. An optimized feature selection technique based on incremental feature analysis for bio-metric gait data classification. Multimedia Tools and Applications: 1-19.

[89] Heng-Chao Li, Wen Hong, Member, Yi-Rong Wu, Ping-Zhi Fan, "Bayesian Wavelet Shrinkage With Heterogeneity-Adaptive Threshold for SAR Image Despeckling Based on Generalized Gamma Distribution", IEEE Transactions on Geoscience and Remote Sensing, Volume: 51, Issue: 4, April 2013) Page(s): 2388 – 2402, 14 September 2012, DOI: 10.1109/TGRS.2012.2211366

[90] R. Sethunadh and T. Thomas, "Spatially adaptive despeckling of SAR image using bivariate thresholding in directionlet domain", Electronics Letters, Volume: 50, Issue: 1, January 2 2014, Page(s): 44 – 45, 09 January 2014, DOI: 10.1049/el.2013.0971

[91] Lei Zhu, Xiaotian Zhao and Meihua Gu, "SAR image despeckling using improved detail-preserving anisotropic diffusion", Electronics Letters, Volume: 50, Issue: 15, July 17 2014, Page(s): 1092 – 1093, 24 July 2014, DOI: 10.1049/el.2014.0293.

[92] Prabhishek Singh, Raj Shree, "Statistical Modelling of Log Transformed Speckled Image", International Journal of Computer Science and Information Security (IJCSIS), Vol. 14, No. 8, August 2016.

[93] Shreyamsha Kumar, B.K. SIViP (2013) 7: 1211. https://doi.org/10.1007/s11760-012-0389-y

[94] Shreyamsha Kumar, B.K. SIViP (2013) 7: 1159. https://doi.org/10.1007/s11760-012-0372-7

[95] A. Buades, B. Coll, and J. Morel. On image denoising methods. Technical Report 2004-15, CMLA, 2004.

[96] Xiaobo Zhang, "Image denoising using local Wiener filter and its method noise", Optik - International Journal for Light and Electron Optics, Volume 127, Issue 17, September 2016, Pages 6821-6828, https://doi.org/10.1016/j.ijleo.2016.05.002

[97] Barri, Adriaan; Dooms, Ann; Schelkens, Peter (2012). "The near shift-invariance of the dual-tree complex wavelet transform revisited". Journal of Mathematical Analysis and Applications. 389 (2): 1303–1314. doi:10.1016/j.jmaa.2012.01.010

[98] James E. Fowler: The Redundant Discrete Wavelet Transform and Additive Noise, contains an overview of different names for this transform.

[99] A.N. Akansu and Y. Liu, On Signal Decomposition Techniques, Optical Engineering, pp. 912-920, July 1991.

[100] M.J. Shensa, The Discrete Wavelet Transform: Wedding the A Trous and Mallat Algorithms, IEEE Transaction on Signal Processing, Vol 40, No 10, Oct. 1992.

[101] M.V. Tazebay and A.N. Akansu, Progressive Optimality in Hierarchical Filter Banks, Proc. IEEE International Conference on Image Processing (ICIP), Vol 1, pp. 825-829, Nov. 1994.

[102] M.V. Tazebay and A.N. Akansu, Adaptive Subband Transforms in Time-Frequency Excisers for DSSS Communications Systems , IEEE Transaction on Signal Processing, Vol 43, No 11, pp. 2776-2782, Nov. 1995.

[103] S. Foucher, G. B. Bni, and J.-M. Boucher, Multiscale MAP filtering of SAR images, IEEE Trans. Image Process., vol. 10, no. 1, pp. 4960, Jan. 2001.

[104] D. L. Donoho, "Denoising by soft-thresholding," *IEEE Trans. Inform. Theory*, vol. 41, no. 3, pp. 613–627, Mar. 1995.

[105] Wavelet basics, Available at: http://www.wavelet.org/tutorial/wbasic.htm

[106] S.Md.Mansoor Roomi, D.Kalaiyarasi, J.Goma Abhinaya, C.Bhavana, Edge Preserving SAR image Despeckling",2011 Third National Conference on Computer Vision, Pattern Recognition, Image Processing, and Graphics.

[107] Prabhishek Singh, Dr. Raj Shree, "Importance of DWT in Despeckling SAR Images and Experimentally Analyzing the Wavelet Based Thresholding Techniques",

published in International Journal of Engineering Sciences & Research Technology, October, 2016, DOI: 10.5281/zenodo.160861

[108] D. E. Molina, D. Gleich, and M. Datcu, "Evaluation of Bayesian despeckling and texture extraction methods based on Gauss– Markov and auto-binomial Gibbs random fields: Application to TerraSAR-X data," IEEE Trans. Geosci. Remote Sensing, vol. 50, no. 5, pp. 2001–2025, May 2012

[109] B. Aiazzi, L. Alparone, S. Baronti, and F. Lotti, "Lossless image compression by quantization feedback in a content-driven enhanced Laplacian pyramid," IEEE Trans. Image Process., vol. 6, no. 6, pp. 831–843, June 1997

[110] Abdullah Al Jumah, "Denoising of an Image Using Discrete Stationary Wavelet Transform and Various Thresholding Techniques", Published Online February 2013, Journal of Signal and Information Processing, 2013, 4, 33-41.

[111] Alka Vishwa, Shilpa Sharma, "Modified Method for Denoising the Ultrasound Images by Wavelet Thresholding", Published Online June 2012 in MECS, I.J. Intelligent Systems and Applications, 2012,6,25-30.

[112] Arun Dixit, Poonam Sharma, "A Comparative Study of Wavelet Thresholding for Image Denoising", I.J. Image, Graphics and Signal Processing, 2014, 12, 39-46 Published Online November 2014 in MECS, DOI: 10.5815/ijigsp.2014.12.06.

[113] Tinku Acharya and Ajoy K. Ray, "Image Processing Principles and Applications", 2005 edition A John Wiley & Sons, Mc., Publication.

[114] D. L. Donoho and I. M. Johnstone, "Ideal spatial adaptation via wavelet shrinkage," Biometrika, vol. 81, no. 3, pp. 425–455, Sep. 1994.

[115] Gregorio Andria, Filippo Attivissimo, Anna M. L. Lanzolla, Mario Savino, "A Suitable Threshold for Speckle Reduction in Ultrasound Images", IEEE TRANSACTIONS ON INSTRUMENTATION AND MEASUREMENT, VOL. 62, NO. 8, AUGUST 2013, Page(s): 2270 – 2279

[116] A. Achim, A. Bezerianos, and P. Tsakalides, "Novel bayesian multiscale method for speckle removal in medical ultrasound images," IEEE Trans. Med. Imaging, vol. 20, no. 8, pp. 772–783, Aug. 2001.

[117] S. G. Chang, ―Adaptive wavelet thresholding for image denoising and compression, IEEE Trans. Image Processing, vol. 9, Sept. 2000, pp. 1532–1546.

[118] C. B. Burckhardt, "Speckle in ultrasound B-mode scans," IEEE Trans. Sonics Ultrasonics, vol. 25, no. 1, Jan. 1978, pp. 1–6.

[119] Wavelet Noise Thresholding, Available: http://www.bearcave.com/misl/misl_tech/wavelets/noise.html

[120] MathWorks Documentation, wthresh (Soft or hard thresholding), Available: https://in.mathworks.com/help/wavelet/ref/wthresh.html

[121] MathsWorks Documentation, ”Wavelet Family”, Available at: http://in.mathworks.com/help/wavelet/ug/wavelet-families-additional-discussion.html

[122] James S. Walker. “A Primer on Wavelets and Their Scientific Applications, Second Edition (Studies in Advanced Mathematics)” [English]. Published by Chapman And Hall, Crc (2008). Ch 2: Daubechies, Book (Online Source) Available: https://www.scribd.com/document/255294926/28851-a-Primer-on-Wavelets-and-Their-Scientific-Applications

[123] R. C. Gonzalez, R. E. Woods, Digital Image Processing, second ed., Prentice-Hall, Inc., 2002.

[124] Nimrod Peleg, “The History and Families of Wavelets”, Update: Dec. 2000, Available: cs.haifa.ac.il/~nimrod/Compression/Wavelets/w3families2000.pdf

[125] E. Hervet, R. Fjørtoft, P. Marthon, and A. Lopès, “Comparison of wavelet-based and statistical speckle filters,” in Proc. SPIE SAR Image Analysis, Modelling, and Techniques III, F. Posa, Ed., 1998, vol. 3497, pp. 43–54.

[126] J. R. Sveinsson and J. A. Benediktsson, “Almost translation invariant wavelet transformations for speckle reduction of SAR images,” IEEE Trans. Geosci. Remote Sensing, vol. 41, no. 510, pp. 2404–2408, Oct. 2003.

[127] S. Solbø and T. Eltoft, “Homomorphic wavelet-based statistical despeckling of SAR images,” IEEE Trans. Geosci. Remote Sens., vol. 42, no. 4, pp. 711–721, Apr. 2004.

[128] M. I. H. Bhuiyan, M. O. Ahmad, and M. N. S. Swamy, “A new homomorphic Bayesian wavelet-based MMAE filter for despeckling SAR images,” in Proc. IEEE Int. Symp. Circuits and Systems (ISCAS), May 2005, vol. 5, pp. 4935–4938.

[129] M. I. H. Bhuiyan, M. O. Ahmad, and M. N. S. Swamy, “Spatially adaptive wavelet-based method using the Cauchy prior for denoising the SAR images,” IEEE Trans. Circuits Syst. Video Technol., vol. 17, no. 4, pp. 500–507, Apr. 2007.

[130] R. Tao, H. Wan, and Y. Wang, “Artifact-free despeckling of SAR images using contourlet,” IEEE Geosci. Remote Sensing Lett., vol. 9, no. 5, pp. 980–984, Sept. 2012.

[131] F. Argenti, T. Bianchi, A. Lapini, and L. Alparone, “Fast MAP despeckling based on Laplacian–Gaussian modeling of wavelet coefficients,” IEEE Geosci. Remote Sensing Lett., vol. 9, no. 1, pp. 13–17, Jan. 2012.

[132] H. Chen, Y. Zhang, H. Wang, and C. Ding, “Stationary-wavelet based despeckling of SAR images using two-sided generalized gamma models,” IEEE Geosci. Remote Sensing Lett., vol. 9, no. 6, pp. 1061–1065, Nov. 2012

[133] L. I. Rudin, S. Osher, and E. Fatemi, “Nonlinear total variation based noise removal algorithms,” Physica D, vol. 60, nos. 1–4, pp. 259–268, Nov. 1992.

[134] J. Shi and S. Osher, “A nonlinear inverse scale space method for a convex multiplicative noise model,” SIAM J. Imaging Sci., vol. 1, no. 3, pp. 294–321, Sept. 2008.

[135] L. Denis, F. Tupin, J. Darbon, and M. Sigelle, “SAR image regularization with fast approximate discrete minimization,” IEEE Trans. Image Process., vol. 18, no. 7, pp. 1588–1600, July 2009.

[136] F. Palsson, J. R. Sveinsson, M. O. Ulfarsson, and J. A. Benediktsson, “SAR image denoising using total variation based regularization with SURE-based optimization of the regularization parameter,” in Proc. IEEE Int. Geoscience and Remote Sensing Symp. (IGARSS), 2012, pp. 2160–2163.

[137] D. Gleich and M. Kseneman, “A comparison of regularization based methods for despeckling of SLC SAR images,” in Proc. 9th European Conf. Synthetic Aperture Radar (EUSAR), 2012, pp. 784–787.

[138] C. Kervrann, J. Boulanger, and P. Coupé, “Bayesian nonlocal means filter, image redundancy and adaptive dictionaries for noise removal,” in Proc. 1st Int. Conf. on Scale Space and Variational Methods in Computer Vision (SSVM), 2007, pp. 520–532.

[139] P. Coupe, P. Hellier, C. Kervrann, and C. Barillot, “Bayesian non local means-based speckle filtering,” in Proc. 5th IEEE Int. Symp. Biomedical Imaging: From Nano to Macro, 2008, pp. 1291–1294.

[140] H. Zhong, Y. Li, and L. Jiao, “SAR image despeckling using Bayesian non-local means filter with sigma preselection,” IEEE Geosci. Remote Sensing Lett., vol. 8, no. 4, pp. 809–813, July 2011.

[141] Y. Yu and S. T. Acton, “Automated delineation of coastline from polarimetric SAR imagery,” Int. J. Remote Sens., vol. 25, no. 17, pp. 3423–3438, Sept. 2004.

[142] J.-S. Lee, J.-H. Wen, T. L. Ainsworth, K.-S. Chen, and A. J. Chen, "Improved sigma filter for speckle filtering of SAR imagery," IEEE Trans. Geosci. Remote Sensing, vol. 47, no. 1, pp. 202–213, Jan. 2009.

[143] J. S. Lee "Digital image smoothing and the sigma filter" Comput. Vis. Graph. Image Process, vol. 24 no. 2 pp. 255-269 Nov. 1983.

[144] C. Tomasi and R. Manduchi, "Bilateral filtering for gray and color images," in Proc. 6th Int. Conf. Computer Vision (ICCV), 1998, pp. 839–846.

[145] W. G. Zhang, Q. Zhang, and C. S. Yang, "Improved bilateral filtering for SAR image despeckling," Electron. Lett., vol. 47, no. 4, pp. 286–288, Feb. 2011.

[146] T. Teuber and A. Lang, "A new similarity measure for nonlocal filtering in the presence of multiplicative noise," Comput. Stat. Data Anal., vol. 56, no. 12, pp. 3821–3842, Dec. 2012.

[147] D. Gragnaniello, G. Poggi, and L. Verdoliva, "Classification based nonlocal SAR despeckling," in Proc. Tyrrhenian Workshop on Advances in Radar and Remote Sensing, 2012, pp. 121–125.

[148] Prabhishek Singh, Raj Shree, "Statistical Quality Analysis of Wavelet Based SAR Images in Despeckling Process", Asian Journal of Electrical Sciences (AJES), Volume 6 No.2 July-December 2017 pp 1-18.

[149] Prabhishek Singh, Raj Shree, "Speckle Noise: Modelling and Implementation", published in International Journal of Control Theory and Applications, 9(17) 2016, pp. 8717-8727 © International Science Press.

[150] Prabhishek Singh, Raj Shree, "Analysis and Effects of Speckle Noise in SAR Images", 2nd International Conference on Advances in Computing, Communication, & Automation (ICACCA) (Fall) Year: 2016, Pages: 1 – 5. (International Conference)

[151] Prabhishek Singh, Raj Shree, "A Comparative Study to Noise Models and Image Restoration Techniques", in International Journal of Computer Applications, Volume 149 - Number 1, Year: 2016.

[152] Prabhishek Singh, Raj Shree, "Despeckling Filtering Techniques to SAR Images", published in National Conference on Information Security Challenges (NCISC-2016), BBAU, Lucknow, 24th Feb 2016. (National Conference)

[153] D. L. Donoho, "Compressed sensing," IEEE Trans. Inform. Theory, vol. 52, no. 4, pp. 1289–1306, Apr. 2006.

[154] S. Foucher, “SAR image filtering via learned dictionaries and sparse representations,” in Proc. IEEE Int. Geoscience and Remote Sensing Symp. (IGARSS), 2008, vol. I, pp. 229–232.

[155] M. Yang and G. Zhang, “SAR image despeckling using overcomplete dictionary,” Electron. Lett., vol. 48, no. 10, pp. 596–597, May 2012.

[156] Y. Hao, X. Feng, and J. Xu, “Multiplicative noise removal via sparse and redundant representations over learned dictionaries and total variation,” Signal Process., vol. 92, no. 6, pp. 1536–1549, June 2012.

[157] Median Filter, Available at: https://homepages.inf.ed.ac.uk/rbf/HIPR2/median.htm

[158] Median filter, Available at: https://en.wikipedia.org/wiki/Median_filter

[159] Manoj Diwakar, Manoj Kumar, “CT image noise reduction based on adaptive wiener filtering with Wavelet packet thresholding”, Parallel, Distributed and Grid Computing (PDGC), 2014 International Conference, 11-13 Dec. 2014, DOI: 10.1109/PDGC.2014.7030722

[160] Microwave Remote Sensing, Synthetic Aperture Radar (SAR), Available at: https://crisp.nus.edu.sg/~research/tutorial/mw.htm

Appendix-A

ABBREVIATIONS

1D	-One dimensional
2D	-Two dimensional
ABPP	-Algorithm Best Performance Percentage
AEV	-Average Entropy Value
ANBPP	-Algorithm Not Best Performance Percentage
ATV	-Advanced Total Variation
BayesWS-HAW	-Bayesian Wavelet Shrinkage Method with Heterogeneity Adaptive Weight
BCMAP	-Bivariate Cauchy Maximum A Posteriori
CC	-Correlation Coefficient
COP	-Constant Of Proportionality
CoWT	-Continuous Wavelet Transform
CRT	-Cathode Ray Tube
CV	-Coefficient of Variation
CWT	- Complex Wavelet Transform
DA-NLMF	-Discontinuity Adaptive Non Local Means Filtering
DD-DWT	-Double Density Discrete Wavelet Transform
df	-Degree of Freedom
DOG	-Derivative Of Gaussian
DS	-Directional Smoothing
DSF	-Directional Smoothing Filter
DT-CoWT	-Discrete Time Continuous Wavelet Transform
DWT	-Discrete Wavelet Transform
EC	-Edge Correlation
EDS	-Enhanced Directional Smoothing

ENL	-Equivalent Number of Looks
ESNR	-Energy Signal to Noise Ratio
FOM	-Figure Of Metric
FSIM	-Feature Similarity Index Metric
FWT	-Fast Wavelet Transform
GGD	-General Gaussian Distribution
HBM3D	-Homomorphic Block Matching 3 Level Decomposition
HFLF	-Homomorphic Filtering with Log Function
HH	-Diagonal Component
HL	-Horizontal Component
HMN-AD	-A New **H**omomorphic SAR Image Despeckling using **M**ethod **N**oise Thresholding and **A**nisotropic **D**iffusion **(Proposed Method 1)**
HMN-CF	-A New **H**omomorphic SAR Image Despeckling using **C**orrelation based **F**usion and **M**ethod **N**oise Thresholding **(Proposed Method 3)**
HMN-DSF	-A New **H**omomorphic SAR Image Despeckling using **D**irectional **S**moothing **F**ilter and **M**ethod **N**oise Thresholding **(Proposed Method 2)**
HPF	-High Pass Filter
HPPB	-Homomorphic Probabilistic Patch Based algorithm
IDPAD	-Improved Detail Preserving Anisotropic Diffusion
IDWT	-Inverse Discrete Wavelet Transform
ISAR	-Inverse Synthetic Aperture Radar
ISUKF	-Importance Sampling Unscented Kalman Filter
LH	-Vertical Component
LL	-Approximate Component
LLMMSE	- Locally adaptive Linear Minimum Mean Squared-Error

LPF	-Low Pass Filter
MAP	-Maximum A Posteriori
MCMAP	-Multivariate Cauchy Maximum A Posteriori
MMSE	-Minimum Mean Square Error
MSE	-Mean Square Error
NLM	-Non Local Mean
NV	-Noise variance
PDF	-Probability Density Function
PSF	-Point Spread Function
PSNR	-Peak Signal to Noise Ratio
RADAR	-'RAdio Detection And Ranging' or' 'RAdio Direction And Ranging'
RAR	-Real Aperture Radar
RLP	-Ratio Laplacian Pyramid
RMSE	-Root Mean Square Error
SAR	-Synthetic Aperture Radar
SAR-BM3D	-SAR Block Matching and 3-D filtering
SNR	-Signal to Noise Ratio
SRAD	-Speckle Reduction using Anisotropic Diffusion
SSIM	-Structure Similarity Index Metric
SURE	-Stein's Unbiased Risk Estimator
SWT	-Stationary Wavelet Transform
TCR	-Target to Clutter Ratio
UIQI	-Universal Image Quality Index

Appendix-B

PLAGIARISM REPORT

Gmail **Prabhishek Singh <prabhisheksingh88@gmail.com>**

Fwd: [Urkund] 8% similarity - shodhganga.bbau@gmail.com

1 message

Periodical Section <gbl.bbau@gmail.com> Tue, Apr 17, 2018 at 5:32 PM
To: Prabhishek Singh <prabhisheksingh88@gmail.com>

Student message: Prabhishek Singh, Department of Information Technology, prabhisheksingh88@gmail.com

---

Document : Prabhishek Singh.pdf [D37658583]

IMPORTANT! The analysis contains 1 warning(s).

About 8% of this document consists of text similar to text found in 91 sources. The largest marking is 201 words long and is 96% similar to its primary source.

PLEASE NOTE that the above figures do not automatically mean that there is plagiarism in the document. There may be good reasons as to why parts of a text also appear in other sources. For a reasonable suspicion of academic dishonesty to present itself, the analysis, possibly found sources and the original document need to be examined closely.

Click here to open the analysis:
https://secure.urkund.com/view/36977262-463784-359162

Click here to download the document:
https://secure.urkund.com/archive/download/37658583-747506-610446

Prabhishek Singh.pdf
3360K

Appendix-C

LIST OF PUBLICATIONS

PAPERS PUBLISHED

1. Prabhishek Singh, Raj Shree, **"A new homomorphic and method noise thresholding based despeckling of SAR image using anisotropic diffusion",** *Journal of King Saud University – Computer and Information Sciences* (2017), **Elsevier**, http://dx.doi.org/10.1016/j.jksuci.2017.06.006, **Scopus**, **ESCI** and **UGC Indexed**.
2. Prabhishek Singh, Raj Shree, Manoj Diwakar, "**A new SAR image despeckling using correlation based fusion and method noise thresholding",** *Journal of King Saud University – Computer and Information Sciences* (2018), **Elsevier**, https://doi.org/10.1016/j.jksuci.2018.03.009, **Scopus**, **ESCI** and **UGC Indexed**.
3. Prabhishek Singh, Raj Shree, **"Statistical Quality Analysis of Wavelet Based SAR Images in Despeckling Process"**, *Asian Journal of Electrical Sciences (AJES)*, Volume 6 No.2 July-December 2017 pp 1-18, **UGC Indexed**.
4. Prabhishek Singh, Raj Shree, **"Speckle Noise: Modelling and Implementation"**, published in *International Journal of Control Theory and Applications*, 9(17) 2016, pp. 8717-8727 © International Science Press, **UGC Indexed**.
5. Prabhishek Singh, Raj Shree, **"A New Computationally Improved Homomorphic Despeckling Technique of SAR Images"**, in *International Journal of Advanced Research in Computer Science*, Volume 8, Number 3, March-April 2017, **UGC Indexed**.

6. Prabhishek Singh, Raj Shree, **"Statistical Modelling of Log Transformed Speckled Image"**, published online in Vol. 14 No. 8 AUGUST 2016 *International Journal of Computer Science and Information Security*, (pp. 426-431).
7. Prabhishek Singh, Raj Shree, **"Quantitative Dual Nature Analysis of Mean Square Error in SAR Image Despeckling"**, in *International Journal on Computer Science and Engineering (IJCSE)*, Volume 9 Number 11 Nov, Page: 619-622. (2017), **UGC Indexed.**
8. Prabhishek Singh, Raj Shree, **"Importance Of DWT In Despeckling SAR Images And Experimentally Analyzing The Wavelet Based Thresholding Techniques"**, in *International Journal Of Engineering Sciences & Research Technology*, 5(10): October, 2016, **UGC Indexed.**
9. Prabhishek Singh, Raj Shree, **"A Comparative Study to Noise Models and Image Restoration Techniques"**, in *International Journal of Computer Applications*, Volume 149 - Number 1, Year: 2016.
10. Prabhishek Singh, Raj Shree, **"Analysis and Effects of Speckle Noise in SAR Images"**, 2nd International Conference on Advances in Computing, Communication, & Automation (ICACCA) (Fall) Year: 2016, Pages: 1 – 5. **(International IEEE Conference)**
11. Prabhishek Singh, Raj Shree, **"Despeckling Filtering Techniques to SAR Images"**, published in National Conference on Information Security Challenges (NCISC-2016), BBAU, Lucknow, 24th Feb 2016. **(National Conference)**
12. Prabhishek Singh, Raj Shree, **"Statistical Assessment of Despeckling Algorithms With and Without Reference Indexes in Synthetic Aperture Radar Images"**, *Advanced Science, Engineering and Medicine*, Vol. 10, 1–4, 2018, **UGC Indexed. (Accepted) (In-Press)**
13. Musheer Vaqur, Prabhishek Singh, Manoj Diwakar, Raj Shree, **"An Edge Preserving Wavelet based Despeckling of SAR Images using**

Anisotropic Diffusion", *Journal of Advanced research in Dynamical Control Systems (JARDCS)*, **Scopus, UGC Indexed. (Accepted) (In-Press)**

PATENT PUBLISHED

TITLE OF THE INVENTION: A DESPECKLING FRAMEWORK OF AGRICULTURAL SAR IMAGES FOR LAND MONITORING

APPLICATION NO: 201711035086 A

PUBLICATION DATE: 24/11/2017

NAME OF INVENTOR: RAJ SHREE, PRABHISHEK SINGH, RAVI PRAKASH PANDEY

Appendix-D

PAPER-1

Authors: Prabhishek Singh, Raj Shree

Title: A new homomorphic and method noise thresholding based despeckling of SAR image using anisotropic diffusion

Journal: Journal of King Saud University – Computer and Information Sciences

Year of publication: 2017

Publisher: Elsevier

DOI: http://dx.doi.org/10.1016/j.jksuci.2017.06.006

Indexing: Scopus, ESCI and UGC Indexed

Journal of King Saud University – Computer and Information Sciences xxx (2017) xxx–xxx

Contents lists available at ScienceDirect

Journal of King Saud University – Computer and Information Sciences

journal homepage: www.sciencedirect.com

A new homomorphic and method noise thresholding based despeckling of SAR image using anisotropic diffusion

Prabhishek Singh [a,*], Raj Shree [b]

[a] Department of Information Technology, India
[b] Department of Information Technology, India

ARTICLE INFO

Article history:
Received 11 April 2017
Revised 8 June 2017
Accepted 30 June 2017
Available online xxxx

Keywords:
Image despeckling
Wavelet transform
Anisotropic diffusion
Method noise

ABSTRACT

In synthetic aperture radar (SAR) images, degradation due to multiplicative speckle noise and detail blurring is one of the common problem. This problem is solved by despeckling method. The main objective of image despeckling is to eliminate the speckle noise and preserve the important details of SAR images such as texture, edges, structures and corners. Usually SAR images are high dimensional images and preserving the edge and corner components is one major issue. Anisotropic diffusion also called Perona-Malik diffusion is used to reduce noise without disturbing the significant parts of the image. An homomorphic scheme is proposed using anisotropic diffusion in db2-type wavelet transform. Linear and non-linear filters are used on the approximate part of the image to remove blurring. Method noise thresholding is used to restore the unfiltered part of the despeckled image. The proposed method is applied and tested on correlated speckle noise as well as uncorrelated speckle noise on the real dataset of SAR images. The performance of the proposed method is evaluated by its visual quality and by using other metrics such as PSNR, SSIM, UIQI and RMSE. The performance and computational time are calculated and compared with standard filters and methods. The critical analysis of the result shows that proposed method gives the brilliant outcome in terms of structure, edge preservation and noise suppression. The proposed method has the ability to be used in practical applications.

1. Introduction

Image restoration is one of the most researched area in the field of image processing where original image is recovered from the noisy image. Satellite imagery is sub field of the image processing, where satellite images are obtained from synthetic aperture radar, This is an form of radar that is fixed on the satellites and aircraft that captures the high resolution images of the broad areas of the earth surface. SAR images are formed by the consistent interaction of the emitted microwave radiation with target areas. This consistent interaction originates arbitrary constructive and destructive nosiness resulting into multiplicative kind of noise known as speckle noise all over the image. There are many despeckling techniques and filters available in spatial as well as frequency domain to handle speckled SAR images by preserving the major information in the image like edge, boundary and objects. Few standard and conventional filters for despeckling purpose in the field of satellite imagery are frost filter (Frost et al., 1982), kuan filter (Kuan et al., 1987), kuwahara filter (Hachimura et al., 1976), (Kyprianidis et al., 2009), lee filter (Lee, 1980; Lee, 1981), mean filter (Acharya and Ray, 2005) and median filter (Jain, 1989). The denoising schemes under homomorphic filtering are highly effective and adaptive. The non homomorphic denoising techniques are also effective but less frequently used due to its complexity.

It is observed that bayesian approaches in transform domain shows better results than bayesian approaches in spatial domain. But there some non-bayesian approaches that gives as better results as bayesian approaches in transform domain. Order Statistics and Morphological Filters (Alparone et al., 1995; Alparone et al., 1996; Crimmins, 1985) are used for preserving edges, retaining textures and smoothing the noisy background, but thicker objects left unprocessed. This method is not built for speckle noise model but still provides fair results in some cases. Anisotropic diffusion (Yuand and Acton, 2004; Perona and Malik, 1990) is a

* Corresponding author.
E-mail address: prabhisheksingh88@gmail.com (P. Singh).

Peer review under responsibility of King Saud University.

Production and hosting by Elsevier

http://dx.doi.org/10.1016/j.jksuci.2017.06.006
1319-1578/

popular technique that retains significant parts mainly edges, lines and other fine details. Speckle Reduction using Anisotropic Diffusion (McConnell and Oliver, 1994) exploits sudden occurring coefficient of variation. It shows better results than conventional methods in the terms of variance minimization, mean preservation and edge localization. SRAD (Yuand and Acton, 2002) (Speckle Reducing Anisotropic Diffusion) developed the pioneer scheme of reducing speckle noise using anisotropic diffusion by validating the new algorithm using both synthetic and real linear scan ultrasonic imagery of the carotid artery. In despeckling based on compressed sensing (Foucher, 2008; Yangand and Zhang, 2012; Hao et al., 2012), it is known that in order to obtain good quality image, multiple degraded images can be merged. Keeping this in mind, compressed sensing is employed to get multiple SAR images from a single SAR image. Other non bayesian approaches that also gives satisfactory results in terms of visual appearance and edge preservation are bilateral filtering (Tomasiand and Manduchi, 1998; Zhang et al., 2011; Li et al., 2013), sigma filter (Lee, 1983) and non-local filtering (Deledalle et al., 2009; Parrilli et al., 2012).

Homomorphic and non-homomorphic filtering are the two bayesian methods in transform domain that provide best schemes in wavelet domain. Homomorphic filtering (Gagnon and Jouan, 1997; Hervet et al., 1998) is used to remove the multiplicative noise using log and exponential operations, while non–homomorphic filtering (Foucher et al., 2001; Argenti and Alparone, 2002; Dai et al., 2004) is less frequently seen in literature as it directly handles multiplicative noise without removing it. Since last two decades, homomorphic filtering is the commonly used method as after transforming multiplicative noise to additive, other additive noise restoration models can be used easily to handle this situation. It is easy understandable method. Non-homomorphic filtering methods directly works on multiplicative noise. This method is comparatively difficult to work upon. Basically homomorphic filtering is used for improving non-homogeneous illumination in images. Classical hard and soft thresholding methods (Donoho, 1995) were implemented in (Guo et al., 1994). The undecimated wavelet transform and the MAP standard have been implemented in the issue of SAR image despeckling (Argenti et al., 2012).

The article is organized in the following way: Section 2 describes the background of anisotropic diffusion, speckle noise model, thresholding mechanism, linear, non linear filters and method noise. Section 3 elaborates the proposed method. Section 4 presents all the experimental results and discusses its comparative performance, finally conclusions are drawn in Section 5.

2. Background

2.1. Anisotropic diffusion

In order to smooth the speckled images, the available methods and filters are based on the diffusion of the pixel values. Diffusion can be either isotropic or anisotropic diffusion. In isotropic, there is a diffusion of pixel values all across the image due to which blurring occurs as it performs the averaging all across the image regardless of any edge or object. It simply averages the image due to which the pixels at edge and objects gets mixed up. Here diffusion is same in every direction regardless of boundaries in the image. In the case of anisotropic diffusion, diffusion varies with the direction. It tries to average the image only at the either side of the edge, object or boundary. It smooths the correct object. This is achieved by the evaluating the gradient of the image (Jacobs, 2005) which is also called as edge stopping function. Basic equation of anisotropic diffusion is,

$$\frac{\partial(I(x,y,t))}{\partial(t)} = div[g(\|\nabla(I(x,y,t))\|)\nabla(I(x,y,t))] \quad (1)$$

here, $I(x,y,0)$ is original image, $\nabla(I(x,y,t))$, is the gradient of the image at time t, t is the time parameter and $g(*)$ is the conductance function that controls the conduction as a function of gradient. The conductance function is selected to satisfy $\lim_{x\to 0} g(x) = 1$, so that the diffusion of pixel values is maximum within the homogeneous regions and $\lim_{x\to 0} g(x) = 0$, so that the diffusion of pixel values gets stopped across the edges. In other words if conductance function is low, then small intensity gradients are capable enough to block conduction and hence diffusion across step edges and if it is large then it decreases the impact of intensity gradients on conduction. Perona and Malik (Perona and Malik, 1990) proposed two function as given below,

$$g_1(x) = \exp\left[-\left(\frac{x}{K}\right)^2\right] \quad (2)$$

and

$$g_2(x) = \frac{1}{1+\left(\frac{x}{K}\right)^2} \quad (3)$$

where, K is the gradient magnitude threshold parameter that controls the speed of the diffusion. Diffusion Eq. 2 provides preferential treatment for high contrast edges over low contrast ones while the diffusion Eq. 3 supports wide regions over smaller ones.

Anisotropic diffusion filtering is an iterative process. It is extremely sensitive to the number of iterations. Choosing the time parameter T is vital, since misjudging it may result in blurring the true edges and boundaries, while undervaluing it may leave unfiltered noise artefacts. Correct choice of conductance function and gradient thresholding parameters may lead to higher PSNR values. The slope of the reduction of PSNR values will be low, keeping the diffused image close to the original one. It is noticed that PSNR value is always maximized in a specific iteration, which is the ideal time to terminate the process.

2.2. Speckle noise model

Speckle noise is mainly found in SAR images and ulrasound images. Speckle has a negative influence on SAR images (Singh and Shree, 2016). Speckle noise is modelled as product of clean image pixel $S(i,j)$ to be estimated from $I(i,j)$ and multiplicative noise with unit mean and standard deviation $N(i,j)$. $I(i,j)$ is degraded pixel of the image. Speckle noise is modelled as,

$$I(i,j) = S(i,j) \times N(i,j) \quad (4)$$

Speckle noise is multiplicative in nature and most of the noise restoration models are additive model. So these models cannot be directly implemented to the SAR image despeckling process. A proper pre-processing step is required to handle this situation. The Lee filter can convert this multiplicative model into an additive one, thus reduces the problem of dealing with speckle noise. Some image enhancement methods can also be used for the same purpose. Log transform is one of them. It degrades the quality of the image (Singh and Shree, 2016) but it is easy and efficient in nature conversion of speckle noise, so it is applied in the work. Exponential transform is applied to perform the reverse operation of log transform to get back its original form.

2.3. Wavelet thresholding and adaptive filters

Wavelets are preferred mathematical function for denoising purpose. MATLAB Wavelet Toolbox offers a function, dwt2 for 2D-DWT which is used to analyse the high-frequency component in the image. Daubechies wavelet (db2) (Walker, 2008) is used as it easily solves the self-similarity properties of a signal or fractal problems. Decomposition is tested and performed up to 5 levels

Please cite this article in press as: Singh, P., Shree, R. A new homomorphic and method noise thresholding based despeckling of SAR image using anisotropic diffusion. Journal of King Saud University – Computer and Information Sciences (2017), http://dx.doi.org/10.1016/j.jksuci.2017.06.006

for visual quality analysis. Decomposition at level 3 delivers the best results. DWT decomposes the image into approximate part (LL) and detailed part (LH, HL and HH). Approximate part is subjected to median and wiener filtering while detailed part is thresholded using bayesian shrinkage rule using soft thresholding.

Median filtering is a nonlinear method for eliminating salt and pepper and impulsive noise. It reduces the random noise and preserves the edges in the image (Huang et al., 1979; Arias-Castro and Donoho, 2009) and is formulated as,

$$y[m,n] = median\{x[i,j],(i,j)\varepsilon w\} \tag{5}$$

where, w is a neighbourhood mask defined by the user, centered around location [m,n] in the image.

Wiener filter is the linear filter mainly used for reducing additive noise and avoid blurring. Wiener filters are commonly practised in the frequency domain (Brown et al., 1996; Wiener, 1949) and defined by,

$$W(f_1,f_2) = \frac{H*(f_1,f_2)S_{xx}(f_1,f_2)}{|H(f_1,f_2)|^2 S_{xx}(f_1,f_2) + S_{\eta\eta}(f_1,f_2)} \tag{6}$$

where, $S_{xx}(f_1,f_2)$ and $S_{\eta\eta}(f_1,f_2)$ are the power spectra of reference image and additive noise respectively and $H(f_1,f_2)$ is the blurring filter.

Threshold choice method includes three classes: universal threshold, sub-band adaptive threshold and spatially adaptive threshold. In universal threshold, the threshold value is uniquely chosen for all wavelet coefficients (Lee, 1980; Dixit and Sharma, 2014). In sub-band adaptive thresholding, the threshold value is selected separately for each detail sub-band (Dixit and Sharma, 2014; Acharya and Ray, 2005). In spatially adaptive threshold way, each detailed wavelet coefficient has its own threshold value (Dixit and Sharma, 2014; Frost et al., 1982). The proposed scheme uses the universal threshold selection category.

Selection of threshold value in satellite images is not a easy task as satellite images are low contrast in nature. Selection of small threshold value causes resultant image to be noisy, while resultant image at the edges and boundaries gets blurred for the large threshold value. Therefore selecting an optimal threshold value is an important task for preserving edges, boundaries and objects. In the proposed scheme, bayes shrink method is used for wavelet thresholding. Bayes Shrink is a mathematical frame where it is expected that all high frequency sub bands of wavelet coefficients are generalized by Gaussian distribution to evaluate the threshold value that reduces the Bayesian risk (Kumar and Diwakar, 2016a,b).

Threshold is calculated using,

$$\lambda = \left(\frac{\sigma_\eta^2}{\sigma_Y}\right) \tag{7}$$

Abramovitch et al. 1998 suggested robust median estimation method using which noise variance is estimated. According to this method thresholding is performed only at the diagonal (HH) component of the detailed part, but here in the proposed scheme, thresholding is performed in all the detailed parts (HL, LH and HH). Noise variance is estimated as:

$$\sigma_\eta^2 = \left[\frac{median(|X(m,n)|)}{0.6754}\right]^2 \tag{8}$$

where, $X(m,n) \in LH_L, X(m,n) \in HL_L$ and $X(m,n) \in HH_L$, and L depicts the level of decomposition in DWT. The standard deviation of noise less image (σ_Y) can be estimated as:

$$\sigma_Y^2 = max(\sigma_X^2 - \sigma_\eta^2, 0) \tag{9}$$

where, $\sigma_X^2 = \frac{1}{b}\Sigma_{i=1}^{b} X_i^2$, and b is the patch size of the input image.

Hard and Soft thresholding are the two most popular thresholding algorithm used for performing thresholding using the selected threshold value. In hard thresholding, every coefficient value is matched with λ and values less than λ are changed to zero while the replacement process in soft thresholding is similar to hard thresholding, moreover remaining coefficients are modified by subtracting threshold values. On comparing, soft thresholding delivers improved performance in terms of visual appearance of images. The soft thresholding is equated as:

$$\widehat{Y} : \begin{cases} 0 & if\ |X| \leqslant \lambda \\ sign(X)(|X| - \lambda) & if\ |X| > \lambda \end{cases} \tag{10}$$

2.4. Method noise

The difference between the noisy image and denoised image shows the noise removed by the algorithm, which is called as method noise. Let say, D is the noisy image and after denoising it we get E as the final denoised image. Now mathematically F is evaluated by below equation,

$$F = D - E \tag{11}$$

Now F contains the noisy part, so further any denoising scheme can be applied to it like thresholding or filtering. After denoising F, let say $E1$ is achieved. Then below equation is performed to get the resultant denoised image, $E2$ which contains the lowest noise.

$$E2 = E + E1 \tag{12}$$

All despeckling approaches depend on the filtering constraint v. This constraint measures the degree of filtering applied to the image. For most of the methods, the parameter v depends on an approximation of the noise variance σ^2. Method noise is a kind of a post processing step. It is used after the filtering is applied. It enhances the result and improves the quality of the image. Method noise is simple to understand and implement.

3. Proposed methodology

The proposed work is based on the homomorphic filtering in wavelet domain. Homomorphic filtering method is adaptive and robust than other methods (Gagnon and Jouan, 1997), (Hervet et al., 1998). Efficient linear and non-linear filters and non-bayesian methods can easily be incorporated in the homomorphic filtering schemes. The proposed algorithm is explained below:

Algorithm 1: Proposed despeckling scheme using method noise and anisotropic diffusion

Input: Speckled SAR image
Output: Despeckled SAR image
1: Apply iterative anisotropic diffusion/filtering on S.
(a) Initiate the parameters, $g(*)$ and K.
(b) Compute Perona-Malik diffusion Eq. 3 using required parameters.
(c) **for** i = 1 to n, i = No. of iterations, **do**
i. solve the standard Eq. 1 of anisotropic diffusion.
ii. update the values.
end for
(d) Resultant image is S_{ad}.
2: Apply log transformation, S_l.
3: for j = 1 to 3, j = level of decomposition, **do**
(a) Apply DWT on S_l.
(b) Decomposition into 4 subbands, approximate part (a1, a2, a3) and detail part (b1 c1 d1), (b2 c2 d2), (b3 c3 d3).

(*continued on next page*)

Please cite this article in press as: Singh, P., Shree, R. A new homomorphic and method noise thresholding based despeckling of SAR image using anisotropic diffusion. Journal of King Saud University – Computer and Information Sciences (2017), http://dx.doi.org/10.1016/j.jksuci.2017.06.006

(c) Apply 2D median filtering on a2 and a3 subbands using 3*3 neighborhood mask using Eq. 5.
(d) Apply 2D adaptive wiener filtering on a1 subbands using 3*3 neighborhood mask using Eq. 6.
(e) Perform thresholding on the detailed part (b1 c1 d1), (b2 c2 d2), (b3 c3 d3) using following step:
i. Estimate noise variance using Eq. 8.
ii. Threshold calculation using Eq. 7.
iii. Apply soft thresholding using Eq. 10 and Eq. 9.

end for

4: Apply inverse DWT.

5: Apply exponential transform, S_e.

5: Apply method noise using input high frequency speckled image (S) and thresholded high frequency subband (S_e).
(a) Subtract S_e from S and get D, as $D = S - S_e$.
(b) Apply step 3(e) on D and then apply IDWT and resultant is H.
(c) Add H and S_e to get D_{ES}, as $D_{ES} = H + S_e$.

4. Experimental results and discussion

In this section, experimental results with their performance aspects are presented on some real SAR images in order to verify the effectiveness of proposed algorithm. The real sample dataset of SAR images shown in Fig. 1. Fig. 2 shows speckled SAR image dataset at $\sigma = 20$. This sample dataset is made noisy by adding speckle noise at various levels ($\sigma \in 4, 10, 20, 30, 40$).

Noisy SAR images are of size 512×512 used to verify the performance of the proposed algorithm for the quantitative and qualitative evaluation. All experiment results are evaluated in MATLAB version = 8.3, name = R2014a on Intel(R) Core(TM) i5-2410 M CPU @ 2.30 GHz, 4 GB RAM and 64-bit operating system. System configuration is necessary to note down as the execution time of the proposed algorithm will be compared to the other techniques on the same system (Singh and Shree, 2017). Anisotropic total variation and diffusion gives the best results in terms of visual appearance as it restores the edges (Lee, 1980; Kumar and Diwakar, 2017). For all the experiments, the window size is fixed for 3×3 but No. of iteration, I is not fixed. I is tested from $(1 - 10)$ and results are presented on the best number of iterations.

In order to validate the proposed algorithm, the experimental results are compared with the results of some well known standard filters and techniques, such as log compression filtering method (Loizou et al., 2014), frost filter (Frost et al., 1982), kuan filter (Kuan et al., 1987), kuwahara filter (Hachimura et al., 1976), lee filter (Lee, 1980), SRAD (Speckle Reduction using Anisotropic Diffusion) (Yuand and Acton, 2002), and HFLF (Homomorphic Filering with Log Function) (Loizou et al., 2014). The code of SRAD (Yuand and Acton, 2002) is taken from Image Despeckle Filtering Toolbox of (Loizou et al., 2014) available on the mathsworks website (Image Despeckle Filtering Toolbox, 2014). The parameters required are No. of iterations I, window size and lambda (time step). I is the common parameter used in all the compared work, window size is fixed to 3×3, used in (Hachimura et al., 1976) and lambda $[0.00 - 0.25]$ is used in (Yuand and Acton, 2002). Except window size, all the other parameters are changed and measured for values of best results. The experimental results are performed at noise variance $\sigma = 20$.

4.1. SAR data

Here in the experiment, five different SAR images are taken of different background nature to verify credibility of the proposed algorithm. Original SAR image dataset in Fig. 1 is taken from public access database (http://photojournal.jpl.nasa.gov/catalog/PIA01763, http://eo.belspo.be/directory/SensorDetail.aspx?senID = 152 and http://www.sandia.gov/RADAR/imagery/). The real speckled SAR image displayed in the Fig. 11 is taken from the dataset of standard 512×512 grayscale test images available at http://decsai.ugr.es/cvg/CG/base.htm. For easy understanding, SAR images in Figs. 1d are denoted as SAR1, SAR2, SAR3 and

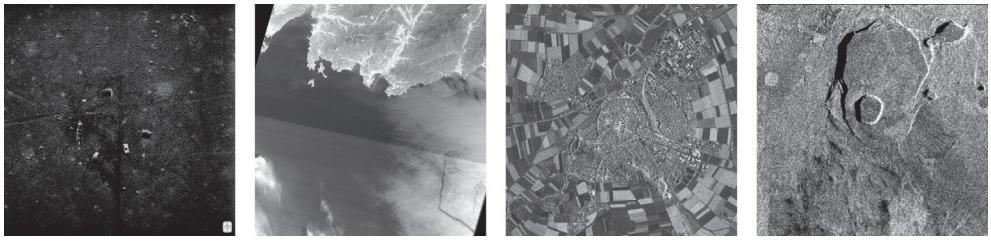

Fig. 1. Original SAR Images.

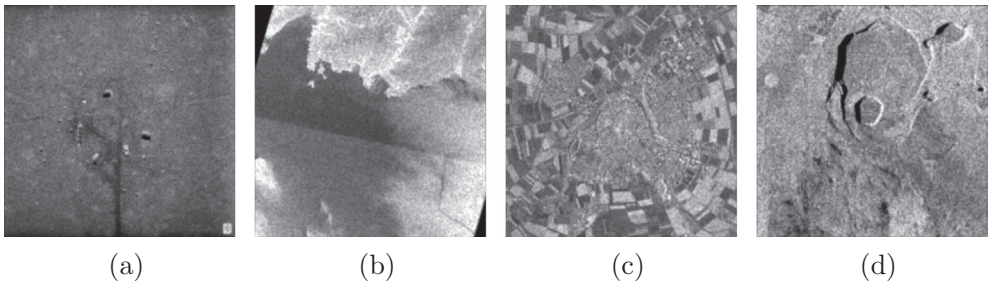

Fig. 2. Noisy SAR image data set $\sigma = 20$.

Please cite this article in press as: Singh, P., Shree, R. A new homomorphic and method noise thresholding based despeckling of SAR image using anisotropic diffusion. Journal of King Saud University – Computer and Information Sciences (2017), http://dx.doi.org/10.1016/j.jksuci.2017.06.006

SAR4, respectively. Apart from SAR images, speckle noise is also seen medical images specially in ultrasound images.

4.2. Performance evaluation

In order to measure the accuracy of the proposed algorithm, there are some commonly used performance metrics with-references indexes of despeckling algorithms like, Root Mean Square Error (RMSE), Signal to Noise Ratio (SNR), Peak Signal to Noise Ratio (PSNR), Energy Signal-to-Noise Ratio (ESNR), Structural Similarity Index Measure (SSIM), Edge Correlation (EC) index and Pratts Figure Of Merit (FOM) (Argenti et al., 2013). Among these metrics, mostly used measures are used like PSNR, SSIM, RMSE and a new measure is used Universal Image Quality Index (UIQI) to analyze the linear correlation, luminance and contrast of the image. SSIM is used measure the similarity between denoised image against reference image. It depends upon three terms, luminance, contrast and structural term. The overall index is a multiplicative combination of the three terms. SSIM is computed by,

$$SSIM(x,y) = \frac{(2\mu_x\mu_y + C_1)(2\sigma_{xy} + C_2)}{(\mu_x^2 + \mu_y^2 + C_1)(\sigma_x^2 + \sigma_y^2 + C_2)} \tag{13}$$

here $\mu_x, \mu_y, \sigma_x, \sigma_y$ and σ_{xy} are the local means, standard deviation and cross variance for images x, y. $C_1 = (0.01 * L)^2$ and $C_2 = (0.03 * L)^2$, where L is the specified dynamic range value. According to the literature (Li et al., 2013) its value lies between -1 to 1, value near to 1 represents better image quality.

PSNR is one of the important performance metric in the case of the denoising procedure. When the value of the PSNR is high, then the quality of the denoised image is good, otherwise considered as bad. PSNR is computed by:

$$PSNR = 10log_{10}\left(\frac{255 \times 255}{MSE}\right) \tag{14}$$

where Mean Square Error (MSE) is calculated as:

$$MSE = \frac{1}{mn}\Sigma_{i=0}^{m-1}\Sigma_{j=0}^{n-1}[X(i,j) - R(i,j)]^2 \tag{15}$$

RMSE also known as Root Mean Square Deviation (RMSD) is one of the most widely used statistics in geographic information system and remote sensing imagery. RMSE measures the error between two images dataset comparing a despeckled image and reference image. RMSE is mostly used in the performance evaluation of geostatistical and remote sensing applications. RMSE is evaluated as:

$$RMSE = \sqrt{MSE} \tag{16}$$

UIQI performs the comparison between reference image and despeckled image on the basis of: luminance, contrast, and structural components. UIQI is a simple and widely used metric that counts only on first and second order statistic of the reference and despeckled SAR images, but sometimes UIQI is considered as a unstable measure as it doesnt correlate with subjective quality assessment of image due to which a new metric is proposed called as SSIM which is explained above and used in the work. UIQI can be written as a product of three components:

$$Q = \frac{\sigma_{xy}}{\sigma_x\sigma_y} \cdot \frac{2\bar{x}\bar{y}}{(\bar{x})^2 + (\bar{y})^2} \cdot \frac{2\sigma_x\sigma_y}{\sigma_x^2 + \sigma_y^2} \tag{17}$$

The first component is used to measures the degree of linear correlation. The second component measures how close the mean luminance is. The third component measures how similar the contrasts of the images are. The range of the three components is in $[0, 1]$. Therefore, the final range of the UIQI is in between $[0, 1]$.

4.3. Experimental evaluation and comparison

Figs. 3–10, show the results of log compression filtering, frost filter, kuan filter, kuwahara filter, lee filter, SRAD, HFLF and proposed algorithm respectively. There are certain measures for analysing the quality of despeckled SAR image through their visual appearance such as, (i) presence of the artifacts; (ii) edge preservation; (iii) visibility of low contrast objects and (iv) texture preservation, but there is no such mathematical formula or specific process available to do so.

The performance measures(PSNR, SSIM, UIQI and RMSE) are evaluated at different noise variances shown in Tables 1 and 2. The best results are shown in bold. The computational time of the proposed algorithm is shown in comparative Table 3. On comparing Table 1–3, it is clear that the results of the proposed algorithm are better than the mentioned standard methods.

Table 1, shows comparative table of various despeckling methods including proposed method based on PSNR and UIQI, while Table 2, based on UIQI and RMSE. The results of kuan and kuwahara filters shows the good performance results in terms of visual appearance of image, but still presence of artifacts and slight disturbance in edges is seen there. The proposed method shows the best results among all the mentioned methods.

On applying all the methods on SAR1 image, it is observed that at noise variance level 40, kuan filter shows the best results in terms of PSNR, while in rest of the noise variances, proposed method shows the best results. On SAR2 image proposed method shows the best results in terms of PSNR and SSIM. On SAR3 image, frost filter shows better results at low variance level i.e. 4 in terms of PSNR. SRAD shows better results at variance level 20 in terms of SSIM, while in rest cases in terms of PSNR and SSIM, proposed method shows the best results as depicted in Table 1.

In SAR1 image, kuan filter shows good result at noise level 30 in terms of UIQI. In SAR2 image, again kuan filter shows good

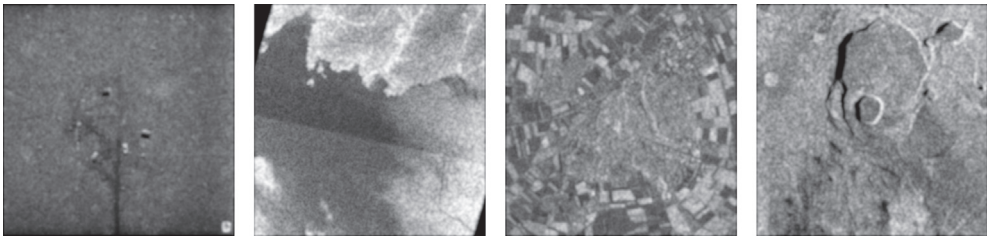

(a) (b) (c) (d)

Fig. 3. Results of Log compression filtering.

Please cite this article in press as: Singh, P., Shree, R. A new homomorphic and method noise thresholding based despeckling of SAR image using anisotropic diffusion. Journal of King Saud University – Computer and Information Sciences (2017), http://dx.doi.org/10.1016/j.jksuci.2017.06.006

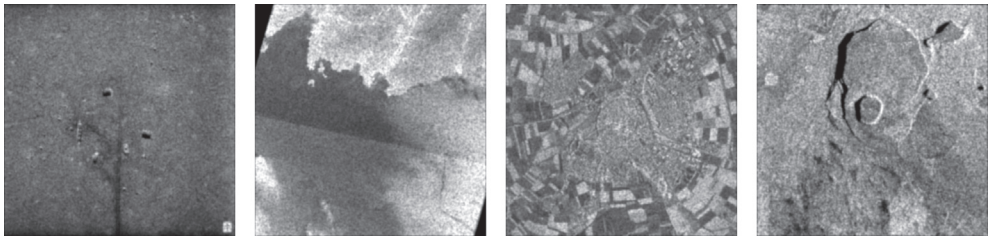

Fig. 4. Results of Frost filter.

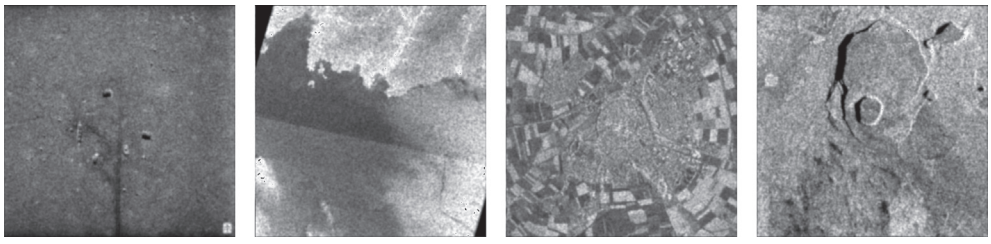

Fig. 5. Results of Kuan filter.

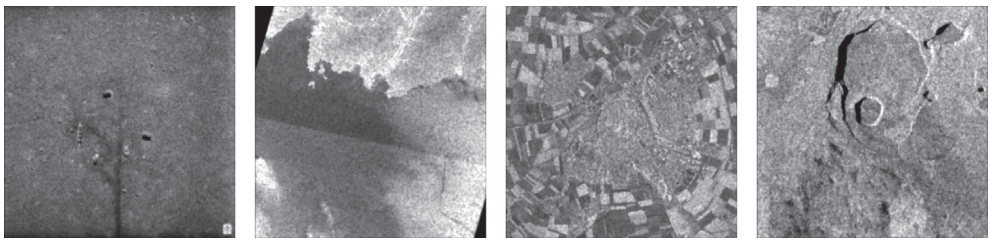

Fig. 6. Results of Kuwahara filter.

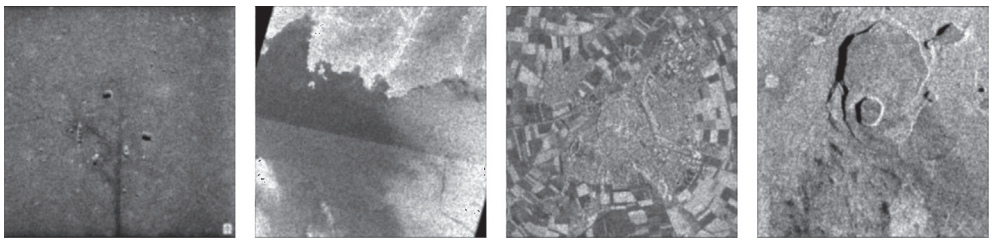

Fig. 7. Results of Lee filter.

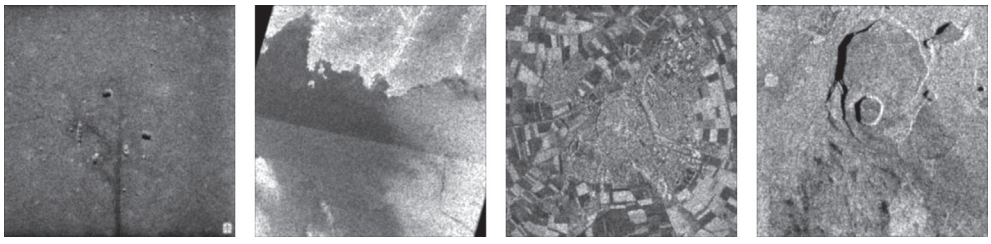

Fig. 8. Results of SRAD filter.

Please cite this article in press as: Singh, P., Shree, R. A new homomorphic and method noise thresholding based despeckling of SAR image using anisotropic diffusion. Journal of King Saud University – Computer and Information Sciences (2017), http://dx.doi.org/10.1016/j.jksuci.2017.06.006

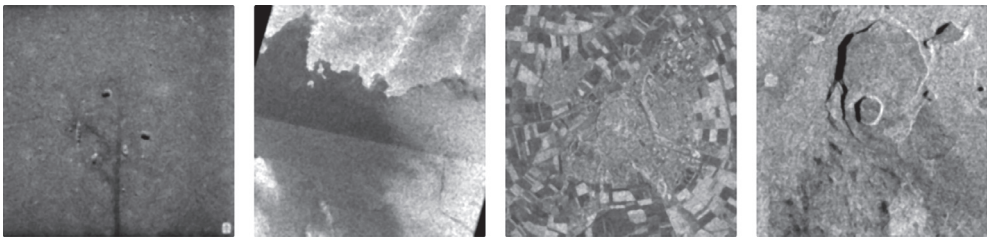

Fig. 9. Results of HFLF filter.

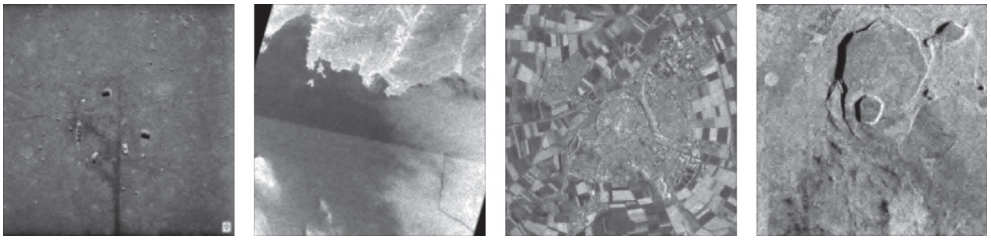

Fig. 10. Results of proposed algorithm

Table 1
PSNR and SSIM of despeckled SAR images.

		PSNR					SSIM				
Image	Noise Variance	4	10	20	30	40	4	10	20	30	40
SAR1	Log Compression	36.647	36.0538	34.9534	33.9844	33.1368	0.7186	0.7186	0.7106	0.7981	0.7589
	Frost	43.112	41.4352	39.0494	36.8906	34.9803	0.9676	0.9472	0.9296	0.8761	0.8247
	Kuan	42.4187	41.3284	38.6061	37.3362	**37.1907**	0.9404	0.9414	0.9597	0.9117	0.9205
	Kuwahara	40.4171	39.4169	37.7651	36.4102	35.2912	0.9443	0.9282	0.9008	0.8756	0.8539
	Lee	42.4187	41.1534	39.0061	37.3362	34.1907	0.9304	0.936	0.9297	0.9151	0.9005
	SRAD	43.2369	40.9462	38.4532	37.9469	35.4101	0.9642	0.9543	0.8962	0.9001	0.8911
	HFLF	38.5577	37.9848	36.7265	35.6321	34.7107	0.947	0.9276	0.8914	0.8573	0.8277
	Proposed	**43.7758**	**41.601**	**39.9001**	**38.4579**	36.6709	**0.9725**	**0.9691**	**0.9358**	**0.9229**	**0.9209**
SAR2	Log Compression	36.1302	34.8258	32.9989	31.665	30.5224	0.9215	0.9016	0.8456	0.8035	0.7752
	Frost	41.9545	38.2017	33.7232	31.5344	30.0437	0.9605	0.9202	0.8272	0.7562	0.7102
	Kuan	33.5174	33.4021	32.7725	32.1921	31.4272	0.9643	0.927	0.9167	0.8901	0.885
	Kuwahara	35.468	34.4955	32.9353	31.9244	30.8737	0.9405	0.907	0.8638	0.8334	0.8113
	Lee	35.7995	35.5979	34.5047	33.667	32.6689	0.9644	0.9371	0.9248	0.8946	0.8851
	SRAD	40.4123	39.4624	35.0432	33.9467	32.1256	0.9423	0.9231	0.9142	0.8991	0.8712
	HFLF	34.6708	33.7066	32.3736	31.3879	30.517	0.9495	0.9021	0.8449	0.8016	0.7723
	Proposed	**42.7729**	**40.7504**	**37.0465**	**34.9169**	**32.8688**	**0.9749**	**0.9489**	**0.9252**	**0.9001**	**0.8914**
SAR3	Log Compression	32.1007	31.5781	30.3034	29.8619	29.2327	0.8246	0.8274	0.7849	0.7512	0.7132
	Frost	**41.1252**	36.4462	34.1957	32.0019	30.8811	0.9797	0.9344	0.8804	0.8258	0.7769
	Kuan	36.125	35.4573	33.8029	34.1759	31.0092	0.926	0.9311	0.915	0.8964	0.8864
	Kuwahara	33.9882	33.4617	32.0788	31.6396	30.9167	0.911	0.8965	0.8702	0.8498	0.8328
	Lee	38.125	36.4763	34.1123	33.9769	30.1694	0.946	0.9211	0.9149	0.8925	0.8164
	SRAD	29.0049	29.4843	32.2613	30.5044	30.2244	0.8848	0.9263	**0.9846**	0.8964	0.8764
	HFLF	34.7756	34.0279	32.4083	31.8244	30.9849	0.9245	0.9009	0.8639	0.8325	0.8059
	Proposed	39.2991	**36.9472**	**34.3189**	**34.9939**	**31.1602**	**0.9808**	**0.9377**	0.9211	**0.9085**	**0.8957**
SAR4	Log Compression	31.8743	31.8187	30.1481	29.2254	28.4631	0.7946	0.764	0.7177	0.6787	0.6522
	Frost	36.8249	32.2271	31.1902	30.0011	29.004	0.8912	0.8783	0.8424	0.7692	0.7244
	Kuan	32.6358	34.4218	31.5743	29.9742	28.9994	0.9002	0.9237	0.8295	0.7692	0.8504
	Kuwahara	32.9419	32.3182	31.2995	30.0035	29.0091	0.8877	0.8713	0.8428	0.8147	0.8022
	Lee	33.6358	33.1421	31.5743	29.3073	28.9461	**0.9254**	0.8759	0.8659	0.8564	0.8491
	SRAD	31.1452	31.0094	30.4683	28.4321	26.4414	0.8843	0.8613	0.8015	0.7751	0.7561
	HFLF	32.6814	31.1111	31.0843	30.0037	29.5014	0.8833	0.8592	0.8174	0.7837	0.7599
	Proposed	**36.9001**	**33.3331**	**31.9939**	**30.0272**	**29.9536**	0.904	**0.9244**	**0.8758**	**0.8655**	**0.8529**

Please cite this article in press as: Singh, P., Shree, R. A new homomorphic and method noise thresholding based despeckling of SAR image using anisotropic diffusion. Journal of King Saud University – Computer and Information Sciences (2017), http://dx.doi.org/10.1016/j.jksuci.2017.06.006

Table 2
UIQI and RMSE of despeckled SAR images.

		UIQI					RMSE				
Image	Noise Variance	4	10	20	30	40	4	10	20	30	40
SAR1	Log Compression	0.7349	0.7009	0.6763	0.6505	0.6268	5.2637	5.6803	6.4474	7.2083	7.9472
	Frost	0.9001	0.8743	0.8631	0.8319	0.7804	1.2712	1.8153	3.6273	5.1585	6.4275
	Kuan	0.9051	0.886	0.8315	**0.9151**	0.8701	2.7083	2.8144	3.3632	3.8926	4.4414
	Kuwahara	0.862	0.8568	0.8419	0.8258	0.8133	3.4102	3.8566	4.6645	5.4519	6.2015
	Lee	0.8916	0.8863	0.8531	0.8452	0.8562	2.7008	2.8144	3.3632	3.8926	4.4498
	SRAD	0.9004	0.8464	0.8345	0.8311	0.8312	0.9041	1.2352	1.3256	1.7432	2.4326
	HFLF	0.8296	0.8168	0.7921	0.7676	0.7492	4.2242	4.548	5.2569	5.9628	6.6301
	Proposed	**0.906**	**0.8952**	**0.8761**	0.8656	**0.8758**	**0.0072**	**0.0094**	**0.0127**	**0.0151**	**0.0164**
SAR2	Log Compression	0.8185	0.8447	0.8033	0.7704	0.7539	5.6305	6.5428	8.0744	9.4146	10.7383
	Frost	0.8715	0.8264	0.8001	0.7328	0.7006	2.0386	4.4358	7.4284	9.5572	11.3467
	Kuan	0.8115	**0.9243**	0.8003	0.8124	0.8148	7.6065	7.7081	8.2877	8.8604	9.676
	Kuwahara	0.8615	0.8447	0.8204	0.8008	0.7902	6.0766	6.7964	8.1337	9.1377	10.3127
	Lee	0.8156	0.8248	0.8248	0.8348	0.8153	5.849	5.9868	6.7892	7.4766	8.3871
	SRAD	0.8123	0.8001	0.8002	0.8124	0.8227	0.8461	1.2034	2.1234	2.9846	3.1456
	HFLF	0.8401	0.8036	0.769	0.7411	0.7276	6.6606	7.4426	8.6772	9.7198	10.745
	Proposed	**0.8773**	0.8458	**0.8384**	**0.8399**	**0.8228**	**0.0072**	**0.0116**	**0.0157**	**0.0201**	**0.0227**
SAR3	Log Compression	0.8021	0.7805	0.7524	0.7295	0.7132	8.954	9.5093	10.5374	11.5867	12.4573
	Frost	0.9074	0.8946	0.8838	0.8376	0.7962	2.5165	4.0846	6.7316	8.6661	10.3039
	Kuan	0.8962	0.8896	0.8846	0.8766	0.8562	4.4751	4.8327	5.5914	6.4037	7.1715
	Kuwahara	0.8856	0.8776	0.8617	0.848	0.8372	7.2052	7.6554	8.5894	9.4422	10.2617
	Lee	0.8664	0.8567	0.8434	0.8764	0.8264	4.4751	4.8328	5.5945	6.4307	7.1715
	SRAD	0.8846	**0.9061**	0.8912	0.8641	0.8162	12.7882	12.1016	8.4109	10.7605	6.1712
	HFLF	0.8919	0.8723	0.8467	0.8227	0.8055	6.5805	7.1723	8.2697	9.2438	10.1815
	Proposed	**0.9079**	0.9016	**0.8921**	**0.8804**	**0.8737**	**0.0153**	**0.0178**	**0.0215**	**0.0245**	**0.0277**
SAR4	Log Compression	0.7412	0.7193	0.6882	0.6611	0.6502	9.1905	9.9473	11.2113	12.4678	13.3374
	Frost	0.8611	0.8179	0.8516	0.7893	0.7544	2.9229	4.9625	7.8985	10.194	11.8836
	Kuan	0.8512	**0.8934**	**0.932**	0.7896	0.7942	4.2195	4.825	6.0026	10.195	7.7929
	Kuwahara	0.8562	0.8145	0.8439	0.8261	0.8156	8.1275	8.7326	9.8193	10.9531	11.9014
	Lee	0.8612	0.8611	0.8421	0.8166	0.7944	4.2195	4.8254	6.0026	6.9453	7.7929
	SRAD	0.8441	0.8292	0.8041	0.776	0.7599	2.2951	3.1375	3.9467	4.6742	5.9919
	HFLF	0.8572	0.839	0.8075	0.7833	0.7667	8.375	8.9423	10.0656	11.1012	12.0777
	Proposed	**0.8681**	0.8648	0.8521	**0.8457**	**0.8375**	**0.0218**	**0.0241**	**0.0282**	**0.0315**	**0.0348**

Table 3
Execution time of different despeckling techniques (in seconds).

Method	Log Compression	Frost	Kuan	Kuwahara	Lee	SRAD	HFLF	Proposed
Time	2.0034	17.5055	24.6968	25.0012	36.612	4.1567	1.7898	3.2136

result at variance level 10 in terms of UIQI. In SAR3 image, SRAD method shows better result at variance level 10 in terms of UIQI. In SAR4 image kuan filter shows good result at noise variance level 10 and 20 in terms of UIQI. On comparing kuan and proposed method in terms of UIQI, the proposed method is better in 80 percent of the cases while kuan shows best results in almost all the rest cases. The result of proposed method are far better than other methods in terms of RMSE. RMSE value should be as low as possible and RMSE value of the proposed method is evaluated very low than others, thus PSNR also shows better results.

In terms of texture and edge preservation kuan, kuwahara and SRAD filter shows the better results, small objects are retained properly and not over smoothed over the homogeneous areas. In SAR4 image, the edges are well preserved by above three methods. Log compression and HFLF does not provide good results as edges gets distorted specially in the SAR1 image and smoothing is also not performed properly as speckle noise can be observed in the results on zooming the images. Frost filter performs better than lee filter, although the results of both methods are satisfactory but still there is a blurriness which can be seen in SAR1 and SAR2 image, but in rest two images results are better.

The Fig. 11 shows the analysis and comparison of proposed method and other compared methods and filters on the real speckled SAR image. This figure shows the result of the proposed method on uncorrelated speckle noise, as in the Fig. 11, the distributional behavior of the speckle can be analyzed and known but the degree of noise variance in the image cannot be estimated. Hence it is a tricky task to despeckle the real noisy SAR image, but still the proposed method shows comparatively good result among the other methods and filters.

On analysing the results of proposed method in SAR1 image, small objects are preserved, details are not blurred and texture is also preserved over homogeneous areas without inclusion of any artefacts. In SAR2 image, edges are well preserved and the visual appearance of the SAR3 and SAR4 image are best among all methods in respect of all parameters. This result shows that this experimental method can be used in various applications like wave forecasting, marine climatology, regional ice monitoring, and ship detection in the coastal regions, while the results of the SAR1, SAR3 and SAR4 of earth's land terrain area shows that it can also be used in field of agricultural and tropical forest monitoring.

Performance percentage of the proposed method is evaluated using all the results at different noise variance cases of

Please cite this article in press as: Singh, P., Shree, R. A new homomorphic and method noise thresholding based despeckling of SAR image using anisotropic diffusion. Journal of King Saud University – Computer and Information Sciences (2017), http://dx.doi.org/10.1016/j.jksuci.2017.06.006

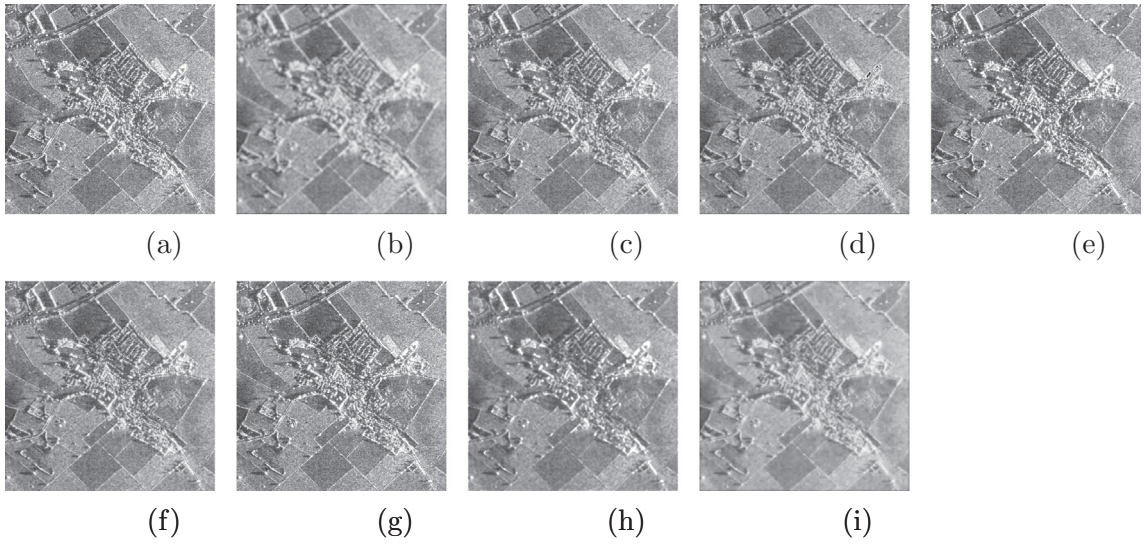

Fig. 11. Analysis on real speckled SAR image: (a) real speckled SAR image; (b) result of log compression; (c) result of frost; (d) result of kuan; (e) result of kuwahara; (f) result of lee; (g) result of SRAD; (h) result of HFLF; and (i) result of proposed algorithm.

performance metrics in the Table 1 and 2. There are 20 cases each for every metrics. There are 4 metrics evaluated. Therefore there are total 80 cases, over which the proposed method is compared with other standard work. Out of 80 cases, the proposed method shows better results in 71 cases. So, the performance percentage of the proposed method is 88.75 percent.

In order to visualize the performance of the algorithm over the real SAR dataset at different classification of the noise variances ($\sigma \in 4, 10, 20, 30, 40$), a concept of confusion matrix (Semwal et al., 2015; Semwal et al., 2015) is used to evaluate the performance and also provides the detailed statistical learning (Singh et al., 2016) at all discussed noise variances in Table 1 and 2. The training images used are the ones shown in Fig. 1 and are corrupted with speckle noise at above defined noise variances. In order to test this classifier performance, the confusion matrix (Semwal et al., 2016) is evaluated as shown in Fig. 12. The major diagonal depicts the percentage of speckled image and not speckled image correctly detected by the proposed method. The secondary diagonal shows the false positives and false negatives.

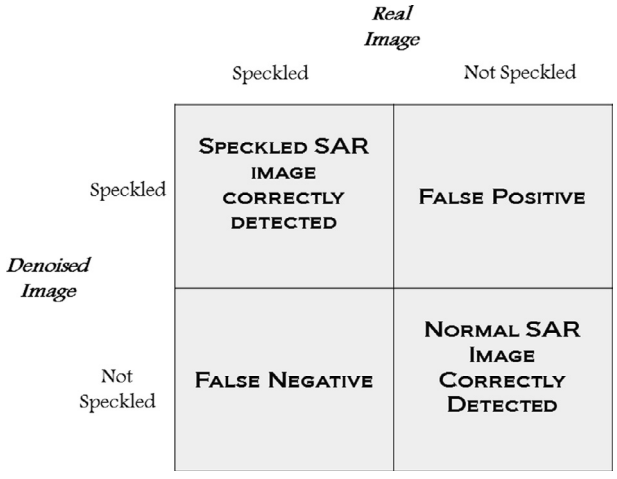

Fig. 12. Confusion matrix.

Now the proposed algorithm is checked at ($\sigma \in 4, 10, 20, 30, 40$) using all four performance metric values used in Tables 1 and 2 and evaluates the performance percentage of the proposed approach while comparing with other mentioned methods and filters. A Table 4 is created using the concept of confusion matrix where the performance percentage is evaluated using metrics values at different noise levels. The table is divided into two major categories, first is Algorithm Best Performance Percentage (ABPP) and second is Algorithm Not Best Performance Percentage (ANBPP). ABPP depicts that percentage when proposed method shows the best result among other methods and filters. ANBPP shows that percentage where other methods and filters overcome the proposed method. The false negative and false positive comes under the category of ANBPP. The ABPP shows the performance percentage at different noise variance level. Using this analysis, average of ABPP can be calculated to define whole sole performance percentage of algorithm which is equivalent to 91.25 according to confusion matrix.

Apart from evaluating an denoised image based on visual appearance and performance metrics, computational time of the algorithm is also one important factor. The execution time of all despeckling algorithm involving proposed method is shown in the Table 3. It can be observed from the Table 3 that the proposed method takes comparatively less computational time than frost, kuan, kuwahara, lee and SRAD but slightly more time than log compression and HFLF. Although the computational time is slightly more than log compression and HFLF, but still proposed method presents the result far better than these two. So, the less time doesn't underrates the proposed method. The computational time

Table 4
Computing performance percentage of proposed method on comparing with different methods and filters.

Algorithm	% Noise variance	% ANBPP	% ABPP
Proposed Algorithm	4	12.5	87.5
	10	6.25	93.75
	20	12.5	87.5
	30	6.25	93.75
	40	6.25	93.75

Please cite this article in press as: Singh, P., Shree, R. A new homomorphic and method noise thresholding based despeckling of SAR image using anisotropic diffusion. Journal of King Saud University – Computer and Information Sciences (2017), http://dx.doi.org/10.1016/j.jksuci.2017.06.006

of the algorithm depends upon the number of iteration involved in the execution. So, it is better to check the algorithm at maximum number of iterations and then later resolve the issue by fixing the values of inner parameters to perform the proposed method iteratively. The results may be gets changed by changing the inner parameter values of the proposed method.

For critically analysing the proposed method, Fig. 13 shows the intensity profile of line on the SAR1 image. Fig. 13 critically analyses and compares the proposed method with the standard work. The accurate overlapping of two waves shows that proposed method delivers the best result. The method is further analysed by drawing the histogram of full reference image and despeckled image on the same plot in Fig. 14. Again overlapping of two histogram is shown at different noise levels to check the impact of proposed method. It can be seen that at noise variance = 40, the method shows good result.

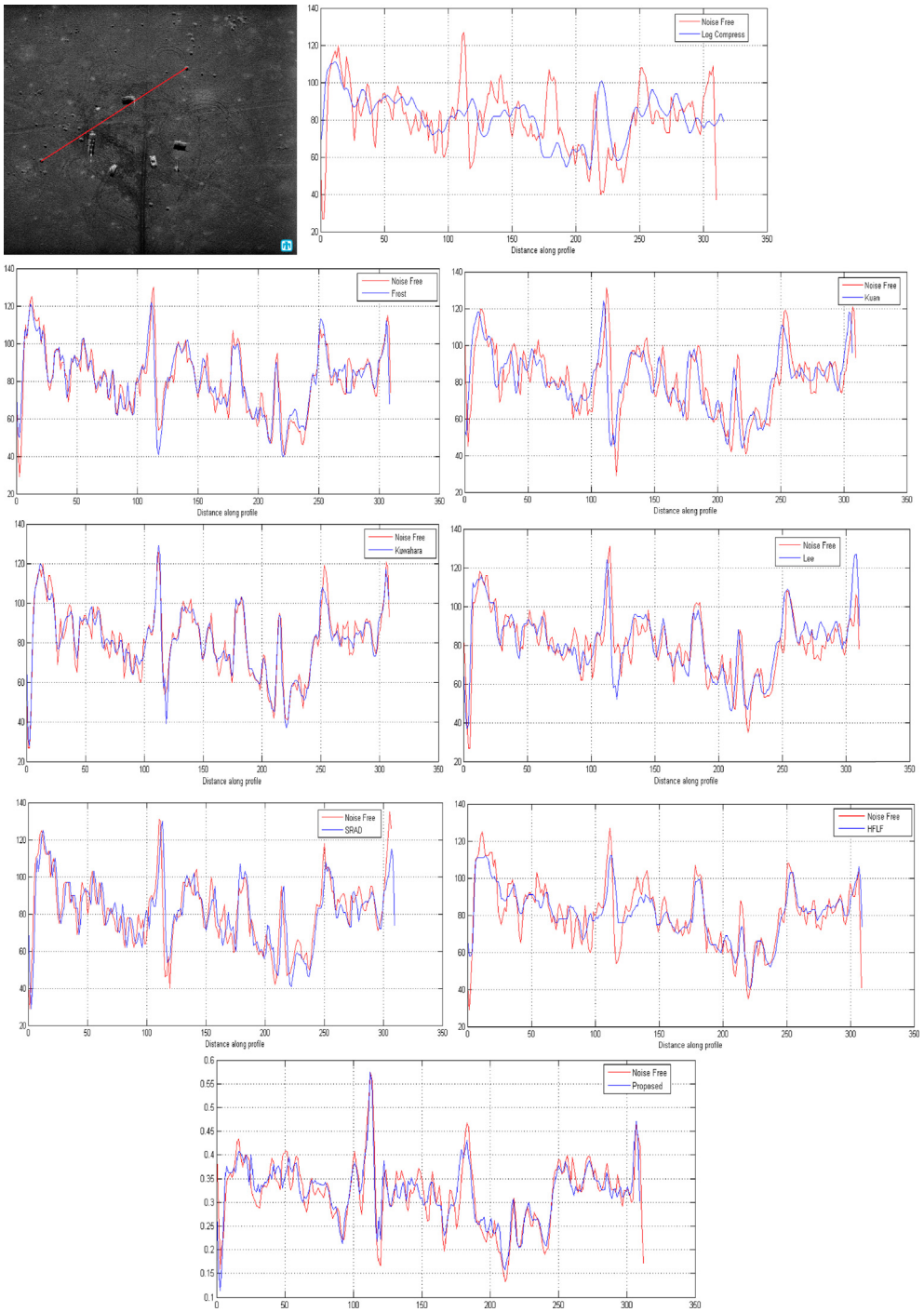

Fig. 13. Intensity profile of a line on SAR1 image. In each plot, the noise free intensity profile is plotted in red and despeckled profile is plotted in blue. For interpretation of the references to colour in this figure legend, the reader is referred to the web version of this article.

Please cite this article in press as: Singh, P., Shree, R. A new homomorphic and method noise thresholding based despeckling of SAR image using anisotropic diffusion. Journal of King Saud University – Computer and Information Sciences (2017), http://dx.doi.org/10.1016/j.jksuci.2017.06.006

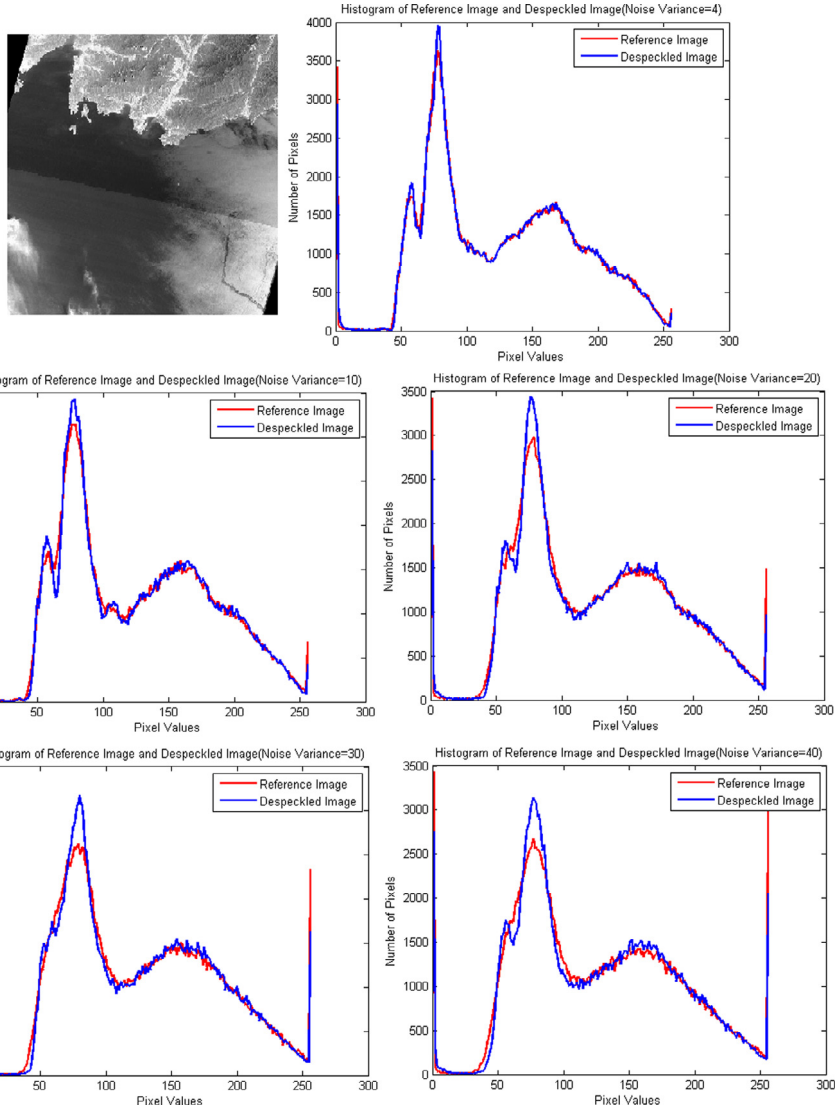

Fig. 14. Histogram of reference image and despeckled image at different noise variance level on SAR2 image using proposed method, in each plot reference image is plotted in red and despeckled image is plotted in blue. For interpretation of the references to colour in this figure legend, the reader is referred to the web version of this article.

5. Conclusion

In this article, a new homomorphic scheme is developed to despeckle the SAR images using anisotropic diffusion. The unfiltered part of the despeckled image is restored using the concept of method noise thresholding. The performance of the proposed method is evaluated by analysing the defined parameters of visual appearance and with different metrics such as PSNR, SSIM, UIQI and RMSE. The performance and computational time of the proposed method is compared with some standard filters and methods using confusion matrix. The proposed method is applied and tested on correlated speckle noise as well as uncorrelated speckle noise on the real dataset of SAR images. From the critical comparative analysis, it can be said that proposed method recovers the speckled image edges and structures of the SAR image. No visual artifacts are generated during the process. The proposed method has the potential ability to be used in various practical applications of SAR images.

References

Acharya, Tinku, Ray, Ajoy K., 2005. Image Processing Principles and Applications. John Wiley & Sons, Mc., Publication.

Alparone, L., Baronti, S., Carl, R., 1995. Two-dimensional rank conditioned median filter. IEEE Trans. Circuits Syst. II 42 (2), 130132.

Alparone, L., Baronti, S., Carl, R., Puglisi, C., 1996. An adaptive order-statistics filter for SAR images. Int. J. Remote Sens. 17 (7), 13571365.

Argenti, F., Alparone, L., 2002. Speckle removal from SAR images in the undecimated wavelet domain. IEEE Trans. Geosci. Remote Sensing 40 (11), 23632374.

Argenti, Fabrizio, Bianchi, Tiziano, Lapini, Alessandro, Alparone, Luciano, 2012. Fast MAP despeckling based on laplacian gaussian modeling of wavelet coefficients. IEEE Geosci. Remote Sens. Lett. 9 (1).

Argenti, Fabrizio, Lapini, Alessandro, Alparone, Luciano, 2013. A tutorial on speckle reduction in synthetic aperture radar images. IEEE Geosci. Remote Sens. Mag.

Arias-Castro, E., Donoho, D.L., 2009. Does median filtering truly preserve edges better than linear filtering? Ann. Stat. 37 (3), 1172.

Brown, Robert, Grover, Hwang, Patrick, Y.C., 1996. . Introduction to Random Signals and Applied Kalman Filtering, third ed. John Wiley & Sons, New York, ISBN 0-471-12839-2.

Crimmins, T.R., 1985. Geometric filter for speckle reduction. Appl. Opt. 24 (10), 14381443.

Dai, M., Peng, C., Chan, A.K., Loguinov, D., 2004. Bayesian wavelet shrinkage with edge detection for SAR image despeckling. IEEE Trans. Geosci. Remote Sensing 42 (8), 16421648.

Deledalle, C.-A., Denis, L., Tupin, F., 2009. Iterative weighted maximum likelihood denoising with probabilistic patch based weights. IEEE Trans. Image Process. 18 (12), 26612672.

Dixit, Arun, Sharma, Poonam, 2014. A Comparative Study of Wavelet Thresholding for Image Denoising, I.J. Image, Graphics and Signal Processing, 12, pp. 39–46.

Donoho, D.L., 1995. Denoising by soft-thresholding. IEEE Trans. Inform. Theory 41 (3), 613627.

Please cite this article in press as: Singh, P., Shree, R. A new homomorphic and method noise thresholding based despeckling of SAR image using anisotropic diffusion. Journal of King Saud University – Computer and Information Sciences (2017), http://dx.doi.org/10.1016/j.jksuci.2017.06.006

Foucher, S., 2008. SAR image filtering via learned dictionaries and sparse representations. In Proc. IEEE Int. Geoscience and Remote Sensing Symp. (IGARSS), vol. I, p. 229232.

Foucher, S., Bni, G.B., Boucher, J.-M., 2001. Multiscale MAP filtering of SAR images. IEEE Trans. Image Process. 10 (1), 4960.

Frost, V.S. et al., 1982. A model for radar images and its application to adaptive digital filtering of multiplicative noise. IEEE Trans. Pattern Anal. Machine Intell. PAMI-4, 157–166.

Gagnon, L., Jouan, A., 1997. Speckle filtering of SAR images: A comparative study between complex-wavelet-based and standard filters. In: Proc. SPIE, Wavelet Applications in Signal and Image processing V, vol. 3169, p. 8091.

Guo, H., Odegard, J.E., Lang, M., Gopinath, R.A., Selesnick, I.W., Burrus, C.S., 1994. Wavelet based speckle reduction with application to SAR based ATD/R. In: Proc. IEEE Int. Conf. Image Processing (ICIP), vol. 1, p. 7579.

Hao, Y., Feng, X., Xu, J., 2012. Multiplicative noise removal via sparse and redundant representations over learned dictionaries and total variation. Signal Process. 92 (6), 15361549.

Hervet, E., Fjrtoft, R., Marthon, P., Lops, A., 1998. Comparison of wavelet-based and statistical speckle filters. In: Proc. SPIE SAR Image Analysis, Modelling, and Techniques III, F. Posa, Ed., vol. 3497, p. 4354.

Huang, T., Yang, G., Tang, G., 1979. A fast two-dimensional median filtering algorithm. IEEE Trans. Acoust., Speech Signal Process. 27 (1), 1318.

Image Despeckle Filtering Toolbox, 2004. Mathworks website, Available: https://in.mathworks.com/matlabcentral/fileexchange/54044-image-despeckle-filtering-toolbox.

Jacobs, David, 2005. Introduction to Image Gradients, Class Notes for CMSC 426, Fall.

Jain, Anil K., 1989. Fundamentals of Digital Image Processing first edition. Prentice Hall Inc..

Kuan, D.T. et al., 1987. Adaptive restoration of images with speckle. IEEE Trans. Acc. Speech Signal Proc. 35 (3), 373–383.

Kumar, M., Diwakar, M., 2016a. CT image denoising using locally adaptive shrinkage rule in tetrolet domain. J. King Saud Univ. Comput. Inf. Sci. http://dx.doi.org/10.1016/j.jksuci.2016.03.003.

Kumar, Manoj, Diwakar, Manoj, 2016b. A new locally adaptive patch variation based CT image denoising. Int. J. Image Graphics Signal Process (IJIGSP) 8 (1), 43–50. http://dx.doi.org/10.5815/ijigsp.2016.01.05.

Kumar, M., Diwakar, M., 2017. A new exponentially directional weighted function based CT image denoising using total variation. J. King Saud Univ. Comput. Inf. Sci. http://dx.doi.org/10.1016/j.jksuci.2016.12.002.

Kuwahara, M., Hachimura, K., Eiho, S., Kinoshita, M., 1976. Processing of RI-angiocardiographic images. In: Preston, K., Jr., Onoe, M. (Eds.), Digital Processing of Biomedical Images. Plenum, New York, p. 187202.

Kyprianidis, J.E., Kang, H., Dllner, J., 2009. Image and video abstraction by anisotropic kuwahara filtering. Comput. Graphics Forum 28, 19551963.

Lee, J.S., 1980. Digital image enhancement and noise filtering by use of local statistics. In: IEEE Trans Pattern Anal. Matching Intell. PAMI-2, 165–168.

Lee, J.-S., 1981. Refined filtering of image noise using local statistics. Comput. Graph. Image Process. 15 (2), 380389.

Lee, J.-S., 1983. Digital image smoothing and the sigma filter. Comput. Vis. Graph. Image Process. 24 (2), 255269.

Li, G.-T., Wang, C.-L., Huang, P.-P., Yu, W.-D., 2013. SAR image despeckling using a space-domain filter with alterable window. IEEE Geosci. Remote Sensing Lett. 10 (2), 263267.

Loizou, Christos P., Theofanous, Charoula, Pantziaris, Marios, Kasparis, Takis, 2014. Despeckle filtering software toolbox for ultrasound imaging of the common carotid artery. Comput. Methods Programs Biomed. 114, 109124.

McConnell, I., Oliver, C., 1994. Comparison of annealing and iterated filters for speckle reduction in SAR. Proc. SPIE Microwave Sensing and Synthetic Aperture Radar 74 2958, 7485.

Parrilli, S., Poderico, M., Angelino, C.V., Verdoliva, L., 2012. A nonlocal SAR image denoising algorithm based on LLMMSE wavelet shrinkage. IEEE Trans. Geosci. Remote Sensing 50 (2), 606616.

Perona, P., Malik, J., 1990. Scale space and edge detection using anisotropic diffusion. IEEE Trans. Image Process. 12 (8), 629639.

Semwal, Vijay Bhaskar et al., 2016. An optimized feature selection technique based on incremental feature analysis for bio-metric gait data classification. Multimedia Tools Appl., 1–19

Semwal, Vijay Bhaskar, Raj, Manish, Nandi, Gora Chand, 2015. Biometric gait identification based on a multilayer perceptron. Rob. Auton. Syst. 65, 65–75.

Semwal, Vijay Bhaskar, Mondal, Kaushik, Nandi, G.C., 2015. Robust and accurate feature selection for humanoid push recovery and classification: deep learning approach. Neural Comput. Appl., 1–10

Singh, Prabhishek, Shree, Raj, 2016. Statistical modelling of log transformed speckled image. Int. J. Comput. Sci. Inf. Secur. 14 (8), 426–431.

Singh, Prabhishek, Shree, Raj, 2016. Analysis and effects of speckle noise in SAR images. IEEE International Conference on Advances in Computing, Communication, & Automation (ICACCA).

Singh, Prabhishek, Shree, Raj, 2017. A new computationally improved homomorphic despeckling technique of SAR images. Int. J. Adv. Res. Comput. Sci. 8 (3).

Singh, Umesh Kumar, Joshi, Chanchala, Gaud, Neha, 2016. Measurement of security dangers in university network. Measurement 155 (1).

Tomasiand, C., Manduchi, R., 1998. Bilateral filtering for gray and color images. In: Proc. 6th Int. Conf. Computer Vision (ICCV), p. 839846.

Walker, James S., 2008. A Primer on Wavelets and Their Scientific Applications, Second Edition (Studies in Advanced Mathematics) [English], Chapman And Hall, Crc. Ch 2: Daubechies, Book (Online Source) Available: https://www.scribd.com/document/255294926/28851-a-Primer-on-Wavelets-and-Their-Scientific-Applications.

Wiener, Norbert, 1949. Extrapolation, Interpolation, and Smoothing of Stationary Time Series. Wiley, New York, ISBN 0-262-73005-7.

Yangand, M., Zhang, G., 2012. SAR image despeckling using overcomplete dictionary. Electron. Lett. 48 (10), 596597.

Yuand, Y., Acton, S.T., 2002. Speckle reducing anisotropic diffusion. IEEE Trans. Image Process. 11 (11), 12601270.

Yuand, Y., Acton, S.T., 2004. Automated delineation of coastline from polarimetric SAR imagery. Int. J. Remote Sens. 25 (17), 34233438.

Zhang, W.G., Zhang, Q., Yang, C.S., 2011. Improved bilateral filtering for SAR image despeckling. Electron. Lett. 47 (4), 286288.

Please cite this article in press as: Singh, P., Shree, R. A new homomorphic and method noise thresholding based despeckling of SAR image using anisotropic diffusion. Journal of King Saud University – Computer and Information Sciences (2017), http://dx.doi.org/10.1016/j.jksuci.2017.06.006

Appendix-E

PAPER-2

Authors: Prabhishek Singh, Raj Shree, Manoj Diwakar

Title: A new SAR image despeckling using correlation based fusion and method noise thresholding

Journal: Journal of King Saud University – Computer and Information Sciences

Year of Publication: 2018

Publisher: Elsevier

DOI: https://doi.org/10.1016/j.jksuci.2018.03.009

Indexing: Scopus, ESCI and UGC Indexed

Journal of King Saud University – Computer and Information Sciences xxx (2018) xxx–xxx

Contents lists available at ScienceDirect

Journal of King Saud University – Computer and Information Sciences

journal homepage: www.sciencedirect.com

A new SAR image despeckling using correlation based fusion and method noise thresholding

Prabhishek Singh [a,*], Raj Shree [a], Manoj Diwakar [b]

[a] Department of Information Technology, Babasaheb Bhimrao Ambedkar University (A Central University), Vidya Vihar, Raebareli Road, Lucknow 226025, India
[b] Department of Computer Science and Engineering, Uttaranchal University, Arcadia Grant, P.O. Chandanwari, Premnagar, Dehradun, Uttarakhand 248007, India

ARTICLE INFO

Article history:
Received 1 November 2017
Revised 7 March 2018
Accepted 9 March 2018
Available online xxxx

Keywords:
DWT
Entropy
Bayesian shrinkage
Bivariate shrinkage
Correlation coefficient
Image fusion

ABSTRACT

This paper presents a new technique for despeckling of Synthetic Aperture Radar (SAR) images using a local correlation based fusion of high-frequency coefficients in Discrete Wavelet Transform (DWT) with method noise thresholding. The decomposition level is decided by analyzing the texture of the input image at each level by calculating entropy. The core idea of the proposed technique lies in the selection of decomposition level in 2D-DWT based on entropy parameter and on the fusion of high-frequency coefficients. On decomposition, the low-frequency coefficients remain untouched and the high-frequency coefficients are thresholded using two different shrinkage rules. Therefore the Bayesian and Bivariate shrinkage methods are applied to the high-frequency coefficients. After performing two different thresholding methods, the improved high-frequency coefficients are fused using local correlation based strategy. The threshold value is calculated by correlation strategy. Later the correlation coefficient (CC) is evaluated between the two improved high-frequency coefficients. The CC is now compared with the threshold value for the fusion purpose. On the basis of defined fusion strategy, the average and maximum operation are applied to perform the fusion of high-frequency coefficients. The despeckling scheme is followed by method noise thresholding in order to preserve the fine details of the image. The performance of the proposed method is assessed using metrics such as Signal-to-Noise Ratio (SNR), Peak-Signal-to-Noise Ratio (PSNR), Structural Similarity Index Metric (SSIM) and visual appearance of the despeckled image. The experimental results demonstrate the effectiveness of proposed work over prior works on SAR image despeckling.

1. Introduction

Image restoration is one of the most investigated fields of image processing where the original image is recovered from the noisy image. In this research work, image restoration is done on SAR images. SAR is one form of radar that is fixed on the satellites and aircrafts that captures the high-resolution images of large area of the earth surface from different view angles. SAR images are formed by the consistent interaction of the emitted microwave radiation with target areas. This consistent interaction originates arbitrary constructive and destructive noisiness that results into granular pattern on captured SAR image. This granular pattern of noise is known as speckle noise. This noise is multiplicative in nature. A granular pattern of speckle noise in the SAR image corresponds to the "salt-and-pepper" kind of noisy effect (Bhattacharya; Guozhong and Xingzhao, 2005). The granular pattern of speckle noise is the interference or fading pattern. The intensity distribution is called the speckle pattern. Speckle is the scattering phenomenon but not the noise (López-Martínez, 2013). The consistent interaction of high-frequency radar waves with a complex set of scatterers are possibly the restrictive aspect of SAR processing system design and application. Fig. 1(b) shows the classical speckle pattern (Singh and Shree, 2017a). In the SAR image processing, the multiplicative nature of speckle noise is modeled in Eq. (1) (Saevarsson et al., 2004). Let $I_L(i,j)$ is the degraded pixel of an observed SAR image with the pixel coordinate (i,j), where the SAR image is assumed as average of L looks and $S(i,j)$ be the speckle-free SAR image that is to be recovered.

* Corresponding author.
E-mail address: prabhisheksingh88@gmail.com (P. Singh).

Peer review under responsibility of King Saud University.

Production and hosting by Elsevier

https://doi.org/10.1016/j.jksuci.2018.03.009
1319-1578/

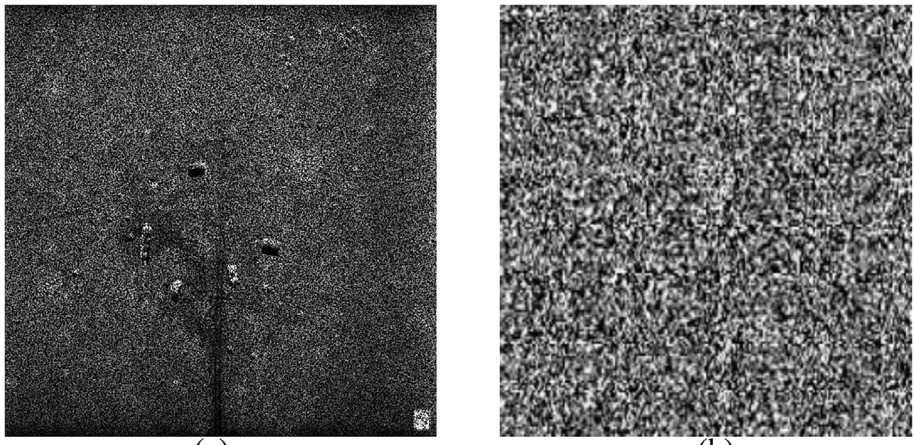

Fig. 1. (a) Real speckled SAR image (b) Classical speckle pattern.

$$I_L(i,j) = S(i,j) * N_L(i,j) \quad (1)$$

In Eq. (1), $N_L(i,j)$ depicts the uncorrelated multiplicative speckle component with unit mean and variance v and L looks (Gao, 2010). An inherent characteristic of SAR images is the presence of speckle noise. Speckle noise is random and deterministic in an image. Speckle has a negative impact on SAR images. Fig. 1(a) depicts the real SAR image.

The sample mean and variance of a single pixel are equal to the mean and variance of the local area (Garg and Kumar, 2012). The points where the interference is constructive are the bright points and the points where the interference is destructive are dark points (López-Martínez, 2013). The statistical properties of a speckle pattern depend on two factors: first on the coherence of the incident light and secondly on the statistics of the scattering surface (Dainty, 1976). It is recognized (Ulaby et al., 1986; Oliver and Quegan, 1998; Walessa and Datcu, 2000) that the perceived intensity of an L-look SAR image conditioned on the underlying reflectivity is gamma distributed (Escamilla and Méndez, 1991; Intajag and Chitwong, 2006). The speckle noise follows gamma distribution (Gao, 2010) which is shown below:

$$P(I|S) = \left(\frac{L}{S}\right)^{L} \frac{I^{L-S}}{\Gamma(\mathrm{L})} e^{-\frac{LI}{S}} \quad (2)$$

Under this model, the multiplicative noise is also gamma distributed (Intajag and Chitwong, 2006; Oliver and Quegan, 1998) . Here, the speckle is treated in a single image as a multiplicative procedure, and the speckle noise probability density function (PDF), N_L, from Eq. (1) is added with gamma distribution Eq. (2). The expected value (E) and variance (V) of N_L are conveyed by moment technique i.e. $E(N_{L)} = 1$ and $E(N_{L)} = 1 + 1/L$, respectively. The single-look amplitude has a Rayleigh (Oliver and Quegan, 1998) distribution; the single-look intensity has a negative exponential distribution (Oliver and Quegan, 1998) with unit mean; the multi-look amplitude has a square root Gamma distribution; the multi-look intensity has a Gamma (or Nakagami-Gamma) (Oliver and Quegan, 1998; Moser et al., 2006a,b; Goodman, 1975) distribution with unit mean (Gao, 2010).

The SAR image despeckling methods come under three categories: Bayesian methods in the spatial domain, Bayesian methods in the transform domain and non-Bayesian approaches. The standard and traditional filters for despeckling in the ground of SAR imagery lies under the category of Bayesian methods in the spatial domain. Some of the effective standard works are Frost filter (Frost et al., 1982), Kuan filter (Kuan et al., 1987); Kuwahara filter (Kuwahara et al., 1976; Kyprianidis et al., 2009) , Lee filter (Lee, 1980, 1981), Mean filter (Acharya et al., 2005) and Median filter (Jain, 1989). These works were obtained by making suppositions on the statistical characteristics of reflectivity and speckle, e.g., pdf and autocorrelation function (Argenti et al., 2013).

In recent times, the theory of least square fidelity minimization (Yan and Lu, 2011a,b, 2012, 2015) is also prevalent to eliminate the noise from images. In order to reduce the least square fidelity term, many regularization functions were examined such as anisotropic diffusion and total variation (TV) approaches. The anisotropic diffusion based methods were projected to improve the fine details of the images by preventing the diffusion at the edges, but it blurred the speckled edges (Catté et al., 1992; Esedoglu and Osher, 2004). In parallel with anisotropic diffusion (Yu and Acton, 2004; Perona and Malik, 1990; Weickert, 1998); TV-based regularization was projected to overcome the smoothness in denoised images (Diwakar and Kumar, 2018). From the past literature, it is observed that TV-based approaches achieve better results in terms of noise reduction, but it had a difficulty of undesirable stair-artifacts (Chambolle and Pock, 2011; Rudin and Osher, 1994; Vogel, 1995; Vogel and Oman, 1996). The benefits of TV and anisotropic diffusion were united to recover the disadvantages of TV method and this grouping is called as anisotropic total variation method (Cai et al., 2009a; Diwakar and Kumar, 2018). Speckle Reduction using Anisotropic Diffusion (McConnell and Oliver, 1994) exploits sudden occurring coefficient of variation. It shows improved outcomes than conventional approaches in the terms of variance minimization, mean preservation and edge localization. The Speckle Reducing Anisotropic Diffusion (SRAD) (Yu and Acton, 2002) established the landmark method of despeckling using anisotropic diffusion by authenticating the new algorithm using both synthetic and real linear scan ultrasonic imagery of the carotid artery enhancing the detailed information of the image, mainly edges. The work presented in (McConnell and Oliver, 1994) and (Yu and Acton, 2002) shows better results in the terms edge and texture preservation and also in visual quality appearance but the speckle reduction in the homogeneous regions is not satisfactory which causes non-uniformity in that area. Lei Zhu (Zhu et al., 2014) introduced a recognized detail-preserving anisotropic diffusion (IDPAD) for despeckling speckled SAR image that undergoes from reduced despeckling presentation mainly at the edges and serious blocking artifacts in uniform areas.

Yao Zhao (Zhao et al., 2015) proposed a dual-formulation-based Adaptive TV regularization scheme which is implemented to explain the TV Regularization. The parameter adaptation of the

Please cite this article in press as: Singh, P., et al. A new SAR image despeckling using correlation based fusion and method noise thresholding. Journal of King Saud University – Computer and Information Sciences (2018), https://doi.org/10.1016/j.jksuci.2018.03.009

TV regularization is grounded on the noise level assessed via wavelets. The work presented shows a great advancement than the previous standard total variation method in terms of speckle reduction in the homogeneous areas and detail preservation in the heterogeneous areas, but still generation of blocky artifacts is observed. Rudin-Osher-Fatemi (R.O.F.) model (Rudin et al., 1992) was suggested to offer the smooth and denoised images using TV approach by L2 norm fidelity optimization. Rudin (Rudin et al., 1992) also argued on the problems like non-linearity and non-differentiability which causes a computational error. Later, R.O.F. model was improved to avoid problems like non-linearity and non-differentiability and enhanced the performance of image denoising (Chambolle, 2004). A non-differential TV method was familiarized using Bregman iteration and it achieves its goal by reducing the problems like non-linearity and non-differentiability. Later, the Bregman iteration was enhanced by applying linearization function (Goldstein and Osher, 2009). Later the work (Goldstein and Osher, 2009) was again stretched to diminish the L1 regularization by familiarizing Split Bregman technique (Deng et al., 2011; Li et al., 2012; Osher et al., 2005; Wotao et al., 2008). Lately, many approaches (Cai et al., 2009a,b,c; Candes et al., 2008; Chen et al., 2015) have been projected via Split Bregman technique by changing norms as well as regularization terms. A number of authors also suggested the mixed models such as L2-L1 (Lou et al., 2015; Zibulevsky and Elad, 2010). These mixed models are focused on higher degree based image denoising (Hu and Jacob, 2012) and gradient-based algorithms for constrained total variation (Beck and Teboulle, 2009). These mixed models show better results than the classical TV method and some of the standard methods, but still, self-generated artifacts can be seen near the noisy edges. To solve this problem, a technique (Sun et al., 2015) was projected grounded on exponentially TV method. Further, image denoising was performed by Split Bregman using exponential TV function. This technique offers improved noise decrease. In recent times, the TV techniques were enhanced such as coefficients driven based TV (Guozhong and Xingzhao, 2005), non-negativity constrained based TV (Osher et al., 2005), to reduce the noise from the noisy images.

The Nonlocal means filters (NLM) filter keeps updating the pixel by a weighted average of the pixels judged to be most similar where neighborhood comparisons are done within a specified search window (Diwakar and Kumar, 2018). The NLM filter delivers a decent outcome in terms of speckle reduction and preserving fine details of the image (Diwakar and Kumar, 2018). In recent years, The NLM (Buades et al., 2005) filter is very prevalent in the field of image denoising. Sara Parrilli (Parrilli et al., 2012) presented a despeckling scheme based on non-local filtering and wavelet shrinkage using probabilistic similarity measure. The results are with consistent PSNR values that show better texture preservation and speckle reduction. Also, the technique has the capacity of better smoothing in the homogeneous areas. The other effective non-local filtering based Bayesian framework is presented in the (Kervrann et al., 2007) which is tested on both the ultrasound (Coupe et al., 2008) as well as SAR images (Zhong et al., 2011). These works present the effectiveness of non-local mean filtering in the domain of despeckling in terms of speckle reduction and maintaining the smoothness in the uniform areas.

The despeckling techniques under homomorphic filtering are effective and highly adaptive. They are easy to understand and implement due to the application of a log and exponential operations. It simplifies the despeckling approach by allowing the use of any additive restoration models in the SAR image despeckling. This is the main reason of high popularity of homomorphic filtering in SAR image despeckling field. The non-homomorphic despeckling methods are also effective and adaptive but still less in use due to its high complexity in understanding and implementation; hence the literature available of non-homomorphic despeckling methods is less in comparison to the homomorphic despeckling methods (Argenti et al., 2013). The available literature shows the Bayesian methods in transform domain demonstrates improved outcomes than Bayesian methods in the spatial domain (Argenti et al., 2013). There are some non-Bayesian methods that also show better results similar to Bayesian methods in the transform domain (Argenti et al., 2013). The homomorphic filtering (Gagnon and Jouan, 1997; Hervet, 1998) is used to convert the multiplicative nature of speckle noise into additive nature using log operations. This simplifies the despeckling procedure and also opens the area of research in various dimensions.

In (Singh and Shree, 2017), a homomorphic method is proposed using method noise thresholding where anisotropic diffusion is applied as a pre-processing step using db2 based 2D-DWT. Median and Wiener filters are used on the approximate part of the image to remove blurring. Method noise thresholding is applied as the post-processing step in the despeckling process that processes the unfiltered part of the despeckled image. This work shows best results in terms of speckle reduction, edge preservation and removing the blurry areas but still there is a scope of improvement by the intelligent use of method noise. Manoj Diwakar (Diwakar and Kumar, 2014) proposed a noise reduction method to enhance the image quality using adaptive Wiener filtering and Wavelet Packet Threshold algorithm. The work is effective to remove the blurring but still, some high contrast and high textured areas are unprocessed. Sonam and Manoj Kumar (2017) proposed a local correlation and directive contrast-based image fusion technique using Discrete Wavelet Packet Transform where low-frequency coefficients are fused using local correlation. The work shows the effective method of fusing the low and high-frequency coefficients. Manoj Diwakar (Kumar and Diwakar, 2016) proposed a two-phase denoising scheme, firstly denoising using wavelet thresholding followed by its method noise thresholding and second phase consists of aggregation in the wavelet domain, the presented work is highly efficient in detail preservation but the two-stage process makes it computationally costly. Here author proposed an effective application of method noise. Heng-Chao Li (Li et al., 2013) proposed a new Bayesian multiscale technique for speckle reduction of SAR images in the non-homomorphic agenda. In order to handle multiplicative speckle noise, linear decomposition is used for speckle contribution. Later in SWT, a two-sided general Gamma distribution is familiarized as an earlier phase to handle the heavy-tailed nature of wavelet coefficients of the speckle-free reflectivity. The used shrinkage rule performs thresholding on the diagonal component of the image which causes the horizontal and vertical component to be unfiltered so there is a high scope for improvement in the denoising process. R. Sethunadh and T. Thomas (2014) presented a new adaptive SAR image despeckling procedure in the spatial domain by using statistical interscale dependency of the directionlet transform coefficients; the work is highly efficient in preserving the high textured region. J. Jennifer Ranjani and S. J. Thiruvengadam (2010) presented a dual-tree complex wavelet transform based SAR image despeckling using interscale dependence. This technique employs maximum a posteriori estimator in the framework. This work is better in suppressing the speckle noise in the uniform areas and has better edge preservation capabilities. Bin Xu (Xu et al., 2015) proposed despeckling method grounded on patch ordering and transform-domain filtering. Log transform with bias correction is implemented on SAR image to transform the nature of speckle from multiplicative to the additive. The proposed technique has very robust speckle reduction capability and execution time of the planned scheme is also suitable for applied applications of SAR image processing.

This article proposes a new method noise thresholding based SAR image despeckling technique based on dual wavelet shrinkage

Please cite this article in press as: Singh, P., et al. A new SAR image despeckling using correlation based fusion and method noise thresholding. Journal of King Saud University – Computer and Information Sciences (2018), https://doi.org/10.1016/j.jksuci.2018.03.009

rule using a local correlation based fusion of high-frequency coefficients. The dual thresholding is applied in parallel using Bayesian and Bivariate shrinkage rule on the detailed part of the speckled SAR image. The Bayesian method evaluates different threshold value for each decomposition level and therefore is subband dependent, while bivariate shrinkage rule uses the parent and child wavelet coefficient for evaluating the threshold value. The Bayesian approach works better at smoothing the flat regions while the bivariate approach is better at smoothing the edge part. The parallel filtered detailed part (by Bayesian and Bivariate shrinkage rule) of the SAR image are fused using local correlation strategy which is grounded on 'avg' and 'max' operations. The decomposition level is decided by the entropy metric depending on the texture of the SAR image. The proposed scheme is compared with some of the latest works of Bayesian (Li et al., 2013) and Bivariate (Sethunadh and Thomas, 2014) thresholding, anisotropic diffusion (Zhu et al., 2014) and total variation method (Zhao et al., 2015).

The article is organized into five sections. Section 2 briefly describes the homomorphic filtering with DWT, wavelet thresholding using Bayesian shrinkage and bivariate shrinkage rule, method noise thresholding and entropy based wavelet decomposition. Section 3 presents the proposed flowchart and step by step procedure of the proposed despeckling scheme. Section 4 shows the experimental results and statistical analysis of work and Section 5 concludes the article with a future scope.

2. Background

2.1. Homomorphic filtering and discrete wavelet transform

Speckle noise is multiplicative in nature. The homomorphic filtering is applied to convert the multiplicative nature of speckle noise into additive. It transforms it into additive noise. Most of the effective image restoration models available works on the additive noises. In order to use these additive restoration models, homomorphic filtering is applied. The log and exponential transform are the operations that are used for the purpose of multiplicative nature conversion. The log transform converts multiplicative speckle noise into additive noise and after the despeckling process, the exponential transform is applied to perform the reverse-log operation.

Wavelets are most commonly used the mathematical function in image denoising. DWT provides the transformation of the image from the spatial to the frequency domain (Singh and Shree, 2016a). 2D-DWT corresponds to multi-resolution approximation expressions. On applying DWT, it transforms the speckled image into four parts: appropriate part (LL) and detailed part (Vertical Noisy Coefficients (LH), Horizontal Noisy Coefficients (HL) and Diagonal Noisy Coefficients (HH)). The approximate component is the low-frequency coefficient while the detailed part is the high-frequency coefficient. The major image information is present in the detailed part as high-frequency corresponds to noise and also to edges. This settles in processing the heterogeneous areas of the image on priority for better detail preservation. Fig. 2 shows the DWT decomposition of the speckled SAR image up to level-2 (Singh and Shree, 2016b).

The LL component is used for further decomposition or other smoothing processing as it has important information of SAR images like the texture and it has less speckle distribution. The LH, HL and HH components have vertical, horizontal and diagonal statistics of an input SAR image (Singh and Shree, 2017a). The input SAR image can be remodeled by considering only LL band image and neglecting other unimportant information from other components.

The only drawback of 2D-DWT is that on applying DWT on the image, at every level it reduces the size of the image to half of the previous level as shown in Fig. 3. This causes loss of information. The article evaluates the loss of information during decompositions and decides the best decomposition level using entropy calculation at each band level using specified formula mentioned in the next sub-section (See Fig. 4).

In order to apply DWT in image denoising, there are certain parameters which need to fix. Firstly the wavelet family basis is desired to be preferred for every decomposition layer like db2, haar, sym etc. Secondly, appropriate n-level decomposition is required to be decided. According to the available literature, most of the time in image denoising, the image is decomposed up to a 3–5 level which is considered as the best decomposition but in reality, there is a loss of information at each decomposition (Singh and Shree, 2017b). This loss of information is needed to be evaluated which should be the considered as a decisive parameter for the exact decomposition level. The article has decided the entropy as a decisive parameter for setting up the decomposition level. Wavelet-based denoising is performed by following three steps:

Step 1: Perform DWT on input speckled SAR image to obtain approximate and detail parts.

Step 2: Perform the denoising using following steps:

i. Estimate noise variance.
ii. Calculate threshold.
iii. Apply thresholding on detail parts.

Step 3: Apply inverse DWT to obtain final despeckled SAR image.

2.2. Wavelet thresholding using Bayesian shrinkage rule

The threshold λ is evaluated using below equation,

$$\lambda = \left(\frac{\sigma_n^2}{\sigma_Y}\right) \tag{3}$$

The noise variance is estimated using robust median estimation method (Abramovich et al., 1998) as follows:

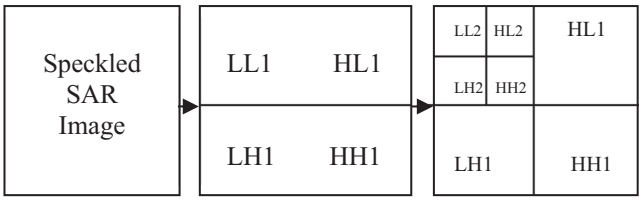

Fig. 2. 2D-DWT decomposition up to two level.

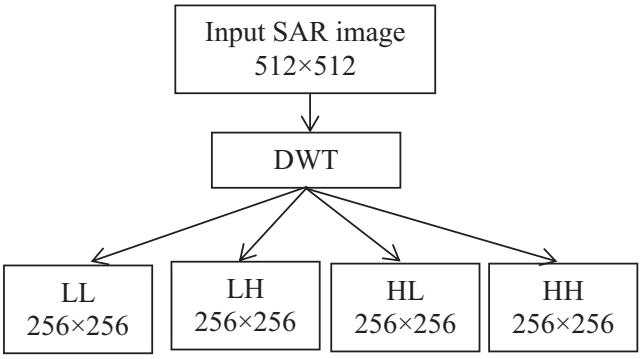

Fig. 3. Frequency band decomposition using DWT.

Please cite this article in press as: Singh, P., et al. A new SAR image despeckling using correlation based fusion and method noise thresholding. Journal of King Saud University – Computer and Information Sciences (2018), https://doi.org/10.1016/j.jksuci.2018.03.009

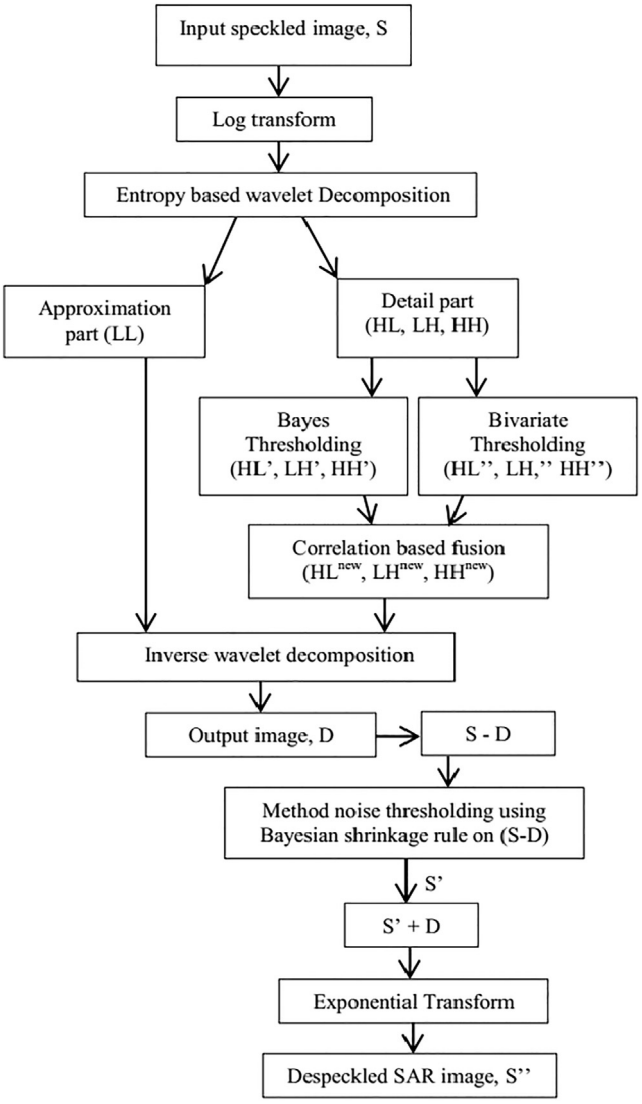

Fig. 4. Flowchart of proposed despeckling method.

$$\sigma_n^2 = \left[\frac{median(|X(x,y)|)}{0.6754}\right]^2 \tag{4}$$

where, $X(x,y)\epsilon LH_L$, $X(x,y)\epsilon HL_L$and $X(x,y)\epsilon HH_L$, and L is decomposition level. The standard method works only on the HH_L, but in the proposed work, it is applied to all the detail components (LH_L, HL_L, HH_L). The standard deviation of noise less image (σ_Y) is calculated using:

$$\sigma_Y^2 = max(\sigma_X^2 - \sigma_n^2, 0) \tag{5}$$

where, $\sigma_X^2 = \frac{1}{c}\sum_{i=1}^{c} X_i^2$, and c is the patch size of the input image.

Thresholding can be done either by hard and soft thresholding. The proposed method uses soft thresholding. It is equated as:

$$\hat{Y} := \begin{cases} 0 & if\ |X| \leqslant \lambda \\ sign(X)(|X| - \lambda) & if\ |X| > \lambda \end{cases} \tag{6}$$

2.3. Wavelet thresholding using Bivariate shrinkage rule

To despeckle the high frequency coefficients, a Bivariate shrinkage function is performed using adaptive thresholding. Suppose, b_{2p} signifies the parent of b_{1p} (b_{2p} is the wavelet coefficient at the identical location as the pth wavelet coefficient b_{1p}, but at the next coarser scale). Then

$$a_{1p} = b_{1p} + n_{1p}$$

$$a_{2p} = b_{2p} + n_{2p} \tag{7}$$

where, a_{1p} and a_{2p} are speckled wavelet coefficients, b_{1p} and b_{2p} are speckle less wavelet coefficients and n_{1p} and n_{2p} are additive noise coefficients. Eq. (7) can be re-written as:

$$a_p = b_p + n_p \tag{8}$$

where, $b_p = (b_{1p}, b_{2p})$, $a_p = (a_{1p}, a_{2p})$ and $n_p = (n_{1p}, n_{2p})$. To despeckle the high frequency coefficients, Bivariate shrinkage rule (Chang et al., 2000) can be conveyed as:

$$\hat{b}_{1p} = \frac{\left(\sqrt{a_{1p}^2 + a_{2p}^2} - \lambda_p\right)+}{\sqrt{a_{1p}^2 + a_{2p}^2}} . a_{1p} \tag{9}$$

The function $(z)_+$ is well-defined as:

$$(z)_+ \sim= \begin{cases} 0, & if\ z < 0 \\ z, & if\ z > 0 \end{cases} \tag{10}$$

The term λ_p in Eq. (9) is the threshold for the pth coefficient, calculated as:

$$\lambda_p = \frac{\sqrt{3}\sigma_n^2}{\sigma_p} \tag{11}$$

To calculate the noise variance σ_n^2 from the noisy wavelet coefficients, a robust median estimator is used from the finest scale wavelet coefficients (LH, HL and HH subbands) stated in the Eq. (4) and marginal variance of σ_p^2 for each wavelet coefficient can be estimated as:

$$\hat{\sigma}_p^2 = \left(\hat{\sigma}_{ap}^2 - \sigma_n^2\right)_+ \tag{12}$$

where, $\hat{\sigma}_{ap}^2$is the marginal variance for noisy coefficients of a_{1p} and a_{2p}. Since, a_{1p} and a_{2p} are modeled as zero mean, $\hat{\sigma}_{ap}^2$ can be estimated as:

$$\hat{\sigma}_{ap}^2 = \frac{1}{|S(p)|}\sum_{a_i \in S(p)} a_i^2 \tag{13}$$

where, $|S(p)|$ is the size of the neighborhood S(p).

2.4. Method noise thresholding

The difference between the noisy image and denoised image shows the noise removed by the algorithm, which is called as method noise (Kumar, 2013); (Shreyamsha Kumar, 2013) . Let say, S is the noisy image and after denoising it, we get D as the final denoised image. Now mathematically F is evaluated by $F = S - D$. Now F contains the noisy residual part which is unfiltered, so further, any denoising scheme can be applied to it like thresholding or filtering. After denoising F, let say S' is achieved. Then $S'' = S' + D$ is performed to get the final denoised image, S'' which contains the lowest noise (Kumar and Diwakar, 2016; Buades et al., 2004; Zhang, 2016). The proposed method implements the method noise thresholding as the post-processing step.

2.5. Entropy-based wavelet decomposition

The 2D-DWT is applied to the log-transformed speckled SAR image up to level n depending on the measurement of texture using entropy parameter for best results. The entropy (E') is used for deciding the decomposition level which is an arithmetical

Please cite this article in press as: Singh, P., et al. A new SAR image despeckling using correlation based fusion and method noise thresholding. Journal of King Saud University – Computer and Information Sciences (2018), https://doi.org/10.1016/j.jksuci.2018.03.009

parameter of measuring the uncertainty of pixel values that can be used to illustrate the texture of the input image (Diwakar and Kumar, 2014).

On the every next decomposition level (n), E' is evaluated for the parent and child node. The higher value of E' of parent node than the child node indicates the presence of information in the image which requires next decomposition for detail preservation. This process continues until the above condition fails. This process of setting the decomposition level gives the best outcome in terms of detail preservation. E' is formulated as,

$$E' = -\sum_i P_i Log_2 P_i \tag{14}$$

3. Proposed methodology

The despeckling technique is tested on the real speckled SAR images and simulated speckled classical images. The assessment of the image quality is performed by comparing the despeckled image with the reference image. The simulation is performed by adding the speckle noise in the classical image. The speckle distribution in the real SAR data is unknown but in simulated classical images, the speckle noise is uniformly distributed. A dual wavelet-based global thresholding rule is executed in parallel (Bayesian and Bivariate shrinkage rule) using local correlation based fusion strategy.

***Step 1*:** The speckled SAR image is multiplicative in nature. Natural log transform is applied to convert this multiplicative nature to the additive. Let the speckled SAR image is S.

***Step 2*:** Entropy-based Wavelet Decomposition to n-level

The entropy-based wavelet decomposition level is decided by following steps:

A: Firstly apply 2D-DWT on the image and set the maximum number of levels.

B: Perform decomposition into four components (LL, LH, HL, HH) for each level.

C: Compute the entropy of each component (LL, LH, HL, HH) for each layer using Eq. (14) and then calculate average entropy value (AEV) for each layer by,

$$AEV = \left(\frac{E'(LL) + E'(LH) + E'(HL) + E'(HH)}{4}\right) \tag{15}$$

D: In top-down approach manner, check the AEV,

i. if (AEV(parent node) > AEV(child node)), then go for next decomposition level.
ii. Otherwise, remove the remaining child nodes.

E: Finish the procedure, if there is no node to decompose.

***Step 3*:** The dual thresholding (Bayesian (**A.**) and Bivariate (**B.**) shrinkage) is applied in parallel on the detailed part. The improved detailed parts of both thresholding are later fused to get more enhanced results.

A. For each decomposition level, apply wavelet thresholding using Bayesian shrinkage rule on the detailed part (HL, LH, HH).
i. Noise variance estimation using Eq. (4).
ii. Threshold calculation using Eq. (3).
iii. Apply soft thresholding using Eqs. (5) and (6), resultant detailed parts are (HL', LH', HH').
B. For each decomposition level, apply wavelet thresholding using bivariate shrinkage rule on the detailed part (HL, LH, HH).
i. Calculate local noise variance σ_n^2 using Eq. (4).
ii. For each coefficient of each high pass subbands
a) Compute $\hat{\sigma}_{ap}^2$ using Eq. (13)
b) Compute $\hat{\sigma}_p^2$ using Eq. (12)
c) Compute the threshold λ_p using Eq. (11)
d) Estimate each coefficient using Eq. (9)
e) Restore the value in $a_{1p.}$ The resultant detailed parts are (HL", LH," HH").

Step 4: Locally correlation based fusion.

The obtained high-frequency coefficients (HL', LH', HH') and (HL", LH," HH") after two different parallel thresholding methods are fused using local correlation based approach. Firstly, the threshold value is calculated using this approach:

Non-overlapping block-wise correlation coefficients (CC) are calculated from these high-frequency coefficients (HL', LH', HH') and (HL", LH," HH") using 3×3 mask size. The average of all the CC is evaluated and is decided as the threshold value. In the proposed work, the evaluated threshold value is denoted as T. The CC (Shi, 2005) is evaluated using the below Eq. (16)

$$CC = \frac{\sum_m \sum_n (A_{mn} - \bar{A})(B_{mn} - \bar{B})}{\sqrt{\left(\sum_m \sum_n (A_{mn} - \bar{A})^2\right)\left(\left(\sum_m \sum_n (B_{mn} - \bar{B})^2\right)\right)}} \tag{16}$$

where, $\bar{A}$ = mean2(A), and $\bar{B}$ = mean2(B). The m and n represents the source images. mean2(A) = $A_l^X(i,j)$ and mean2(B) = $B_l^Y(i,j)$. $A_l^X(i,j)$ and $B_l^Y(i,j)$ are mean values of their respective high frequencies subbands. 2D-DWT is applied up to l-level of decomposition over the source images X and Y. (i,j) represents the pixel coordinates. The value of CC lies between [-1 to 1] range, where '1' specifies a strong positive relationship, '-1' specifies a strong negative relationship. A CC of '0' specifies no relationship at all.

In the local correlation based fusion strategy of obtained high-frequency coefficients (HL', LH', HH') and (HL", LH," HH"), a non-overlapping block-wise CC are calculated from these high frequencies using 5×5 mask size using Eq. (16). Here, the acquired CC is compared with the threshold value (T). If the CC value is less than or equal to the T, then the maximum operation is executed. In maximum operation, fusion is implemented by choosing the largest values from both of the transformed images. Or else, the average operation is applied, which calculates the average value using both of the transformed images to perform fusion. Local correlation-based fusion strategy is given as follows:

$$A_l^{new} = \begin{cases} \max(A_l^X, B_l^Y) & if (CC \leqslant T) \\ \text{avg}(A_l^X, B_l^Y) & otherwise \end{cases} \tag{17}$$

In the Eq (17), the operations "max" and "avg" stand for maximum and average values, respectively, and A_l^{new} for the fused coefficients (HL^{new}, LH^{new}, HH^{new}).

Theoretically, when $(CC \leqslant T)$, this means that the similarity rate between the detailed despeckled components is less, so "max" operation is used to take the best despeckled component between the two which helps to preserve the edges. When $(CC \leqslant T)$, this means the similarity rate between the detailed despeckled components is more and both the components are almost equivalent, so it is better to average them. On the experimental note, the detailed despeckled components are experimentally tested and fused using 'max', 'min' and 'avg' operations and on the basis of experimental evaluation, it is observed this formulation i.e. Eq. (17) gives the best result.

Step 5: Finally, apply inverse DWT to get out denoised SAR image using low-frequency coefficients (LL) and shrinkage and fused high-frequency coefficients (HL^{new}, LH^{new}, HH^{new}). This output denoised image is D.

Please cite this article in press as: Singh, P., et al. A new SAR image despeckling using correlation based fusion and method noise thresholding. Journal of King Saud University – Computer and Information Sciences (2018), https://doi.org/10.1016/j.jksuci.2018.03.009

Step 6: Apply method noise thresholding.

Perform (S - D) operation. Now apply 2D-DWT on (S - D) up to n-level of decomposition using step 2. The detailed part is filtered using Bayesian thresholding method. After performing this step, the output image S'. Now perform addition operation i.e. (S' + D). The final step is to perform an exponential operation on (S' + D). The output image is the despeckled SAR image, S''.

4. Experimental results and discussion

In this section, statistical and experimental results with respect to image quality performance measurements are shown on the real SAR data and simulated speckled classical images. It validates the practicality of the proposed method. The dataset of real SAR images for noise variance at $\sigma = 20$ is shown in Fig. 5. The experimentation is performed on real SAR dataset for various noise variance level i.e. [$\sigma = 5$; 10; 20; 30; 40]. The proposed method is also tested on simulated speckled classical images Figs. 11 and 12) and the results are presented in the Fig. 13. The experimental analysis is performed on the images of size 512×512 in order to authenticate the performance of the proposed scheme. The experimental analysis is performed on following system configuration: MATLAB version = 8.3, name = R2014a on Intel(R) Core(TM) i5-2410 M CPU @ 2.30 GHz, 4 GB RAM and 64-bit operating system. The system configuration is essential to note down for the evaluation of the computational time of the proposed algorithm. The proposed methodology is a multi-step procedure which contains various changeable parameters which are user sensitive. The experimental results are performed using db2 based 2D-DWT and the level of decomposition is set after calculating the entropy metric. The standard bivariate shrinkage rule and modified Bayesian shrinkage rule are applied using soft thresholding method on the detailed components separately. The [3×3] mask is used for calculating the threshold value. The [5×5] mask is used for performing the fusion based on local correlation strategy. The discussed modified Bayesian shrinkage rule is applied in the method noise thresholding section also. The remaining parameters remain the same.

For validating the proposed scheme, the experimental and statistical results are compared with the outcomes of some well-known techniques in the field of SAR images despeckling such as ATV (Zhao et al., 2015), BayesWS-HAW (Li et al., 2013), Bivariate thresholding (Sethunadh and Thomas, 2014) and IDPAD (Zhu et al., 2014). The result of the proposed algorithm on simulated classical images is shown in Fig. 13.

In this research work, results and discussion are presented on three different kind of SAR images. The real SAR data is taken from the open public database. SAR1 image shown in Fig. 5(a) is Ka-band image of a variety of military vehicles in the desert near Albuquerque, NM, taken from the Sandia National Laboratories, Airborne ISR, available at http://www.sandia.gov/RADAR/imagery/, SAR2 depicted in Fig. 5(b) is Space Radar Image of Kilauea, Hawaii - Interferometry 1, taken from the database of Jet propulsion laboratory, California Institute of Technology, available at: https://photojournal.jpl.nasa.gov/catalog/PIA01763 and the SAR3 image shown in Fig. 5(c) is the aerial photography of the cemetery of Cologne, Germany which is available at open public access database (DATASET OF STANDARD; Test Images).

4.1. Performance evaluation

PSNR is one of the most used performance evaluation metrics in denoising or despeckling used to describe the overall texture of the image. The high value of PSNR indicates better image quality. The unit of PSNR is dB. PSNR is computed by:

$$10\log_{10}\left(\frac{255 \times 255}{MSE}\right) \tag{18}$$

where,

$$MSE = \frac{1}{N}\sum_{j=0}^{N-1}(X - Y)^2 \tag{19}$$

SSIM is used to measure the similarity between the despeckled image and the reference image. It depends upon three parameters: luminance, contrast and structure. It is a perceptual metric that calculates the degradation in the image quality caused by data compression or data transmission losses. It is grounded on visible structures present in the image. It is an improved version of the UIQI. The overall index is a multiplicative combination of the luminance, contrast and structure. SSIM is computed by,

$$SSIM(x, y) = \frac{(2\mu_x\mu_y + C_1)(2\sigma_{xy} + C_2)}{(\mu_x^2 + \mu_y^2 + C_1)(\sigma_x^2 + \sigma_y^2 + C_2)} \tag{20}$$

According to the literature (Cho and Lee, 2016), the standard range of SSIM varies from −1 to 1.

SNR is frequently used performance metric in the field of denoising or despeckling. SNR is used to measure the sensitivity of the image. SNR is evaluated as the ratio of noise-free image variance to the MSE. The noise-free image variance is calculated from the difference of average signal and background values and the MSE is defined from the background region. It is expressed in dB. SNR is calculated by,

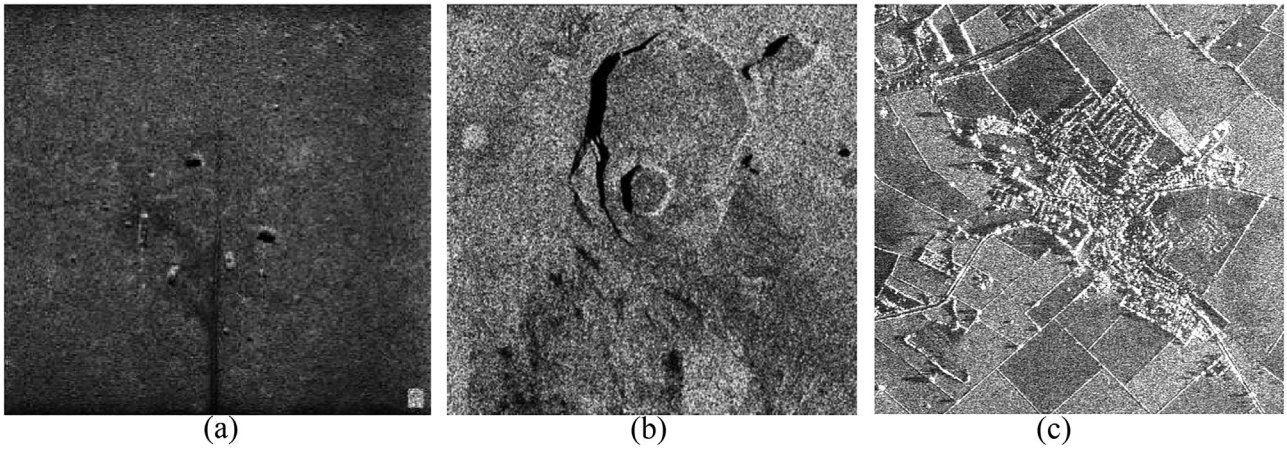

Fig. 5. Speckled SAR images.

Please cite this article in press as: Singh, P., et al. A new SAR image despeckling using correlation based fusion and method noise thresholding. Journal of King Saud University – Computer and Information Sciences (2018), https://doi.org/10.1016/j.jksuci.2018.03.009

$$SNR = 10\log_{10}\left[\frac{Var[f]}{MSE}\right] \quad (21)$$

where $Var[f]$ = noise-free image variance.

4.2. Analysis of Locally correlated detailed subbands

The resultant high-frequency subbands of Bayesian and Bivariate shrinkage methods are fused using local correlation based strategy. Table 1 shows the degree of similarity i.e. correlation between the despeckled detailed subbands of Bayesian and Bivariate shrinkage methods for various noise variance level i.e. (σ = 5, 10, 20, 30, 40).

Let, at σ = 20, the despeckled detailed subbands of Bayesian and Bivariate shrinkage rule are (HL', LH', HH') and (HL'', LH,'' HH'') respectively, the correlation coefficient (CC) is calculated using Eq. (16).

Table 1
Correlation values between detailed subbands at various noise levels.

Noise variance	LH subband	HL subband	HH subband
σ = 5	0.9527	0.9658	09,758
σ = 10	0.9159	0.9158	0.9258
σ = 20	0.8759	0.8598	0.8479
σ = 30	0.8143	0.8258	0.8157
σ = 40	0.7589	0.7656	0.7458

At σ = 20,

$$CC(LH', LH'') = 0.8759,$$

$$CC(HL', HL'') = 0.8598,$$

$$CC(HH', HH'') = 0.8479.$$

Similarly, the correlation of rest of the subbands is evaluated. This analysis determines the degree of similarity between these two subbands. Based on this correlation similarity factor, the local correlation based fusion strategy is designed that fuses the two enhanced high-frequency coefficients.

4.3. Experimental evaluation and comparison

The experimental results are shown in this section represented in the Figs. 6–10 for SAR image dataset and in Figs. 11–13 for classical image dataset. The reference SAR images are shown in Fig. 5. The Figs. 6–10 show the result of the despeckling methods i.e. ATV, BayesWS-HAW, Bivariate thresholding, IDPAD and proposed method. There are certain parameters for analyzing the despeckled SAR image quality on the basis of visual appearances such as (i) occurrence of the artifacts; (ii) edge preservation; (iii) visibility of low contrast objects and (iv) texture and structure preservation. Since there is not any

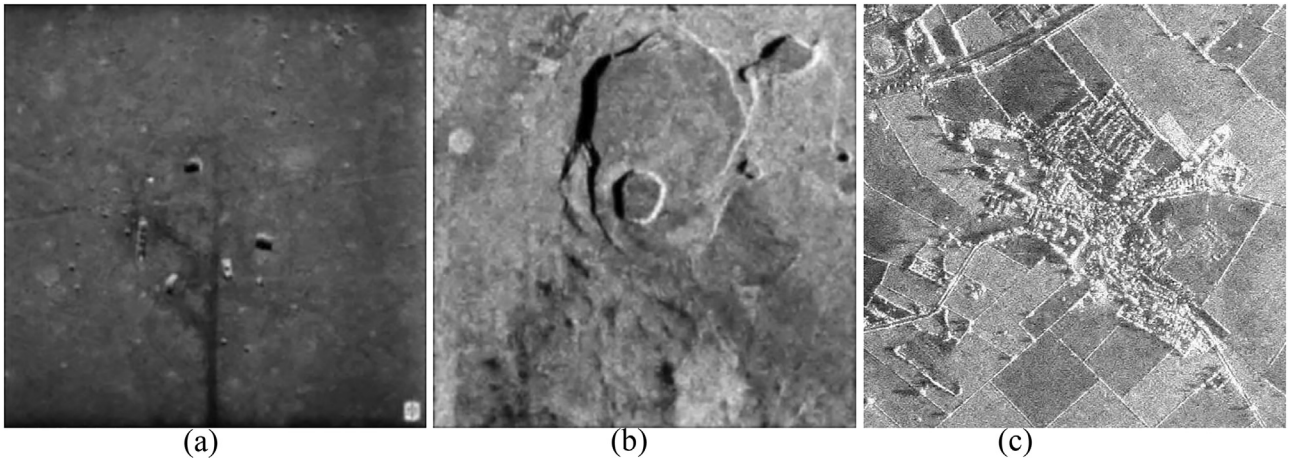

Fig. 6. Results of ATV.

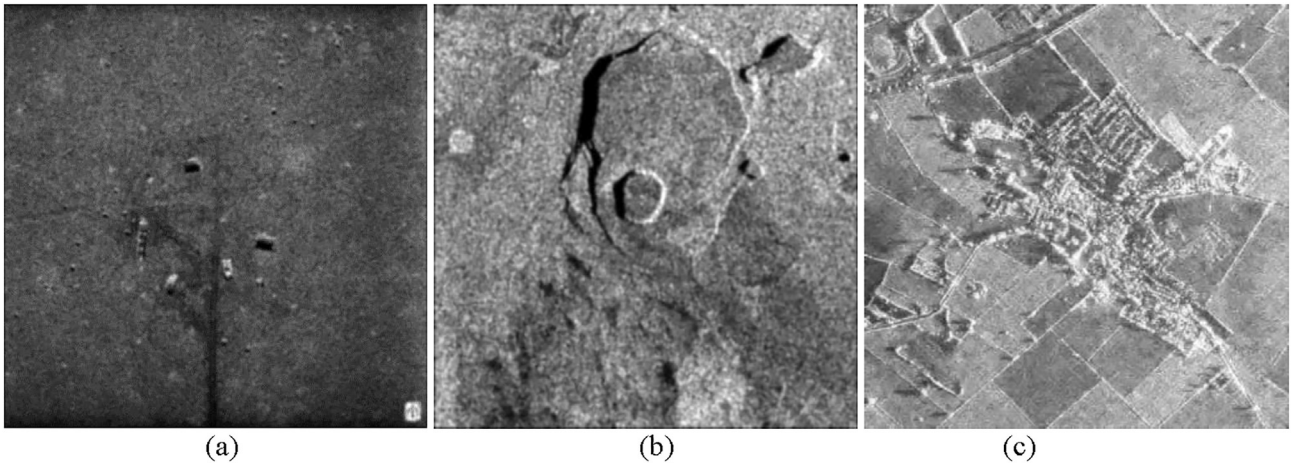

Fig. 7. Results of BayesWS-HAW.

Please cite this article in press as: Singh, P., et al. A new SAR image despeckling using correlation based fusion and method noise thresholding. Journal of King Saud University – Computer and Information Sciences (2018), https://doi.org/10.1016/j.jksuci.2018.03.009

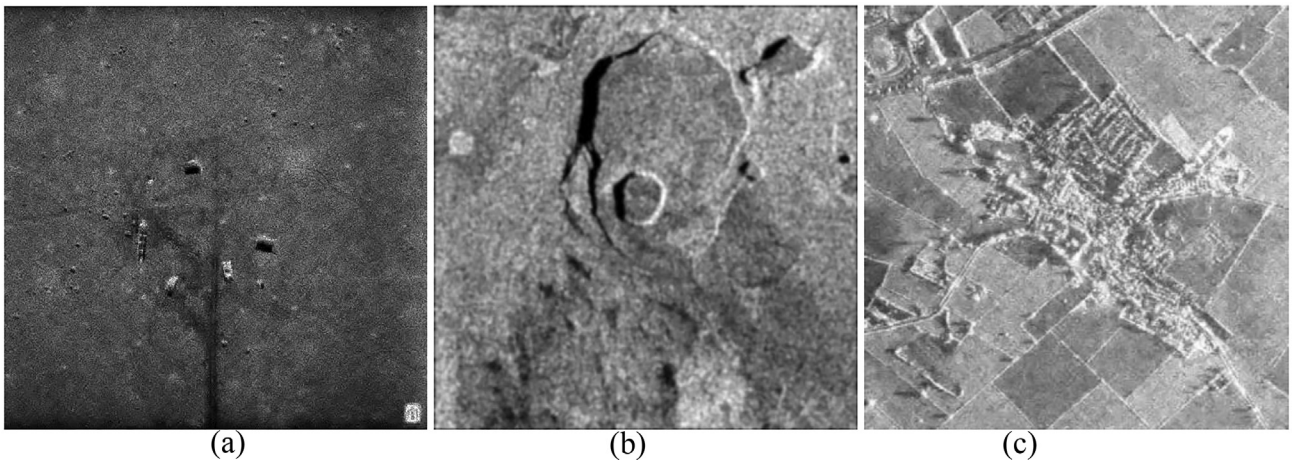

Fig. 8. Results of Bivariate thresholding.

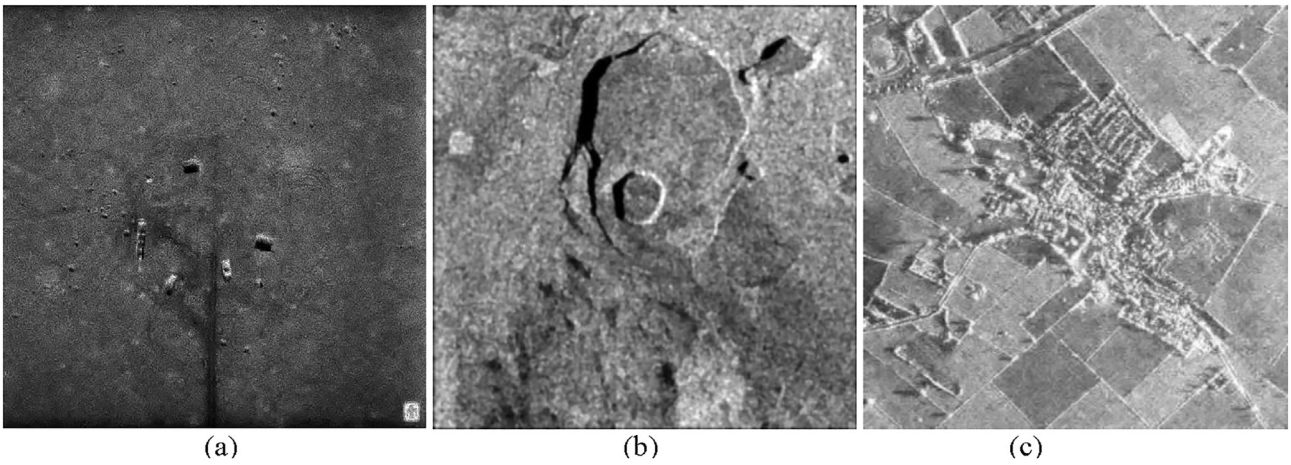

Fig. 9. Results of IDPAD.

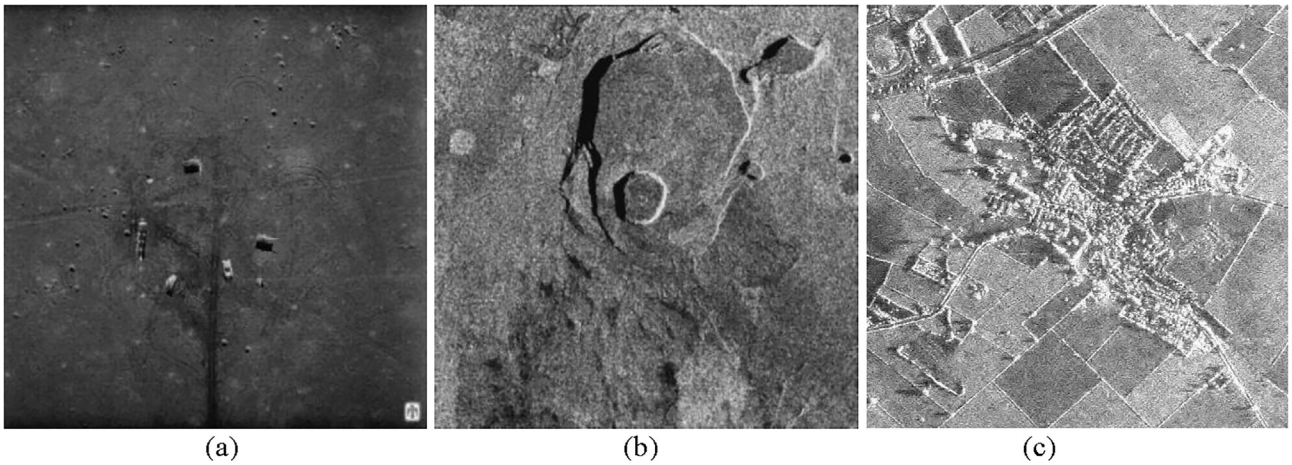

Fig. 10. Results of the proposed method.

scientific principle available to do so, therefore the analysis is done through a visual appearance on the basis of these above-discussed parameters. The level of decomposition in the proposed method is set on the basis of the entropy metric. The decomposition level is not fixed and it is different on different SAR images due to varying texture.

The Bivariate thresholding and IDPAD show decent despeckling results. The results of ATV method appear over smooth and minor details are lost. The results of Bayesian (BayesWS-HAW) also show some loss of information as output images appear quite blurred. The proposed method overcomes all the compared methods in terms of edge and texture preservation.

Please cite this article in press as: Singh, P., et al. A new SAR image despeckling using correlation based fusion and method noise thresholding. Journal of King Saud University – Computer and Information Sciences (2018), https://doi.org/10.1016/j.jksuci.2018.03.009

In terms of artifact generation in the output images, it is seen that there is no occurrence of artifacts in the results of proposed scheme. BaysWS-HAW shows some occurrence of blocking artifacts in the output results. ATV, bivariate and IDPAD don't generate any artifacts. The structures of the objects seen in the output images of proposed methodology are well preserved. The SAR images are basically low contrast images and speckle noise disturbs the overall texture of the image, in the despeckling results, it can be seen that in proposed method output, the low contrast objects are well preserved.

On analyzing the details of the output images in Figs. 6–10, it is observed that the proposed method shows the best result in terms of preservation of the significant information. The proposed method utilizes meritorious attributes of both Bayesian and Bivariate shrinkage methods, as it can be seen the corners and edges are well preserved and even the smoothness over the homogeneous areas are well maintained. The despeckling scheme is grounded on the local correlation based fusion strategy of high-frequency coefficients. It provides the effective enhancement of the high-frequency coefficients. A mask of 3×3 is used to calculate the optimal threshold value using correlation coefficient. The work is tested on the 5×5, 7×7 and 9×9 masks. As the mask size increases the despeckled image quality degrades, this proves the importance of the threshold value in this scheme. The 'average' and 'max' operation depends on the threshold value. Hence the fusion strategy depends on the threshold value. The scheme uses the db2 wavelet family basis in DWT operation. The wavelet decomposition level is set using the entropy factor. The decomposition is performed till the level nth until the entropy value of level n is approximately equal to the level n-1.

Tables 2, 3 and 4, respectively show the PSNR (dB), SSIM and SNR (dB) values of the despeckled SAR images using proposed and existing methods. The finest values among all the approaches are denoted in bold. The outcomes displayed in tables validate the superiority of the proposed method among other methods. The improvement in the quantitative measures (PSNR, SSIM, and SNR) is analyzed by studying their values before and after the despeckling process. It provides an analysis of incremental improvement in the despeckled image with respect to its reference image using proposed method.

In Table 2, the PSNR values of the proposed method show the best result among the compared method. The IDPAD method at $\sigma = 10$ in SAR image 2 shows the best result among all methods but still, the overall texture of the proposed method is better than IDPAD at $\sigma = 10$. In SAR image 3, the proposed method shows best result at $\sigma = 10$, 30 and 40. The BayesWS-HAW and IDPAD shows

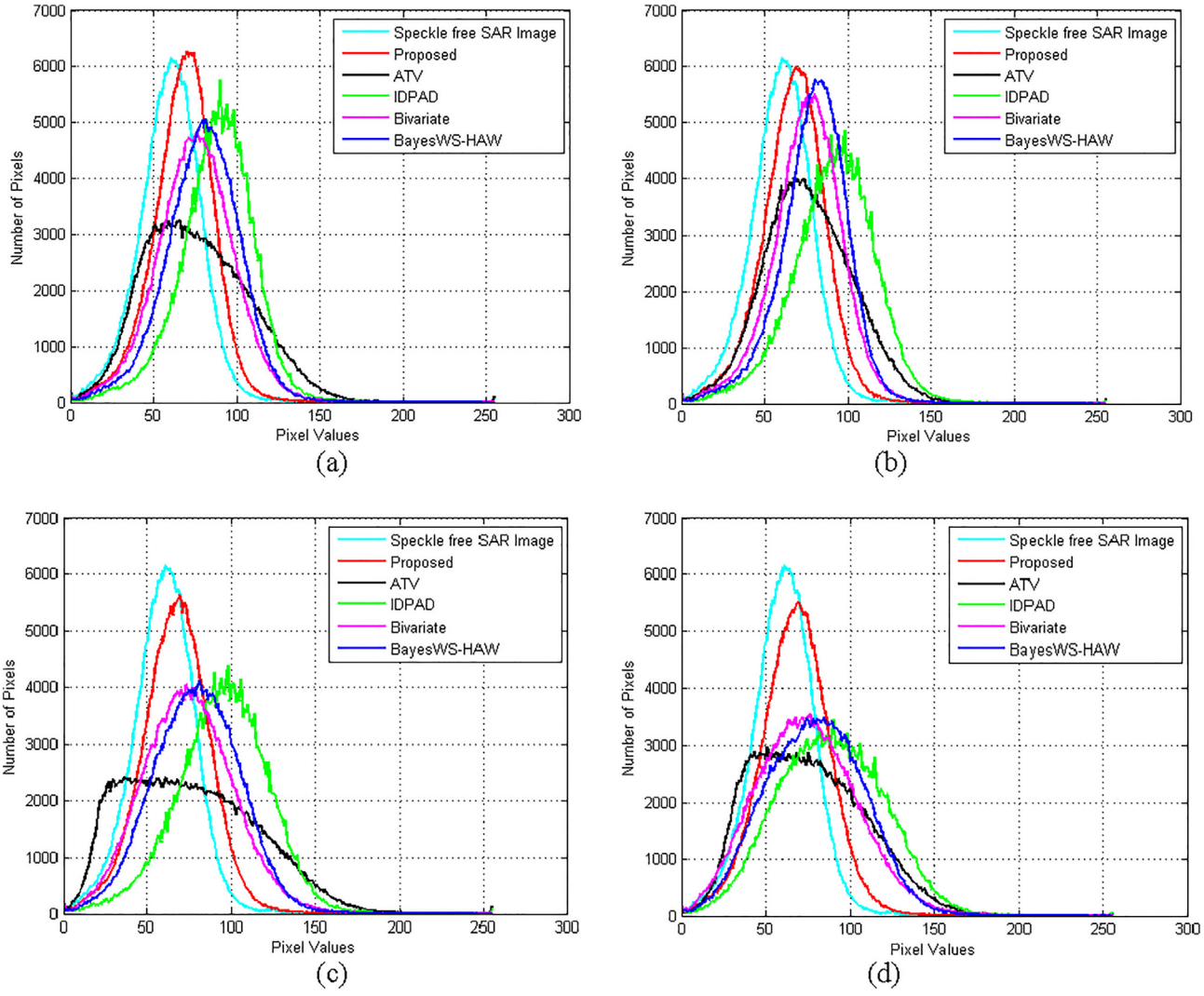

Fig. 11. Plotting noise-free SAR image and results of proposed, ATV, IDPAD, Bivariate and BayesWS-HAW methods using histogram at (a) $\sigma = 10$ (b) $\sigma = 20$ (c) $\sigma = 30$ (d) $\sigma = 40$.

Please cite this article in press as: Singh, P., et al. A new SAR image despeckling using correlation based fusion and method noise thresholding. Journal of King Saud University – Computer and Information Sciences (2018), https://doi.org/10.1016/j.jksuci.2018.03.009

better result than proposed method at σ = 20 and 5 respectively in terms of PSNR. In Table 3, The SSIM of the proposed method also shows the best result among all compared methods. The ATV method at σ = 30 in SAR image 2 shows the best result but on zooming the output image it is seen that the minor detail parts are lost and overall structure of the image is also over smooth. The method based on anisotropic diffusion (IDPAD) shows a better result in terms of texture and edge preservation. In SAR image 3, en efficient preservation of structures is observed at σ = 5, 10, 30 and 40 by the proposed method. The IDPAD method shows better result at σ = 20 than the proposed method. In Table 4, the results of the proposed method are compared on the basis of SNR values.

Fig. 12. Speckle-free classical images.

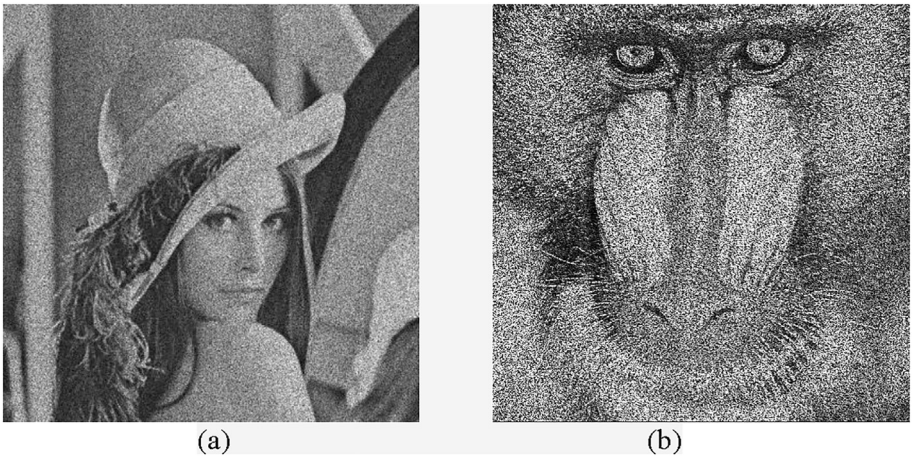

Fig. 13. Speckled classical images at σ = 20.

Table 2
PSNR of Despeckled SAR Images.

Image	σ	Before Despeckling	After Despeckling				
		Default PSNR Values	ATV (Zhao et al., 2015)	BayesWS-HAW (Li et al., 2013)	Bivariate Thresholding (Sethunadh and Thomas, 2014)	IDPAD (Zhu et al., 2014)	Proposed Method
SAR Image 1	5	25.1588	44.6736	43.2879	43.9918	44.8527	**48.8954**
	10	22.1475	44.5672	43.2341	42.7834	44.4261	**45.1272**
	20	19.1526	44.6732	42.5641	41.5642	43.7659	**44.8522**
	30	17.3726	43.2431	42.9867	41.4451	43.0909	**43.7231**
	40	16.2027	42.1101	41.6739	40.0934	41.6452	**42.6387**
SAR Image 2	5	20.2091	46.5643	43.3923	44.1983	46.1131	**46.7341**
	10	17.3042	45.6294	42.4562	43.8563	**45.9321**	45.7563
	20	14.4775	45.0095	42.2231	43.1951	44.0774	**45.1247**
	30	12.8544	44.6719	42.2495	42.6443	44.2341	**44.7684**
	40	11.7723	44.0035	41.0941	42.0902	43.7675	**44.1191**
SAR Image 3	5	18.6959	42.6598	43.0202	43.0298	**44.2368**	43.2368
	10	15.8382	42.1010	41.9056	42.1350	42.3569	**42.3910**
	20	13.0255	39.3598	**40.3659**	39.5913	40.2598	40.3265
	30	11.4343	37.2946	38.2159	38.1278	37.9898	**38.2791**
	40	10.3691	35.0303	36.0891	35.2136	36.1297	**36.2590**

Please cite this article in press as: Singh, P., et al. A new SAR image despeckling using correlation based fusion and method noise thresholding. Journal of King Saud University – Computer and Information Sciences (2018), https://doi.org/10.1016/j.jksuci.2018.03.009

All the SNR quantitative values show the better performance than the other compared methods. Only two methods i.e. BayesWS-HAW and IDPAD show better results than the proposed method at σ = 10 and 20 respectively. In SAR image 3, the SNR values of IDPAD at σ = 5 and ATV at σ = 20 shows better result than the proposed method. In the rest cases, the SNR values of the proposed method are better. The Table 2, 3 and 4 shows the quantitative analysis of the despeckling methods before and after despeckling. It helps in understanding the effectiveness and capability of the despeckling algorithms at different noise variances.

The Fig. 14. shows the comparative graphical analysis of the output result of despeckling methods at various noise variances

Table 3
SSIM of Despeckled SAR Images.

Image	Σ	Before Despeckling	After Despeckling				
		Default SSIM Values	ATV (Zhao et al., 2015)	BayesWS-HAW (Li et al., 2013)	Bivariate Thresholding (Sethunadh and Thomas, 2014)	IDPAD (Zhu et al., 2014)	Proposed Method
SAR Image 1	5	0.6281	0.9878	0.9543	0.9673	0.9784	**0.9989**
	10	0.4682	0.9564	0.9432	0.9564	0.9453	**0.9647**
	20	0.3144	0.9153	0.9274	0.9241	0.9213	**0.9389**
	30	0.2380	0.9057	0.9094	0.9075	0.9091	**0.9182**
	40	0.1950	0.8954	0.8971	0.8745	0.8875	**0.8973**
SAR Image 2	5	0.7895	0.9785	0.9674	0.9666	0.9817	**0.9853**
	10	0.6575	0.9666	0.9561	0.9654	0.9563	**0.9756**
	20	0.4959	0.9514	0.9153	0.9482	0.9063	**0.9541**
	30	0.3992	**0.9219**	0.9085	0.9131	0.9063	0.9191
	40	0.3364	0.8974	0.8751	0.8821	0.8874	**0.9093**
SAR Image 3	5	0.7492	0.9251	0.9511	0.9256	0.9354	**0.9546**
	10	0.6072	0.9018	0.9154	0.8959	0.9025	**0.9157**
	20	0.4390	0.8512	0.8467	0.8415	**0.8559**	0.8549
	30	0.3416	0.8057	0.7989	0.8027	0.8125	**0.8127**
	40	0.2808	0.7301	0.7250	0.7125	0.7259	**0.7325**

Table 4
SNR of Despeckled SAR Images.

Image	σ	Before Despeckling	After Despeckling				
		Default SNR Values	ATV (Zhao et al., 2015)	BayesWS-HAW (Li et al., 2013)	Bivariate Thresholding (Sethunadh and Thomas, 2014)	IDPAD (Zhu et al., 2014)	Proposed Method
SAR Image 1	5	20.4960	24.1256	25.0068	23.5674	24.0019	**25.3430**
	10	19.2512	23.4561	**24.9989**	23.1258	24.2985	24.3198
	20	17.4705	23.0258	23.9898	22.9478	**24.3333**	24.1021
	30	16.2215	22.5689	23.0258	22.0201	23.0589	**23.1230**
	40	15.2771	22.0145	22.9157	21.5698	22.9971	**23.0090**
SAR Image 2	5	13.7497	21.2365	22.3495	21.2598	23.0989	**23.1964**
	10	13.0248	22.3598	22.1254	21.0547	22.9589	**23.0101**
	20	11.9114	21.1211	21.2864	20.3256	22.5646	**22.9184**
	30	11.0817	20.1254	21.0597	20.0201	22.0358	**22.1614**
	40	10.4375	20.0032	20.7613	20.5632	21.9898	**22.1009**
SAR Image 3	5	13.0469	21.5478	21.5987	21.8780	**22.0040**	21.9870
	10	12.3241	21.2658	21.2910	21.3294	21.4560	**21.5897**
	20	11.1980	**21.1254**	20.8910	20.8978	20.0992	21.0123
	30	10.3512	20.8478	20.3325	20.1587	20.5894	**20.9878**
	40	9.6860	20.1015	20.1214	20.0121	19.5656	**20.5898**

Fig. 14. Despeckled classical images using the proposed method.

Please cite this article in press as: Singh, P., et al. A new SAR image despeckling using correlation based fusion and method noise thresholding. Journal of King Saud University – Computer and Information Sciences (2018), https://doi.org/10.1016/j.jksuci.2018.03.009

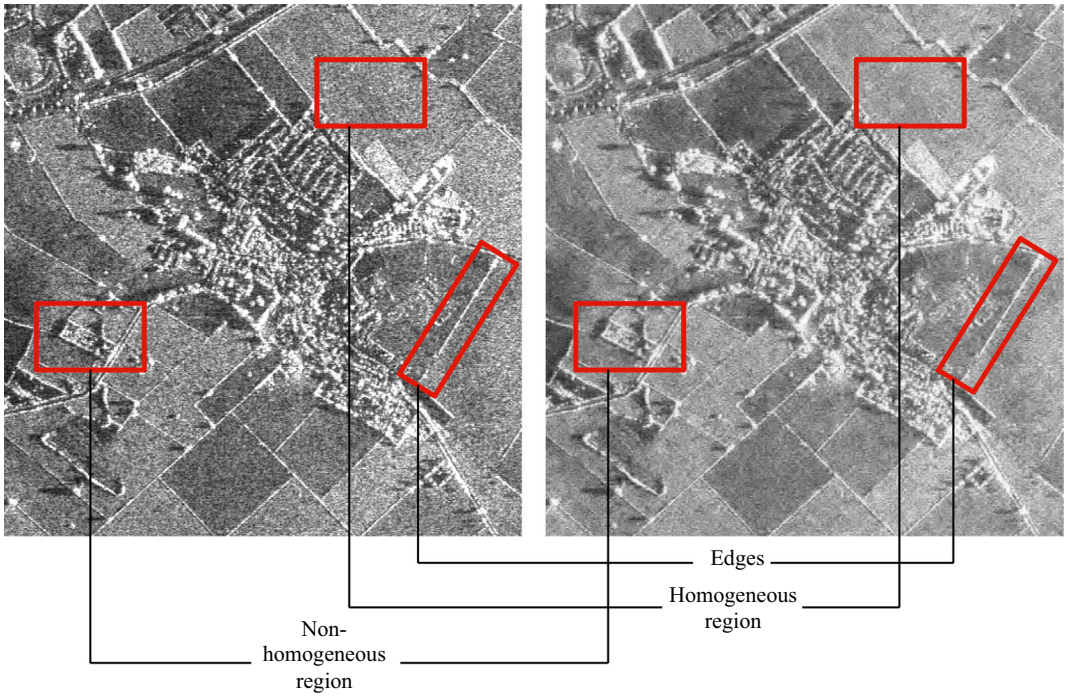

Fig. 15. Analysis of speckle reduction and detail preservation in the proposed method on SAR image 3.

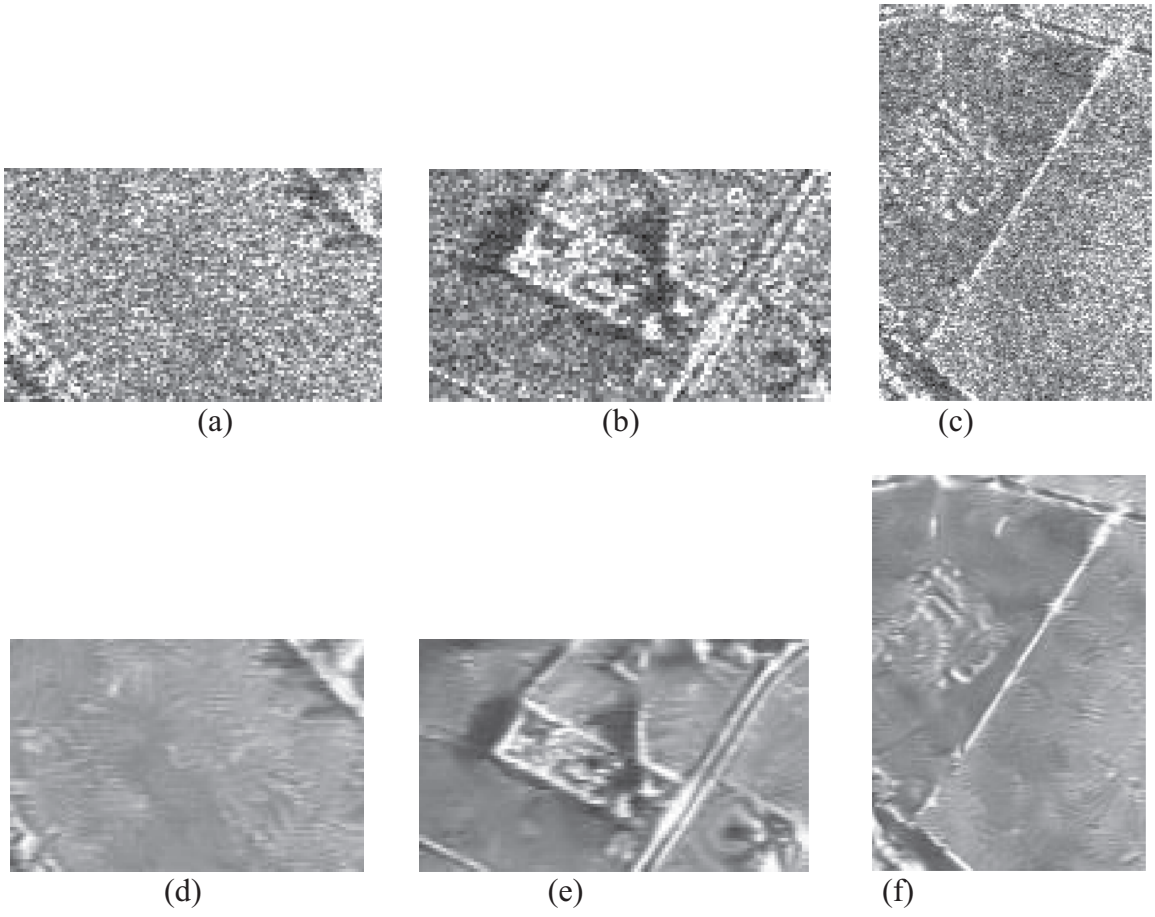

Fig. 16. Analysis of zoomed part of the despeckled SAR image 3 using proposed method assessing the detail preservation like edge preservation, smoothness in the homogeneous region, texture preservation in the heterogeneous region and speckle reduction.

Please cite this article in press as: Singh, P., et al. A new SAR image despeckling using correlation based fusion and method noise thresholding. Journal of King Saud University – Computer and Information Sciences (2018), https://doi.org/10.1016/j.jksuci.2018.03.009

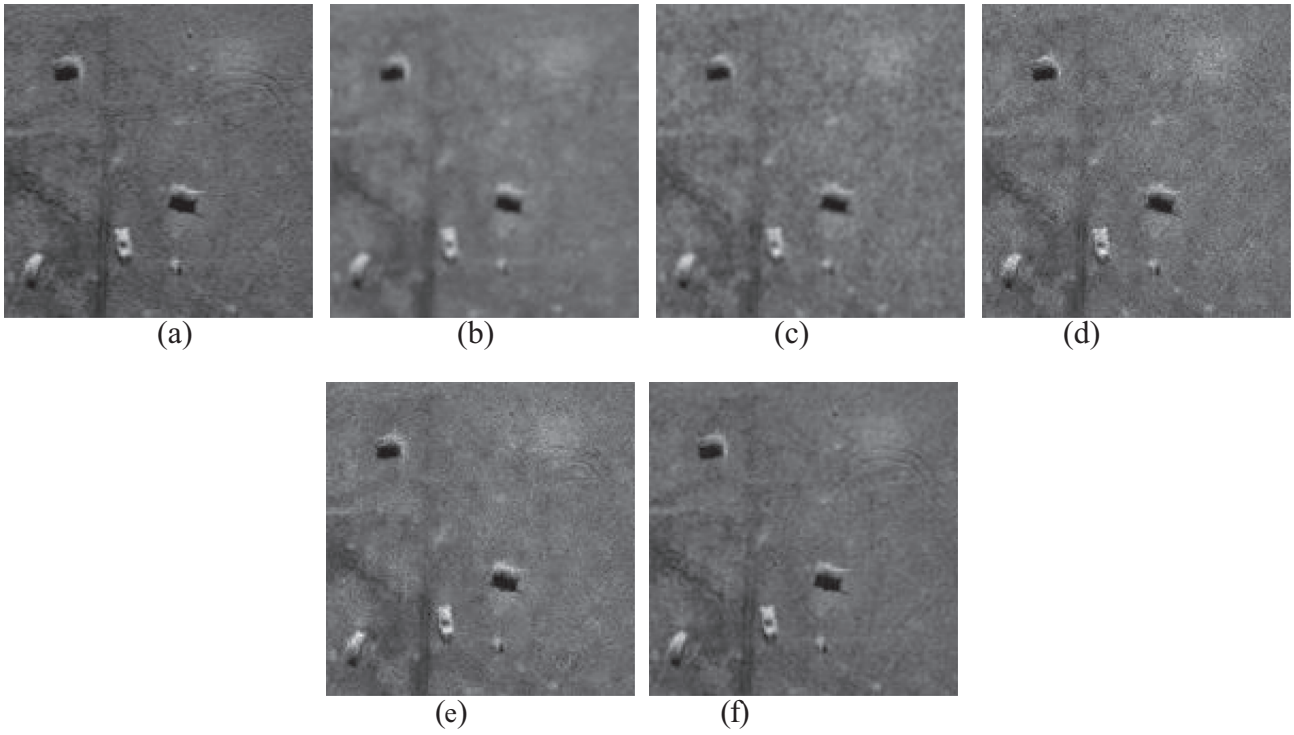

Fig. 17. Results of zoomed areas of SAR image 1 using different despeckling algorithm (a) reference SAR image (b) results of ATV (c) results of BayesWS-HAW (d) results of Bivariate thresholding (e) results of IDPAD (f) results of the proposed method.

(σ = 10, 20, 30, 40). The plot is generated of all despeckling results using the histogram. It depicts the similarity and closeness of the despeckling output result with the reference SAR image. It can be easily seen that the result of the proposed method show the best results and it is closest to the noise-free SAR image in comparison to other compared work.

The despeckling scheme performs successfully on real SAR data. Since the SAR images are already influenced by the speckle noise and distribution of noise pattern in SAR images is unknown. The capability and strength of designed despeckling scheme are tested by applying it to the classical digital images like 'Lena', and 'Baboon'. The proposed algorithm experiments on these classical images at noise variance (σ) = 20 shown in the Figs. 11–13. In this case, the quality of the despeckled image can be checked easily and efficiently. Here the original speckle-free i.e. clean reference image is available which can be used for performance analysis. The result of the proposed method on speckled classical images is tested by visual quality. It is observed that the high visual quality of the despeckled image in Fig. 13 is achieved. The smoothness in the homogeneous areas is obtained. The granular pattern i.e. speckle noise is also eliminated.

The Figs. 15 and 16 shows the zoom-in result of the proposed method in terms of edge preservation and smoothness in the homogeneous and heterogeneous areas. The smoothness and the speckle reduction in the homogeneous regions are well achieved. The structure preservation in the heterogeneous areas is efficiently achieved using proposed method.speckle noise reduction, smoothness in homogenous region, preservation of edges, point scatterers and textured regions are compared in Fig. 17. On comparing the zoomed-in result of despeckling schemes i.e. Fig. 17(b–f); it is observed that the proposed method Fig. 17(f)) shows the best preservation of fine detail in the SAR image as a comparison to other methods Fig. 17(b–e)). The Fig. 17(a) shows the reference zoomed-in SAR image. On visual inspection, the Fig. 17(f) shows that it is the closest to the Fig. 17(a). It proves the best speckle reduction and detail preservation in the proposed method.

5. Conclusion and future scope

In this research work, a new homomorphic SAR image despeckling scheme is developed using local correlation based fusion in wavelet transform. The developed scheme uses two different wavelet shrinkage rule i.e. Bayesian and Bivariate shrinkage rule for filtering the high-frequency coefficients. The Bayesian method smoothes the uniform region but it is sensitive to the edges. The bivariate method analyses the dependence between the child coefficient and its parent coefficient and enhances the edge component of the image. The high-frequency coefficient components of both the shrinkage rules are fused using local correlation based strategy. After fusion of two improved high frequency coefficient components, then the despeckled image results into a higher quality image. Entropy-based wavelet decomposition decides the decomposition level of the wavelet transform. The method noise thresholding is applied to process the unfiltered components of the image and to restore the remaining fine details of the image. This concept is capable of restoring the significant information like edges and corners which remain unfiltered in the initial stage of despeckling. The performance of the proposed method is assessed by the visual appearance of the despeckled SAR image and with the help of quantitative metrics like PSNR, SSIM, and SNR. From the critical comparative analysis, it can be said that proposed method preserves the edges and structure of the object in the SAR image. This research shows that no visual artifacts are generated during the process. Therefore proposed method has the potential ability to be used in various practical applications of SAR images.

The authors believe that there is a lot of scope for adding new dimensions in the proposed scheme. In the proposed scheme the authors set the decomposition level using entropy factor by analyzing the texture feature. So there are also other ways that can decide the decomposition level like, local range, MSE, contrast etc. There is the scope of using advanced transform like curvelet, shearlet, and many others. The researchers can develop a new way

Please cite this article in press as: Singh, P., et al. A new SAR image despeckling using correlation based fusion and method noise thresholding. Journal of King Saud University – Computer and Information Sciences (2018), https://doi.org/10.1016/j.jksuci.2018.03.009

to evaluate the threshold value. A new fusion strategy can be developed. The developed despeckling model is highly adaptive and robust.

References

Abramovich, F., Sapatinas, T., Silverman, B.W., 1998. Wavelet thresholding via a bayesian approach. J. R. Stat. Soc. Ser. B 60, 725–749.

Bhattacharya, A., Speckle Filtering/Speckle Statistics, (Slide courtesy Prof. E. Pottier and Prof. L. Ferro-Famil).

Saevarsson, Birgir Bjorn, Sveinsson, Johannes R., Benediktsson, Jon Atli, 2004. Combined Wavelet and Curvelet Denoising of SAR Images. In: Proceedings of IEEE, 2004.

Chen, Guozhong, Liu, Xingzhao, 2005. Wavelet-Based Despeckling SAR Images Using Neighbouring Wavelet Coefficients. In: Proceedings of IEEE, 2005.

Frost, V.S., et al., 1982. A model for radar images and its application to adaptive digital filtering of multiplicative noise. IEEE Trans. Pattern Anal. Machine Intell. PAMI-4, 157–166.

Kuan, D.T. et al., 1987. Adaptive, restoration of images with speckle. IEEE Trans. Acc. Speech Signal Proc. 35 (3), 373–383.

Kuwahara, M., Hachimura, K., Eiho, S., Kinoshita, M., 1976. Processing of RIangiocardiographic images. In: Preston, K., Onoe, M. (Eds.), Digital Processing of Biomedical Images. Plenum, New York, pp. 187–202.

Kyprianidis, J.E., Kang, H., Dllner, J., 2009. Image and Video Abstraction by Anisotropic Kuwahara Filtering. Comput. Graph. Forum 28, 19551963.

Lee, J.S., 1980. Digital image enhancement, and noise filtering by use of local statistics. IEEE Trans. Pattern Anal. Matching Intell PAMI-2 (1980) 165–168.

Lee, J.-S., Apr. 1981. Refined filtering of image noise using local statistics. Comput. Graph. Image Process. 15 (2), 380389.

Acharya, Tinku, Ray, Ajoy K., 2005. Image Processing Principles Applications. John Wiley Sons, Mc., Publication.

Anil K. Jain, 1989. Fundamentals of Digital Image Processing first edition. Prentice Hall, Inc.

Yu, Y., Acton, S.T., Sept. 2004. Automated delineation of coastline from polarimetric SAR imagery. Int. J. Remote Sens. 25 (17), 34233438.

Perona, P., Malik, J., 1990. Scale space and edge detection using anisotropic diffusion. IEEE Trans. Image Process. 12 (8), 629639.

McConnell, I., Oliver, C., 1994. Comparison of annealing and iterated filters for speckle reduction in SAR. Proc. SPIE Microwave Sens Synthetic Aperture Radar 74. 2958, 7485.

Yu, Y., Acton, S.T., Nov. 2002. Speckle reducing anisotropic diffusion. IEEE Trans. Image Process. 11 (11), 1260–1270.

Gagnon, L., Jouan, A., 1997. Speckle filtering of SAR images: a comparative study between complex-wavelet-based and standard filters. In: Proc. SPIE, Wavelet Applications in Signal and Image processing, 1997, vol. 3169, pp. 8091.

Hervet, E., Fjrtoft, R., Marthon, P., Lops, A., 1998. Comparison of wavelet-based and statistical speckle filters. In: Posa, F. (Ed.) Proc. SPIE SAR Image Analysis, Modelling, and Techniques III, 1998, vol. 3497, pp. 4354.

Singh, P., Shree, R., 2017. A new homomorphic and method noise thresholding based despeckling of SAR image using anisotropic diffusion. J. King Saud Univ.–Comput. Information Sci. http://dx.doi.org/10.1016/j.jksuci.2017.06.006.

Sonam, Kumar M., 2017. A Local Correlation and Directive Contrast Based Image Fusion. In: Raman, B., Kumar, S., Roy, P., Sen, D. (Eds.) Proceedings of International Conference on Computer Vision and Image Processing. Advances in Intelligent Systems and Computing, vol 459. Springer, Singapore.

Diwakar, Manoj, Kumar, Manoj, 2014. CT image noise reduction based on adaptive wiener filtering with Wavelet packet thresholding. In: Parallel, Distributed and Grid Computing (PDGC), 2014 International Conference, 11–13 Dec. 2014, doi:10.1109/PDGC.2014.7030722.

Kumar, Manoj, Diwakar, Manoj, 2016. New Locally Adaptive Patch Variation Based CT Image Denoising. Int. J. Image Graph. Signal Process. (IJIGSP) 8 (1), 43–50. https://doi.org/10.5815/ijigsp.2016.01.05.

Chang, S.G., Yu, B., Vetterli, M., 2000. Adaptive wavelet thresholding for image denoising and compression. IEEE Trans. Image Proc. 9 (9), 1532–1546.

Shi, Wenzhong, Zhu, Chang Qing, Tian, Yan, Nichol, Janet, 2005. Wavelet-based image fusion and quality assessment. Int. J. Appl. Earth Observ. Geoinformation 6 (3–4), 241–251.

Cho, Choongsang, Lee, Sangkeun, 2016. Effective Five Directional Partial Derivatives-Based Image Smoothing and a Parallel Structure Design. IEEE Trans. Image Process. 25 (4), 1617–1625. https://doi.org/10.1109/TIP.2016.2526785.

Zhao, Yao, Liu, Jianguo, Zhang, Bingchen, Hong, Wen, Yirong, Wu., 2015. Adaptive Total Variation Regularization Based SAR Image Despeckling and Despeckling Evaluation Index. IEEE Trans. Geosci. Remote Sens. 53 (5), 2765–2774.

Li, Heng-Chao, Hong, Wen, Member, Yi-Rong Wu, Fan, Ping-Zhi, 2013. Bayesian Wavelet Shrinkage With Heterogeneity-Adaptive Threshold for SAR Image Despeckling Based on Generalized Gamma Distribution. IEEE Trans. Geosci. Remote Sens. 51 (4), 2388–2402. https://doi.org/10.1109/TGRS.2012.2211366.

Sethunadh, R., Thomas, T., 2014. Spatially adaptive despeckling of SAR image using bivariate thresholding in directionlet domain. Electr. Lett. 50 (1), 44–45. https://doi.org/10.1049/el.2013.0971.

Zhu, Lei, Zhao, Xiaotian, Meihua, Gu, 2014. SAR image despeckling using improved detail-preserving anisotropic diffusion. Electr. Lett. 50 (15), 1092–1093. https://doi.org/10.1049/el.2014.0293.

Parrilli, Sara, Poderico, Mariana, February 2012. Cesario Vincenzo Angelino, and Luisa Verdoliva, "A Nonlocal SAR Image Denoising Algorithm Based on LLMMSE Wavelet Shrinkage". IEEE Trans. Geosci. Remote Sens. 50 (2).

Kervrann, C., Boulanger, J., Coupé, P., 2007. Bayesian nonlocal means filter, image redundancy and adaptive dictionaries for noise removal. In: Proc. 1st Int. Conf. on Scale Space and Variational Methods in Computer Vision (SSVM), 2007, pp. 520–532.

Coupe, P., Hellier, P., Kervrann, C., Barillot, C., 2008. Bayesian non local means-based speckle filtering. In: Proc. 5th IEEE Int. Symp. Biomedical Imaging: From Nano to Macro, 2008, pp. 1291–1294.

Zhong, H., Li, Y., Jiao, L., July 2011. SAR image despeckling using Bayesian non-local means filter with sigma preselection. IEEE Geosci. Remote Sensing Lett. 8 (4), 809–813.

Ranjani, J.J., Thiruvengadam, S.J., Jun. 2010. Dual tree complex wavelet transform based despeckling using interscale dependency. IEEE Trans. Geosci. Remote Sens. 48 (6), 2723–2731.

Bin, Xu, Cui, Yi, Li, Zenghui, Zuo, Bin, Yang, Jian, Song, Jianshe, 2015. Patch Ordering-Based SAR Image Despeckling Via Transform-Domain Filtering. IEEE J. Selected Top. Appl. Earth Observ. Remote Sens. 8 (4), 1682–1695. https://doi.org/10.1109/JSTARS.2014.2375359.

Cai, J.-F., Osher, S., Shen, Z., 2009. Convergence of the linearized Bregman iteration for 1-norm minimization. Math. Comput. 78 (268), 2127–2136.

Cai, J.-F., Osher, S., Shen, Z., 2009. Linearized Bregman iterations for compressed sensing. Math. Comput. 78 (267), 1515–1536.

Cai, J.-F., Osher, S., Shen, Z., 2009. Split Bregman methods and frame based image restoration. Multiscale Model. Simul. 8 (2), 337–369.

Candes, E.J., Wakin, M.B., Boyd, S.P., 2008. Enhancing sparsity by reweighted minimization. J. Fourier Anal. Appl. 14 (5–6), 877–905.

Chen, H., Wang, C., Song, Y., Li, Z., 2015. Split Bregmanized anisotropic total variation model for image deblurring. J. Vis. Commun. Image Represent. 31, 282–293.

Shreyamsha Kumar, B.K., SIViP, 2013. 7, 1211. https://doi.org/10.1007/s11760-012-0389-y

Shreyamsha Kumar, B.K., SIViP, 2013. 7, 1159. https://doi.org/10.1007/s11760-012-0372-7

Buades, A., Coll, B., Morel, J., 2004. On image denoising methods. Technical Report 2004-15, CMLA, 2004.

Zhang, Xiaobo, 2016. Image denoising using local Wiener filter and its method noise. Optik – Int. J. Light Electron Optics 127 (17), 6821–6828. https://doi.org/10.1016/j.ijleo.2016.05.002.

Singh, Prabhishek, Shree, Raj, 2016. Statistical Modelling of Log Transformed Speckled Image, published online in Vol. 14 No. 8 AUGUST International Journal of Computer Science and Information Security, pp. 426–431.

Singh, Prabhishek, Shree, Raj, 2016. Analysis and effects of speckle noise in SAR images, published in 2nd International Conference on Advances in Computing, Communication, & Automation (ICACCA) (Fall) Pages: 1–5, IEEE Conference Publications.

Singh, Prabhishek, Shree, Raj, 2017a. Statistical Quality Analysis of Wavelet Based SAR Images in Despeckling Process. Asian J. Electr. Sci. (AJES) 6 (2), 1–18.

Singh, Prabhishek, Shree, Raj, 2017b. Quantitative Dual Nature Analysis of Mean Square Error in SAR Image Despeckling. Int. J. Comput. Sci. Eng. (IJCSE) 9 (11), 619–622.

López-Martínez, Carlos, 2013. Speckle Noise Characterization and Filtering in Polarimetric SAR Data, 2nd Advanced course on radar polarimetry, ESA-ESRIN, 21–25 Jan 2013.

Dainty, J.C., 1976. The Statistics of Speckle Patterns. In: Wolf, E. Progress in Optics XIV © North-Holland.

Escamilla, Héctor M., Méndez, Eugenio R., 1991. Speckle statistics from gamma-distributed random-phase screens. J. Opt. Soc. Am. A 8, 1929–1935.

Intajag, Sathit, Chitwong, Sakreya, 2006. Speckle Noise Estimation with Generalized Gamma Distribution. In: SICE-ICASE International Joint Conference, Oct 2006, 18–21, in Bexco, Busan Korea.

Ulaby, F.T., Moore, R.K., Fung, A.K., 1986. Microwave Remote Sensing, Active and Passive, Volume III. from Theory to Applications, Artech House.

Oliver, C., Quegan, S., 1998. Understanding Synthetic Aperture Radar Images. Artech House, Boston.

Walessa, M., Datcu, M., 2000. Model-based despeckling and information extraction from SAR Images. IEEE Trans. Geosc. Remote Sensing 38 (5), 2258–2269.

Gao, Gui, 2010. Statistical Modeling of SAR Images: A Survey. Sensors (Basel) 10(1) 775–795. doi:10.3390/s100100775

Garg, R., Kumar, Er. Abhijeet, 2012. Comparison of Various Noise Removals Using Bayesian Framework. Int. J. Mod. Eng. Res. 2 (1), 265–270.

Moser, G., Zerubia, J., Serpico, S.B., 2006. SAR amplitude probality density function estimation based on a generalized Gaussian model. IEEE Trans. Image Process. 15, 1429–1442.

Moser, G., Zerubia, J., Serpico, S.B., 2006. Dictionary-based stochastic expectation–maximization for SAR amplitude probability density function estimation. IEEE Trans. Geosci. Romote Sens. 4(1).

Goodman, J.W., 1975. Statistical Properties of Laser Speckle Patterns, Laser Speckle and Related Phenomena. Springer Verlag, Heidelberg, Germany, pp. 9–75.

DATASET OF STANDARD [512×512] GRAYSCALE TEST IMAGES, Available at: http://decsai.ugr.es/cvg/CG/base.htm

Test Images, Available at: http://decsai.ugr.es/cvg/dbimagenes/

Argenti, Fabrizio, Lapini, Alessandro, Bianchi, Tiziano, Alparone, Luciano, 2013. A Tutorial on Speckle Reduction in Synthetic Aperture Radar Images. IEEE Geosci. Remote Sens. Mag. 1 (3), 6–35.

Please cite this article in press as: Singh, P., et al. A new SAR image despeckling using correlation based fusion and method noise thresholding. Journal of King Saud University – Computer and Information Sciences (2018), https://doi.org/10.1016/j.jksuci.2018.03.009

Catté, F., Lions, P.-L., Morel, J.-M., Coll, T., 1992. Image selective smoothing and edge detection by nonlinear diffusion. SIAM J. Numer. Anal. 29 (1), 182–193.

Esedoglu, S., Osher, S.J., 2004. Decomposition of images by the anisotropic Rudin–Osher–Fatemi model. Commun. Pure Appl. Math. 57 (12), 1609–1626.

Weickert, J., 1998. Anisotropic Diffusion in Image Processing, vol. 1, Teubner Stuttgart.

Chambolle, A., Pock, T., 2011. A first-order primal-dual algorithm for convex problems with applications to imaging. J. Math. Imaging Vis. 40 (1), 120–145.

Rudin, L.I., Osher, S., 1994. Total variation based image restoration with free local constraints. In: IEEE International Conference, Image Processing, 1994, Proceedings, ICIP-94, vol. 1, IEEE, 1994, pp. 31–35.

Vogel, C.R., 1995. A multigrid method for total variation-based image denoising. In: Computation and Control IV, Springer, pp. 323–331.

Vogel, C.R., Oman, M.E., 1996. Iterative methods for total variation denoising. SIAM J. Sci. Comput. 17 (1), 227–238.

Diwakar, Manoj, Kumar, Manoj, 2018. A review on CT image noise and its denoising. Biomed. Signal Process. Control 42, 73–88. https://doi.org/10.1016/j.bspc.2018.01.010.

Chambolle, A., 2004. An algorithm for total variation minimization and applications. J. Math. Imaging Vis. 20 (1–2), 89–97.

Goldstein, T., Osher, S., 2009. The split Bregman method for L1-regularized problems. SIAM J. Imaging Sci. 2 (2), 323–343.

Deng, J., Li, H., Wu, H., 2011. A CT image denoise method using curvelet transform. In: Communication Systems and Information Technology, Springer, pp. 681–687.

Li, W., Li, Q., Gong, W., Tang, S., 2012. Total variation blind deconvolution employing split Bregman iteration. J. Vis. Commun. Image Represent. 23 (3), 409–417.

Osher, S., Burger, M., Goldfarb, D., Xu, J., Yin, W., 2005. An iterative regularization method for total variation-based image restoration. Multiscale Model. Simul. 4 (2), 460–489.

Wotao, Y., Stanley, O., Donald, G., Jerome, D., 2008. Bregman iterative algorithms for minimization with applications to compressed sensing. SIAM J. Imaging Sci. 1 (1), 143–168.

Rudin, L.I., Osher, S., Fatemi, E., 1992. Nonlinear total variation based noise removal algorithms. Phys. D: Nonlinear Phenom. 60 (1), 259–268.

Lou, Y., Zeng, T., Osher, S., Xin, J., 2015. A weighted difference of anisotropic and isotropic total variation model for image processing. SIAM J. Imaging Sci. 8 (3), 1798–1823.

Zibulevsky, M., Elad, M., 2010. L1–L2 optimization in signal and image processing. IEEE Signal Process. Mag. 27 (3), 76–88.

Hu, Y., Jacob, M., 2012. Higher degree total variation (HDTV) regularization for image recovery. IEEE Trans. Image Process. 21 (5), 2559–2571.

Beck, A., Teboulle, M., 2009. Fast gradient-based algorithms for constrained total variation image denoising and deblurring problems. IEEE Trans. Image Process. 18 (11), 2419–2434.

Sun, C., Tang, C., Zhu, X., Ren, H., 2015. Exponential total variation model for noise removal, its numerical algorithms and applications. AEU Int. J. Electron. Commun. 69 (3), 644–654.

Yan, J., Lu, W.-S., 2011. New algorithms for sparse representation of discrete signals based on lp-l2 optimization. In: 2011 IEEE Pacific Rim Conference on Communications, Computers and Signal Processing (PacRim), IEEE, 2011, pp. 73–78.

Yan, J., Lu, W.-S., 2011. Power-iterative strategy for lp-l2 optimization for compressive sensing: towards global solution. In: 2011 Conference Record of the Forty Fifth Asilomar Conference on Signals, Systems and Computers (ASILOMAR), IEEE, 2011, pp. 1153–1157.

Yan, J., Lu, W.-S., 2012. Smoothed p–2 solvers for signal denoising, in: 2012 IEEE International Conference on Acoustics, Speech and Signal Processing (ICASSP), IEEE, 2012, pp. 3801–3804.

Yan, J., Lu, W.-S., 2015. Image denoising by generalized total variation regularization and least squares fidelity. Multidimens. Syst. Signal Process. 26 (1), 243–266.

Buades, A., Coll, B., Morel, J.-M., 2005. A review of image denoising algorithms, with a new one. Multiscale Model. Simul. 4 (2), 490–530.

Please cite this article in press as: Singh, P., et al. A new SAR image despeckling using correlation based fusion and method noise thresholding. Journal of King Saud University – Computer and Information Sciences (2018), https://doi.org/10.1016/j.jksuci.2018.03.009